Development of a "Pro-Matrix" Advanced Cell Scaffold Biomaterial to Support Mesenchymal Stem Cell Therapy

Thesis

Development of a “Pro-Matrix” Advanced Cell Scaffold Biomaterial to Support Mesenchymal Stem Cell Therapy

Catriona Bethan Inverarity

Department of Life, Health and Chemical Sciences,

The Open University

A thesis submitted in partial fulfilment of the degree of Doctor of Philosophy

June 2020

Sponsored by The Open University and Consorcio Regenero

Hosted by the Institute of Biomedical Engineering, University of Oxford

Abstract

Cell therapies are typically limited by the rapid dispersal of cells on delivery. Scaffolds offer an approach of enhancing therapeutic efficiency and efficacy as a delivery vehicle and implantable niche. This project aimed to combine the bio-intelligent properties of fibrin-based scaffolds with the potential of MSC cell therapies for activating healing in chronic wounds.

A highly porous fibrin-based biomaterial scaffold was developed using an optimised emulsion templating technique. Templating enables reproducible manufacture of materials with a regular, highly porous structure with a high degree of pore interconnectivity and consistent pore size distribution. The method was optimised to generate a range of pore diameters suitable for skin tissue engineering, but it could be adjusted for other purposes. What differentiates this method is that the emulsion is amenable to incorporation of protein monomers without causing any denaturation, which allows the creation of a native-like structure during fibrin formation. The initial structure is then stabilised by glutaraldehyde cross-linking. The resulting scaffold is suited to cell ingress and supporting angiogenesis and allows fluid and nutrient exchange between the scaffold and the wound environment.

The experimental work undertaken to design a suitable emulsion produced results which, to the authors' knowledge, have not been reported elsewhere. The two distinct patterns of behaviour identified suggest specific surfactant traits that make certain kinds of surfactants extremely useful in supporting high internal phase emulsions. The reason(s) for this are unclear, but the overall trend has potential utility in emulsion formulation. 'Oil carrying capacity' (OCC) is proposed as an index for ranking surfactants by the oil fraction (in an oil-in-water emulsion) for which stability is greatest.

This project is divided into two main sections: emulsion formulation and using the optimised emulsion to template a scaffold that was then refined to produce a material with appropriate structural, mechanical, and biochemical properties for skin tissue engineering. Emulsion design encompassed degradation kinetics and achieving appropriate internal phase droplet size, packing and size distribution for cell and blood vessel ingress. Successful emulsions were then tested for protein compatibility and used to template various fibrin-based scaffolds. By iterative redesign, refined and reproducible scaffolds were produced that were characterised by various means to assess their suitability as skin tissue engineering scaffolds.

This work describes a novel biocompatible fibrin scaffold with optimised microstructure for cell ingress and angiogenesis, excellent handling capabilities in both freeze-dried and rehydrated forms and biocompatibility as demonstrated by in vitro assays.

Acknowledgements

There are many people who have helped me over the last four years to whom I am profoundly grateful. I would like to thank my supervisors Dr Julian Dye, Dr Duncan Banks, and Dr Martin Bootman. Special thanks to Julian for the thoughtful provision of homemade jam and mince pies.

This project was made possible by funding from The Open University and a Chilean stem cell consortium, Regenero Consorcio, based at the Universidad de los Andes, Santiago.

Thank you to Dr. Marcus Green and Dr. Igor Dyson (University of Oxford) and Dr. Igor Kraev (The Open University) for their technical support. I would particularly like to thank Gordon Imlach (The Open University) for his time and patience training me to use the SEM. While I took all the images myself, the quality is due to the dedicated and thorough training I received from Gordon. Thanks also to Karen Evans, Iwona Loza and especially Agata Stramek of the Biomedical Research Unit at The Open University. Their support and commiseration during the most challenging and frustrating part of my project was most appreciated.

Although I am a student at The Open University, the project has been generously hosted by the Department of Engineering Science at the University of Oxford. The tissue engineering group, led by Prof. Zhanfeng Cui and Prof. Cathy Ye, were welcoming and supportive. The friends I made at the lab were a wonderful source of advice and comic relief.

Finally, I am immensely grateful to my family for their constant support and encouragement. The past four years have been both an academic and a personal challenge and I could not have done this without them.

Table of contents

List of figures

3.4	2	Timeline of chick embryo development, based on Hamburger-Hamilton stages, alongside key stages from the CAM assay protocol
3.4	3	Diagram showing pre-orientation of embryos; method of cracking eggs and placement in culture dishes
3.4	4	CAM development at time points after scaffold placement
3.4	5	Number of blood vessels interacting with scaffold samples
3.4	6	Cyanmethemoglobin (mg/ml) detected using Drabkin's Reagent at 540 nm (R^2=0.9995)
3.4	7	Embryo mortality arising from (A) catastrophic yolk rupture, (B) slow rupture after 2 days in culture and (C) low humidity (60-65%). Mortality was detectable by (D) blood accumulating at the periphery of the capillary plexus and (E) whitening of vessels and the embryo.

Future work

4	1	Sketch of proposed semi-automated scaffold rig to support scaled-up manufacture

List of tables

List of equations

Experimental work

List of abbreviations

bFGF	Basic fibroblast growth factor
BM-MSC	Bone marrow-derived mesenchymal stem cell
CAM	chick chorioallantoic membrane
CCK-8	Cell counting kit
CXCL-5	A chemokine, also known as epithelial-derived neutrophil-activating peptide 78
DMEM	Dulbecco's Modified Eagle's Medium
EDC	1-ethyl-3-(3-dimethylaminopropyl) carbodiimide
ECM	Extracellular matrix
ELISA	Enzyme-linked immunosorbent assay
EtOH	Ethanol (absolute; ~70% vol)
ETPM	Emulsion templated fibrin-based scaffold
FPA	Fibrinopeptide A
FPB	Fibrinopeptide B
FBS	Foetal bovine serum
G-CSF	Granulocyte-colony stimulating factor
GFP-MSC	Fluorescently labelled mesenchymal stem cells
GTA	Glutaraldehyde
H&E	Haematoxylin and eosin (histological stains)
HA	Hyaluronic acid
HH	Hamburger-Hamilton (stages of chick embryo development)
HIPE	High internal phase emulsion
HLB	Hydrophile-lipophile balance
HUVECs	Human umbilical vein endothelial cells
IL	Interleukin (-6,-8, -11 etc.)

LM	Light microscopy
M-CSF	Macrophage-colony stimulating factor
MES	2-morpholin-4-ylethanesulfonic acid
MMP	Matrix metalloproteinase
MSC	Mesenchymal stem cell
MTT	3-(4,5-dimethylthiazol-2-yl)-2,5-diphenyltetrazolium bromide
M_w	Molecular weight (g/mol)
NHS	N-hydroxyfulfosuccinimide
NICE	National Institute for Health and Care Excellence
NPIMR	Northwick Park Institute for Medical Research
OCC	Oil carrying capacity
O/W	Oil-in-water emulsion (i.e. oil droplets are dispersed in a continuous aqueous phase)
PBS	Phosphate buffered saline
PEG	Polyethylene glycol
PDGF-B	Platelet-derived growth factor B
PHBV	Poly (3-hydroxybutyrate-co-3-hydroxyvalerate)
PLGA	Poly (lactic-co-glycolic acid)
PLLA	Poly (L-lactic acid)
PM0	Foamed fibrin-based scaffold
POE	Polyoxyethylene
PolyHIPE	Scaffold templated from HIPE
PS	Penicillin-streptomycin
PVA	Poly vinyl alcohol
qPCR	Quantitative polymerase chain reaction
REM	Rapid eye movement

RI	Refractive index
SDF-1	Stromal cell-derived factor 1
SEM	Scanning electron microscope/graph
STSG	Split thickness skin graft
TGF-β1	Transforming growth factor β1
Three Rs	(or 3R principles) Refinement, reduction, and replacement of animals in research
TSI	Turbiscan™ stability index
TX	Triton™ X (surfactant series)
UTS	Ultimate tensile strength
VEGF	Vascular endothelial growth factor
W/O	Water-in-oil emulsion (i.e. aqueous droplets are dispersed in a continuous oil phase)

Publications and presentations

Manuscripts in preparation

1. Ranking surfactants by oil carrying capacity: A systematic approach to selecting surfactants to emulsify known oil fractions in oil-in-water emulsions
2. PolyHIPEs for skin tissue regeneration I: Formulation and characterisation of oil-in-water emulsions for templating highly porous protein structures
3. PolyHIPEs for skin tissue regeneration II: Manufacture and characterisation of novel fibrin-based hierarchical scaffolds
4. The chick chorioallantoic membrane (CAM) assay for assessing angiogenic potential of biomaterial scaffolds

Presentations and published abstracts

1. Characterisation of microstructural, mechanical, and biological properties of a novel fibrin-based bio-intelligent scaffold for *in situ* skin tissue engineering. Catriona Inverarity, Jimena Cuenca, Duncan Banks, Martin Bootman, Maroun Khoury and Julian Dye. eCM Meeting Abstracts 2018, collection 4, Tissue and Cell Engineering Society (TCES) conference (page 61).
2. Microstructural, mechanical, and biological characterisation of a novel fibrin scaffold for skin tissue engineering. Catriona Inverarity, Jimena Cuenca, Duncan Banks, Martin Bootman, Maroun Khoury and Julian Dye. 5th TERMIS World Congress 2018. Poster 01-P194.
3. Interplay between composition, mechanical properties, and biological properties in a fibrin-based bio-intelligent scaffold for skin tissue engineering. Catriona Inverarity, Jimena Cuenca, Duncan Banks, Martin Bootman, Maroun Khoury and Julian Dye. 29th Annual Meeting of the European Society for Biomaterials. Poster 598, session C.
4. Bio-intelligent scaffolds for regeneration of full-thickness skin injuries. Catriona Inverarity, Jimena Cuenca, Duncan Banks, Martin Bootman, Maroun Khoury and Julian Dye. STEM for Britain 2019, group 1 (Biosciences and Engineering). Presented at the Houses of Parliament March 2019.

Patents and IP

1. In progress

Aims

Skin is the largest organ of the body and is instrumental in homeostatic regulation as well as forming a physical barrier to infection (Percival, 2002; Walters and Roberts, 2002). When skin is wounded and this protective barrier is breached, it is important to repair the damage quickly to restore function (MacNeil, 2007). However, some wounds do not heal readily, leaving patients in pain and at risk of secondary illnesses (Ehrlichman et al., 1991; Guest et al., 2015). These non-healing wounds may be chronic wounds such as ulcers, but another example is extensive partial- or full-thickness burns. The normal wound healing mechanism may not be impaired in the same way that it is in chronic wounds, but the extent of severe burn injuries means that the time required to restore the epidermal layer can be excessively long (Papini, 2004; Percival, 2002). There may also be insufficient healthy tissue remaining for graft repair, the current gold standard (Atiyeh and Costagliola, 2007; Dai et al., 2018; Hrabchak et al., 2006).

In these cases, intervention is required to facilitate healing. Where conventional therapies fail, tissue engineering strategies may be deployed (Boyce and Lalley, 2018; Garcia-Gareta, 2019; Vig et al., 2017; Yu et al., 2019). This may take the form of transplanted cells, growth factors or biomaterial scaffolds of various composition (Bhardwaj et al., 2017; Chua et al., 2016; Frueh et al., 2016; Whang et al., 2000; Yu et al., 2019).

The aim of the project is to produce an appropriate scaffold to support regeneration of skin tissue damaged by burns or chronic wounds, such as diabetic ulcers. It is generally accepted that tissue engineering scaffolds must fulfil a series of biological, structural and mechanical requirements to achieve *in vivo* efficacy (Garcia-Gareta, 2019; Hutmacher, 2001; Jones et al., 2002; Yannas and Burke, 1980). As a minimum, the scaffold produced for this project must meet the following requirements.

1) The scaffold must be capable of physically filling the defect caused by the tissue damage (or the excised wound site) and integrating with the healthy surrounding tissue (Schulz et al., 2000; Yannas and Burke, 1980). This may be achieved by either ingress of migratory cells and migration of wound margin keratinocytes, or cellular colonisation of the scaffold before implantation; or a combination of the two (Zhong et al., 2010).

2) Engineering approaches to scaffold manufacture have sought to integrate the scaffold with the surrounding tissue by matching their elasticity and tensile strength (Janson and Putnam, 2015; Sander et al., 2014; Vidal et al., 2019). The scaffold must have a high degree of porosity with good interconnectivity to allow for the movement of cells and diffusion of nutrients and waste (Busby et al., 2001; Thomson et al., 1995; Whang et al., 2000). Pores must be of an appropriate

size to host cells and allow them to develop an appropriate morphology and proliferate (Bokhari et al., 2007; Busby et al., 2001; Dagalakis et al., 1980; Sultana and Wang, 2008).

3) The biomaterial must be non-cytotoxic and biocompatible with the host tissue to avoid an inflammatory response that could lead to rejection (Hutmacher, 2001; MacNeil, 2007). Appropriate material selection (or coating) may even be beneficial to the healing wound. The scaffold must persist long enough to adequately support the fragile wound site but degrade in line with the rate of tissue repair to safe, readily metabolisable products (Busby et al., 2001; Langer and Vacanti, 1993).

The project is industrially sponsored and is intended for eventual commercialisation. This influenced decisions about both method and materials from the outset to ensure the scaffold had the potential for straightforward technology transfer. Ease of manufacture and potential scalability are therefore additional, though secondary, considerations. So too is the cost/benefit ratio of the scaffold, the selection criteria for many health advisory services such as NICE.

Scope of thesis

This thesis discusses the design, development, and characterisation of a biomaterial scaffold from first principles. It aims to explain the rationale for such a material, given the large number of commercially available 'wound healing' products and attempt to summarise the overwhelming and at times contradictory literature surrounding these products. The experimental work encompasses the design of the scaffold and also of the emulsions used to template them. These processes were not mutually exclusive and were performed concurrently in an iterative manner. For the sake of clarity, the work is not presented chronologically and is instead arranged to follow a logical narrative.

The thesis comprises four chapters, the first of which provides an overview of the normal structure and function of skin; the pathology of normal wound healing and the instances where wound healing is impaired. It further discusses the clinical and socioeconomic need to resolve recalcitrant wounds, and introduces the role of tissue scaffolds in addressing this need.

The second chapter summarises the relevant literature, covering the development of tissue engineering scaffolds; their successes and limitations; the relative merits of different manufacturing techniques and the scaffold properties arising. Emulsion templating is evaluated in more depth as a method of manufacturing scaffolds. The 'ideal' biological, structural, and mechanical scaffold properties are discussed, as is the relevance of fibrin as a scaffold material to achieve these criteria.

Chapter three presents the experimental work in four different sections. Firstly, emulsions were prepared, evaluated, and refined for stability and droplet size. Secondly, emulsions with appropriate stability were used to template scaffolds, with fibrinogen and thrombin incorporated into the continuous phase. The emulsions were further optimised, taking into account salinity of the buffer and concentration of the aqueous phase, to maintain stability while increasing the oil fraction to generate stable emulsions capable of producing highly interconnected porous materials. In the third section, candidate materials were evaluated for mechanical strength (tensile and bulk compression testing), cytocompatibility and degradation in storage as well as wound environments. Assessment of the angiogenic potential of optimised scaffolds and commercial products is presented in the fourth section of the experimental chapter. This work was performed using fertilised hens' eggs in an *in vitro*/*in vivo* bridge model.

The fourth and final chapter presents the conclusions arising from this project and presents suggestions for future work. The scaffolds produced for this project have only been manufactured in a small laboratory setting and would require extensive and rigorous testing to meet regulatory requirements before translation to the clinic.

1. Introduction

Chronic wounds, such as diabetic ulcers, affect 200,000 people in the UK alone (Posnett and Franks, 2008), and cost the NHS an estimated £3bn a year to treat (D McColl et al., 2009). There are an estimated 24,000 UK hospital admissions for diabetic foot ulcers alone. With NICE estimating the number of people living with diabetes to almost double between 2013 and 2025, this figure is only expected to increase (NICE, 2015). Amid growing pressures on health services and care provision, there is a requirement to move towards treatment, rather than management, of chronic wounds. This would not only reduce the economic burden of such wounds, but also more importantly improve patient outcome and quality of life.

Biomaterials have long been investigated as a means of supporting regeneration of tissue damaged by burns or chronic conditions. The use of scaffolds for tissue grafting and repair using allogenic cells has been under development for the last 25 years (Langer and Vacanti, 1993); however, few scaffolds are being produced and marketed at the scale, cost and speed required to seriously tackle the burden of chronic wounds.

A scaffold is a substrate material into which cells may be loaded for transplantation. Much like building scaffolding, it creates a supportive structural framework which plugs a physical gap in the injured tissue, while providing an internal microenvironment that houses cells (such as stem cells), allowing them to communicate, produce extracellular matrix and ultimately regenerate the wound by producing healthy tissue that integrates into its surroundings. The scaffolding material itself may promote wound healing by direct interaction with ingressing cells, or by release of bioactive agents. This may be achieved by selection of a compatible, bioactive material such as a native protein, or an inert substrate functionalised with a bioactive coating.

While scaffolds may be applied acellularly (de la Puente and Ludeña, 2014), and rely on colonisation by cell ingress and vascular invasion from the wound margin (Klin et al., 2007); it is generally accepted that successful wound regeneration by tissue regeneration requires suitable scaffolds to be used in combination with a cellular component and/or a bioactive component (Ahmed et al., 2008; Whang et al., 2000). The bioactive component may promote proliferation and differentiation of cells transplanted in the scaffold or host cells.

In the last century there has been enormous development in the treatment of serious skin injuries, particularly with the advent of modern tissue engineering. However, there has always been a lag between laboratory developments and improved clinical outcomes. Historically this has been due to lack of detailed knowledge of the pathophysiology in these complex wound environments. More

recent challenges include how to promote regeneration (newly formed matrix resembling native tissue, with total function and no scarring) as opposed to loss of tissue or healing with scarring, contracture, or other loss of function.

Successful future therapies should draw on the successes of the past and combine to create a treatment that promotes regeneration or at least improved healing. Research has shown that supply of stromal cells and/or biochemical agents such as growth factors have the potential to achieve this. Biomaterial scaffolds offer the opportunity to replicate the success of autologous cell therapies with a single biopsy rather than several painful harvesting surgeries which further expose immune-compromised patients to risk of infection.

This project was a collaboration between The Open University and Consorcio Regenero/Cells for Cells, a stem cell company based in Chile. The goal of the project is to design and create suitable scaffolds to support stem cells, provided by Regenero, in order to deliver them into wound environments and promote their proliferation and differentiation into skin-type cells that can remodel damaged tissue. The particular focus was on healing skin damaged by burns or chronic wounds.

Scaffold samples were sent to Chile for testing with Regenero's cells. The results are held by Regenero and are not discussed or disclosed in this thesis. The work therefore focused on development of the scaffold material and manufacturing techniques. There were two novel aspects to this work: firstly, the pattern of emulsion behaviours described in Chapter 3.1 have not, to our knowledge, been reported previously. Secondly, the manufacturing process here enables tightly controlled templating of highly porous protein scaffolds with their native structure retained. This is an important distinction from other protein scaffolds made from comparable methods, as the conditions and/or reagents commonly used denature proteins and remove the native hierarchical structure.

Skin and its structure

Skin forms a barrier over almost the entire surface of the body and is a vital barrier to the environment that protects against infection. The various structures and components of skin together give rise to its global physiology. These structures are illustrated in Figure 1 and described below.

The outer epidermal layer confers barrier function. The underlying dermis provides mechanical support and thermal regulation. It contains a wide variety of cells types and supporting structures. Under the dermis is the hypodermis which acts as an energy reserve, releasing fats from its adipocytes when required.

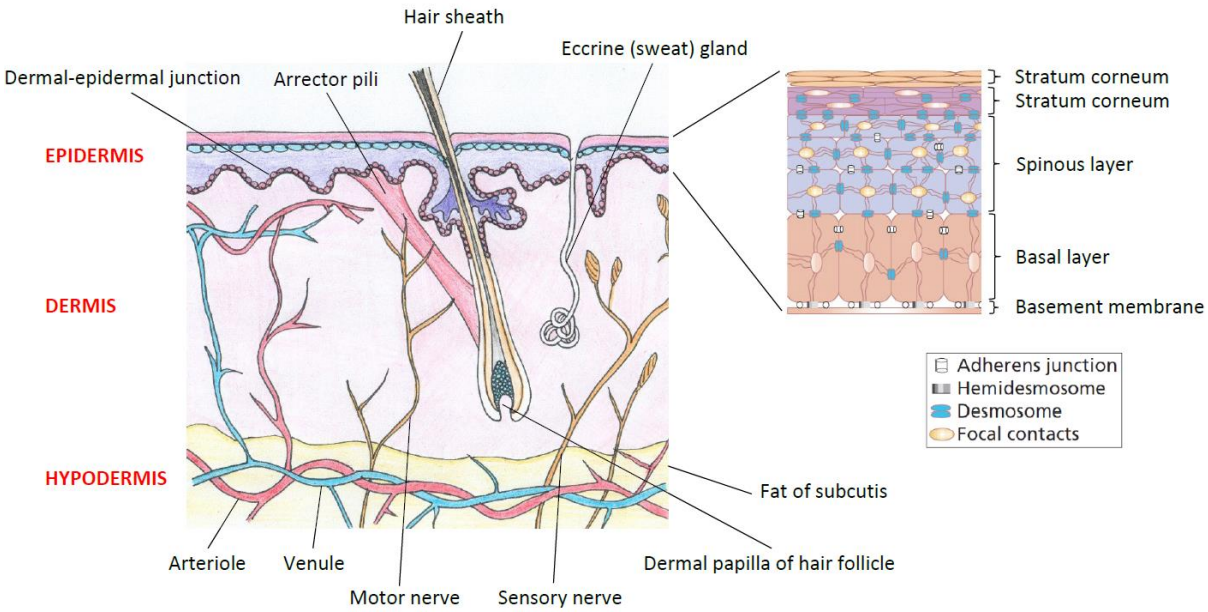

Fig. 1: Cross-sectional view of full thickness human skin. Skin comprises three distinct layers: the epidermis, dermis, and hypodermis. The epidermis comprises five sub-strata, culminating in the stratum basale, which forms the boundary with the underlying dermis. The dermis is the thickest layer of skin. It contains two sub-strata; one of loosely packed collagen and one of thicken collagen bundles. Elastin and proteoglycans are also present, providing elasticity and hydration to the extracellular matrix surrounding the dermal fibroblasts. The deepest layer of skin is the hypodermis, or subcutaneous layer. This is largely composed of subcutaneous fat tissue. Image adapted from Rook's Textbook of Dermatology (McGrath et al., 2004).

The outermost layer, the **epidermis**, constantly renews by sloughing off dead cells and replacing them with cells migrating upwards from lower levels. These cells change in their characteristics to become keratinized (hardened and senescent) as they migrate to the surface.

The epidermis comprises five sub-strata, the first of which, the stratum corneum, consists of a layer of these keratinized cells and forms a waterproof barrier to the environment. The stratum lucidum, most notable in thicker epidermis, is a thin layer of dead cells. These slough off and are replaced by underlying cells as part of the dynamic skin renewal process. The stratum granulosum is a thin layer formed by keratinocytes migrating up from the stratum spinosum underneath. This layer is so named due to its spiny appearance (Montagna and Parakkal, 2012), arising from microfilaments between desmosomes shrinking when stained for histological imaging (Bensouilah and Buck, 2006). The stratum basale is the lowest layer of the epidermis and forms the boundary with the dermis below.

The epidermis is primarily composed of keratinocytes. Small numbers of other cells types with a diverse array of functions are also present. These include Langerhans cells, antigen-presenting immune cells, present in all layers except the stratum corneum. Together with the barrier function of the stratum corneum, these cells help protect the skin from infection. Present in the stratum basale are melanin-producing melanocytes, and Merkel cells ('light touch' mechanoreceptors) (Kamel et al., 2013; Montagna and Parakkal, 2012; Szabo, 1967). Melanocyte density is dependent on the location – for example, it is higher on the face and other regions frequently exposed to sunlight (Szabo, 1967).

Below the epidermis is the **dermis**, the thickest of the three layers of skin, composed of connective tissue. The dermis supports the derivative structures of skin, such as hair follicles and sweat glands (Bensouilah and Buck, 2006). It is highly vascularised by the dermal plexus, a dense capillary network (Schulz et al., 2000). This capillary network is supported by venules and arterioles in the hypodermis. The epidermis, however, is avascular.

The dermis comprises two sub-layers: a thin papillary layer, and a thicker reticular layer. The papillary layer lies next to the stratum basale of the epidermis and contains a loose mesh of collagen fibres. Underneath, thicker bundles of collagen lie parallel to the various strata – this is the reticular layer (Bensouilah and Buck, 2006; Montagna and Parakkal, 2012).

These collagen fibre meshes provide mechanical strength and structural integrity to the dermis. They allow the dermis to provide structural support to the epidermis and underlying tissues. The thickness of the hydrated dermis also helps provide thermal insulation. The primary cell type present is fibroblasts, but some immune cells (mast cells and macrophages) are also present. Dermal fibroblasts produce collagen, elastin and proteoglycans – the components of extracellular matrix (ECM) (Tessmar

and Göpferich, 2007). The principal component is collagen (70%) which gives the dermis mechanical strength and toughness. Elastin improves flexibility and elasticity. Proteoglycans impart hydration and a degree of viscosity to the dermal ECM (Bensouilah and Buck, 2006).

The dermis also carries motor and sensory nerve endings. Nerve density varies with location. Sensory nerves in the skin serve to sense pain, temperature, and pressure. Conditions in which sensory function is impaired, such as diabetic neuropathy or traumatic injuries which destroy nerve endings, can cause delays in detecting wounds and seeking treatment (Sidawy, 2006). An example is diabetic ulcers, another co-morbidity of diabetes which may occur alongside diabetic neuropathy and which arises from venous insufficiency. These ulcers commonly occur in less visible locations, such as the soles of feet. Neuropathic patients who cannot feel pain from the ulcer may not realise there is a wound. Intervention is delayed, during which time the ulcer is likely to worsen. Neuropathic patients are also more likely to obtain traumatic injuries like burns as their autonomic aversion response (for example, to extremely high temperatures) is impaired (Falanga, 2005). Nerves are therefore a vital component of skin in normal homeostasis and in early detection and response to wounds.

The third, deepest, layer is the **hypodermis**; composed of loose connective tissue and adipose tissue (Bensouilah and Buck, 2006). Some deeper sweat glands also extend into the hypodermis (Montagna and Parakkal, 2012).

Classification of wound type and severity

Wounds may be classified by the type of injury, their depth, and propensity to heal in a defined timeframe. Wounds are broadly divided into acute wounds, which heal in a timely fashion according to a classical model of wound healing; and chronic wounds – recalcitrant wounds that heal very slowly or may not heal at all without appropriate intervention (Li et al., 2007; Robson, 1997). Such wounds may not be as immediately severe as acute wounds, but the longer a chronic wound remains unhealed the more susceptible it is to infection (Landis, 2008). This results in increased pain for the patient and may lead to sepsis. A summary of different types of both chronic and acute wounds is given in Tables 1 and 2.

Acute wounds	
Surgical incisions	Thin wounds made with a sharp edge. Wounds may be deep, but narrow enough to suture to allow healing by primary intent. Little damage to surrounding soft tissue; little disruption to vasculature.
Burns	Burns are classified according to depth. Superficial burns may heal easily; partial burns are increasingly damaging with depth into the dermis. Maintaining a clean, moist wound is vital. Full thickness burns are excised to remove necrotic tissue to promote healing. Scarring is common.
Degloving	Injuries caused by a shearing force to the skin edge. Skin may appear mottled. Disruption to skin surface may be minimal but de-vascularisation to skin and soft tissue can be significant. This can lead to tissue necrosis, leading to infection and slowed healing. Excision is vital before suturing.
Crushing	Skin may not be broken, but crushing force may cause cell death. Wound may require excision or debridement to remove necrotic tissue. Wound closed with non-viable tissue left *in situ* will result in excessive scarring.

Table 1: Examples of acute skin injuries (Li et al., 2007; Papini, 2004; Percival, 2002).

Chronic wounds	
Pressure sores/ulcers *(also known as bed sores, decubitus ulcers and ischemic ulcers)*	Pressure sores are common in patients with limited or no mobility where skin is compressed under body weight. Regions of compressed tissue may receive insufficient blood supply, causing damage and eventually becoming necrotic. Once the epidermis is necrotised, the ulcer is susceptible to infection as supply of white blood cells is reduced by impaired vasculature. Pressure ulcers are most common on bony areas of the body – heels, ankles, hips, and coccyx.
Diabetic ulcers	Patients with severe or poorly managed diabetes are at risk of a subset of pressure ulcers, known as diabetic ulcers. Reduced capillary perfusion in the extremities, often coupled with atherosclerotic arteries, can lead to microangiopathy. Blood flow and perfusion are further compromised by pressure, so diabetic ulcers commonly occur on the soles of the feet. Patients with diabetic neuropathy do not feel pain from the injured region, allowing injuries to progress undetected.
Venous ulcers	Venous ulcers arise from venous insufficiency, for example due to impaired venous valves that causes blood to pool in the vein. Fluid leakage from the vein into surrounding tissue can cause necrosis and lead to ulceration. Ulcers typically occur on the lower leg or ankle. Venous ulcers are the most common form of leg ulcers (70-90%).

Table 2: Examples of chronic skin injuries (Belcaro et al., 2006; Callam et al., 1987; Cullum et al., 2001; Harding et al., 2002; Mustoe, 2004; Shea, 1975; Snyder, 2005).

Skin is a dynamic system that constantly renews by sloughing off dead cells and replacing them with cells migrating outwards from lower levels. Therefore, the epidermis has an inherent mechanism for self-repair and renewal, supported by migration of keratinocytes from the wound margin (Gurtner et al., 2008; Papini, 2004). As such, the depth of a wound is a critical factor in the healing outcome. Wounds that extend deeper than the epidermis cannot heal in this way without intervention.

Clinically, a 'healed' wound is simply one in which the epidermal barrier is restored. 'Regeneration' is a more rigorous term referring to the restoration of the structure and function of the injured tissue are restored to their uninjured state.

First degree, or partial thickness, injuries affect only the outer layer of skin. Breaching the epidermis impairs the barrier function of skin, but the dermis below remains intact. The mechanical support provided by the dermis prevents the wound gaping or distorting and helps limit the size of the defect. In the case of superficial burn injuries, the epidermis is injured but remains intact (Papini, 2004). The barrier function of skin remains, so the risk of infection is low and the wound remains hydrated, enabling healing to occur more quickly (Cope et al., 1947).

Injuries restricted to the epidermis are capable of total regeneration with no noticeable change from the uninjured tissue, as long as there remains a dermal substrate over which these keratinocytes can migrate (Schulz et al., 2000; Yannas et al., 1989). No scar tissue forms as the underlying dermis is not damaged no extracellular matrix (ECM) deposition occurs in response to the injury (Shevchenko et al., 2009).

However, adult human dermis is not generally thought to be capable of spontaneous regeneration (Yannas et al., 1989). As a result, deeper injuries are not able to fully regenerate and instead proceed through a process of healing and remodelling, but original tissue structure is not fully restored.

Partial thickness wounds extend into the dermis. Superficial partial thickness injuries are painful, as nerves in the upper dermis are exposed in the wound (Papini, 2004). Healing of the epidermis occurs by migration of keratinocytes from the wound margin and dermis adnexa (Ito et al., 2005). Regeneration is slower than in superficial injuries, and the rate is determined by the density of adnexa. Thicker, hairier skin heals more quickly than thinner hairless skin. Deeper partial thickness wounds, where most of the dermis is affected, heal more slowly as the density of dermal adnexa reduces with depth (Papini, 2004).

In superficial, partial thickness burn wounds, cooling the wound and maintaining a moist environment are important in preventing progression of the injury to deeper tissue. Deeper partial thickness wounds that are not cooled in this way may be still capable of healing in healthy individuals where a warm, moist, clean wound environment are maintained; however, bad scarring is likely (Cuttle et al., 2006; Papini, 2004). To promote better healing, deep partial thickness burns are often excised to remove damaged and necrotic tissue and present an amenable surface for healing. The excised wound is commonly treated with grafting (Kaufman et al., 1990).

In full thickness wounds, all three layers of skin are damaged. Adnexa and native structures capable of supporting regeneration are damaged or destroyed in the wound and there is no remaining supportive tissue underneath the wound (Schulz et al., 2000). Therefore, healing can only occur by migration of cells from the wound margin, which slows down the healing process considerably. As migration only occurs laterally, the rate of healing is also strongly dictated by the diameter of the wound. Wounds greater than 1 cm in diameter contract strongly and in doing so impair function of the tissue (Papini, 2004).

Full thickness wounds can occur due to trauma (Graham et al., 2013; Weigert et al., 2011); necrotising infection (which may require excision) (Akhtar et al., 2006); following surgery (i.e. tumour resection) (Tufaro et al., 2007) or as a result of severe burns (Böttcher-Haberzeth et al., 2010; Pham et al., 2007). Clinically, these wounds are often treated by application of split-thickness skin graft (STSG) (Frueh et al., 2016). This approach is clearly limited – it contains only epidermal keratinocytes and therefore lacks the potential to regenerate the complex arrangement of ECM and dermal cells in the deeper tissue. The dermis will instead fill with granulation tissue as a defensive mechanism to cover the wound (Schulz et al., 2000). Scarring ensues, leading to contraction and a poor cosmetic and functional result. Additionally, harvesting STSG results in donor site morbidity so it is not desirable to harvest a large quantity of skin graft for patients with extensive injuries (Boyce et al., 2017). In practice, full thickness wounds are not considered to be capable of restorative healing by conventional techniques (Shevchenko et al., 2009).

Burn wounds are commonly classified in the same way as other wounds, but using a different terminology: first, second or third degree. First degree burns are superficial, second degree burns affect the dermis, and third-degree burns affect the full thickness of skin.

A brief history of burns and their classification

Burns have affected mankind since Neanderthals learnt to create and control fire. Early records of their treatment date back to 1500 BC during the time of the ancient Egyptians (Artz, 1970; Liu et al., 2016). Subsequent civilisations throughout history have created their own remedies using materials at hand. These treatments range from the bizarre (wine and myrrh) to the truly unpleasant (cattle dung and bees wax) but many ancient treatments contained materials and principles that are still used today (Liu et al., 2016). The Chinese were using tea leaves to treat burns over 2500 years ago; recent research suggests that green tea leaves provide useful antioxidants to promote healing and may stimulate angiogenesis (Liu et al., 2016; Qin et al., 2013; Wang et al., 2004). Hippocrates reportedly

applied pig skin mixed with bitumen resin and vinegar solution – an early example of a biological xenogeneic skin substitute, with acid perhaps to sterilise the wound. That Hippocrates chose pig skin is interesting, as it closely resembles human skin and pigs are still commonly used as model systems in clinical trials today.

Maggots were widely used for debridement to prepare the wound bed. Whilst unpleasant, maggots specifically target necrotic tissue and are therefore highly effective at preparing a wound bed (for burns or other types of wounds requiring excision) without removing healthy tissue – something that would be extremely difficult to achieve by surgical or chemical means without advanced knowledge and equipment.

Early treatments were limited by a lack of fundamental understanding of the pathophysiology. Guillaume Dupuytren (1777-1835), an eminent French surgeon, was the first to create a formal classification system to assess the severity of burns according to their depth. His six-stage system categorised wounds by increasing severity (Androutsos et al., 2011):

1) Skin redness
2) Blisters
3) Partial destruction of the skin
4) Total destruction of the skin
5) Charring of muscle tissue
6) Charring of bones

His treatment regimen included debridement and application of silver nitrate (a solution which blackens the wound on oxidation but provides broad spectrum antimicrobial action) as well as “perforated compresses spread with cerate, lint, emollient cataplasms, and calming drinks”. Dupuytren importantly recognised the importance of postoperative care and rehabilitation, using immobilisation and traction devices to restore the position and function of limbs after injury. He was also the first to describe lines of skin tension (Langer lines) which dictate the way that wounds grow following incision (Langer, 1861). A practical application is the deliberate orientation of surgical incisions to minimise wound size. Though Dupuytren did not use skin grafting in his own work, his legacy heavily influenced future reconstructive plastic surgery practices (Goldwyn, 1969).

Dupuytren’s attempt at burn classification was a useful contribution to the field, but was cumbersome and thus superseded by Boyer’s three-stage classification system: erythema, blistering and eschar formation (Jackson, 1970; Sneve, 1906).

A common system for definition and categorisation of burns, with agreed and precise terms, is essential for assessment and comparison of injuries. Historical systems like Boyer’s and Dupuytren’s classified burns by criteria such as appearance, depth of necrosis or circulatory state. Assessments like these fail to take account of the fact that while the surface appearance of new burns indicates the

intensity of skin burning, but this may not align with the depth of necrosis and therefore the range of tissues damaged (Jackson, 1970). This has implications for prognosis, treatment options and postoperative care. As such, the system most commonly used in recent years classifies wounds by depth.

Normal wound healing

Wounds may heal by primary or secondary intention. Healing by primary intention involves the wound edges being drawn together, for example with the aid of surgical staples or sutures. Wounds in which necrotic tissue is debrided prior to suturing are said to heal by 'delayed primary intention'. In both cases, epidermal closure may be achieved by keratinocyte migration across the narrowed wound site. If a wound is too large to close, healing by secondary intention occurs instead. The defect remains open throughout the healing process and is therefore prone to infection. The large defect size means wound repair is slower and more complex than for healing by primary intent (Beldon, 2010). The typical process of healing by secondary intention is outlined below.

There are three stages of repair in the classic model of wound healing by secondary intention: inflammation, formation of new tissue and remodelling of the new tissue (Broughton et al., 2006; Gurtner et al., 2008). There may be some overlap between each phase; and the duration and success of each stage is specific to the health and environment of the injured individual (Falanga, 2005).

The response to skin injury is immediate. Inflammatory pathways, cellular components of the immune system and the coagulation cascade (discussed in detail below) are all activated (Gurtner et al., 2008). Keratinocytes at the wound periphery release IL-1 and TNF-α, signalling to the surrounding cells that the epidermis is injured (Kondo and Ishida, 2010). The priority is to seal the defect to prevent blood loss. Vasoconstriction occurs, reducing vessel lumen diameter (Broughton et al., 2006). Thrombin-activated endothelial cells cease production of anticoagulant materials and instead produce von Willebrand factor. Thrombin also activates platelets, which become 'sticky' and adhere to each other and the site of the vessel defect (Marder et al., 2012). Once the wound is stabilised, the inflammatory process dilates blood vessels and increases their permeability to support movement of inflammatory cells, such as neutrophils attracted by TNF-α and IL-1 (Broughton et al., 2006; Kondo and Ishida, 2010).

The damage to blood vessels limits the supply of oxygen to the wound bed, creating a hypoxic environment (Chen et al., 2008; Falanga, 2005). This hypoxic effect stimulates the progress of healing by promoting keratinocyte migration, proliferation of fibroblasts and synthesis of growth factors such as PDGF-B, endothelin and TGF-β1 (Falanga, 2004, 2005; Falanga et al., 1991; Kourembanas et al.,

1990, 1991). These growth factors recruit dermal cells and circulating monocytes to the wound environment over the following 2 to 3 days. When sufficient numbers of each are present, neutrophils interact with platelets in the wound, causing platelets to release lipoxin A4 or A5 (Broughton et al., 2006). Lipoxin can resolve inflammation processes in a variety of cell types (Chandrasekharan and Sharma-Walia, 2015). It counteracts the pro-inflammatory cytokines to prevent the inflammatory response persisting unnecessarily, as doing so may be detrimental.

The fibroblasts that migrate into the wound bed deposit a disorganised, loosely packed collagen matrix. Granulation tissue fills defects but lacks the functionality of intact tissue. It is visually different from healthy tissue and may appear unsightly, and it lacks the mechanical strength and elasticity of surrounding healthy tissue. This makes granulation tissue more susceptible to further damage or injury as it cannot respond to mechanical stress in the same way as the intact tissue surrounding it.

In an ideal wound healing scenario, tissue is restored to the same level of structural and functional integrity as it held prior to injury. Whilst this is not achievable by current methods, and injured adult skin will never regain its initial strength, it is possible to restore some native structure and function (Levenson et al., 1965). This is achieved during the third and final stage of wound healing in which the temporary granulation tissue is remodelled to resemble intact tissue more closely. Remodelling begins two to three weeks after injury and can last for a year or even longer. Any residual activity from the inflammatory and new tissue formation stages reduces and ceases during the remodelling process. Most of the endothelial cells, macrophages and myofibroblasts that were recruited during these earlier stages cease activity in the wound area – either migrating away from the area or undergoing apoptosis (Gurtner et al., 2008).

Following this reduction of cell mass in the dermis, a quantity of tissue – comprised largely of type III collagen and other ECM proteins – remains in the injury site (Gurtner et al., 2008). Collagen III provides tensile strength in the dermis (Cen et al., 2008). A few cells remain, such as fibroblasts and mesenchymal stem cells, which are thought to interact to regulate homeostatic function of the remodelling skin (Szabowski et al., 2000). The remaining fibroblasts, macrophages and endothelial cells that were recruited to the wound in early stages secrete matrix metalloproteinases, which gradually remodel the disorganised type III collagen matrix to a matrix composed primarily of type I collagen (Lovvorn et al., 1999). Type I collagen is the primary component of intact skin. It is arranged in randomly oriented bundles, loosely interwoven in a ‘basket weave’ structure. Tissue remodelling, replacing disorganised type III with more structured type I collagen and accompanied by secretion of ECM proteins, allows for the tissue to withstand greater strain. Remodelled tissue has greater elasticity and strength than transitional (granulation) tissue.

Meanwhile, the recruited monocytes differentiate into macrophages. These are thought to be involved in coordinating the later stages of healing, although their role is not understood (Gurtner et al., 2008). In addition to inflammatory cells, progenitor and stem cells may potentially also be recruited (Chen et al., 2008). These, in turn, release a cocktail of growth factors. Recruited fibroblasts and endothelial cells begin to form granulation tissue (Falanga, 2005). This begins wound contraction.

Contraction occurs when these growth factors stimulate fibroblasts to differentiate into myofibroblasts (Mirastschijski et al., 2004). Myofibroblasts contract by an actin-myosin mechanism, collectively acting to cause wound contracture. ECM proteins such as collagen, fibronectin and vitronectin support the new tissue and provide guidance for cellular movement and contraction (Falanga, 2002). Myofibroblasts can cause a wound to contract to less than 10% of its initial size. While this effectively reduces the exposed wound surface, the result is a scarred defect with permanent loss of function (Schulz et al., 2000).

The duration of the remodelling phase is influenced by management of the wounds and the general health of the patient. By the end of the remodelling phase, the epidermis is restored, and the defect filled with mature scar tissue.

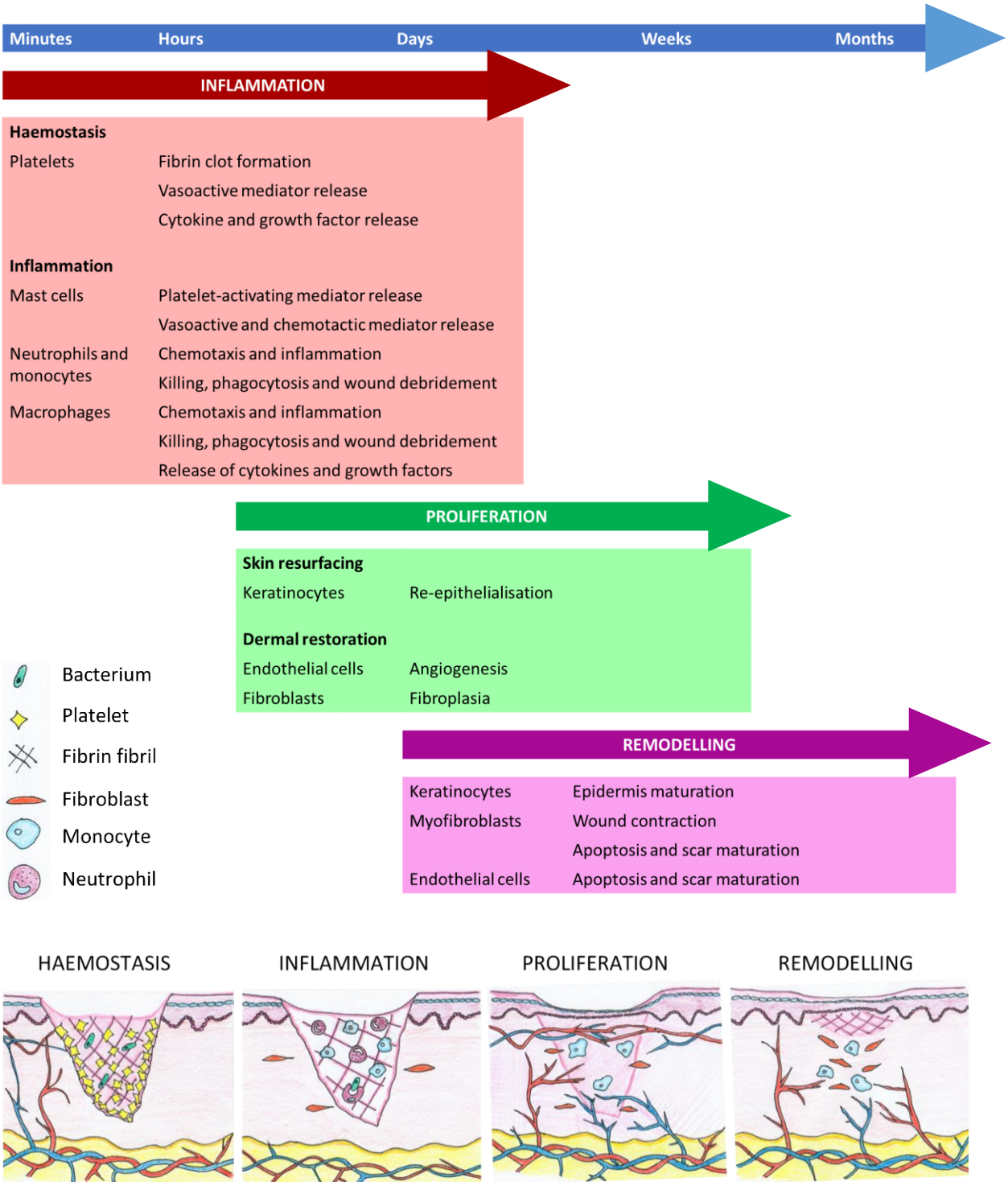

Figure 2: Schematic diagram illustrating the chronological events of wound healing. The three major phases of wound healing are distinct in their action, but may overlap as events of wound healing are controlled by soluble factors, such as cytokines and growth factors, which take time to secrete, diffuse and stimulate a response from target receptors. Overlap of phases ensures a continuous, persistent movement towards healing an injury. The major cells types involved in each phase are shown alongside their role in wound healing. Chronology diagram adapted from Li et al (2007); healing stages image adapted from Opneja et al. (2019).

2. Literature Review

Current treatments

There are various strategies to achieving wound healing. Narrow incision-type wounds may be cleaned to prevent infection and sutured to promote healing by primary intent. This is the best-case scenario, as keratinocyte migration and support from the undamaged surrounding dermal appendages allows for total regeneration. Wound edges must be clean, in close proximity and not necrotic or otherwise unviable for this mode of healing.

Larger defects must be assessed according to their width and depth to determine an appropriate method of treatment. Wounds with a large surface area but shallow penetration, such as abrasions, may heal readily by keratinocyte migration and support from underlying dermal structures. However, the loss of epidermis impairs barrier function in the wound and the area is susceptible to infection by environmental pathogens. Keeping the wound clean is important in preventing infection and supporting timely healing.

In deeper, wider wounds, healing will occur by secondary intention and the wound will fill with granulation tissue. Such wounds may be actively treated, or simply covered to keep clean and allowed to progress through healing by secondary intent. This may be the case for small, acute wounds where healing is expected and the scar will be small and unobtrusive.

Active treatment is desirable in larger wounds or those expected not to heal without intervention, such as recalcitrant chronic wounds. This may be achieved by seeking to seal the epidermis to restore the barrier function (i.e. by the application of keratinocytes or a synthetic silicon covering) and allowing the underlying tissue to form granulation tissue. The graft may be initially applied using surgical staples, sutures or adhesive, but gradually adheres to the wound bed by ingrowth of granulation tissue (Jones et al., 2002). Alternatively, constructs may seek to support both epidermal and dermal repair by provision of biological stimuli or of a construct designed to support native cells and ECM structures.

The strategies for treating superficial and deeper wounds by tissue engineering constructs are discussed briefly below.

When the epidermis is breached in a superficial wound, keratinocytes migrate from the wound periphery and bed, leading to total regeneration with no visible scar. For larger epidermal defects, keratinocyte migration from the wound margins alone is not sufficient to cover the wound and restore the epidermal barrier (Jones et al., 2002). A single sheet layer of cultured keratinocytes can be used

to replace irreparably damaged epidermis (MacNeil, 2007). However, in deeper wounds that extend into the dermis, the dermal structures that support healing are compromised and tissue will scar rather than regenerate.

The dermis is not capable of regeneration so this technique is insufficient to adequately replace a full-thickness defect, either cosmetically or functionally (Schulz et al., 2000). To replicate the thickness, durability, and difference in both anatomical and mechanical structures, a second 'dermal' layer is required.

Early synthetic scaffolds sought to restore epidermal barrier function by creating a seal to prevent infection and fluid loss. The materials used were typically bioinert organic polymers which adhered to the wound and provided no stimulus to influence or promote wound healing (Burke et al., 1981). The recognition of biocompatible and bioactive materials led to the creation of more ambitious constructs. These aimed not only to replace missing epidermis, but also to support the damaged dermis by provision of a bilayered construct. (Burke et al, 1981). This tenet provided the basis for Integra® *(Integra LifeSciences; Plainsboro, NJ, USA)*; comprising a temporary Silastic outer layer and a porous collagen-chondroitin 'dermis'. The silicon 'epidermal' layer is initially bonded to the 'dermis' once the porous dermal component has integrated with host tissue, the Silastic may be peeled away, allowing the epidermis to heal from the wound margin and burgeoning dermal wound bed, or by the application of autograft. The porous collagen-chondroitin scaffold supports in-migration of cells from the surrounding dermis, and was found to vascularise within 3 to 5 days of implantation (Burke et al., 1981). Integra® was an important development in the treatment of burn wounds, arguably the most significant since the Second World War, as it represented a shift in thinking from merely sealing the wound to reduce mortality, to healing the wound and restoring appearance and functionality (Cope et al., 1947; Jones et al., 2002; Yannas and Burke, 1980). First patented in the 1980s, Integra® remains a leading commercial product in the field.

More recently, Boyce et al (1999) showed that cultured autologous keratinocytes and fibroblasts, seeded onto a collagen-based sponge, could be used in conjunction with Integra® in place of an autograft. This approach requires a biopsy to harvest autologous cells, but removes the necessity for repeated autograft harvests. If the biopsy is taken early, the cells may be sufficiently expanded to apply when the Silastic layer is ready for removal. There is no need to wait for re-epithelialisation of graft sites to harvest autografts, and the smaller area and duration of exposed tissue from biopsy reduces the risk of infection.

MySkin *(Regenerys, Cottenham, Cambridge, UK)* also uses the concept of *in vitro* expansion of autologous keratinocytes to avoid the need for extensive and repeated autograft harvest in burns and

chronic wounds patients. Traditionally taking a similar form to the cultured skin substitute described by Boyce et al (1999), keratinocytes are expanded *in vitro* and delivered to the wound on a polymer carrier dressing, allowing a convenient patch method of applying cells to the wound (Moustafa et al., 2007). MySkin is also available as a spray, where keratinocytes are delivered in a suspension and may be applied by spraying directly onto the wound bed.

Some existing skin replacement constructs present both dermal and epidermal components that interact dynamically with each other during *in vitro* maturation (Stark et al, 2006) and also after transplantation (Klingenberg et al, 2010).

Dermal scaffolds are designed to support cells that will mimic the native dermis. The dermis is highly vascularised; it supports the keratinised avascular epidermis by nutrient exchange diffusion (Jones et al., 2002; MacNeil, 2007). As such, a key feature of dermal scaffolds – as opposed to typical dressings or epidermal scaffolds – is the ability to induce, encourage, or support angiogenesis into the wound site (Frueh et al., 2016). This will sustain the regenerating tissue and allow the damaged dermis to continue to support the regenerating epidermis above. Dermal scaffolds may be optimised to enhance angiogenic potential by modifying the size, number and interconnectivity of pores; using bioactive materials, releasing agents or coatings to stimulate angiogenesis; or by chemically modifying the scaffold to present a more biocompatible surface to the wound margin (Cam et al., 2015; Frueh et al., 2016; Wilcke et al., 2007).

It is worth noting that although human skin comprises three distinct layers, tissue-engineered skin substitutes currently available for clinical and commercial use lack the subcutaneous layer (i.e. hypodermis) (Monfort et al., 2013). Whilst it may not be as important as an epidermal or dermal replacement in terms of filling the defect and causing cellular regeneration of the wound, the hypodermal layer contributes to the mechanical durability and thermal regulation capability of skin. Current commercial skin substitutes and scaffolds only comprise two layers, so the functionality of the third, hypodermal, layer is lacking. This may be a factor in their disappointing clinical performance. However, there is limited literature on the creation or performance of tri-layered skin substitutes. While published results are encouraging, (Monfort et al., 2013; Perng et al., 2008; Trottier et al., 2008) there has been no move towards commercialisation and little clinical data exists on *in vivo* efficacy. Further evidence is required to demonstrate sufficient improvement over a bilayered product to justify the additional cost and complexity of manufacturing a tri-layered product.

Classification	Usage		Example product
i. Anatomical structure	Epidermal		Split-thickness skin graft
	Dermal		MatriDerm®; Hyalomatrix®
	Dermo-epidermal (composite)		Apligraf®
ii. Duration of cover	Permanent		Analogue material; graft
	Semi-permanent		Material later remodelled (e.g. Suprathel®)
	Temporary		Biobrane®
iii. Permanence	Non-resorbable (permanent)		-
	Non-resorbable (removable)		Nylon- and silicon- backed materials (e.g. EpiDex®)
	Resorbable/biodegradable		e.g. MatriDerm®
iv. Type of biomaterial	Biological	Autologous	Skin graft
		Allogeneic	Cadaveric skin graft; OrCel
		Xenogeneic	Porcine skin graft
	Synthetic	Biodegradable	e.g. Dermagraft®
		Non-biodegradable	Nylon- and silicon- backed materials
v. Skin substitute composition regarding cellular components	Cellular		e.g. EpiDex
	Acellular		e.g. Biobrane®
vi. Primary biomaterial loaded with cellular components	*In vitro*		Pre-seeded scaffold
	In vivo		Acellular scaffold

Table 1: Classification of currently available skin-substitute products. Collated from multiple sources (Atiyeh et al., 2005; Atiyeh and Costagliola, 2007; Clark et al., 2007; Horch et al., 2005, 2005; Jones et al., 2002; MacNeil, 2007; Patel and Fisher, 2008; Shevchenko et al., 2009). Products are summarised in Tables 2 and 3.

Skin substitutes have been commercially available since the advent of modern tissue engineering in the 1970s (Yannas and Burke, 1980). This began with the pioneering of autograft techniques, providing a rapid wound covering without the need for donor screening or the risk of immune rejection. However, the procedure is painful and may cause donor site morbidity and exposes additional surface area to infection in an already compromised patient. Autograft is therefore unsuited to treatment of extensive injuries. The use of artificial skin overcomes the drawbacks of the use of autograft and allograft/xenograft. There is no donor site morbidity and no wait for donor recruitment and screening. Synthetic products can be engineered to render them non-immunogenic. A range of products, for treatment of both chronic wounds and burns, is now commercially available for therapeutic use in patients where autograft is not a tenable solution (Jones et al., 2002).

While autograft remains the gold standard, skin substitutes have the potential match their performance without the requirement for painful graft harvesting.

The application of skin substitutes has been shown to reduce morbidity in patients with severe burns (>50% total body surface area burnt) (Boyce et al., 2017). Treatment of these burns requires that necrotic tissue be removed to create a viable wound bed and prevent excessive inflammation. This cannot be achieved using standard wound dressings alone (Hansbrough, 1990). The use of autograft or allograft provides immediate, but temporary, coverage to sustain patients while repair takes place. Synthetic dermal substitute products (see Tables 2 and 3) offer not just coverage but depth, structure, and support to the regenerating tissue.

As a minimum, a skin substitute should replace the basic barrier function of the wounded skin, preventing dehydration and infection as well as aiding thermoregulation (Kamel et al., 2013). However, this only restores epidermal function. The goal is regeneration of the full thickness of the damaged tissue. The challenge of skin substitutes is to replace or promote repair of the dermal layer that would not otherwise regenerate. This would restore the thickness and function of skin to the wound area. However, quality of healing is vital. Excessive contracture or scarring achieves physical wound closure but the new tissue is both functionally and cosmetically impaired (Frueh et al., 2016). In their pioneering work during the early days of skin tissue engineering, Yannas and Burke (1980) identified two goals of artificial skin – to achieve wound closure, and to replace lost or damaged tissue. In the short term, substitutes must stabilise patients by establishing a barrier to infection and fluid loss. However, preventing functional skin loss requires intervention to reduce scarring and contraction.

Skin substitutes may be excised donor skin (autograft, allograft or xenograft) synthetic or bio-synthetic (Pham et al., 2007). Autograft remains the gold standard for re-epithelialisation of critically damaged

skin with best restoration and least contracture of the wound site (Boyce, 2001; Mahjour et al., 2015). However, limited availability and high risk of donor site morbidity present a need for alternative therapy (Böttcher-Haberzeth et al., 2010). Allograft and xenograft (commonly porcine tissue) counter these issues, but present problems of graft rejection, ethical issues and the risk of disease transmission (Eisenbud et al., 2004; Yannas and Burke, 1980). Non-cellular components of skin grafts – primarily ECM proteins and collagen – have low immunogenicity. However, the difficulty of removing immunogenic cellular components of these grafts mean that allogenic grafts are ultimately rejected and are only suitable for temporary use (Wainwright, 1995).

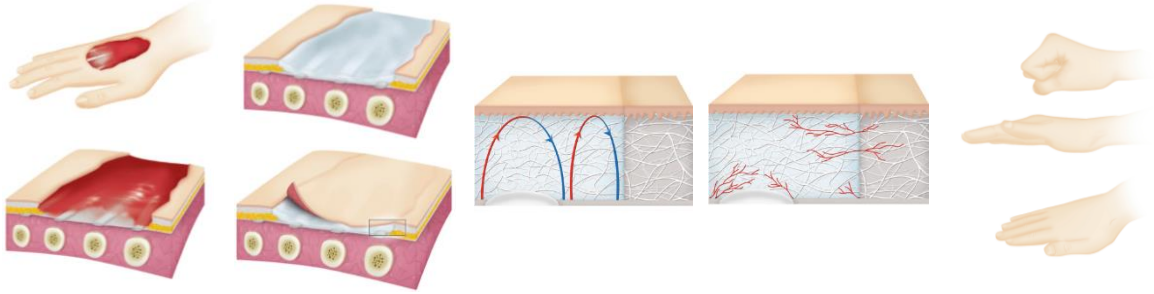

Injury	Day 0	Days 3-5	Days 5-7	Healing
Assessed for coverage and depth	Scaffold and split thickness skin graft (STSG) applied	Resident cells nourished by passive blood and plasma diffusion	Micro-vessels invade from excised wound bed support tissue	Wound cavity fills and remodels over time to restore function

Fig. 1: The use of artificial skin substitutes for repair of injured tissues. Adapted from MatriDerm® promotional materials from the MedSkin Solutions Dr. Suwelack website, http://www.medskin-suwelack.com/en/matriderm. Page last accessed 16th August 2017.

Current commercial bioengineered skin substitutes do not match the results achieved by autograft, but they do achieve some restoration (Klingenberg et al., 2010). They may be used in combination with split-thickness autograft, significantly reducing the area of graft tissue required (Boyce et al., 2006). This reduces both donor morbidity and the number of surgeries required. Bioengineered skin substitutes combine biocompatible polymers with cultured cells such as fibroblasts and keratinocytes (Klingenberg et al., 2010). There are now a number of commercially available temporary and permanent skin substitute products available (Schulz et al., 2000). These are summarised in Table 2 (products made with naturally derived products) and Table 3 (products based on synthetic materials).

Product name	Manufacturer	Material(s)	Indications
Products for superficial/epidermal repair			
Jaloskin®	Fidia Advanced Biopolymers S.r.l.; Padova, Italy	Semi-permeable transparent film of HYAFF®11, a benzyl ester of hyaluronic acid (HA derived from bacterial fermentation).	Indicated for management of superficial moderately exudating wounds (i.e. venous, pressure, diabetic and chronic vascular ulcers; surgical or trauma wounds and first- and second-degree burns).
OrCel	Forticell Bioscience, New York, NY, USA	Bilayered allogeneic product used in combination with STSG. Fibroblasts seeded on porous side of bovine collagen sponge; keratinocytes seeded on non-porous side.	Originally designed to treat epidermolysis bullosa. OrCel has been used for burns also.
Products for partial/deep or full thickness repair			
AlloDerm	LifeCell; Branchburg, NJ, USA	Derived from cadaveric human skin from tissue banks. Epidermis and all cellular components removed, leaving dermal matrix. Freeze-dried; rehydrate to use. Contains intact collagen fibres to support ingrowth of new tissue, elastin filaments to provide strength, and hyaluronan and proteoglycans for cell attachment and migration.	Burns, traumatic or oncologic wounds with deep structure exposure, hernia repair, breast, and other tissue reconstruction.
Apligraf®	Organogenesis, Inc.; Canton, MA, USA	Living bilayered skin substitute comprising an 'epidermal' layer of human keratinocytes and a 'dermal'	Intended for use in conjunction with compression treatment of partial and full-thickness venous skin ulcers (>1 month duration).

		layer of human fibroblasts in a bovine type I collagen matrix. Cells are originally derived from donated human neonatal male foreskin tissue.	Contraindicated for use in infected wounds and patients with known hypersensitivity to bovine collagen or agarose (Apligraf shipping medium).
Cymetra	LifeCell; Branchburg, NJ, USA	Injectable micronized particulate form of AlloDerm. Dry form, packaged in syringe, rehydrated prior to use with either normal saline or lidocaine for injection.	Cosmetic soft tissue augmentation and treatment of vocal cord paralysis by injection laryngoplasty.
Hyalomatrix®	Anika Therapeutics, Inc.; Bedford, MA, USA	Hyaluronic acid-based dressing consisting of a biomaterial (esterified hyaluronic acid materials).	Indicated for use in the management of partial and full-thickness wounds, second degree burns, ulcers (pressure, venous, diabetic, and chronic vascular), surgical wounds, tunnelled wounds, trauma wounds and draining wounds.
MatriDerm	Dr. Suwelack Skin & Health Care, Billerbeck, Germany	3D matrix consisting of native structured collagen from bovine dermis, and elastin from bovine nuchal ligament. Available in different sizes and thicknesses, selected according to the demands of the wound.	Burns; surgical reconstruction of soft tissue defects.
OASIS® Wound Matrix	Cook Biotech, Inc.; West Lafayette, IN, USA	ECM derived from porcine sub-mucosal small intestine, primarily composed of collagen, proteoglycans cell adhesion proteins, ECM proteins, growth factors and GAGs.	Indicated for use in chronic vascular, diabetic, pressure and venous ulcers; trauma wounds, management of partial and full thickness wounds. Not indicated for use in third-degree burns.

Puracol Plus Microscaffold Collagen	Medline Industries, Inc.; Mundelein, IL, USA	Silver containing version also available ('Puracol Plus Ag+). Bovine collagen (predominantly type I) processed to retain a higher degree of tertiary triple helix structuring than more heavily processed collagen products.	Indicated for the management of partial and full thickness wounds; pressure, venous, diabetic, and mixed vascular aetiology ulcers; first- and second-degree burns; donor sites and bleeding wounds; abrasions, trauma wounds and surgical wounds. Not suitable for third degree burns. Contraindicated for patients with known sensitivity to collagen.

Table 2: Examples of current commercial scaffolds for skin tissue engineering made using natural materials. This includes both cryopreserved and decellularised tissue, as well as scaffolds synthesized from naturally occurring organic polymers such as collagen. Information sourced from Frueh et al (2016); Romanelli et al (2007); Schulz et al (2000) and company websites.

Product name	Manufacturer	Material(s)	Indications
Products for superficial/epidermal repair			
MySkin	Regenerys Ltd.; Cottenham, Cambridge UK	Autologous keratinocytes seeded onto a plasma polymerised carrier dressing. Keratinocytes may also be sprayed directly on the wound. Product maturation takes 2-3 weeks from biopsy to application.	Used for severe extensive burns, or chronic wounds and ulcers. Required biopsy size 4c m^2; 0.5 mm thickness
Products for mid-partial thickness repair			
Biobrane® Temporary Wound Dressing	Mylan Institutional; Canonsburg, PA, USA	Bilayered product comprising a thin outer semi-permeable silicone membrane, bonded to a matrix of knitted fabric with adherent purified peptides from porcine dermal collagen. Native blood clots in the nylon/collagen matrix, providing additional adherence	Debrided superficial to 'mid-partial' thickness burns with viable wound beds.
Products for partial/deep or full thickness repair			
Dermagraft®	Organogenesis, Inc.; Canton, MA, USA	Cryo-preserved 3D human dermal substitute composed a bioabsorbable scaffold of polyglactin mesh with human fibroblasts seeded. These are intended to proliferate to fill the mesh interstices and	Indicated for treatment of full thickness diabetic foot ulcers (>6 weeks duration), in conjunction with standard wound care regimens.

	(Developed by Advanced Tissue Sciences Inc.; La Jolla, San Diego, CA, USA).	produce ECM and other physiological factors prior to cryo-preservation, so the final product resembles dermal matrix.	Contraindicated for infected wounds, wounds with insufficient blood supply or ulcers with sinus tracts; and in patients with known hypersensitivity to bovine products (may contain traces from manufacturing and storage media).
DermaMatrix	Synthes CMF, West Chester, PA, USA	Cadaver human skin from tissue banks. Donor skin is processed to remove all cellular components, including epidermis, and then is freeze-dried. Rehydrate to use.	Soft tissue repair, breast reconstruction, abdominal hernia repair, head and neck reconstruction.
EpiDex	EuroDerm Biotech & Aesthetics, Stuttgart, Germany	Autologous keratinocytes (from stem cells of follicular outer root sheath of anagen hair) cultured on silicone sheets to form a multi-layered epidermal equivalent. Production of EpiDex takes 6 weeks after hair plucking to harvest keratinocytes. 50-200 hairs are required per patient.	Chronic wounds – those where the wound has not healed with optimum standard of care within 3 months. A new patch must be applied every 3 weeks.
Integra® Dermal Regeneration Template	Integra LifeSciences; Plainsboro, NJ, USA	Bilayered product comprising a thin outer layer of silicon and the thick inner matrix layer of pure bovine collagen and glycosaminoglycans (derived from shark collagen).	Post-excisional treatment of full-thickness or deep partial thickness burns; repair of scar contractures.

			Contraindicated for infected wounds and patients with known hypersensitivity to bovine collagen and chondroitin.
Suprathel®	PolyMedics Innovations GmbH; Denkendorf, Germany	Semi-permeable PLA-based elastic membrane.	Indicated for use with superficial and deep dermal/partial thickness skin loss diseases, or small full thickness areas (e.g. burns, STSG donor sites, large abrasions, reconstructive surgery, scar corrections and dermabrasion, and non-healing wounds (i.e. leg ulcers and diabetic foot).
Transcyte® *(formally known as Dermagraft-TC)*	Shire Regenerative Medicine, Inc.; San Diego, CA, USA	Synthetic epidermis consisting of fibroblasts (donor allogenic cells) cultured on a nylon mesh and cryopreserved in situ.	Indicated for use for treatment of partial- and full-thickness venous skin ulcers (>1 month duration) and diabetic foot ulcers (>3 weeks duration) which extend through, but no deeper than the dermis. Contraindicated for use on infected wounds and in patients with known allergies to bovine collagen or agarose shipping medium.

Table 3: Examples of current commercial scaffolds for skin tissue engineering made using synthetic materials. This includes scaffolds also incorporating a naturally derived element, such as bilayered products; synthetic scaffolds supplied seeded with cells; and composite scaffolds comprising both natural and synthetic biomaterials. Information sourced from Frueh et al (2016); Jones et al (2002); Schulz et al (2000) and company websites.

Pipeline products and clinical trials

The market for wound products for skin is vast. As the largest and outermost organ, skin is not only the most susceptible to injury but also the most visible. Products therefore span those that seek to address immediate threat to life, for example by preventing infection, to products that address cosmetic concerns. At the time of writing, there are over 3,300 trials regarding wounds and skin injuries listed on ClinicalTrials.com (last accessed September 2019). These trials encompass new products, new and expanded uses of existing products (particularly those already well established on the market, such as Biobrane (Table 3, Table 4), StrataGraft® (Table 4) and Hyalomatrix® Hyaluronic Acid Regenerative Matrix (Table 5)) and the use of non-product based therapies (such as behavioural and peri- and postoperative care approaches to supporting wound healing).

Despite a wealth of research in the field and advances in materials, technology and rehabilitative therapies, the number of innovative new products coming to market is relatively small compared to the number of clinical trials (Table 6). This may be attributed to the cost and time required to develop, test, and achieve regulatory approval for new products. This system is biased in favour of large commercial entities marketing products with close similarities to existing regulated products.

This gives rise to a large number of similar products modified and marketed for highly specific applications rather than a diverse range of products, or those custom-designed to best treat different types of wounds.

Given the overwhelming number of products available to treat a broad spectrum of types and severities of skin injury, there is some confusion and hesitancy on the part of many physicians to adopt new bioengineered products for use. Inertia with clinical and commercial uptake is a further commercial barrier to new and innovative or niche products, particularly those produced by SMEs, microenterprises and start-ups that lack the resources, networking capabilities and marketing experience of established companies.

As yet, off-the-shelf, full-thickness skin replacements (as a medical device or as a template to promote tissue regeneration) are not available, despite the marketing claims of some current commercial products. However, there are many products on the market that go some way to meeting these requirements. These materials may be used as vehicles, incorporating various cell types (such as keratinocytes, fibroblasts and stromal cells) or other growth-enhancing substances like cytokines and growth factors to improve the biological functionality and relevance of the scaffolds (Branski et al., 2009). Using well-known materials and well-characterised cell lines, or expanded autologous cells, would reduce regulatory requirements and therefore time and financial barriers to market.

Gene transfer technology is another interesting future avenue for therapy. Delivery by scaffold in direct contact with the wound bed is advantageous to topical delivery as it offers greater control over dosage and uptake.

	Status	Study title	Conditions	Interventions	Inclusions	Exclusions	Comments
NCT03005054	Active, not recruiting (4 centres)	StrataGraft® Skin Tissue as an alternative to autografting full-thickness complex skin defects	Trauma-related wounds Burns Skin wounds	StrataGraft® Skin Tissue Autograft	Age 18-65 Sufficient healthy skin for donor site in case StrataGraft site requires autografting Complex skin defects of up to 49% TBSA (can come from >1 area) Full thickness complex skin defects requiring excision & autografting Treatment sites on torso and limbs may be up to 200 cm^2 (cohort 1) or 400 cm^2 (cohort 2) For thermal burns only, first excision &grafting of treatment sites	Pregnant women and prisoners Subjects receiving systemic immunosuppressive therapy Known history of malignancy Pre-admission insulin-dependent diabetics Expected survival <3 month Suspected infection at anticipated treatment sites Treatment sites adjacent to unexcised eschar Chemical & electrical burns	Phase II open-label, controlled, randomised, multi-centre dose-escalation study Safety, tolerability and efficacy of single or multiple applications for healing excised full thickness defects from acute traumatic skin loss (<49% TBSA)

NCT01437852	Completed, has results (6 centres) (30 participants)	StrataGraft® Skin Tissue as an alternative to autografting deep partial-thickness burns	Trauma-related wounds Burns Skin wounds	StrataGraft® Skin Tissue Some adverse events reported possibly due to SG. One probable – rash vesicular (1/30)	As above, but: 3-49% TBSA Deep partial thickness thermal burn(s) with total area 88-880 cm^2	Treatment sites with exposed tendon or bone Face, head, neck, hands, buttocks, perineum and over-joint areas Chronic wounds Current conditions at discretion of investigator	Phase 1b open-label, dose-escalation Safety, tolerability and efficacy 2 cohorts receive product stored by refrigeration; 1 receives cryopreserved, thawed product

NCT03005106	Active, not recruiting (16 centres) (71 enrolled participants)	StrataGraft® Skin Tissue in the promotion of autologous skin regeneration of complex skin defects due to thermal burns that contain intact dermal elements	Trauma-related wounds Burns Skin wounds	StrataGraft® Skin Tissue Autograft (both – to different areas on the same patient)	≥18 y/o w/ thermal burn(s) on torso, arms or legs – first excision and grafting of study treatment sites Sufficient healthy skin reserved for donor site if needed Clinical expectation donor site will heal without grafting Complex skin defects 3-49% TBSA (≥1 area) Thermal burns with intact dermal elements for which excision + autografting are clinically indicated.	Prisoners, pregnancy, expected survival <3 months; subjects receiving systemic immuno-suppressive therapy, with a known history of malignancy, pre-admission insulin-dependent diabetics; other concurrent conditions (discretionary); participation in treatment group of another study within 90 days prior to enrolment Chronic wounds or full-thickness in the treatment area; treatment sites immediately adjacent to unexcised eschar; signs of infection at anticipated treatment sites; treatment sites on the face, head, neck, hands, feet, buttocks or over joints.	Phase III Safety & efficacy study

NCT04123548	New posting 11/10/19 Status not yet posted so presumably not started recruiting yet (14 locations)	StrataGraft® Skin Tissue expanded access at specific study sites (StrataCAT)		StrataGraft skin tissue Applied once to no more than 3 separate burn sites, totalling a max. study treatment area of no more than 1000 cm^2, and using no more than 10 tissues	Provide written informed consent Have enough health skin to reserve as donor site(s) in case autografting becomes necessary Have protocol-defined thermal burns on torso, upper extremities and lower extremities: - The right size for treatment areas - With intact dermal elements for which excision and autografting are clinically indicated - Wounds have not been previously excised and grafted	Pregnant, prisoner, or expected to live less than 3 months Has any other condition that, per protocol or in the opinion of the investigator, may compromise the patient's safety or the study objectives Has participated in an investigational study within 90 days before enrolment	Provide expanded access to StrataGraft for thermally induced deep partial-thickness burns that contain intact dermal elements and for which surgical excision and autograft are clinically indicated Multi-centre, open-label study in adults

NCT00618839	Completed, has results (2/3 centres)	StrataGraft™ Skin Tissue (Human Donor Skin) in the surgical management of complex skin defects	Third degree burns Burns Wound infection Degloving injury	StrataGraft™ Skin Tissue Cadaver allograft All patients received StrataGraft skin tissue and an intrapatient control area treated with cadaver allograft in a split-wound design 3 serious and 10s of other adverse events reported but deemed unrelated to StrataGraft®	Aged 18+, with complex skin defects requiring sequential debridement under anaesthesia with temporary biological dressing (allogeneic grafting) prior to autografting Full thickness skin defects Informed consent	Pregnant/lactating women; prisoners; immune-compromised patients Venous stasis ulcers of the lower leg; diabetic foot ulcers; donor site wounds Wounds of <5% BSA; wounds of the hands, face and feet Prior entry into this study Expected survival <3 months Concomitant processes sustained at time of dermal injury (i.e. cardiac/ respiratory damage; destabilised organs from trauma) Active malignancy	Phase I/IIa clinical trial Open-label, randomised, comparative study with max. 15 patients Sequential surgical procedures involving surgical debridement and temporary cadaveric allografting and various or contiguous wound sites

Table 4: Selected clinical trials regarding use of StrataGraft™ from ClinicalTrials.gov. Last accessed October 2019. StrataGraft™ (Stratatech, a Mallinckrodt company) skin tissue is provided as a suturable circular patch of stratified epithelial tissue composed of a living dermal matrix (containing dermal fibroblasts) overlaid with human epidermal cells (NIKS™ cells). The standard of care for temporary coverage of full thickness skin defects is coverage with cadaver allograft until the wound can be autografted.

	Status	Study title	Conditions	Interventions	Inclusions	Exclusions	Comments
NCT02930499	Suspended (investigator relocation)	Effect of hyaluronic acid ECM on venous ulcers	Venous ulcers	Hyalomatrix extra-cellular matrix Mepilex wound dressing (a siliconized non-adhesive foam wound dressing) Each product applied once weekly	Age 21-90 (18-85) Chronic venous insufficiency and the presence of venous ulceration for >2 months Subjects and/or caregiver willing and able to tolerate multi-layered compression bandages Must be reliable, responsible, and able to visit the clinic weekly to the full 16-week period	Non-venous ulcers; sensitivity to HA; presence of wound infection; peripheral arterial disease Has received growth factor therapy (e.g. autologous platelet-rich plasma gel, becaplermin, bilayered cell therapy, dermal substitute, ECM) within 2 weeks Pregnancy or lactation at time of treatment Currently (or within 3 months of randomisation) receiving/ed radiation or chemotherapy Currently enrolled in another investigational device, drug of biological trial (or within 30 days of baseline) History or alcohol or drug abuse Allergic to primary & secondary dressing materials and adhesives, including occlusive dressings	Randomised, comparative study to determine whether Hyalomatrix is as effective as Integra™ Meshed Bilayer Wound Matrix when used in subjects who receive concurrent treatments with both products on their first- and/or second-degree burns located on both hands. Interventional, randomised, parallel assignment, open label, Phase IV.

NCT02363543	Withdrawn (0 participants) (sponsor decided to withdraw)	Comparison of Hyalomatrix and Integra Wound Matrix on Burn Wounds (Hyalomatrix)	Bandages	Hyalomatrix Integra (both products concurrently on $1^{st}/2^{nd}$ degree burns on both hands)	Written consent First and/or second degree burns on both hands Subject must be enrolled within 48 hours of the injury occurrence	Breastfeeding, pregnancy (current or planned) Prognosis indicating unlikely survival past the study period Third degree burns Electrical/chemical or frostbite burns Inhalation-related burn trauma On-going bone fractures Known sensitivity to silicone, hyaluronan, bovine collagen, chondroitin and/or derivatives Prior treatment that may affect study outcome Medical condition that may impede wound healing beyond what would be typically expected	Randomised, comparative study to determine efficacy of Hyalomatrix compared to Integra™ Meshed Bilayer Wound Matrix Phase IV

NCT03107546	Recruiting (40 participants) (1 location)	Comparison of scar formation in syndactyly release surgery with full thickness skin graft versus skin graft substitute	Syndactyly.	Hyalomatrix Skin graft (used to cover the newly separated fingers (exposed tissue) in place of autograft).	Age up to 17 years Patients requiring syndactyly release surgery with skin grafting for one or more web spaces on their hand(s)	Previous surgery on the web that requires a subsequent syndactyly release Diagnosis of macrodactyly Those who otherwise do not meet the inclusion criteria	Study purpose: compare effectiveness, wound healing, scar formation and potential associated complications of current skin graft technique with new Hyalomatrix technique following surgery Randomised parallel assignment,; double-blind (by location of each comparator material)

Table 5: Select clinical trials regarding use of Hyalomatrix® Tissue Reconstruction Matrix (Anika Therapeutics) listed on ClinicalTrials.gov. Last accessed October 2019. Hyalomatrix® is a bi-layered, sterile, single-use and flexible 'advanced' wound dressing. It is composed of a non-woven pad with a contact layer of fibrous-form hyaluronic acid derivative with an outer layer of a semi-permeable silicone membrane.

New products by development stage

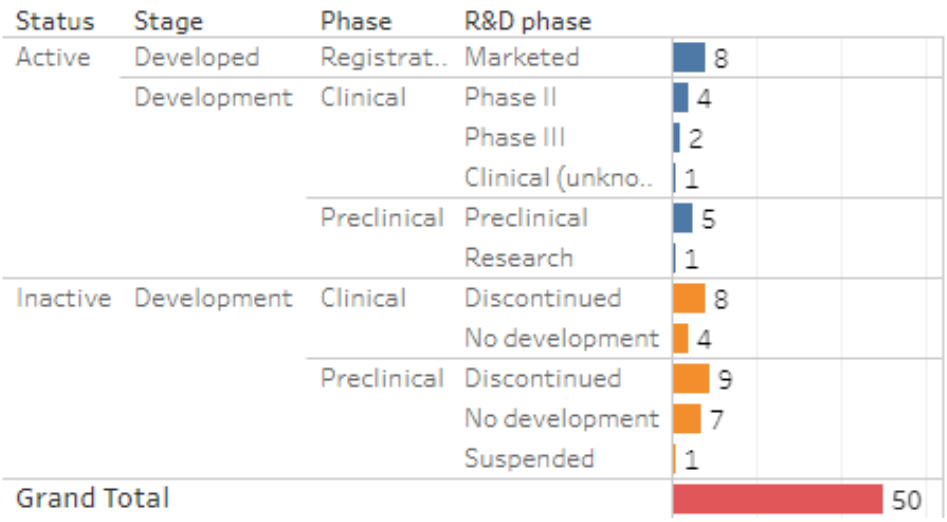

New products by route of administration

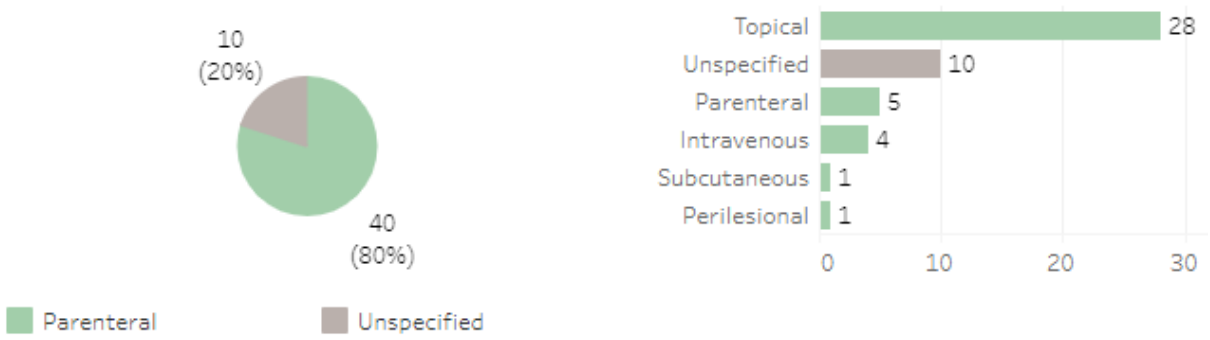

Table 6: An overview of the status and development of new burns products registered on the World Health Organisation Research Observatory database. Despite a wealth of academic research, few products translate to market. The duration and high cost of clinical trials may be a barrier, particularly to small companies and spinouts. Of those that do translate, most are classified as 'topical', which carry the lowest regulatory requirements. Data available online at https://www.who.int/research-observatory/en/ last accessed October 2019.

Stem cells and wounds

Stem cells can be defined as pluripotent or multipotent, depending on the number of cell types they are capable of differentiating into. Mesenchymal stem cells (MSCs) are multipotent, and can differentiate into a range of lineages, including bone, cartilage, fat, tendon, ligament and muscle (Oreffo et al., 2005; Pittenger et al., 1999). This plasticity renders MSCs of great interest in the field of regenerative medicine as their potential applications are wide ranging.

MSCs are primarily located in adult bone marrow, as well as in umbilical cord, adipose tissue and menstrual blood. Marrow is also a major reservoir for hematopoietic stem cells, which synthesise blood cells to renew those in circulation (Pittenger et al., 1999). MSCs can also migrate from bone marrow and circulate through blood vessels. In the context of skin tissue regeneration, MSCs in circulation may be chemically recruited to a wound by inflammatory cytokines (Chen et al., 2008).

One study found that the provision of IL-1α to *in vitro* cultured mesenchymal stem cells increased their expression of various growth factors (G-CSF, M-CSF, IL-6 and IL-11) (Haynesworth et al., 1996). In a wound environment, keratinocytes are known to release IL-1, so MSCs may be able to support regeneration by influencing and recruiting other cell types in the wound by growth factor expression (Kondo and Ishida, 2010).

Controlling the environment of stem cells influences their differentiation. In a wound environment, MSCs may differentiate into fibroblasts to directly aid wound repair, or endothelial cells and perivascular smooth muscle cells to form new blood vessels and support the wound (Pittenger et al., 1999). MSCs derived from adipose tissue have been shown to elicit a strong angiogenic response from host tissue. Their implantation in scaffolds improves vascularisation compared to comparable avascular scaffolds (Laschke et al., 2013). This vascularisation is important in the integration of an implanted scaffold and integral to the viability of resident cells. The oxygen diffusion limit has been observed to be approximately 150-200 μm from the nearest blood vessel (Folkman and Hochberg, 1973). Scaffolds are designed to aid repair in large defects, where the centre of the scaffold could reasonably be in the order of several times this range from the wound bed and 100 times the range from the lateral wound margins. The ability to quickly vascularise a scaffold is therefore essential as a large area is isolated from intact vasculature and is susceptible to necrosis. While this has been achieved by seeding endothelial cells, harvesting autologous cells is difficult (i.e. HUVECs from umbilical cord); yield is low and *in vitro* expansion difficult (Laschke et al., 2013; Tremblay et al., 2005).

Adipose-derived stem cells are of interest as they are readily available in adults and relatively straightforward to harvest (i.e. by liposuction) (Aust et al., 2004; Cheng et al., 2012). The ease of extraction makes adipose tissue a useful autologous source of MSCs. Using autologous adipose MSCs avoids the ethical implications that

are associated with the harvest of stem cells from other sources (i.e. embryonic; umbilical). The yield from harvest is also significantly higher than stem cell yield from bone marrow (Laschke et al., 2013).

It has been shown that human MSCs respond to signals from keratinocytes – migrating towards them, or towards conditioned media and away from keratinocytes (Mishra et al., 2012). This demonstrates a precedent for use of MSCs in scaffolds, as they may be more disposed to colonise a scaffold and migrate outwards towards signals from the keratinocytes in the surrounding healthy tissue.

MSCs have been shown to have important effects via regulation of the immune system, making it possible for allogenic cells to evade the host immune system (Koç et al., 2000). The mechanisms for this are not understood, but the theory is supported by a small number of studies. For example, Koç et al. (2002) found no evidence of alloreactive T cells in patients treated with MSCs.

This creates new avenues of opportunity for cellular tissue engineering, moving away from the requirement for autogenic cells. However, precise understanding of the physiological behaviour and mechanisms of differentiation is lacking, hindering the development of more sophisticated, targeted therapies (Sasaki et al., 2008). Tuan et al (2002) similarly suggest that more understanding is required to unlock the therapeutic potential of MSCs, and further that the key to their success may be the ability to successfully control, manipulate and expand them *in vitro*.

Therapeutic use of stem cells

Stem cells retain their ability for self-renewal. They are also able to differentiate into mature cells of a range of lineages depending on physical, chemical and biological environment signals from surrounding tissues *in vivo* (Arwert et al., 2012; Jiang et al., 2002) or under simulated conditions in vitro (Sasaki et al., 2008). After injury, stem cells utilise both of these capabilities in turn: proliferating to replenish the damaged or missing cells, then differentiating into an appropriate lineage (Watt and Driskell, 2010) – for example, myofibroblasts.

Differentiated cells are responsible for secretion of extracellular matrix components (Tessmar and Göpferich, 2007). The successful creation of new tissue, similar in composition to healthy native tissue, requires the cells in the scaffold to differentiate into appropriate lineages. This may be achieved by the provision of an appropriate microenvironment alongside biochemical triggers such as cytokines (e.g. SDF-1, IL-8, IL-6, VEGF and CXCL-5) (Mishra et al., 2016; Nissen et al., 1998).

Bone marrow-derived stem cells (BM-MSCs) secrete greater quantities of some of these cytokines, including VEGF and keratinocyte growth factor, than dermal fibroblasts (Chen et al., 2008). Interestingly, they also

secreted lower amounts of other cytokines, such as IL-6, which are implicated in various diseases when found in elevated quantities.

"Enhanced" growth factor secretion, either by up- or down-regulation, contributes to the enhanced wound healing capability of BM-MSCs compared to differentiated cell lineages such as dermal fibroblasts (Wu et al., 2007). Cancer cells also express elevated levels of growth factors, which may explain their ability to proliferate and colonise rapidly (Goldman, 2004).

Applying this principle to healing of chronic or recalcitrant wounds by delivering growth factors to the wound, directly or indirectly using BM-MSCs, has therapeutic potential. BM-MSCs have been shown to migrate to epithelial wounds, suggesting they do indeed support wounds healing by this mechanism in model systems. In one such system, the BM-MSCs were principally located in the upper dermis, below the wounded epithelium, suggesting a paracrine mode of action whereby BM-MSCs do not enter the wound, but express growth factors into it to promote healing (Chen et al., 2008; Yamaguchi et al., 2007).

Scaffolds: a structured approach to soft tissue repair

Porous scaffolds are widely used in in the treatment of injured or diseased tissue (Sultana et al, 2008; Bannasch et al, 2003). They may be used as a physical plug to fill an extensive cavity and prevent excessive contraction or scarring. Principally, however, they are used to provide a suitable structure to allow for cell infiltration and encourage tissue regeneration.

Porous materials are highly desirable as scaffolds as interconnected cavities provide space for vascularisation and angiogenesis, and aid the supply of nutrients and chemical stimuli and removal of waste from the regenerating tissue (Thomson et al, 1995; Busby et al, 2001; Whang et al. 2000). A highly porous material will allow for increased and more uniform infiltration of cells (Brauker et al, 1995; Carnachan et al, 2006; Glowacki et al, 1983; Klawiter and Hulbert, 1971; Lu et al, 2012; Mooney et al, 1991; Nade et al, 1983; Whang et al, 2000).

Current commercial scaffolds display very different microstructures to ideal characteristics cited in the literature. This may relate to reduced plasma diffusion and cell or blood vessel motility within the scaffold and, in turn, reduced *in vivo* performance. Porosity is created in Integra® Dermal Regeneration Template (Integra Lifesciences) by snap-freezing a dispersion of liquid particles within their matrix (Yannas et al., 1985). While porosity is high (Figure 2A) – the patent claims up to 95% porosity by this method – the material suffers from low interconnectivity between pores (Figure 2B). Additionally, the space between droplets in the dispersion results in impenetrable protein walls which restrict cellular or vascular migration. Matriderm® (Dr. Suwelack Skin and Health Care) also displays porosity with low interconnectivity (Figure 2D). In this case, porosity is

generated by the freeze-drying process (Schoof et al., 2001; Wieland and Haas, 2013). In both cases, the method of producing porosity is scalable and amenable to use with protein-based materials, but the conservative approach fails to achieve the high degree of interconnected porosity and low density that would maximise cell and vascular colonisation and promote rapid healing.

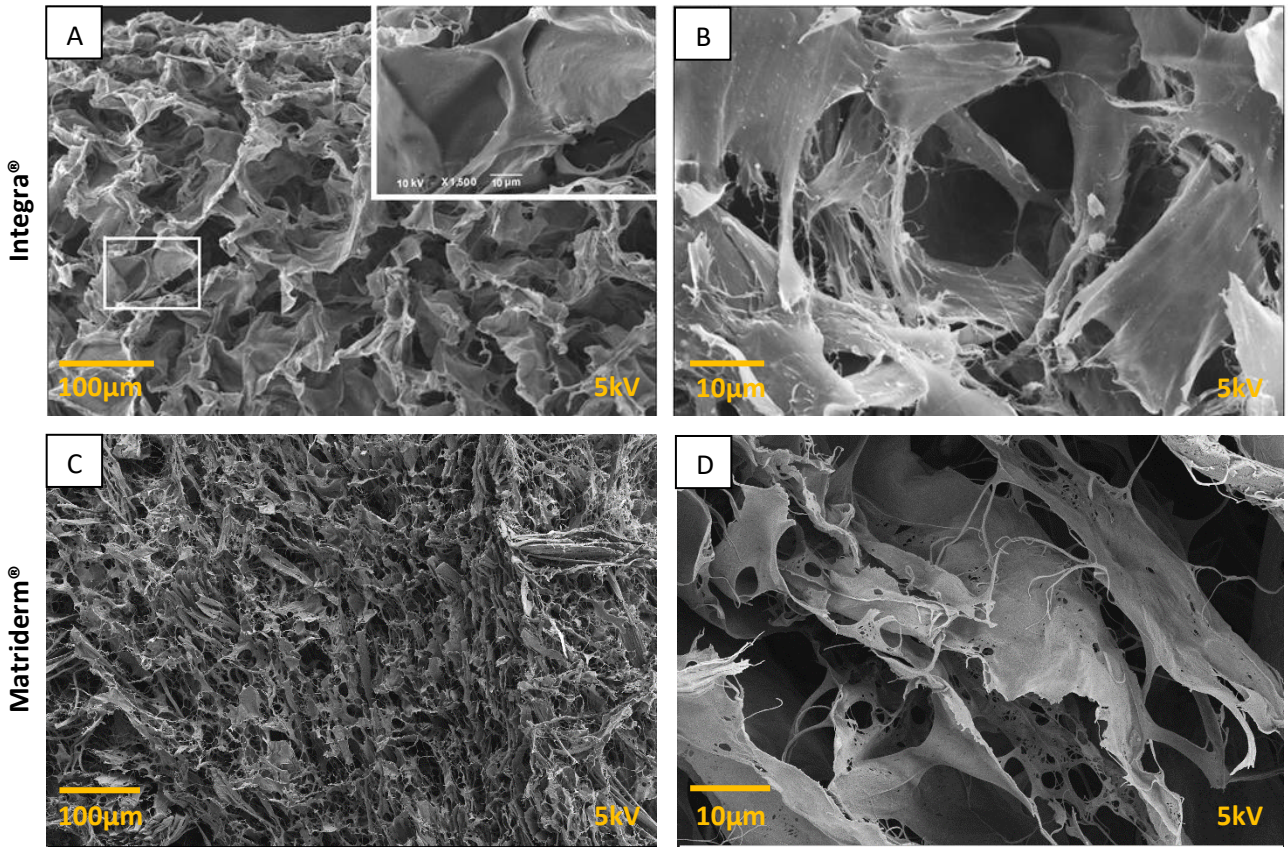

Fig. 2: Scanning electron micrographs showing cross-sections of commercially available skin scaffolds, Integra® Dermal Regeneration Template (Integra Lifesciences) and Matriderm® (Dr. Suwelack Skin & Health Care). Integra is shown at [A] 200 times and [B] 1,500 times magnification (images taken from (Jeremias et al., 2014)). Matriderm is shown at [C] 500 times and [D] 5,000 times magnification (primary images).

Vascularisation is key to the success of a tissue engineered construct – insufficient vascularisation results in impaired exchange of nutrients and waste and impedes immune response. As such, infection, localised necrosis or even loosening and rejection of the implant may occur (Sahota et al, 2003; Hendrickx et al, 2010).

Vascularisation of acellular scaffolds may be encouraged by modification of the structural or physicochemical properties of the scaffold or biological activation by release of growth actors (Frueh et al, 2016). Indeed, enrichment with VEGF/bFGF has been shown to accelerate vascularisation of the collagen scaffold Integra® Dermal Regeneration Template (Integra Life Sciences, NJ, USA) (Wilcke et al, 2007).

The size of pores is important to properly accommodate cells, enabling them to adhere to and interact with the scaffold (Bokhari et al, 2007). The degree of porosity, and the size of the pores, can greatly affect the behaviour of cells in a scaffold. Pore size is therefore an important criterion when developing a scaffold for use with any cell type, but especially stem cells as the implications may be profound (Viswanathan et al, 2012).

Work by Choi et al (2013) suggests that pore sizes larger than 200 µm tend to give rise to the formation of a low-density network of large blood vessels which are capable of penetrating deep into the scaffold. Pore sizes less than 200 µm give rise to high-density networks of small blood vessels, but penetration depth is reduced. As such, large pore sizes are desirable for large 3D scaffolds, whereas smaller pore sizes are more suited to smaller, thinner scaffolds such as those required for skin substitutes (Choi et al, 2013). Existing products Integra® (Integra Life Sciences, Plainsboro, NJ) and Matriderm® (Dr. Suwelack Skin & Health Care AG, Billerbeck, Germany) both fall into the latter category (Frueh et al, 2016).

Optimum pore sizes for skin scaffolds quoted in literature vary, but authors commonly quote pore sizes from a few microns ranging to 200 or 300 µm (Busby et al, 2001; Sultana et al, 2008).

Further to pore size, the size of the interconnections is almost important is promoting vascularisation of the scaffold. Large interconnections (~150 µm) show enhanced vascularisation compared to comparable scaffolds with smaller interconnections (Bai et al, 2010). This is likely a direct result of growing blood vessels being presented with a more open, less tortuous path into the implanted scaffold.

High porosity is achieved by maximising the surface area: volume ratio. Very little bulk material is therefore required to create a scaffold, rendering the scaffold fairly fragile. The scaffold must be sufficiently tough to be readily handleable, but also must provide a suitable physical environment for cell ingress and formation of new tissue in vivo.

Scaffolds may be applied acellularly, relying on native cells to migrate in and colonise. They may also be pre-populated with relevant cell types (such as fibroblasts, keratinocytes, or stem cells capable of differentiating into these cells).

There is evidence to suggest that implanting cellularised scaffolds may result in improved or accelerated healing. Lu et al., 2012 reported that their PLLA-collagen and PLLA-gelatin scaffolds, implanted in nude mice with full-thickness dorsal skin injuries, produced a thicker epidermis after 28 days than the same scaffolds used acellularly. A similar result was produced by (S. B. Lee et al., 2003) using gelatin/glucan scaffolds.

Alternative strategies to enhance wound healing may be achieved in either cellularised or acellular scaffolds by incorporating proteins, such as growth factors, to create a ‘smart’ or ‘physiologically active’ scaffold (Tessmar and Göpferich, 2007). The proteins may be adherent to the surface, encouraging the surrounding tissue to integrate with the scaffold edge, or released in a controlled manner (Bryant et al., 2007; Kim et al.,

2003; Whang et al., 2000). This type of carrier scaffold may be used to administer therapeutic doses of drugs to the wound over a defined period.

Once the wound has regenerated, scaffold materials remaining in the wound may often separate and elicit an inflammatory response (Lu et al., 2012). This is a particular problem with some polymeric materials, such as PLLA, PGA and PLGA, which degrade into acidic by-products (Li and Chang, 2005; Taylor et al., 1994). Appropriate material selection, degree of cross-linking, and scaffold dimensions (i.e. wall thickness) help ensure scaffold materials do not persist in the healed wound. Scaffolds for tissue regeneration should instead degrade steadily during healing and leave no debris (Busby et al., 2001; Langer and Vacanti, 1993; Tessmar and Göpferich, 2007). This allows space for generation of new ECM products (Vepari and Kaplan, 2007).

Tissue engineering scaffolds combine materials science with a biological element (i.e. a polymeric scaffold seeded with cells *ex vivo*, or intended to integrate with native cells *in vivo*). As such, the ideal scaffold must have both mechanical and biochemical properties optimised in order to perform well as an engineered construct and support living cells in a wound environment.

Scaffolds must be capable of maintaining a moist wound environment, replacing the hydrating properties of intact dermis. This may be beneficial in reducing formation of bad scars (Chang et al., 1995). Hydration must be held in balance; it is also beneficial for scaffolds to have the capacity to absorb wound debris such as exudate (Choi et al., 1999). Absorption of exudate is an additional advantage of the porous sponge-like structure most scaffolds adopt.

Mechanical strength is vital for the survival of a scaffold, not only to withstand gross movement and external impact, but also to counter contractile forces exerted by cells within the scaffold (Dado and Levenberg, 2009; Lu et al., 2012). Cell-mediated contraction can lead to shrinkage of the scaffold that may alter the structure, and will also prevent the scaffold from creating an effective seal of the wound bed.

However, excessive mechanical strength of a scaffold may also be detrimental. Increased strength is often associated with reduced flexibility of the scaffold, reducing its ability to conform to the wound as it repairs. Limited flexibility and elasticity of the scaffold will impair the elasticity of the ECM in contact with the scaffold. Mesenchymal stem cells have demonstrated a high level of sensitivity to matrix elasticity in differentiating to different cell lineages (Engler et al., 2006). As the mechanical properties of ECM and gross tissue are closely linked, the flexibility and elasticity of the scaffolding material is therefore very specific to the target tissue (Dutta et al., 2017; Janson and Putnam, 2015).

Additionally, strength may be associated with a longer proteolytic degradation time. A scaffold should be optimally tuned to degrade at the same rate that a wound repairs, to maintain a steady volume in the wound cavity. The inherent strength of synthetic polymers makes them well suited as biomaterials for tissue

engineering of ‘hard’ tissues (Dutta et al., 2017). It could be suggested, therefore, that natural polymers are better suited to applications in soft tissue engineering, such as the regeneration of skin.

Mechanical strength derives from the physical (e.g. microstructure, porosity, and homogeneity) and mechanical (e.g. elasticity, stiffness, and isotropy) properties of the scaffolding material (Dutta et al., 2017). Given that many of these characteristics have tight optimal parameters for defined scaffolding applications, altering the strength without detriment to other features can be challenging. One method of increasing strength without affecting the bulk material is fibre reinforcement (Lu et al., 2012). The fibres may be randomly dispersed to achieve anisotropy. The surface area to volume ratio is very high for thin fibres, increasing the area for degradation, so unwanted *in vivo* persistence is avoidable.

The internal structure of a scaffold is vital to its effectiveness. What differentiates a bioinert structure from a truly biocompatible, integrative structure is its ability to support the regenerating tissue. Scaffolds must encourage cells to infiltrate, proliferate and communicate. These cell colonies require the support of a vascular network to apply the supply of nutrients and physiological cues (i.e. growth factors) and removal of waste (Thomson et al., 1995; Whang et al., 2000). Insufficient vascularisation impairs exchange of waste and nutrients, which is detrimental to healing, and impedes immune response. This may lead to necrosis of the wound area, loosening of the scaffold and even rejection from the wound bed (Hendrickx et al., 2010; Sahota et al., 2004).

Vascularisation may be encouraged biochemically, by the provision of growth factors (Frueh et al., 2016). Indeed, the use of VEGF and bFGF has been shown to accelerate the vascularisation of the collagen scaffold Integra® Dermal Regeneration Template (Integra Life Sciences, NJ, USA) (Wilcke et al., 2007).

Alternatively, the internal architecture of the scaffold may encourage its vascularisation. High porosity and interconnectivity between pores allow for pervasion of capillaries from the wound periphery, and their distribution throughout. This connects the scaffold to the infrastructure of the surrounding tissue and is therefore vital to creating an integrative scaffold (Bannasch et al., 2003; Busby et al., 2001; Hollister, 2005). Porosity enhances the permeability of a material, promoting release of bioactive materials loaded onto a scaffold and diffusion of native soluble factors into the scaffold and the cells supported within (Leach and Schmidt, 2005). These materials allow for increased and more uniform infiltration of cells into the implanted scaffold (Brauker et al., 1995; Carnachan et al., 2006; Klawitter and Hulbert, 1971; Lu et al., 2012; Nade et al., 1983; Whang et al., 2000).

Scaffold structure

A scaffold's structure should closely mimic the tissue it is designed to replace to encourage native or near-native behaviour. It is known that porosity and topography directly influence cultured cell behaviour, such as migration (Frueh et al., 2016). Bokhari et al (2007) found pore diameters of 100 µm and interconnect diameters (diameter of connections between larger pores) of 25 µm optimal for penetration of osteoblastic cells into a scaffold. Close control of the microstructure is crucial to optimise these parameters, and to achieve homogeneity throughout the scaffold so that cells are likely to interact in the same way regardless of their position. Thus, the cells are disposed to act as a single population, rather than small colonies each responding to different microenvironments (Bokhari et al., 2007).

Pore size is a critical parameter in the success of a tissue engineering scaffold, especially those designed to support angiogenesis into the wound site (Linnes et al., 2007). In engineering of soft tissue, such as skin, scaffolds with pores of 35 µm diameter showed enhanced angiogenesis compared to scaffolds with smaller or larger pores (Marshall et al., 2005), although vascularisation occurred throughout more of the scaffold with 70 µm diameter pores (Marshall et al., 2004).

Choi et al. (2013) further demonstrated that scaffolds with larger pores (>200 µm diameter) promote the formation of low-density networks of larger blood vessels. Conversely, scaffolds with smaller pores (<200 µm diameter) promote the formation of high-density networks of smaller blood vessels. However, these networks do not penetrate deeply into the cultured construct. As such, smaller pore diameter scaffolds are more suited to smaller, thinner tissue substitutes, such as skin (Choi et al., 2013; Frueh et al., 2016).

Scaffolds with a narrow pore size distribution are typically favoured. However, as the literature suggests different sizes for pore and interconnect diameter for different purposes, it may be desirable to achieve narrow distributions at two pore diameters. This would encompass pore sizes optimised for angiogenesis, vascularisation and cell migration and settlement.

The spatial distribution of these differently sized pores may have to be optimised to support formation of homogenous tissue, and this could prove challenging using current methods.

However, interconnect size may be a more dominant parameter than pore size. Optimised interconnect diameter promotes vascularisation by promoting proliferation, adhesion and migration of endothelial cells through scaffolds (Xiao et al., 2015). Scaffolds with larger interconnections have been shown to exhibit improved vascularisation over those with smaller diameter interconnections, up to a maximum of 400 µm beyond which no significant difference is observed (Bai et al., 2010). However, the optimal pore sizes suggested above are many times smaller than this value. Scaffolds with interconnect diameters exceeding pore diameter are clearly meaningless, so direct application of this data is not useful. *In vitro* verification for

specific cell types in defined scaffolds is advisable to confirm optimum pore and interconnect diameters. However, the results suggest that wider interconnect diameters enhance vascularisation by provision of a more open and direct route through the scaffold.

The shape of pores may also affect scaffold interaction with cells. Funnel-shaped porous structures have been shown to improved fibroblast adhesion, and allow for high cell seeding efficiency (Lu et al., 2012).

The number and distribution of pores is directly linked to the cell-loading capability of a scaffold, and also the spacing between these cells. The density of cells in a scaffold affects the rates of cell proliferation and deposition of new ECM (Cheng et al., 2006; Lu et al., 2012). These two factors play a major role in the properties of the resultant tissue.

The bulk material is selected for both its engineering properties and its biocompatibility. There is an arsenal of such materials, approved for use in a variety of biomedical applications by the FDA and other international regulatory bodies, including natural and synthetic polymers. Treating the surface of the bulk material affects the way it interacts *in vivo*. Surface treatment can be used to enhance *in vivo* performance, or to broaden the selection of appropriate materials by providing a biocompatible surface to a less favourable substrate.

Chemically modifying the material surface has been shown to influence cellular adhesion, allowing control in the way cells interact with the implant (Viswanathan et al., 2012). Biomaterial surfaces may also be biologically treated, for example with the immobilisation of growth factors, to promote or otherwise influence cell adhesion, proliferation and behaviour (LeBaron and Athanasiou, 2000). Cells respond in a very sensitive manner to biomaterial surfaces. Topography can govern the mode of adhesion, the extent and direction of migration, and even differentiation (Bokhari et al., 2007).

The role of fibrin in wound repair

After injury, the coagulation and fibrinolytic cascades are important in providing rapid and appropriate haemostasis to minimise blood loss. If the vascular system is damaged, the coagulation cascade is activated, leading to the release and activation of thrombin (Factor IIa). Thrombin then acts to polymerise soluble fibrinogen (Factor I) to fibrin. The fibrin fibrils that form cross-link and recruit other proteins to aid stability. Together, these actions form a clot, or thrombus, to seal the puncture and prevent further blood loss (Blombäck, 2000; Standeven et al., 2005).

Fibrinogen is one of the most abundant proteins in human plasma (Anderson and Anderson, 2002). It is synthesized by hepatocytes at a rate of approximately 1.7 – 5 g/day (Takeda, 1966). It then leaves the liver and circulates the body in blood plasma at a typical concentration of 2.5 – 3 mg/ml. When circulating cytokines

such as IL-6 are provoked (i.e. in response to epidermal breach), pro-inflammatory agents are released which strongly upregulate the plasma concentration of fibrinogen. Elevated levels increase the potential for coagulation to occur (Blake and Ridker, 2001; Sidhu et al., 2003).

Fibrinogen is a large soluble glycoprotein (approximately 330 kDa in size) with an unusual tri-nodular structure, arising from the fact that it possesses the properties of both fibrous and globular proteins (Standeven et al., 2005; Weisel and Medved, 2001). A schematic of the primary structure of fibrinogen is shown in Figure 3, below.

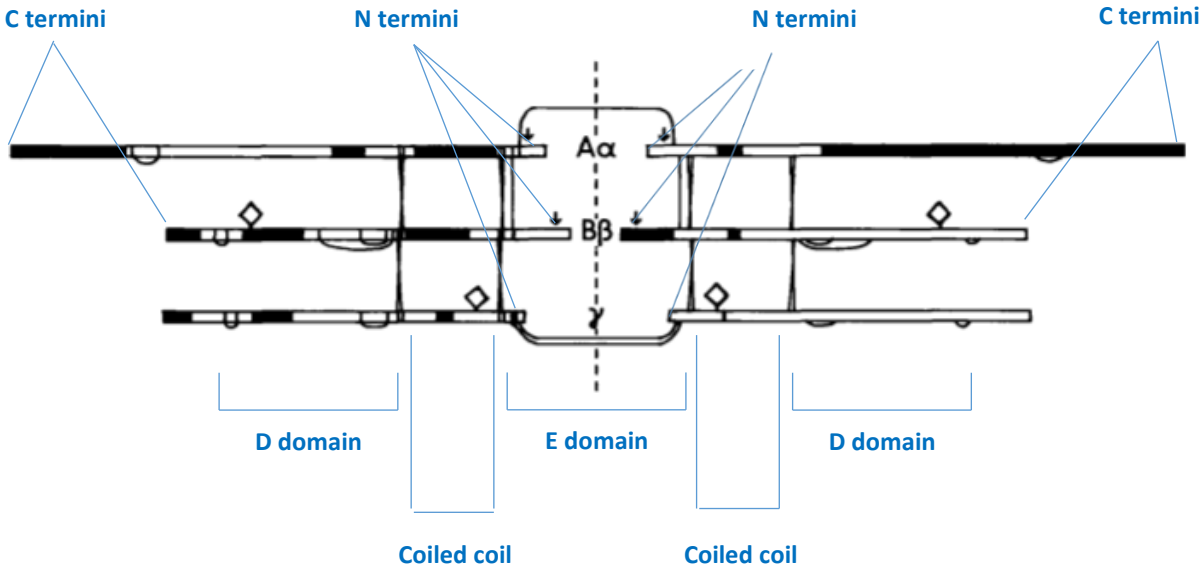

Fig. 3: Primary structure model of human fibrinogen. This simplified diagram shows the primary protein structure of fibrinogen, with the six chains arranged in order, and the N-terminals facing towards the central E domain. A, B and γ refer to the paired protein chains; α and β refer to fibrinopeptides FpA and FpB located at the C-termini of the A and B chains, respectively. Image adapted from Henschen et al., 1983.

The fibrinogen molecule comprises six chains with three identical pairs. These are denoted as Aα, Bβ and γ. The N-termini of all these chains face towards the centre of the fibrinogen molecule, the E domain. These chains intertwine from the central E domain, forming α-helical coiled-coil structures that are supported by disulphide bridges. This results in a generally linear molecule. However, while the Bβ and γ chains extend the length of fibrinogen, ending distally at one of two D regions, the Aα chains instead loop back towards the E domain (Standeven et al., 2005; Weisel and Medved, 2001). This tertiary structure, and its common bending conformations, are illustrated in Figure 4, below.

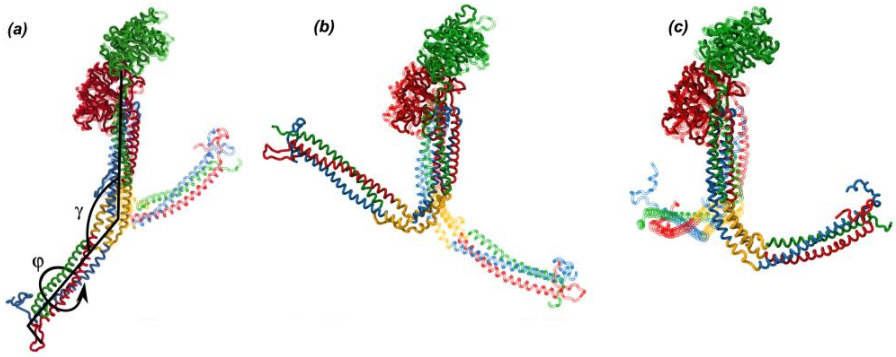

Fig. 4: Tertiary structure and bending conformations of the fibrinogen molecule, with the hinge region coloured yellow. The Aα, Bβ and γ chains are coloured blue, red and green respectively; carbohydrates are shown in orange. The bending angle *γ* is the angle that the hinge region forms between the E domain and the D region. *φ* is the torsion angle. This is defined by two different parts of the E domain, the hinge region, and the D region. Image adapted from Köhler et al., 2015.

During the coagulation cascade, fibrinogen polymerises to fibrin. This occurs when thrombin cleaves the N-terminal sequences on the Aα and Bβ chains by proteolysis, releasing the surface-bound fibrinopeptides FpA and FpB, and in doing so exposing specific binding sites (Bailey et al., 1951; Riedel et al., 2011; Standeven et al., 2005). The chain cleavage and release of FpB causes a drop in solubility that causes the molecules to aggregate laterally and increases the availability of α-chains to cross-linking by Factor XIII (Gorkun et al., 1994; Standeven et al., 2005; Weisel, 1986).

The precise roles of FpA and FpB are not fully understood, as lateral protofibril aggregation can occur without FpB, but equally clot formation can occur with only FpB. However, this latter mechanism is unlikely to occur *in vivo*, as thrombin preferentially cleaves the N-terminal of the Aα first. Cleavage of both Aα and Bβ, releasing FpA and FpB respectively, likely works synergistically to strengthen the bonding between the aggregating molecules, producing stronger fibres (Shainoff and Dardik, 1983; Weisel, 1986). FpB is also associated with faster fibrin formation and increased rate of lateral aggregation (Blombäck, 2000; Shainoff and Dardik, 1983).

As well as Aα and Bβ, fibrinogen contains two γ chains. These are cross-linked at the branch points of higher molecular weight molecules, such as trimers and tetramers (Mosesson et al., 1989; Standeven et al., 2005). The formation of these γ polymers is favoured in certain conditions, such as high Ca^{2+} concentration or slow polymerisation of fibrinogen to fibrin (Mosesson et al., 2001). Additionally, two species of fibrinogen exist: fibrinogen 1 and fibrinogen 2. Fibrinogen 1 contains two identical γ chains, whereas fibrinogen 2 contains a γ and a γ’ chain. γ’ has a different C-terminal sequence. While cross-linking of both resultant fibrinogens is

comparable, fibrinogen 2 is found to produce finer branched fibre networks than fibrinogen 1 (Siebenlist et al., 2005). This is likely due to the delayed release of FpA resulting from the altered thrombin binding site at the C-terminal of γ' on fibrinogen 2. This indirectly supports, and gives physiological relevance, to the findings of the *in vitro* work of Shainoff and Dardik (1983), who found that release of both FpA and FpB gave rise to stronger protofibril and fibre binding.

During cross-linking, protofibrils of fibrin begin to form. When these protofibrils reach a critical length, they start to assemble into double-stranded twisted fibrils. The thickness of these fibres is limited by the degree of twisting, as the constituent protofibrils are also twisted and this limits the distance they can stretch (Standeven et al., 2005; Weisel, 1986). These fibrils branch out, by a combination of two proposed mechanisms, to create intricate networks (Weisel, 1986). In the first, the fibrils align adjacent to one another and form a branch point of two or four molecules. This lends mechanical strength to the clot. In the second, most likely occurring when proteolytic cleavage of fibrinogen is slow, three fibrin molecules bind three protofibrils (Standeven et al., 2005).

Haemostasis and thrombus formation are achieved so rapidly because as fibrin forms, the cleavage of Factor XIII activation peptides by thrombin is accelerated. This ensures that the level of Factor XIII available in the wound site is sufficient to maintain rapid cross linking of the polymerised fibrin protofibrils (Curtis et al., 1983; Lewis et al., 1985).

Eventually, an elastic gel forms (Blombäck and Bark, 2004). The structural and mechanical characteristics are highly dependent on a number of factors. *In vitro* experiments revealed that clotting time remained the dominant factor in clot structure determination through varying ionic strength, fibrinogen concentration and H^+ concentration (Blombäck and Okada, 1982; Okada and Blombäck, 1983). A faster clotting time correlates to a short gelling time, with more lateral fibre aggregation (Weisel, 1986).

Additionally, pH, ionic strength and the presence of various ions and proteins are capable of modifying clot structure. Calcium and chloride ions, albumin and collagen have all been shown to alter clot structure (Standeven et al., 2005).

The presence of calcium ions shortens the clotting time of fibrinogen and gives rise to the production of fibrils with increased mass: length ratios. The resultant fibrin fibres are therefore thicker and stronger (Carr et al., 1986; Hardy et al., 1983). Type IV collagen, typically found in the basement membrane of skin, likewise influences fibrinogen polymerisation. Jones and Gabriel (1988) found that when type IV collagen is present during fibrinogen coagulation, the fibrin fibres produced are thicker for a given fibre length than when collagen is not present.

Conversely, the presence of chloride ions leads to the production of thinner, less stiff, fibrin fibres. This is due to the ions inhibiting lateral aggregation of protofibrils during coagulation (Di Stasio et al., 1998). Human albumin similarly limits lateral growth of fibrils by an alternate mechanism of steric hindrance (Galanakis et al., 1987; Wilf et al., 1985).

Whilst these molecules are all physiologically relevant, the work cited above was all *performed in vitro*. It is therefore more pertinent to tissue engineering work for generation of fibrin constructs, rather than to *in vivo* mechanisms. For example, while isolated fibrinogen and thrombin are capable of causing thrombus formation, the fibres formed are of smaller diameter than fibrin fibres formed by the interaction of fibrinogen and thrombin in plasma (Carr, 1988).

Increasing pH leads to creation of a finer, more friable, clot structure composed of thinner fibrils. Perhaps counter-intuitively, given the evidence that shorter clotting time produces thicker fibrils in the presence of Ca^{2+} and collagen, this occurs in conjunction with a reduced clotting time (Ferry and Morrison, 1947).

Finally, the relative concentrations of fibrinogen and thrombin themselves have a significant influence on polymerisation and resultant clot structure. Increased concentration of thrombin reduces the lag period during which protofibrils grow before aggregation. Therefore, when thrombin concentration is increased, the protofibrils produced will be thinner (Hantgan and Hermans, 1979). An *in vivo* study by Wolberg (2007) showed that this is true only at prothrombin concentrations above physiological levels. At very low prothrombin levels (<10% plasma levels) clots were weak and malformed (Wolberg, 2007). As prothrombin is the precursor molecule to thrombin, it is reasonable to draw the same conclusions about the effect of thrombin concentration. These results indicate that there exists an optimum thrombin concentration range that must be achieved for appropriate coagulation.

Conversely, an increased concentration of fibrinogen increases the lag time, giving more time for protofibrils to grow laterally prior to aggregation. The fibrils and resultant fibres are longer and thicker with increased fibrinogen concentration, and the maximum rate of fibre assembly also increases (Weisel and Nagaswami, 1992). However, when the concentration of fibrinogen exceeds the concentration of thrombin by a factor of approximately 15x, clotting time increases and the reverse is observed (Ferry and Morrison, 1947).

Fibrin scaffolds

Fibrin has been widely investigated as a scaffold for a diverse range of tissue engineering applications including engineering of small blood vessels and heart valve prostheses, cartilage, bone and skin, and as a carrier for transplanted stem cells (Bensaïd et al., 2003; Geer et al., 2002; Jockenhoevel et al., 2001; Perka et al., 2001; Swartz et al., 2005; Yasuda et al., 2009). The use of fibrin composite tissue engineering constructs, with materials such as fibrin-agarose, fibrin-collagen, fibrin-alginate, fibrin-PCL, fibrin-PLLA-PLGA and fibrin-polyurethane has also been described (Carriel et al., 2012; Collen et al., 2003; S. B. Lee et al., 2003; Lesman et al., 2011; Levenberg and Lesman, 2014; Ma et al., 2012, 2003; Schagemann et al., 2010; Serbo and Gerecht, 2013; Shikanov et al., 2009; Swieszkowski et al., 2007; Weinberg, 1989).

Fibrin scaffolds have been used as vehicles for controlled-release drug delivery (Catelas et al., 2008; Jeon et al., 2005; Lee et al., 2003). Fibrin products are also used as adhesives (Borst et al., 1982; Brennan, 1991; Brown et al., 1992; Currie et al., 2001; Dahlstrøm et al., 1992; Rose and Dresdale, 1986), making use of the high tensile strength of bound fibrin constructs. This strength of adhesion derives from the ability of fibrin to bind to cells (de la Puente and Ludeña, 2014) either directly, via integrin receptors, or indirectly via ECM proteins such as fibronectin (binding to fibroblast and phagocyte receptors) (Makogonenko et al., 2002) and vitronectin (binding to collagen and endothelial cell receptors) (Preissner and Jenne, 1991).

Fibrin has been used as a haemostatic agent for over 100 years (Loeb, 1909). Its therapeutic use was inspired by its native action in the coagulation cascade, and it is used to rapidly seal a wound and prevent blood loss in extreme scenarios, such as battlefield injuries (Borst et al., 1982; Granville-Chapman et al., 2011; Vournakis et al., 2003). This versatility in application may derive from the characteristic structure of fibrinogen, and the many ways of producing fibrin from fibrinogen.

Fibrin gels match other biomaterials, such as collagen, for high cell seeding efficiency and the uniform distribution of cells achieved therein and is thus proposed as a candidate scaffold material (Swartz et al., 2005). Further, fibrin offers many advantages over other protein-based biomaterials. For example, processing does not damage protein functionality. Conversely, extraction and processing of collagen to make it suitable for implantation irrevocably damages the higher protein structure. Extraction of fibrin is from whole blood, which may be harvested readily from an autologous donor without incurring donor site morbidity. Allogenic or xenogenic (bovine) blood may also be used.

In normal physiology, the persistence of natural fibrin constructs – blood clots – is regulated by the interplay between the coagulation and fibrinolysis cascades (Clark, 2003; Standeven et al., 2005). Regulation of artificial fibrin scaffolds is likewise tuneable by mechanical or enzymatic means. The number, diameter and density of fibrin fibrils affects degradation rate; as does the biochemical environment, including proteolytic enzymes.

One problem with the use of fibrin for implantable biomaterials is its rapid degradation *in vivo*. Protease inhibitors like aprotinin or tranexamic acid can delay proteolytic degradation, prolonging the persistence of implanted fibrin constructs as required to support the repairing tissue (de la Puente and Ludeña, 2014; Jockenhoevel et al., 2001).

In vivo, cross-linking of newly-formed soluble fibrin fibrils by activated coagulation factor XIII stabilises the fibrils to form a strong, elastic insoluble clot (Standeven et al., 2005). The same effect may be achieved in artificial fibrin constructs by chemical cross-linking with reagents such as genipin (Dare et al., 2009; Linnes et al., 2007), glutaraldehyde (McManus et al., 2006) or carbodiimides such as EDC in NHS buffer (Grasman et al., 2012); or by photo crosslinking with the aid of a ruthenium catalyst (Bjork et al., 2011).

Fibrin and fibrinogen can be used to make an extensive and varied range of scaffold constructs, including microspheres, micro- and nanofibres, microtubes, nanoparticles and hydrogels (Rajangam and An, 2013).

Scaffold preparation techniques

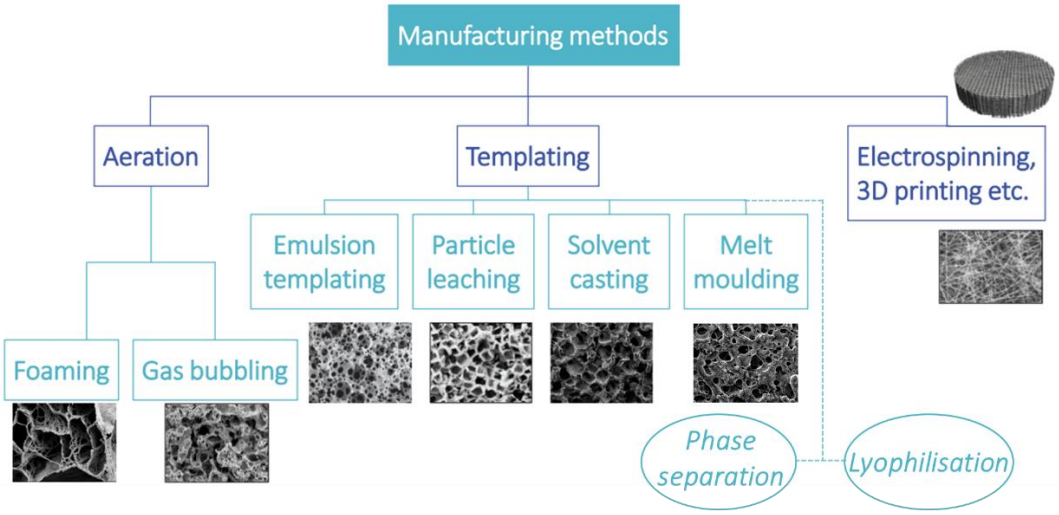

Fig. 5: Summary of manufacturing approaches to produce porous scaffolds for tissue engineering, classified by method of generating porosity.

Scaffolds are designed with the intention of supporting cells within the matrix, by guiding migration and promoting adhesion. They must also support a vascular network to support these cells, and allow the supply of nutrients and physiological cues (i.e. growth factors) and removal of waste. As such, highly porous structures are desirable for scaffold architecture (Bannasch et al., 2003; Busby et al., 2001; Hollister, 2005; Sultana and Wang, 2008).

Some materials, such as foams, are inherently porous (Baldwin and Saltzman, 1996), as are fibrous materials that form an interwoven mesh. This may be accomplished by weaving, knitting or electrospinning. For other materials, porosity may be achieved by a variety of means (Figure 5).

However, certain limitations (e.g. pH, temperature, toxicity) may apply to retain the integrity of the material used and ensure its biocompatibility. This is particularly true of biological polymers, such as proteins, whose structure and functionality is highly dependent on their environment (Tessmar and Göpferich, 2007). At elevated temperatures, proteins are likely to denature, which may alter their structure such that their desired function is impaired or lost. This is supported by a study from Lu et al. (2012) who found that in scaffolds made of gelatin, a denatured form of collagen, cell proliferation was lower than in comparable scaffolds of a less processed form of collagen. Thus, they suggested that increased bioactivity of the matrix protein may confer increased proliferative activity to the cells it supports. Care should therefore be taken to process proteins within tolerable physiological ranges of temperature (37°C) and pH (~pH 7).

Scaffolds are typically formed from solutions, whose structure is formed during solidification. Porosity may be introduced by a number of methods, such as particulate leaching, gas bubbling, phase separation, melt moulding, foaming and emulsion templating (Dutta et al., 2017; S. Yang et al., 2001).

Particulate leaching employs solid particles as porogens. These porogens are dispersed through the liquid scaffold mixture and the scaffold is solidified with the porogens trapped inside. The scaffold is then treated, for instance by washing, to remove the porogen, leaving a cavity in its place. The size and shape of the porogen determines the size and shape of the resultant pore. The density and packing arrangement of the porogens determines the number, spacing and interconnectivity of the pores.

Traditional porogens include soluble materials such as salt and glucose, but porogen selection is only limited by ability to establish a means of its non-destructive removal from the scaffold (Busby et al., 2001; Holy et al., 1999).

Several groups have used hydrocarbons, such as paraffin and beeswax, as porogens (Shastri et al., 2000). These hydrocarbon porogens may be accurately sized and shaped to offer control over scaffold porosity. Removal of the porogen is only possible through interconnected pores, so this method is only suitable for an open pore system. Heat must be applied to melt the waxes in order to remove them, which may not be suitable for protein scaffolds to avoid denaturation and compromised tertiary structure. However, the melting points of paraffin and beeswax are relatively low (61-65°C) so the method is suitable for a range synthetic polymers widely used in tissue engineering, such as PLLA, PLGA, PMMA and PEO (Bogdanov, 2004; Shastri et al., 2000).

Kang et al. (1999) created porous scaffolds by using ice in swollen gelatin hydrogels. This simple method offers advantages of low porogen cost, no biocompatibility issue in case of incomplete porogen removal and no aggressive leaching treatment is required.

The use of particulate leaching to induce porosity is typically limited to production of very thin scaffolds up to 3 mm thick, owing to the difficulty of ensuring porogen removal (S. Yang et al., 2001). In practise, such thin scaffolds have limited applications for *in vivo* tissue engineering. Additive manufacturing may be applied to build up a multi-layered scaffold. For example, by creating many thin scaffolds and layering them to create a thicker three-dimensional construct. This also introduces a possibility for controlled variable porosity throughout the scaffold.

Bubbling inert gas through the liquid scaffold is another method of introducing porosity. Polymer emulsions, such as PLGA in methylene chloride, are saturated with supercritical gas (such as carbon dioxide) in a sealed vessel. The supersaturation replaces the solvent with carbon dioxide. The vessel is rapidly vented, causing the gas to form bubbles. At the same time, the polymer precipitates, leaving behind a solid porous scaffold (Hile et al., 2000). This method may be used in combination with other methods, such as particulate leaching, to enhance the scaffold porosity or to introduce a subset of pore sizes within the scaffold (Shea et al., 1999).

Freeze drying is widely used to preserve scaffold architecture and create a stable, dehydrated product to extend shelf life prior to implantation. It is used as a final processing step in the manufacture of scaffolds with both synthetic (PLGA, PLA, PLLA) and natural polymers (gelatin, fibrin, collagen) (Kang et al., 1999; Nam and Park, 1999; Tessmar and Göpferich, 2007; Whang et al., 2000; Yayon et al., 2010).

In some instances, perhaps where the system is less stable (i.e. soft polymer constructs), snap freezing super-cools water to prevent its crystallisation to ice. The crystallisation process may cause the liquid to pull away from the scaffold, and the shape of the ice crystals may distort the round pores. ‘Snap’ freezing may be achieved using liquid nitrogen or a -80°C freezer prior to freeze drying. This process was originally devised for manufacture of pure polymer scaffolds but has since been used more widely, for example in the lyophilisation of synthetic and composite (HA/PHBV, PLLA, PLGA) or natural polymer (chitosan, collagen/chitosan, fibrin) scaffolds (Kim et al., 2003; Liu and Ma, 2004; Ma et al., 2003; Rapp, 2002; Sultana and Wang, 2008; Whang et al., 1995). Alternatively, scaffolds may be dried under vacuum at room temperature (Bokhari et al., 2007).

Emulsions

An emulsion is a mixture of two or more immiscible phases, typically an oleic and an aqueous phase. Upon mixing, these liquids form a dispersion of droplets (the dispersed phase) in a continuous phase (Hentze and Antonietti, 2001; Tadros, 2013).

Emulsions are thermodynamically unstable systems and inevitably tend towards phase separation (Wang et al., 2010). The stability of the emulsion is determined by the rate at which it decays; i.e. the droplets change size and distribution by processes such as creaming and sedimentation, coalescence and flocculation (Kato et al., 1985; Prinderre et al., 1998; Yarranton et al., 2007) (fig. 6). Gravitational separation occurs when the dispersed particles migrate upwards ("creaming") or downwards ("sedimentation") depending on their relative density to the continuous phase. Droplets may also clump together to form aggregates. If these droplets retain their original integrity, this process is known as flocculation. If the droplets merge together and grow, the process is coalescence. Ostwald ripening is another process of droplet growth, whereby smaller droplets feed larger ones by mass transport through the continuous phase. Phase inversion occurs when the continuous and dispersed phases swap (i.e. an oil-in-water emulsion becomes water-in-oil, or vice versa). Emulsions can destabilise by one or many of these processes. Technological advances, such as the development of automated light scattering equipment, allow real-time data collection to monitor the change in dispersed droplet diameter and spacing at different heights in the sample (Mengual et al., 1999). This allows comparison of both the rate and type of emulsion destabilisation in different formulations.

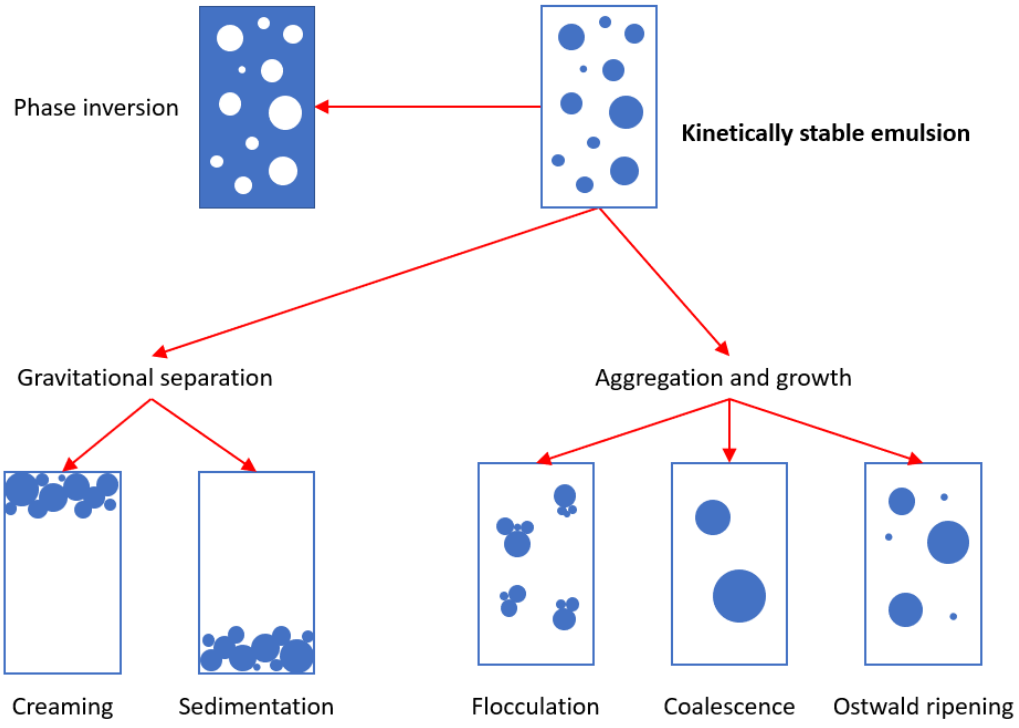

Fig. 6: Mechanisms of emulsion instability and breakage. Image adapted from (McClements, 2007). In stable emulsions, the internal phase droplet number, diameter and spacing remain unchanged. This is thermodynamically unfavourable; emulsions have a tendency to separate to reduce the interfacial area and hence energy. Emulsions can break by migration of the denser phase (creaming or sedimentation, depending on whether the internal phase is more or less dense than the continuous phase). Emulsions can also break by droplets coming together, displacing the continuous phase. Droplets may adhere as floccs (flocculation), merge into larger droplets (coalescence) or feed larger droplets by mass transport (Ostwald ripening).

In general, emulsions with smaller droplet diameters in the dispersed phase are more stable. The change in viscosity of an emulsion system is also a good indicator of its stability. Small variations in viscosity are indicative of emulsion stability (Friberg et al., 1968). An amphiphilic molecule, such as a surfactant, may be added to promote stability of the emulsion (Hentze and Antonietti, 2001). Surfactants have both lipophilic and hydrophilic regions, allowing organised assembly at the interface between the oil and aqueous phases. The barrier they create slows instability. The ratio between the size of the hydrophilic and lipophilic regions of a surfactant molecule is expressed by as HLB (hydrophilic-lipophilic balance) (Boyd et al., 1972; Davies, 1957).

A water-in-oil emulsion (w/o) has oil droplets dispersed in an aqueous continuous phase. An oil-in-water (o/w) emulsion has aqueous droplets dispersed in an oleic continuous phase (Tadros, 2013). The propensity for formation of a w/o or o/w emulsion is determined by the balance of hydrophobicity and hydrophilicity of the solutions in the mixture (Davies, 1957). This may be simply determined using the HLB scale (Griffin, 1955). Oleic phase reagents are assigned an HLB number, determined experimentally, that allows for selection of an appropriate surfactant to cause emulsification with the aqueous phase (Aulton, 1988). This is not a precise method; factors such as temperature, and salt content of the aqueous phase, alter the required HLB.

Required HLB numbers may be indirectly confirmed using conductivity measurements, by determining the nature and temporal stability of a protein emulsion (Prinderre et al., 1998). Emulsion conductivity increases significantly after homogenisation then reduces as the emulsion decays. The rate and duration of the reduction of the conductivity is therefore an indicator of emulsion stability (Kato et al., 1985). Further, experimental data from o/w emulsions has shown that by plotting emulsion conductivity against HLB, the steep region of the curve corresponds to ‘critical’ HLB (Prinderre et al., 1998; Puisieux and Seillier, 1983).

Common name	Chemical designation	HLB	Emulsifying character
-	Sorbitan tetra stearate	0.5	***Lipophilic (oil soluble)***
Span 85	Sorbitan tri oleate	1	
Span 65	Sorbitan tri stearate	2.1	
GMS	Glycerol mono stearate	3.8	
Span 80	Sorbitan mono oleate	4	
Arlacel P135	Polyethylene-30 dipolyhydroxystearate	5.6	
Span 40	Sorbitan mono palmitate	6.7	
-	n-butanol	7	***Water dispersible***
Span 20	Sorbitan mono laurate	8.6	
Arlatone T	PEG-40 sorbitan peroleate	9	
Tegosoft GC	PEG-7 glyceryl coacetate	10	
Tween 81	Polyethylene sorbitan mono oleate	11	***Hydrophilic (water soluble)***
Synperonic NP8	Nonylphenol polyglycol ether 8 EO	12.3	
Tween 21	Polyethylene sorbitan mono laurate	13.3	
Tween 60	Polyethylene sorbitan mono stearate	14.9	
Tween 80	Polyethylene sorbitan mono oleate	15	
Tween 40	Polyethylene sorbitan mono palmitate	15.6	
Tween 20	Polyethylene sorbitan mono laurate	16.7	
Na oleate	Sodium oleate	18	
K oleate	Potassium oleate	20	
Synperonic PE/F 68	Tri-block copolymer of ethylene oxide and propylene oxide	29	
SDS	Sodium dodecyl	40	

Table 7: Common emulsifying surfactants arranged across the HLB range from lipophilic to hydrophilic in character. The hydrophilic-lipophilic balance (HLB) scale is a semi-quantitative method

for assessing the relative contributions of the hydrophilic and lipophilic regions of non-ionic surfactants by molecular weight. HLB 2-3 are antifoaming agents; HLB 3-6 are w/o emulsifying agents, HLB 7-9 are wetting agents, HLB 8-16 are o/w emulsifying agents, HLB 13-15 are detergents and HLB 15-18 are solubilising agents. The overlap shows that behaviour is highly dependent on the emulsion system and surfactant used. Adapted from Davies (1957); Griffin (1955); Kang et al (2010); Lee et al (2005); Pays et al (2002) and Sobisch and Lerche (2005).

The average diameter of dispersed droplets in an emulsion is typically in the order of several μm. The droplet size distribution is often broad. However, additional processing, such as fractionation, may be employed to separate and remove droplets with diameters outside the desired range (Zhang and Cooper, 2005). Emulsion droplet size can be controlled and varied by altering the interfacial tension between the oleic and aqueous phases. For example, increasing surfactant concentration reduces interfacial tension between the dispersed and continuous phase leads to a reduction in the diameter of the droplets of the dispersed phase (Ho et al., 1994).

Homogenisation of an emulsion system, for example by shear mixing, reduces droplet size to a minimum after which no further decrease is observed. The smallest droplets are achieved by mixing at the highest speed for the shortest time, until the theoretical minimum droplet size is achieved, then the mixing time has no further effect (Prinderre et al., 1998; Solans et al., 2005). Ultra-high speed/frequency mixing can be used to make very small droplets in nano-emulsions (Floury et al., 2000; Leong et al., 2009).

The minimum droplet size is governed by interfacial tension and the availability of surfactant in the emulsion system. Homogenisation promotes droplet formation by distributing surfactant throughout the system to enable assembly around a greater number of interfaces. This can also be achieved by, or in conjunction with, increasing the concentration of surfactant.

In addition to affecting the droplet size of the dispersed phase, mixing time also has a strong effect on viscosity, even after droplet size is minimised (Prinderre et al., 1998). (Floury et al., 2000) suggest that this occurs because at high homogenisation pressure, flocculated particles are disrupted. The viscosity reduces until all droplets exist as discrete spheres, or the number of ‘floccs’ reaches a minimum. Further, they observed that at increasing homogenisation pressures, emulsions exhibit Newtonian behaviours, whereas they show shear-thinning behaviours at lower homogenisation pressure.

The density of droplets in the dispersed phase is varied by changing the ratio between the continuous and dispersed phases. There is a theoretical maximum dispersed phase ratio, beyond which the continuous phase

is insufficient to surround all the droplets of the dispersed phase. In practise, instability results in breakdown of the emulsion before this is achieved.

Emulsions offer an attractive method of manufacture for tissue engineering scaffolds. The dispersed phase acts as a set of liquid phase porogens. Thus, the emulsion creates a 'template' for the scaffold (Kimmins and Cameron, 2011; Thomas et al., 2008). The versatility of emulsion templating arises from the ability of emulsions to form readily controllable droplets. Either hydrophilic or hydrophobic polymers may be used depending on the emulsion type used. Hydrophilic polymers dissolve in the aqueous phase to form a scaffold matrix around oil droplets in an o/w emulsion.

Emulsion templating

The ability of emulsions to form droplets of readily controllable size gives many applications in cell and tissue engineering, from micelles or microbeads used to deliver proteins (Tessmar and Göpferich, 2007), drugs (Ho et al., 1994) and DNA/RNA (Kulkarni et al., 2011) (where the dispersed phase is the desired functional output) to templated scaffolds (where the continuous phase creates a porous sponge-like structure after removal of the dispersed phase).

Emulsion templating is a widely used and highly versatile method of introducing porosity (Kimmins and Cameron, 2011; Zhang and Cooper, 2005). The dispersed phase acts as a set of liquid phase porogens. Thus, the emulsion creates a 'template' for the scaffold (Kimmins and Cameron, 2011; Thomas et al., 2008). The versatility of emulsion templating arises from the ability of emulsions to form readily controllable droplets. Either hydrophilic or hydrophobic polymers may be used depending on the emulsion type used. Hydrophilic polymers dissolve in the aqueous phase to form a scaffold matrix around oil droplets in an o/w emulsion.

Methods of using emulsions to create porosity include:

- traditional o/w or w/o emulsions
- TIPS (thermally induced phase separation) (Whang et al., 1995)
- polyHIPEs (poly high internal phase emulsions, where the dispersed phase exceeds 74% total emulsion volume) (Busby et al., 2001; Cameron and Sherrington, 1996)
- polyHIPEs combined with porogens, whereby some of the monomer in the continuous phase is replaced with an inert solvent (porogen) that is immiscible with the dispersed phase. On polymerisation, a series of much smaller pores forms in the walls of the larger ones (Busby et al., 2001; Cameron and Barbetta, 2000; Hainey et al., 1991).

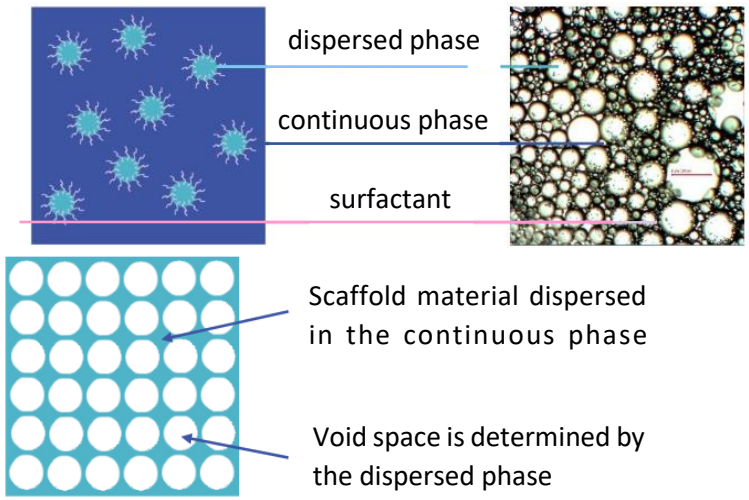

Fig. 7: A simple emulsion comprises an oleic and an aqueous phase. A surfactant may be added to improve stability by assembly at the interface, with hydrophobic regions in the oil phase and hydrophilic regions in the aqueous phase. Porous scaffolds may be produced by dissolving monomers in one phase and initiating polymerisation while the emulsion remains stable. The structure of the emulsion is preserved in the solid scaffold, giving rise to the term 'templating'.

Alternatively, the polymer may be dissolved into the dispersed phase (i.e. a hydrophobic polymer in an o/w emulsion) to form micelles or template microbeads. These polymer microbeads may be used to deliver a variety of substances *in vivo*, such as proteins, drugs and DNA/RNA (Ho et al., 1994; Kulkarni et al., 2011; Tessmar and Göpferich, 2007).

In a porous templated scaffold, the volume fraction of the dispersed phase of the emulsion dictates scaffold porosity and also influences wall thickness by closeness of adjacent droplets. Droplet diameter gives pore diameter. The average diameter of dispersed droplets in an emulsion is typically in the order of several µm. The droplet size distribution is often broad. However, additional processing, such as fractionation, may be employed to separate and remove droplets with diameters outside the desired range (Zhang and Cooper, 2005). Emulsion droplet size can be controlled and varied by altering the interfacial tension between the oleic and aqueous phases. For example, increasing surfactant concentration reduces interfacial tension between the dispersed and continuous phase leads to a reduction in the diameter of the droplets of the dispersed phase (Ho et al., 1994).

Homogenisation of an emulsion system, for example by shear mixing, reduces droplet size to a minimum after which no further decrease is observed. The smallest droplets are achieved by mixing at the highest speed for the shortest time, until the theoretical minimum droplet size is achieved, then the mixing time has no further effect (Prinderre et al., 1998; Solans et al., 2005). Ultra-high speed/frequency mixing can be used to make very small droplets in nano-emulsions (Floury et al., 2000; Leong et al., 2009). The minimum droplet size is governed

by interfacial tension and the availability of surfactant in the emulsion system. Homogenisation promotes droplet formation by distributing surfactant throughout the system to enable assembly around a greater number of interfaces. This can also be achieved by, or in conjunction with, increasing the concentration of surfactant.

In addition to affecting the droplet size of the dispersed phase, mixing time also has a strong effect on viscosity, even after droplet size is minimised (Prinderre et al., 1998). Floury et al. (2000) suggest that this occurs because at high homogenisation pressure, flocculated particles are disrupted. The viscosity reduces until all droplets exist as discrete spheres, or the number of 'floccs' reaches a minimum. Further, they observed that at increasing homogenisation pressures, emulsions exhibit Newtonian behaviours, whereas they show shear-thinning behaviours at lower homogenisation pressure.

The density of droplets in the dispersed phase is varied by changing the ratio between the continuous and dispersed phases. There is a theoretical maximum dispersed phase ratio, beyond which the continuous phase is insufficient to surround all the droplets of the dispersed phase. In practise, instability results in breakdown of the emulsion before this is achieved.

Stability of emulsions is key for templating. An emulsion that breaks by creaming or sedimentation will produce a heterogeneously porous scaffold, with one surface having much lower porosity than the other. Instability arising from coalescence or flocculation will give rise to irregular pore size and non-homogeneous pore distribution. This would produce varied wall thicknesses, with some too thin and liable to rupture, and others too thick to allow diffusion and potentially thick enough to provoke an adverse immune response. However, engineered and well-characterised emulsions are capable of generating scaffolds with tunable and reproducible properties from a variety of materials. It is therefore an interesting technique for producing tissue engineering scaffolds. The batch-to-batch reproducibility is well suited to satisfying regulatory requirements. There is no need for costly and specialised equipment to produce the emulsions, making emulsion templating an economically attractive option for the clinic.

3.0 Experimental work: polyHIPEs for skin tissue engineering

This chapter is presented in four sections: surfactant selection for o/w emulsions (section 3.1), optimisation of the emulsion to template fibrin from solubilised fibrinogen (3.2), characterisation and refinement of fibrin polyHIPEs (polymerised structures from high internal phase emulsions) (3.3) and a study of their angiogenic potential (3.4).

The work is presented in a logical, rather than strictly chronological, order for the sake of clarity. Emulsion stability experiments and surfactant selection were carried out in tandem with templating trials. These were initially performed at low internal volume fractions (50 or 60%) before gradually increasing to high internal phases in order to ascertain the best surfactant for templating as well as inherent emulsion stability. As such, some surfactants and formulations are not described in all sections, as earlier experiments (which may for clarity be presented in subsequent sections) demonstrated lower suitability for templating.

The first section (3.1) presents a strategy for surfactant selection by 'oil carrying capacity'. A series of systematic experiments, testing stability of multiple different families, was used to establish the oil fraction at which peak stability was observed. Two distinct categories of behaviour were observed.

In section 3.2, surfactants with oil carrying capacity in the HIPE (high internal phase emulsion) regime (≥74% internal phase) were considered as potential candidates and trialled in templating. Their performance was re-assessed with protein (for stability of emulsion and function of protein). Oil fraction was gradually increased to create scaffolds with the most desirable microstructure in terms of porosity, interconnectivity, fibre diameter and density and wall thickness. These experiments were carried out alongside work presented in sections 3.1 and 3.3.

Having established a working protocol to templating, the resulting highly porous scaffolds (made from HIPEs with an internal phase comprising ~90% total emulsion volume) were evaluated for mechanical and biological properties in vitro. The scaffold recipe was then refined to improve the performance based on initial in vitro results. The effects of different scaffold compositions on microstructure, bulk mechanical behaviour, cyto-compatibility and degradation rate are presented in section 3.3.

The final section, 3.4, describes the effect of different scaffold structures and compositions on blood vessel interactions in a chick chorioallantoic membrane assay. This *in vitro-in vivo* bridge model was deployed to gain an understanding of scaffold performance in a dynamic system. Scaffolds were evaluated against well established, clinically used scaffolds (Matriderm® and Integra® Dermal Regeneration Template). This tested angiogenic potential of the scaffold materials. More data is required; this will be a priority if future work is to be undertaken.

This experimental section summarises scaffold development from template design and refinement through to early compatibility studies. It will form the basis of future investigations including *in vivo* clinical studies.

An overview of the iterative design process for template design, revisited throughout sections 3.1 and 3.2, is shown in fig. 1 below.

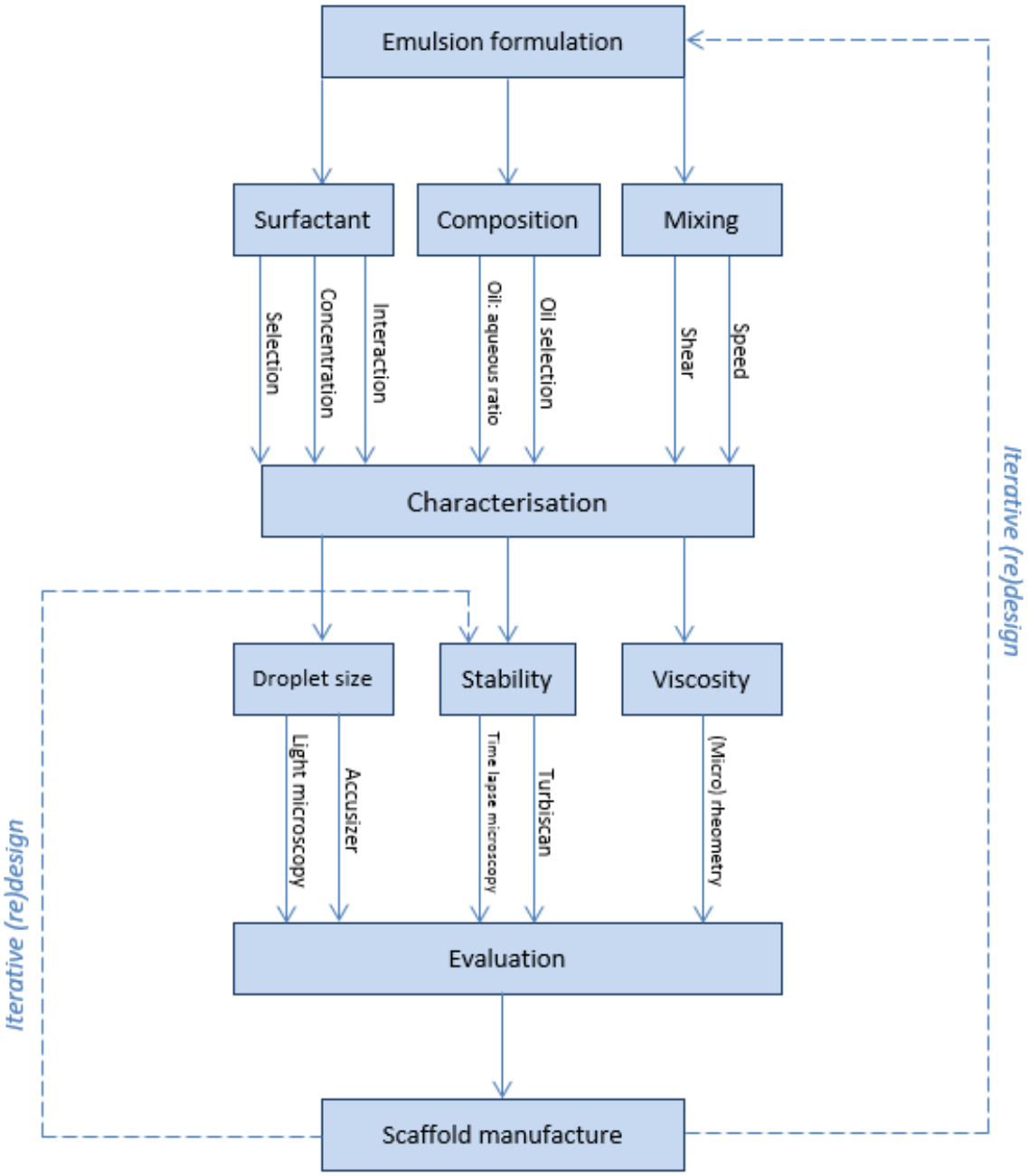

Fig. 1: Overview of experimental work, from surfactant selection and emulsion design to scaffold formulation and characterisation.

3.1 Characterising emulsion stability

ABBREVIATIONS

HIPE	High internal phase emulsion	RI	Refractive index
HLB	Hydrophilic-lipophilic balance	TSI	Turbiscan™ stability index
O/W	Oil-in-water emulsion	TX	Triton™ X
OCC	Oil carrying capacity	W/O emulsion	Water-in-oil (inverse)
POE	polyoxyethylene		

ABSTRACT

Emulsions are used in myriad applications, from paint to petroleum; mayonnaise to medicines. The properties of these products, including density and viscosity, are directly governed by the emulsion. Increasing the oil content, especially beyond 74% of the total volume, greatly changes the behaviour of the emulsion. This can be exploited to generate useful structures or generate higher product yields. However, stability is the limiting design factor and requires careful selection of stabilising surfactants.

The HLB system is the principle quantified method for selecting appropriate (non-ionic) surfactants. It assigns numeric value to the lipophilic and hydrophilic portions of surfactants, attempting to quantify the 'contribution' to stabilising a given oil. While a useful measure, surfactant HLB is only one measure and is not robust enough to accurate select surfactants. This remains a 'dark art' with lengthy experimentation and personnel experience hugely important in formulation.

We propose a novel supplementary surfactant screening tool, "oil carrying capacity". Using a test emulsion comprising decane, aqueous buffer and common industrial surfactants, we assessed short-term dynamic emulsion stability at increasing oil fractions using static multiple light scattering. Surfactants included Tweens, Tergitols, Brijs and Tritons from HLB 9.8 to 17.6.

Emulsion stability data was used to rank surfactants for their ability to generate high internal phase oil-in-water emulsions in the test system. Two distinct patterns of behaviour were observed among the surfactants tested. Branched chain and reduced forms of surfactants displayed enhanced stability at extremely high oil fractions and less contribution of HLB compared to other surfactants of the same family.

This system of determining the oil fraction at which optimum emulsion stability occurs, the 'oil carrying capacity' of each surfactant, is intended as a tool for surfactant selection in a system where the desired oil

fraction is known. Equally, it may be used to optimise oil fraction 'carried' in the emulsion when a particular surfactant is required.

INTRODUCTION

Achieving stable emulsions of known oil: aqueous volume fractions is highly desirable in a broad range of applications. In the petroleum industry, emulsifying heavy oil may improve flow for transportation. The production of reduced fat foodstuffs, such as ice cream or mayonnaise, requires low internal phase (oil) fraction (McClements and Demetriades, 1998). In the pharmacology and biomedical industries, emulsions may be used to template porous scaffolds to support cells in regenerating tissues, or to produce microbeads for delivery of drugs or cellular therapies (Chen et al., 2011; Ho et al., 1994; Tan and Takeuchi, 2007; Zhang et al., 2013). Emulsion templating of delicate structures such as scaffolds requires an extremely high internal phase volume fraction.

The range of emulsions for industrial application is huge and diverse, and the requirements of internal (dispersed) phase volume fraction and duration of stability are equally wide-ranging. Emulsions are inherently thermodynamically unstable, so operational stability must simply exceed shelf life or the duration of a processing step. It is therefore highly specific to the recipe, storage conditions and application.

A robust system of screening surfactants is required to minimise dependence on lengthy experimentation and improve efficiency of emulsion formulation. The purpose of this work was to systematically evaluate surfactant efficacy and efficiency in a high internal phase emulsion (HIPE) system of decane and aqueous buffer. The goal was to identify surfactants that could adequately stabilise high internal phase oil-in-water emulsions with a minimum concentration of non-ionic surfactant.

For non-ionic surfactants, the best screening method remains the HLB system, devised by Griffin in 1955 (Griffin, 1955). This is a semi-quantitative measure of the relative molecular weights of the hydrophilic and lipophilic regions of a surfactant molecule assigned on a scale from 0.5 (extremely lipophilic) to 19.5 (extremely hydrophilic) (fig. 2). The HLB system has been extended to include ionic surfactants, some exceeding HLB 20; however, these are relative figures derived experimentally and not achieved mathematically (Haw, 2004).

While Griffin's work remains important and a useful starting point, HLB only describes the behaviour of surfactants in aqueous solutions and does not consider the environment (including salinity or temperature of the system) or other surfactant characteristics such as structure (Witthayapanyanon et al., 2008). HLB alone was not a useful predictor of surfactancy in this system.

There have been several other proposed tools for predicting emulsions properties and guiding formulation. These include the hydrophile-lipophile deviation (HLD) and the phase inversion temperature (PIT) (Nguyen et

al., 2019; Salager et al., 1979; Shinoda and Arai, 1964). The HLD model considers the emulsion system more holistically than the HLB system, encompassing the system temperature and salinity, the effective alkane carbon number of the oil and the hydrophilic/phobic nature of the surfactant. However, it remains less widely used than the HLB system, possibly owing to the significant increase in complexity of calculations (which do not remove the need for extensive testing). Experience and experimentation are arguably the most important requirements in selecting surfactants for emulsion formulation (Salager et al., 2010).

A common approach is to add surfactant to a system of known, fixed oil: aqueous fraction until emulsification is achieved. Surfactant is added in excess to improve emulsification. However, increased use of surfactant in this way may be undesirable in a number of applications, particularly in the pharmaceutical and biomedical industries where higher surfactant concentrations could denature proteins incorporated in the aqueous phase or cause cytotoxic and irritant effects *in vivo*.

In this study, non-ionic surfactants from distinct families (Tergitol™, Brij®, Tween® and Triton™) were used to emulsify increasing oil fractions to create oil-in-water emulsions. Emulsion stability, and the kinetics of emulsion decay, were measured using a static multiple light scattering technique (Turbiscan™ LAB). Emulsion stability was used to rank surfactants for their ability to generate high internal phase oil-in-water emulsions in the test system. Surfactant HLB and functional groups were considered as variables.

Principles of static multiple light scattering

Stability was reported using the Turbiscan™ stability index (TSI). This non-destructive, non-invasive technique gives the stability of the sample over its whole selected height as a function of transmitted and backscattered light compared to the same measurements at the previous timepoint. Kinetic stability is built up over sequential scans. The pattern of change across the height of the sample gives a 'fingerprint' characteristic of the mode of destabilisation. TSI is defined in equation 1:

$$\mathrm{TSI} = \sum_i \frac{\Sigma_\mathrm{h}|\mathrm{scan_i(h)} - \mathrm{scan_{i-1}(h)}|}{\mathrm{H}} \qquad \text{(eq. 1)}$$

where $scan_i$ is the backscattering value at a given timepoint, $scan_{i-1}$ is the backscattering value from the previous timepoint, h is the height of the scan and H is the total sample height from the first to the last scan. TSI is the sum of the differences between sequential scans and thus represents the stability of the sample over a defined timeframe. TSI reduces with increasing stability.

This novel system of determining the oil fraction at which optimum emulsion stability occurs, the 'oil carrying capacity' (OCC) of the surfactant, is intended as a supplementary tool for surfactant selection in a system where the desired oil fraction is known.

Equally, it may be used to optimise oil fraction 'carried' in the emulsion when a particular surfactant is required. It is a practical tool to be used in conjunction with other metrics, such as HLB, but its simplicity and broad application make it versatile and easy to implement to formulation practises.

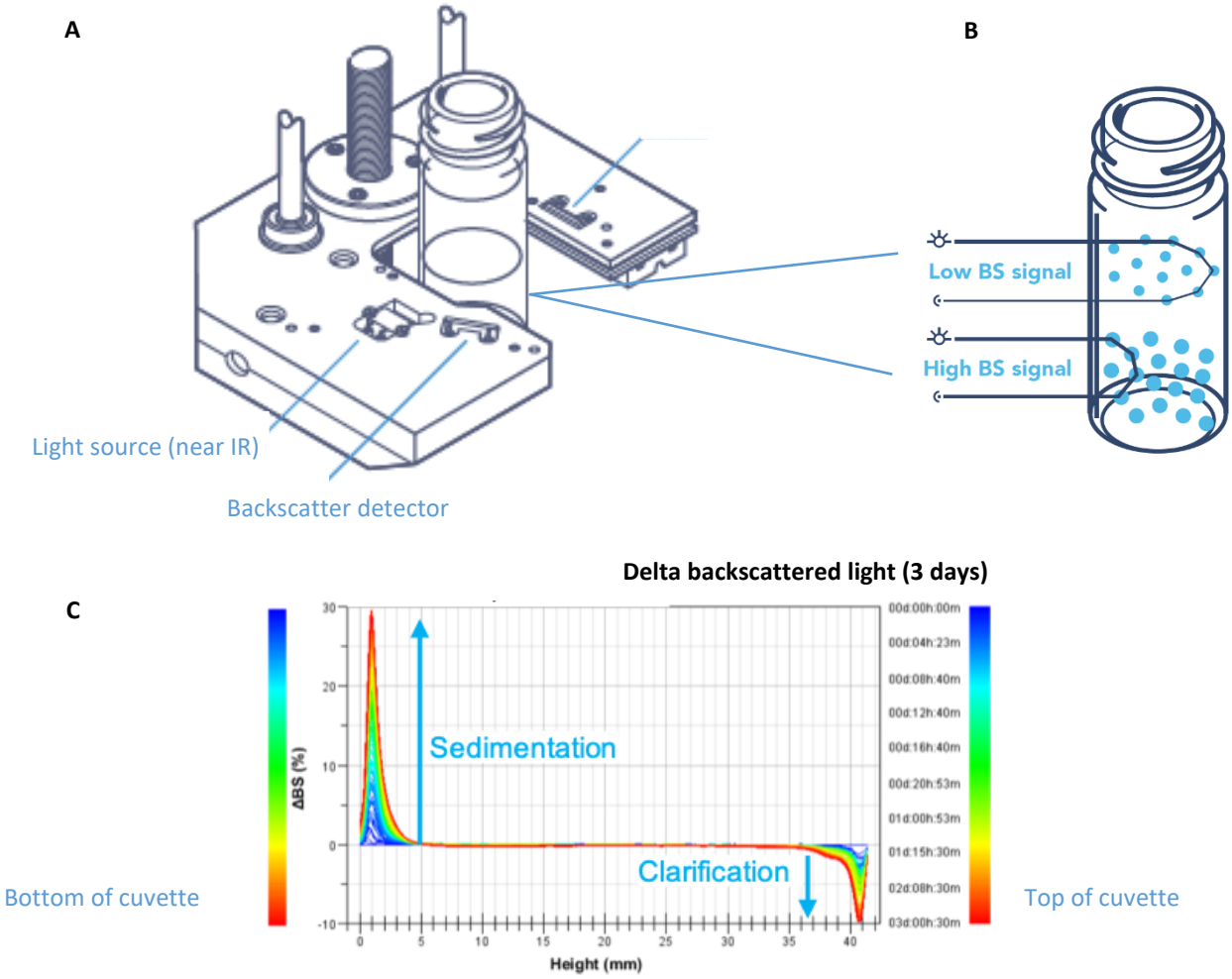

Fig. 1: Measuring kinetic stability using Turbiscan™ Lab static multiple light scattering technology. **[A]** A light source traverses the height of a glass cuvette. A pair of detectors read at 40 µm intervals. **[B]** A backscattering detector on the same side as the light source detects light reflected back from the sample; a transmission detector on the other side of the platform detects transmitted light. **[C]** The levels of transmitted and backscattered light reflect both the concentration of particles in a dispersion and the droplet diameter at different heights in the sample. Sequential scans display real-time change in emulsion characteristics. Images sourced from the Formulaction Knowledge Centre website (last accessed June 2020).

This work focuses on a range of commonly used surfactants used in with oil-in-water (O/W) emulsions. They all lie in the HLB range 9.8 – 17.6 (see table 1). The volume fractions of the oil (internal phase) range from classical emulsions (50, 60, 70% oil by volume) to high internal phase emulsions (HIPEs; 80 and 90% oil by volume). Emulsification and stabilisation of inverse (water-in-oil) emulsions falls outside the scope of the present work. Therefore, no lower volume fractions of oil were considered; neither were lipophilic surfactants with HLB below 10 (the only exception being Triton X-45 (HLB 9.8) which was included to create a full HLB series of Triton X surfactants).

Particle sizing

The size of the droplets of the internal phase is closely linked with the rheological properties of the emulsion, and thus the stability (Lee, 2006). Droplet size is also an important consideration in product design; either dictating pore or bead size in emulsion templating or influencing the bulk flow of materials like creams and lotions (Busby et al., 2002; Tessmar and Göpferich, 2007).

Droplets of the internal phase are generally spherical. This minimises the surface area of contact between the continuous and internal phase and is most thermodynamically favourable. Assuming uniform droplet diameter of perfect spheres, the maximum volume fraction of the internal phase 74% (Cameron and Sherrington, 1996; Tai et al., 2001). Emulsions with an internal phase exceeding 74% total volume are called high internal phase emulsions (HIPEs). The spherical droplets become deformed into polyhedra and the continuous phase is compressed into thin films at the interface (Pal, 1999). The rheological properties change dramatically in HIPEs. HIPEs exhibit high storage modulus and yield stress under low shear, so droplet deformation is insufficient to result in bulk flow. Under high shear when the yield stress is exceeded, the emulsion changes from displaying elastic to viscous behaviour (Lee, 2006). These properties arise from the combined effect of some independent variables (internal phase volume fraction) and some dependent variables (interfacial tension, droplet size and range of droplet size).

Measurement and refinement of droplet size is therefore an important consideration in emulsion formulation. The method is important to ensure that the emulsion is not distorted during measurement attempts. Application of emulsions to microscope slides allows excellent imaging and visualisation of emulsion decay, but the hydrophilic or phobic nature of the slide alters the emulsion at the interface and changes droplet size and dispersity.

Light scattering is a commonly used technique to measure droplet size in emulsions and other dispersions and is well described (International Organization for Standardization, 2009; United States Pharmacopoeia, n.d.).

The Turbiscan LAB Analyser uses static multiple light scattering to measure particle size. The principle advantage of this instrument is the capability to analyse HIPEs up to 95% internal volume fraction without

dilution (Abismaïl et al., 2000). It uses data collected from a pair of sensors to record both backscattered and transmitted light at incremental heights of a sample-containing cuvette. Transmitted light is defined as the ratio of the intensity of light entering (I_0) and exiting (I) a sample medium:

$$T = \frac{I}{I_o} \qquad \text{(eq. 2)}$$

The backscattered light (BS) detected by the Turbiscan is inversely proportional to l^*, the mean free path of a photon travelling in a dispersion:

$$BS = \frac{1}{\sqrt{l^*}} \qquad \text{(eq. 3)}$$

From Mie theory, l^* is proportional to the mean diameter (d) and inversely proportional to the volume fraction of dispersed phase droplets (Φ):

$$l^*(d, \Phi) = \frac{2d}{3\Phi(1-g)Q_s} \qquad \text{(eq. 4)}$$

Mie theory is a solution to Maxwell's equations that, applied to emulsions, describes scattering of light by homogenous spherical particles (dispersed phase) of a different refractive index to that of the surrounding medium (continuous phase) (Acharya, 2017). The Turbiscan software enables computation of mean particle diameter given the volume fraction and the refractive indices of both the dispersed (internal) and continuous phases.

The principles of Turbiscan measurement come from Mie Theory and Beer-Lambert law (eq. 5).

$$A = \varepsilon \text{ x } b \text{ x } c \qquad \text{(eq. 5)}$$

where A is the absorbance (dimensionless), ε is the wavelength-dependent molar absorptivity coefficient ($M^{-1}cm^{-1}$), b is the path length (cm), and c is the sample concentration (M). Absorbance is related to transmitted light as follows:

$$A = -\log_{10} T \qquad \text{(eq. 6)}$$

While Mie Theory accounts for light scattering in a dispersion, Beer-Lambert law relates the absorbance and concentration of the sample medium. Together, they describe light travelling through a sample of mono-disperse spheres through an absorbent medium.

However, there are some limitations to Beer-Lambert law that translate to instrument limitations and should be considered during sample analysis. At high concentrations (0.01 M) Beer-Lambert law deviates from linearity due to the close arrangement of molecules. This proximity results in increased scattering,

fluorescence, changes in refractive index and changes in the absorbance coefficients due to electrostatic interactions between molecules.

Some particle sizing instruments require dilution of samples to obtain accurate measurements in order to maintain linearity of Beer-Lambert law. Given the unique properties of HIPEs, dilution of these emulsions is not desirable in case it affects the measurement.

Static multiple light scattering (fig. 1) offers a method of analysing real-time particle size and migration and the change over time. The method is not intrusive and does not require dilution and so was ideal for studying stability of high internal phase emulsions (up to 95% v/v dispersed phase).

EXPERIMENTAL PROCEDURES

Materials

Tween® (20, 40, 80), Tergitol™ (15-S-7, 15-S-9, 15-S-15), Triton™ (X45, X100, X102, X114, X165, X405; X100 reduced, X114 reduced), Brij® (58, O20), decane and MES hydrate and sodium chloride were purchased from Sigma Aldrich. Brij® O10 was obtained from Croda International (Table 1).

MES/NaCl (25 mM/150 mM) was dissolved in water and adjusted to pH 7.4. This formed the aqueous phase for emulsions. All tested were performed at 37°C.

Preparation of emulsions

Stock solutions of surfactants were prepared in 7 ml polystyrene bijou by dispersing 0.1% (v/v) surfactant in decane so that surfactant scaled with oil fraction. These stock solutions were shaken briefly to disperse the surfactants before adding the deionised water. 4 ml mixtures were prepared in triplicate for each surfactant at various oil fractions (50, 60, 70, 80, 90% v/v oil-surfactant). Each sample was vortexed for 1 minute using WhirliMixer™ (Fisherbrand) to homogenise immediately prior to stability measurements.

Turbiscan stability measurements

3 ml of the sample was pipetted into a borosilicate glass cuvette, taking care to maintain a clean meniscus, and analysed using Turbiscan™ LAB Analyser (Formulaction, Toulouse, France) scanning every 30 seconds for a total of 15 minutes.

Turbiscan stability index (TSI) was plotted for each surfactant as a function of oil fraction in the emulsion preparation, HLB, or time. Lower TSI indicates less change in the transmitted light, or less change in particle size and position.

The oil fraction at the lowest TSI after 15 minutes was identified as the 'oil carrying capacity' (OCC) of that surfactant. Further oil/buffer/surfactant mixtures were prepared at 5% oil fractions either side of this minimum (i.e. an initial minimum of 70% oil fraction would be tested then at 65% and 75% oil fraction).

Refractive index

Refractive index of the MES/NaCl buffer was measured using an Abbe 60/HR refractometer with W type prism and sodium lamp. Entering the refractive index of the aqueous and oil phases, along with the respective volume fractions in each case, to the Turbisoft software enables generation of an estimate of dispersed particle phase over time.

The refractive indices of the decane and MES/NaCl buffer were recorded as 1.409 and 1.335, respectively.

The transmission level of the continuous phase was set at 59.64 from the t=0 reading of the MES/NaCl in the Turbiscan.

Particle sizing

Particle size was determined using Turbisoft software using optical parameters. The refractive index of both the oil and aqueous phases was measured in triplicate using the Abbe 60/HW refractometer with W prism. Transmission level was determined by scanning a continuous phase control (MES/NaCl buffer) with the Turbiscan™. Volume fraction was equal to the amount of decane (internal phase) in each emulsion, ranging from 45% to 90% v/v.

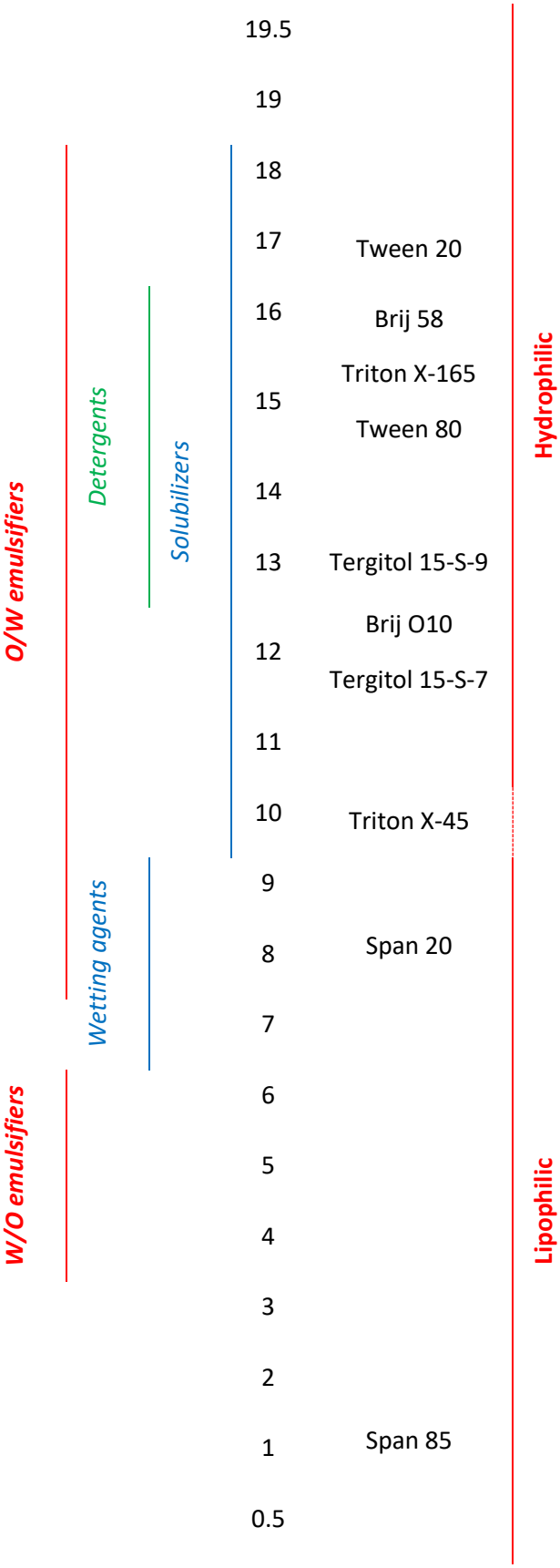
19.5
19
18
17
Tween 20
16
Brij 58
Triton X-165
15
Tween 80
14
13
Tergitol 15-S-9
Brij O10
12
Tergitol 15-S-7
11
10
Triton X-45
9
8
Span 20
7
6
5
4
3
2
1
Span 85
0.5
O/W emulsifiers
W/O emulsifiers
Detergents
Solubilizers
Wetting agents
Hydrophilic
Lipophilic

Table 1: HLB scale of surfactants (adapted from the ICI Americas guide 'The HLB System' (ICI Americas, Inc., 1984)). The surfactants with the highest and lowest HLB from those tested are given for each family.

Surfactant		HLB	Linear formula	Skeletal formula
Tergitol	15-S-7	12.1	$C_{11\text{-}15}H_{23\text{-}31}O(CH_2CCH_2O)_7H$ *C11-15 pareth-7*	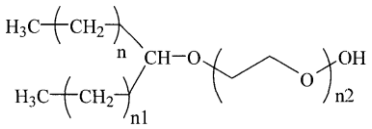
	15-S-9	13.3	$C_{11\text{-}15}H_{23\text{-}31}O(CH_2CCH_2O)_9H$ *C11-15 pareth-9*	
	15-S-15	15.4	$C_{11\text{-}15}H_{23\text{-}31}O(CH_2CCH_2O)_{15}H$ *C11-15 pareth-15*	
Tween	20	16.7	$C_{58}H_{114}O_{26}$ *Polyethylene glycol sorbitan monolaurate*	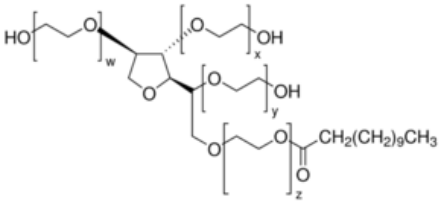
	40	15.6	$C_{22}H_{42}O_6.(C_2H_4O)_n$, n= ~20 *Polyoxyethylene sorbitan monopalmitate*	
	80	15	$C_{64}H_{124}O_{26}$ *Polyethylene glycol sorbitan oleate*	
Brij	O10	12.4	$C_{18}H_{35}(OCH_2CH_2)_nOH$ *Polyoxyethylene (10) oleyl ether*	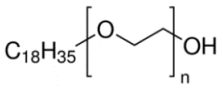
	O20	15	$C_{18}H_{35}(OCH_2CH_2)_nOH$ *Polyoxyethylene (20) oleyl ether*	
	58	15.7	$C_{16}H_{33}(OCH_2CH_2)_nOH$ *Polyoxyethylene (20) cetyl ether*	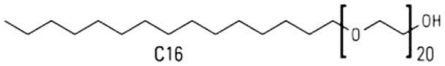
Triton	X-45	9.8	$(C_2H_4O)_n\ C_{14}H_{22}O$, n = ~5 *Polyethylene glycol 4-tert-octylphenyl ether*	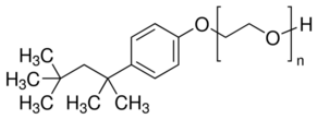
	X-100	13.4	t-Oct-C_6H_4-$(OCH_2CH_2)_nOH$, n= 9-10 *Polyethylene glycol tert-octylphenyl ether*	
	X-102	14.4	$(C_2H_4O)_n\ C_{14}H_{22}O$, n = 12 *Octylphenol ethoxylate*	
	X-114	12.3	$(C_2H_4O)_n\ C_{14}H_{22}O$, n = 7-8 *Polyethylene glycol tert-octylphenyl ether*	
	X-165	15.5	$(C_2H_4O)_n\ C_{14}H_{22}O$, n = 16 *Octylphenol ethoxylate*	
	X-405	17.6	$(C_2H_4O)_n\ C_{14}H_{22}O$, n = 35 *Polyoxyethylene (40) isooctylphenyl ether*	

Table 2: Group A ('main') commonly used industrial surfactants studied, arranged by family and HLB.

Surfactant		HLB	Linear formula	Structure
Tergitol	TMN-6	13.1	$C_{11\text{-}15}H_{23\text{-}31}O(CH_2CCH_2O)_7H$ *Polyethylene glycol trimethylnonyl ether*	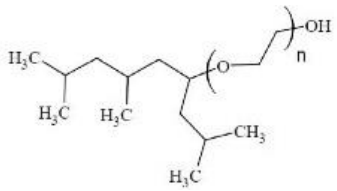
	TMN-10	14.4	$C_{11\text{-}15}H_{23\text{-}31}O(CH_2CCH_2O)_9H$ *Polyethylene glycol trimethylnonyl ether*	
	NP-10	13.2	$C_9H_{19}.C_6H_6.(OCH_2CH_2)_nOH$ *Nonylphenol ethoxylate*	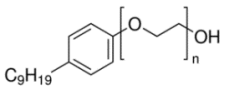
Triton	X-100 reduced	9.8	$(C_2H_4O)_n\ C_{14}H_{22}O$, n = ~5 Polyethylene glycol 4-tert-octylphenyl ether	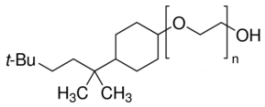
	X-114 reduced	13.4	t-Oct-C_6H_4-$(OCH_2CH_2)_n$OH, n= 9-10 Polyethylene glycol tert-octylphenyl ether	
	N-101 reduced	14.4	$(C_2H_4O)_n\ C_{14}H_{22}O$, n = 12 Octylphenol ethoxylate	
Ecosurf	EH-9	12.5	Ethylene oxide-propylene oxide copolymer mono(2-ethylhexyl) ether	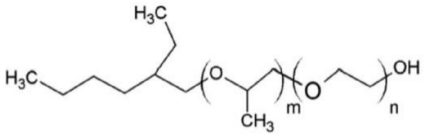

Table 3: Group B ('alternative') surfactants studied, arranged by family and HLB. These surfactants were segregated for their branched structure (Ecosurf, Tergitols) or as being reduced forms of equivalent 'main' surfactants (see Table 2) (Tritons).

RESULTS & DISCUSSION

Stability of emulsions at increasing oil fraction

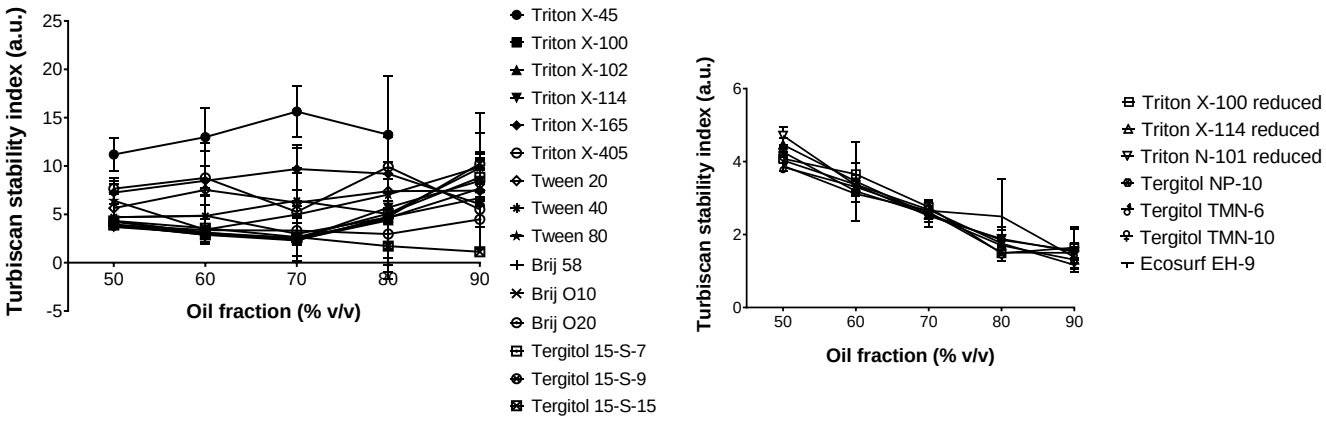

Fig. 2: Stability of emulsions stabilised with 0.1% (v/v) surfactant at increasing oil fractions. Stability (TSI) was measured at 15 minutes after emulsification; lower TSI indicates higher stability. **[A]** 'main' surfactants are traditional options; **[B]** 'alternative' surfactants differ in that they are reduced or branched chain surfactants. Emulsions were tested in triplicate.

Surfactants studied can be divided into two distinct groups (figs. 2A and 2B) based on pattern of stability with increasing oil fraction. Group A (table 2) show maximal stability at or below 70% oil fraction. There was no common trend in stability with increasing oil fraction at fixed surfactant concentration (0.1% v/v). However, the difference in stability of emulsions at each oil fraction was significantly different between different surfactants ($P<0.0001$) (fig. 2A).

Group B (table 3) show increasing stability with increasing oil fraction, even into the HIPE regime above 74% oil fraction.

The TSI of emulsions stabilised with Triton X-45 (HLB 9.8) increased with each step change in oil fraction, indicating reduced stability with increased oil volume fraction. The surfactant HLB was below the required HLB of the decane oil phase (HLB 10-13) so the surfactant provided poor emulsion stability. As oil fraction increased, the surfactant was dispersed over greater surface area and stability further reduced. At 80% oil fraction, the TSI reduced – but stability also reduced. This discrepancy arises from the Turbiscan measurement principles. TSI is a kinetic measurement and relies on the differential light transmission/backscattering between each scan. Samples that decay too quickly – with the most rapid droplet deformation occurring before the first time point – register a lower TSI as a result. TSI measurements for less stable systems were always considered alongside bottle stability test observation.

The other surfactants – in the HLB range 12-17 – show a different pattern of stability with increasing oil fraction. Stability increased (lower TSI) as oil fraction increased up to a certain point, after which stability reduced, often rapidly. This behaviour is characterised by a U-shaped curve with the minimum representing the optimum oil fraction for emulsion stability with each surfactant – the “oil carrying capacity” of the surfactant.

Group B surfactants (table 3), such as reduced Tritons and branched Tergitols, showed a very strong pattern of increased stability (reduced TSI) with increasing oil fraction that continues into the HIPE regime ($P<0.0001$) (fig. 2B).

The difference in stability in branched Tergitols (TMN-6, TMN-10) compared to Tergitol T-S-7, -9 and -15 suggests a structural contribution, but the mechanism is unknown.

Among Tergitols, the conventional surfactants span a wider HLB range (Table 2) than the branched variants (Table 3). Both Tergitol T-S-9 and Tergitols TMN-6 and NP-10 have HLB ~13, matching the experimentally determined required HLB range for decane. These results show a much greater dependence on other surfactant properties, such as structure, rather than HLB.

The pattern of behaviour is different with other classes of surfactant (fig. 2B). The oil carrying capacity metric is a method of distinguishing these classes of surfactant and identifying those suitable for stabilising HIPEs as opposed to lower internal phase emulsions (oil fraction <74%).

Stability of emulsions made with different surfactant families, at different oil fractions

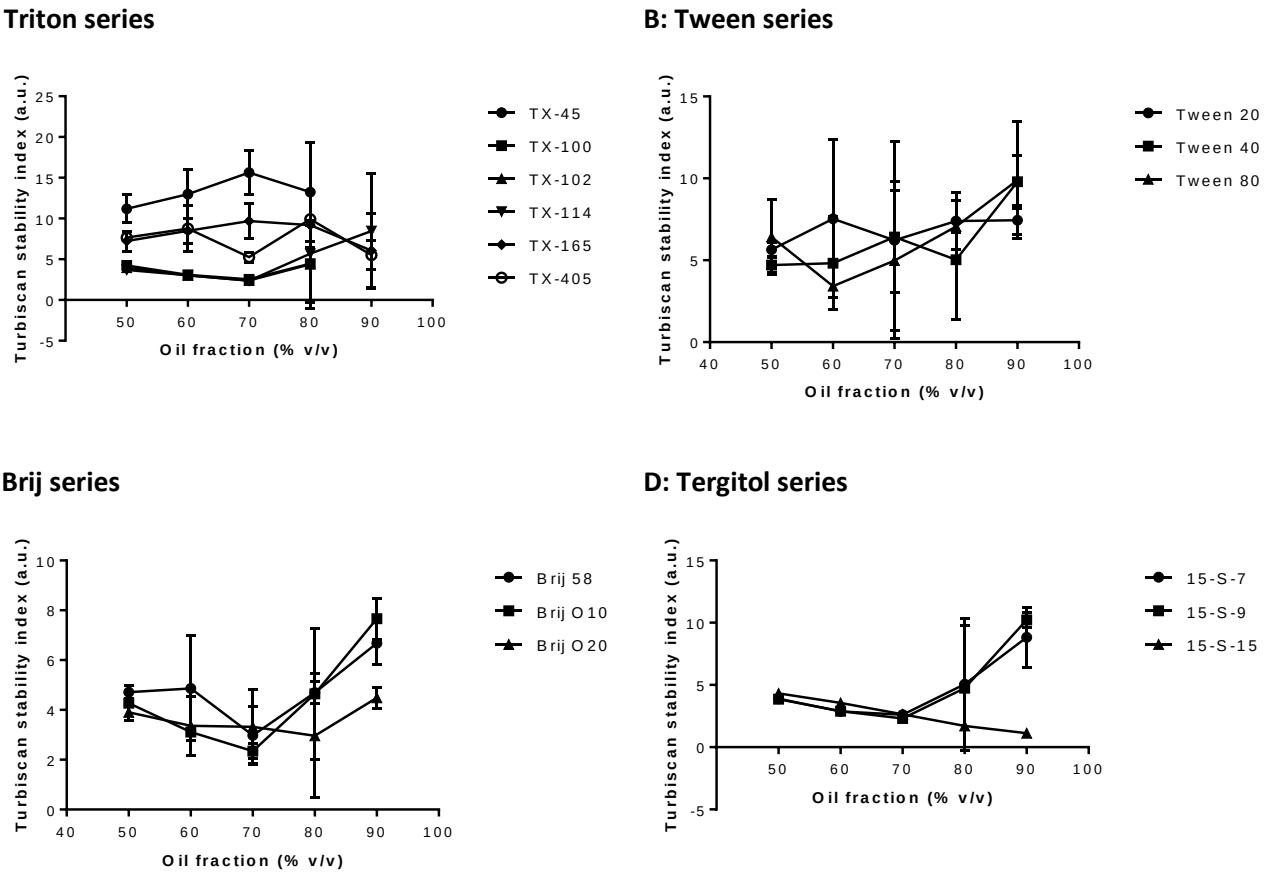

Fig. 3: Stability of emulsions stabilised with 0.1% (v/v) surfactant at increasing oil fractions. Stability (TSI) was measured at 15 minutes after emulsification; lower TSI indicates higher stability. Emulsions are grouped by the family of surfactants used in each case: [**A**] Triton; [**B**] Tween; [**C**] Brij; [**D**] Tergitol. Graphs show mean and standard deviation; n=3.

Among the surfactants in Fig 2A, the different surfactant families show different patterns of behaviour with increasing oil fraction. Emulsions containing Triton surfactants X-100, X-102, X-114 and X-405 all display maximum stability at 70% oil fraction (fig. 3A). With TSI<3, TX-102 and TX-114 were particularly effective at 70% v/v oil fraction, though they are less effective at higher or lower oil: aqueous compositions. The use of different Triton surfactants was highly influential in the stability of the resultant emulsion (P<0.0001). Triton

X-45 shows a symmetrically opposite pattern of behaviour, arising from its low HLB, beneath the o/w emulsifying regime.

Triton X-165 also failed to adequately stabilise emulsions in this test, despite an appropriate HLB (15.5). It should be noted that method (vortex) and time (1 minute) of mixing was standardised for the sake of direct comparison. However, vigorous shaking of Triton X-165 containing mixtures by hand did result in emulsification with good stability. Emulsification of X-165 mixtures was characterised by sudden transition to a highly viscous, opaque phase which gradually incorporated all liquid on further shaking. The extreme viscosity makes emulsification by vortex impractical; the vortex separates the phases rather than incorporating them to create an homogenous emulsion. With shear mixing or vortex, the denser viscous phase sank and did not incorporate with the less dense decane. Shaking lidded containers by hand forcibly reincorporated the oil phase and promoted further mixing until total emulsification was achieved. While this mixing effect was observed to with many surfactants, it was most pronounced with Triton X-165.

Considering stability by family, where hydrocarbon tail length is constant, indicates that variation in HLB is dependent on variable carbon number of the hydrophilic head group rather than reduced lipophilic chain length.

The Tween surfactants had comparable HLB (16.7, 15.6, 15) to Tritons but displayed poorer emulsion stabilisation. OCC of Tween 40 and 80 were 60%, but TSI>3 indicated poor stability even at optimum oil fraction. Tween 20 failed to adequately stabilise emulsions at any oil fraction; reduction in TSI at 80% oil was due to almost instantaneous phase separation after mixing. Most separation and droplet deformation occurred before the first scan started.

All three Brij surfactants tested behaved comparably (fig. 3C) despite the range of HLB (15.7, 12.4, 15 for 58, O10 and O20, respectively). Brij 58 and O10 displayed OCC of 70%, while Brij O20 emulsions were most stable at 80% oil. Notably, O20 emulsions displayed stability (TSI<3) across a range of oil fractions, with 60-80% v/v internal phase systems all measuring stability with TSI<3.

Tergitols 15-S-7 and 15-S-9 showed almost identical emulsion stability (fig. 3D) with OCC 70% and minimum TSI of 2.6 and 2.1 respectively (2 sf). The general pattern of behaviour was similar to that of Brij surfactants, with rapid destabilisation (increase in measured TSI) above the OCC. Tergitol 15-S-15 emulsions also behaved very similarly to T-S-7 and T-S-9 emulsions at lower oil fractions below the HIPE regime (fig. 3D). However, in high internal phase systems (>74%) T-S-15 emulsions showed a continued improvement in stability rather than the expected rapid emulsion breakage (**, P=0.0032). OCC was 90%, with TSI=1.1 (2 sf) indicating extremely good stability. T-S-15 is a larger molecule than either of the others, but the additional -CH may be shared between either of the 3 branches in any ratio so the relative size and shape change may be symmetrical or

distorted. Knowledge of the chain distribution would be useful in determining whether surfactant length or bulk was more effective at stabilising HIPEs.

Effect of surfactant HLB on stability

HLB is a qualitative measure of the contribution of the lipophilic (hydrocarbon tail) and hydrophilic (group group) of surfactants. Plotting TSI against surfactant HLB (fig. 4A) shows that surfactants across a range of HLB values – 12 to 15.5 – generated stable emulsions with TSI<3. The required HLB of the oil should not be considered as a precise figure, but rather as a guide with tolerance above and below depending on the specific surfactant used.

Triton X-114 and Brij O10 (HLB 12.4) and Tween 80 and Brij O20 (HLB 15) are surfactants with identical HLB but with differing TSIs in the test emulsions (fig. 4B; fig. 4C). Triton X-114 and Brij O10 are structurally similar molecules. Although the degree of stability is increased in emulsions containing Brij O10, the OCC and pattern of behaviour across all oil fractions is comparable (P=0.844).

However, Tween 80 and Brij O20 show different stability patterns in emulsions with increasing oil fractions. Tween 80 has OCC of 80% internal volume whereas Brij O20 has OCC 80%; the level of stability is significantly greater in emulsions with Brij O20 (**, P=0.0024) and the stability tolerance is greater across all oil fractions. In contrast, Tween 80 emulsions dramatically reduce in stability away from the OCC composition. In this case, the Tween and Brij molecules have very different structures (Table 2).

The Tween surfactants head groups are large and bulky with limited rotation, whereas the Brij molecules are much narrower and almost linear. This may mean that Brij is able to pack more closely at the interface with less steric repulsion, enabling more effective coverage at the droplet surface and conferring enhanced stability.

Separating the results by surfactant family (fig. 5) highlights the difference in behaviours between each surfactant family – likely, some form of structural contribution. Tritons (fig. 5A) show greatest stability between HLB 12-14, with stability reducing above this value. However, Tergitols with HLB 12-15.5 display emulsion stability with lower TSI at higher HLBs (fig. 5D).

Tweens (fig. 5B) also have higher HLBs but provided least emulsion stability across all surfactants tested (excepting Triton X-45, HLB 9.8, which is below the accepted HLB range for o/w emulsifying).

Brijs tested spanned a range of HLBs but despite this, showed similar stabilising ability at each oil fraction (P=0.0512).

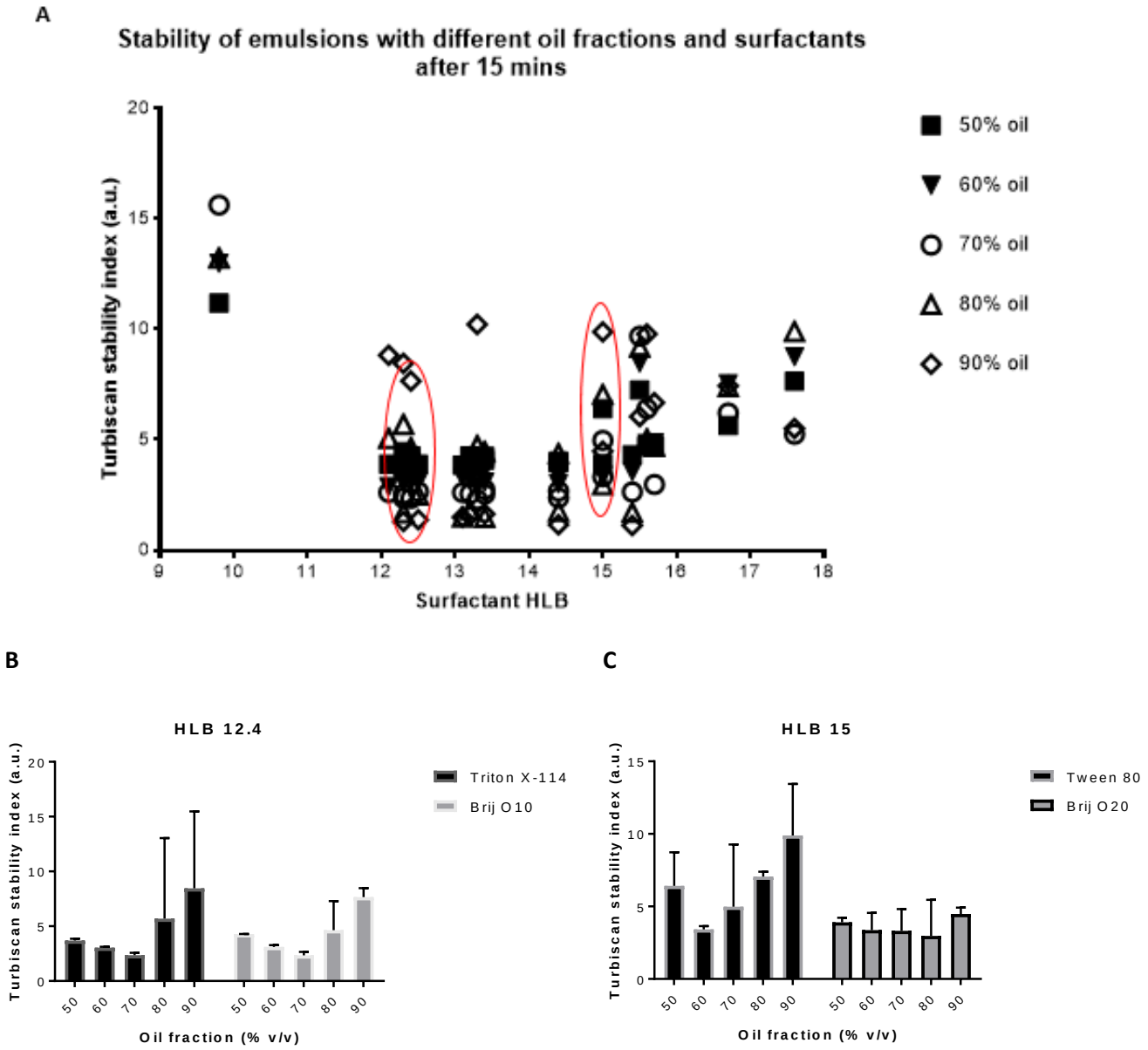

Fig. 4: Effect of surfactant HLB on emulsion stability. Stability (TSI) was measured at 15 minutes after emulsification. All emulsions were made with 0.1% (v/v) surfactant. **[A]** shows the stability of emulsions made with Tritons, Tweens, Brijs or Tergitols as previously. Results at HLB 12.4 and 15.0 are circled as these have overlap with two different surfactants (illustrated separately in **[B] and [C]**. Emulsions were prepared with 0.1% (v/v) surfactant and increasing oil fractions from 50% to 90% (v/v).

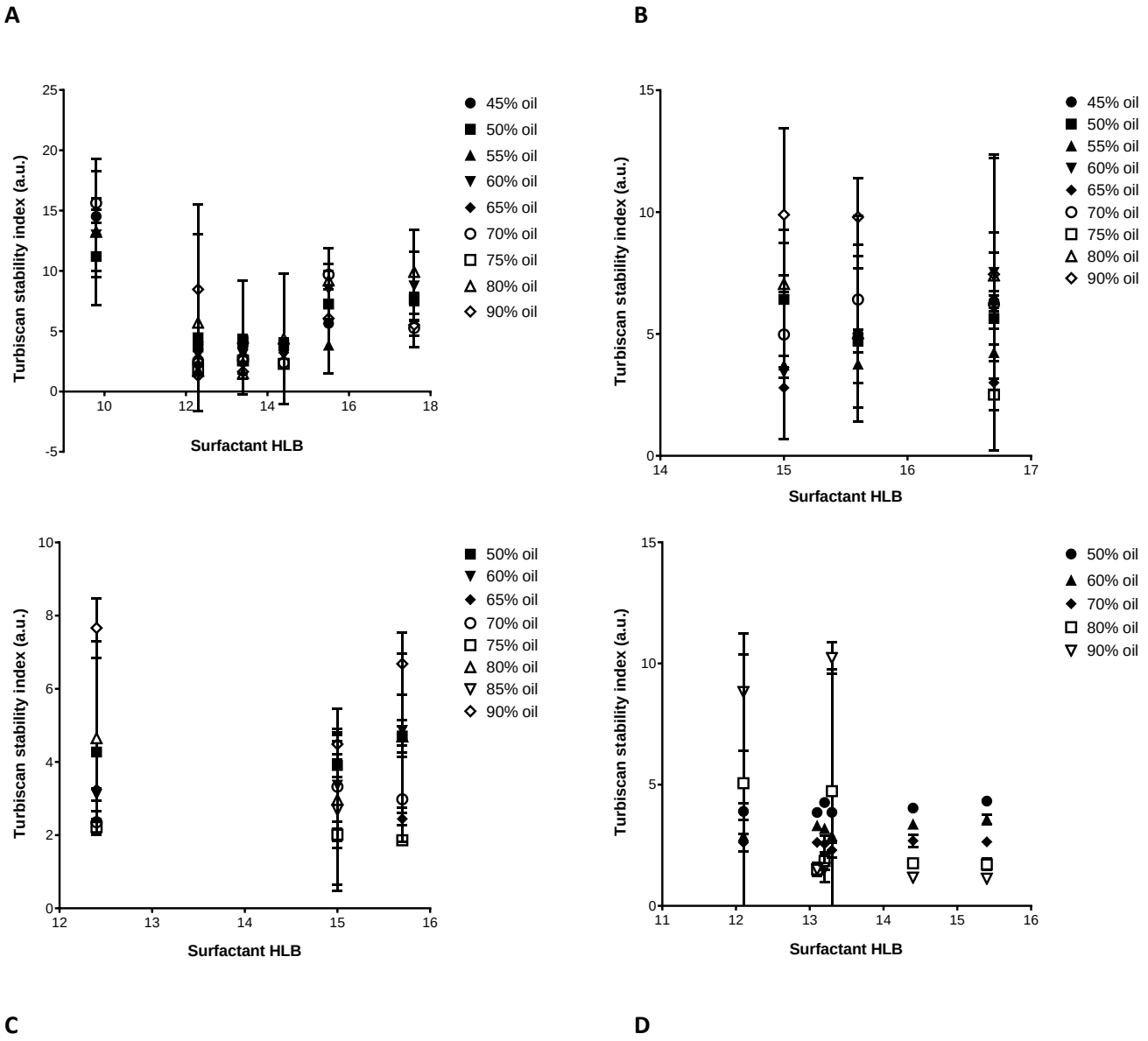

Fig. 5: Effect of surfactant HLB on emulsion stability for emulsions prepared with different families of surfactant. Emulsions were prepared with 0.1% (v/v) surfactant: **[A]** Triton; **[B]** Tween; **[C]** Brij; **[D]** Tergitol, then the stability recorded 15 minutes after mixing in each case.

These results all suggest a significant contribution of the surfactant structure to stability, However, there is no suggestion as to the specific features which work to enhance stability, or why. These numbers do not take into account branching or other conformations. In o/w emulsions, surfactants assemble at the interface and self-orientate with hydrocarbon tails in the dispersed oil phase and hydrophilic head groups in the continuous aqueous phase. Droplet size affects the number of surfactants able to assemble at the interface, with the limiting factor being the circumference and radius of the droplet (limiting tail width and length, respectively).

Droplet size may also, to a small extent, affect the packing from hydrophilic head groups. Smaller droplets have reduced surface area in the dispersed phase. The convex droplet surface creates more space in the continuous phase than in the dispersed one so head group packing would be more affected than hydrophobic tails in the continuous oil phase.

In an attempt to quantify relative contribution head and tail regions, surfactants were arranged by carbon number of the hydrophobic hydrocarbon tail group and hydrophilic head group to determine the effect of the hydrophilic surfactant tail on stability.

Effect of increasing surfactant head group size at increasing oil fraction

Emulsions containing 50%, 60% and 70% v/v oil fraction (those below the HIPE regime) show similar stability behaviour (fig. 6). Stability was generally better in 60% and 70% oil emulsions. The pattern is comparable with the results separated by HLB (fig. 5) but not identical. The stability at 90%, in the HIPE regime, was generally much lower, with the only exceptions being reduced and branched surfactants (Table 3). The tolerance in chain length for stability reduced, with only surfactants with 11-15 carbon tails (Tergitol 15-S-15 and Triton X-10- reduced) achieving suitable stability (TSI<3). However, not all surfactants with this hydrocarbon tail length (or approximate hydrophobic tail: hydrophilic head, expressed by HLB) proved capable of stabilising 90% HIPEs – notably, non-reduced equivalent Tritons.

Effect of increasing hydrocarbon tail length at increasing oil fraction

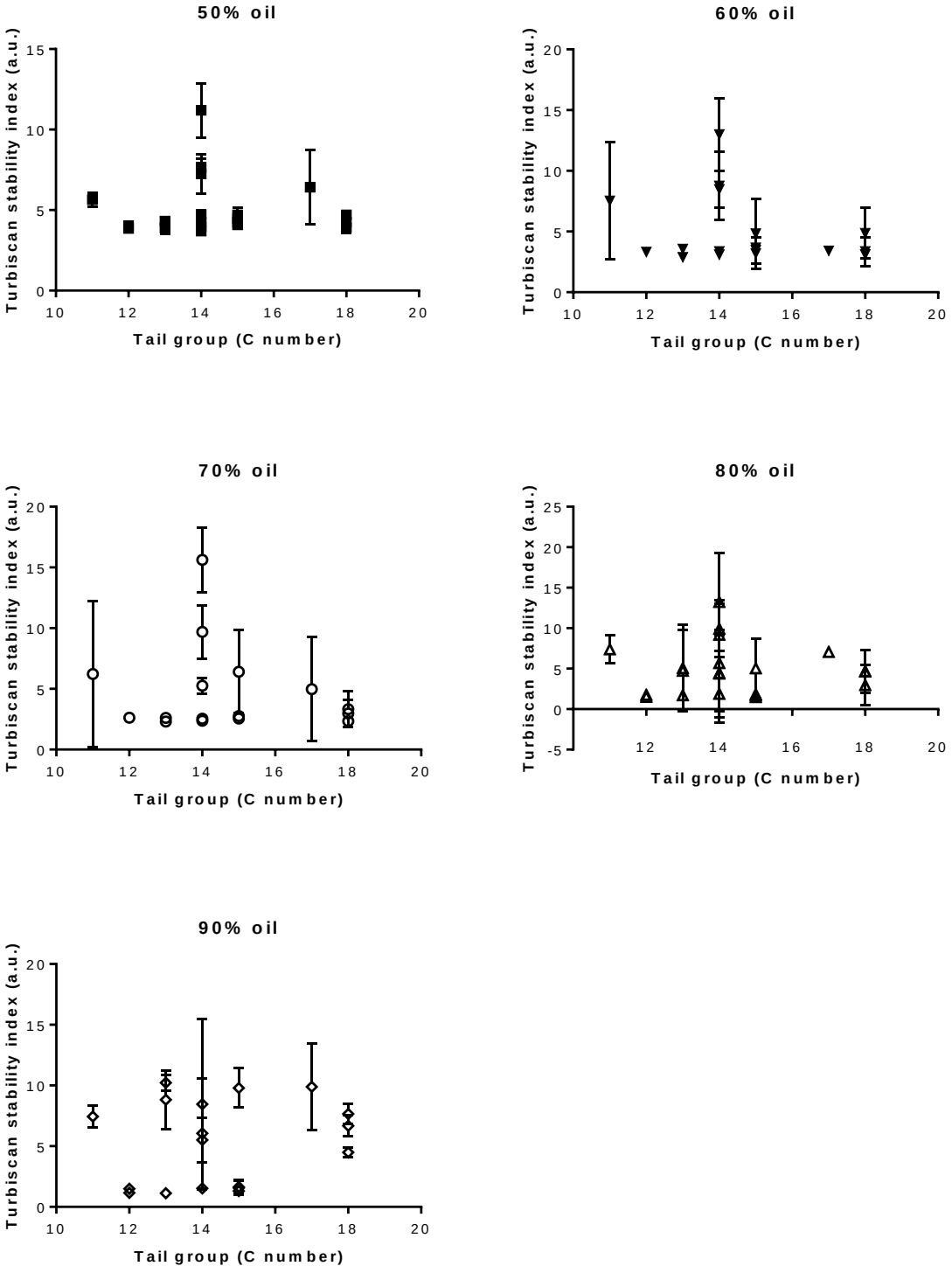

Fig. 6: Effect of surfactant hydrophobic tail length on emulsion stability at increasing oil fractions. Emulsions were prepared with 0.1% (v/v) surfactant and **[A]** 50% oil; **[B]** 60% oil; **[C]** 70% oil; **[D]** 80% oil and **[E]** 90% oil, then the stability recorded 15 minutes after mixing in each case.

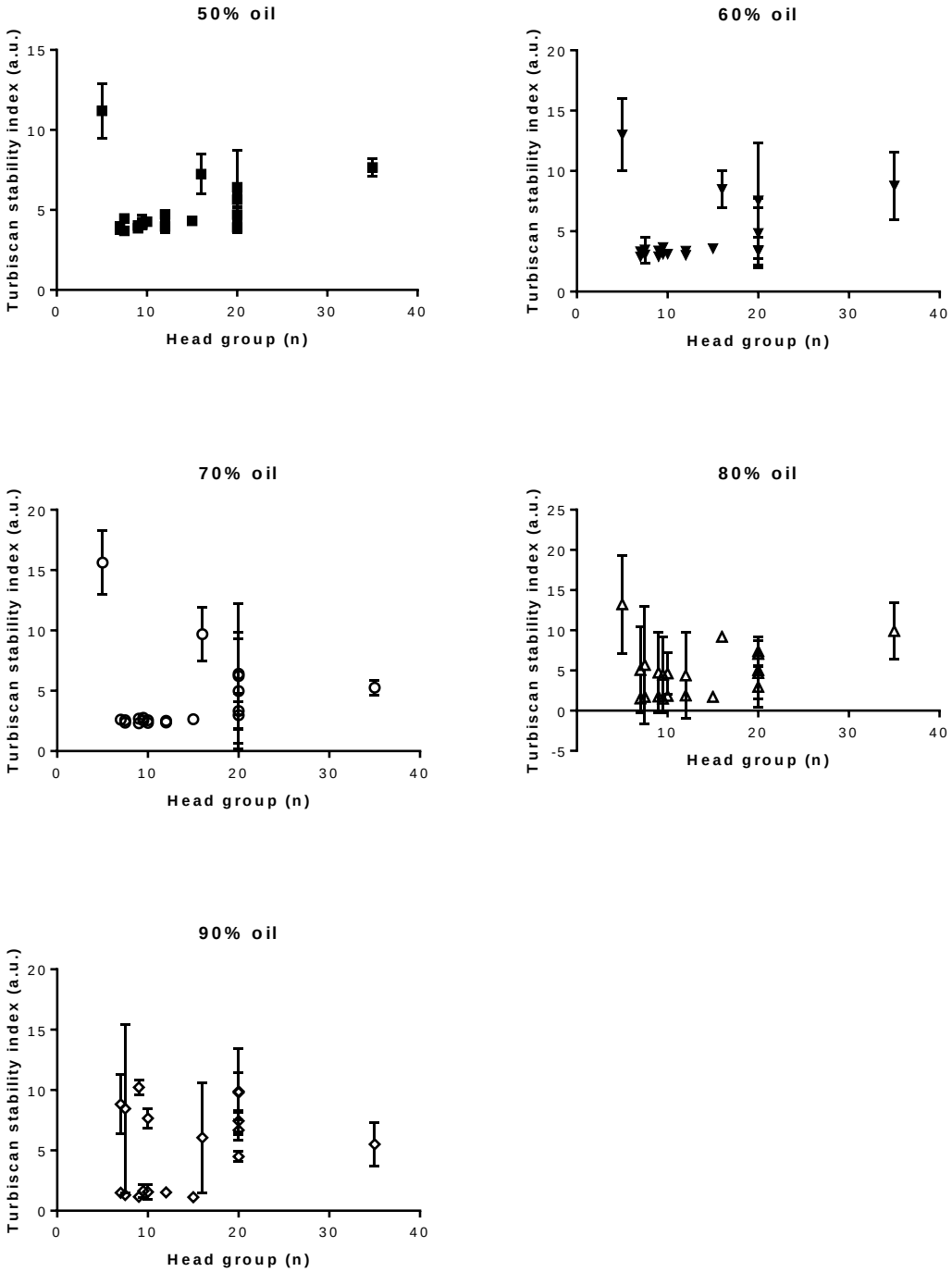

Fig. 7: Effect of surfactant head group size on emulsion stability at increasing oil fractions. Head group size was quantified by number of repeat units (n) such as 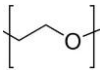

Emulsions were prepared with 0.1% (v/v) surfactant and **[A]** 50% oil; [**B**] 60% oil; [**C**] 70% oil; [**D**] 80% oil and **[E]** 90% oil, then the stability recorded 15 minutes after mixing in each case.

Stability was generally similar across all oil fractions, with surfactants with approximately 9-15 repeated units of the head group having best stability at all oil fractions. Triton X-405 (HLB 17.6) was tested as a significantly larger variant of the other Triton molecules (having 35 POE units rather than the more typical 5-15). Despite having HLB comfortably in the o/w emulsifying range, Triton X-405 emulsions displayed only intermediate stability (TSI~5). Triton X-405 emulsions displayed no variation in stability across any of the oil fractions tested, either above or below the HIPE threshold of 74% internal phase.

Stability with surfactants of 20 carbon head groups

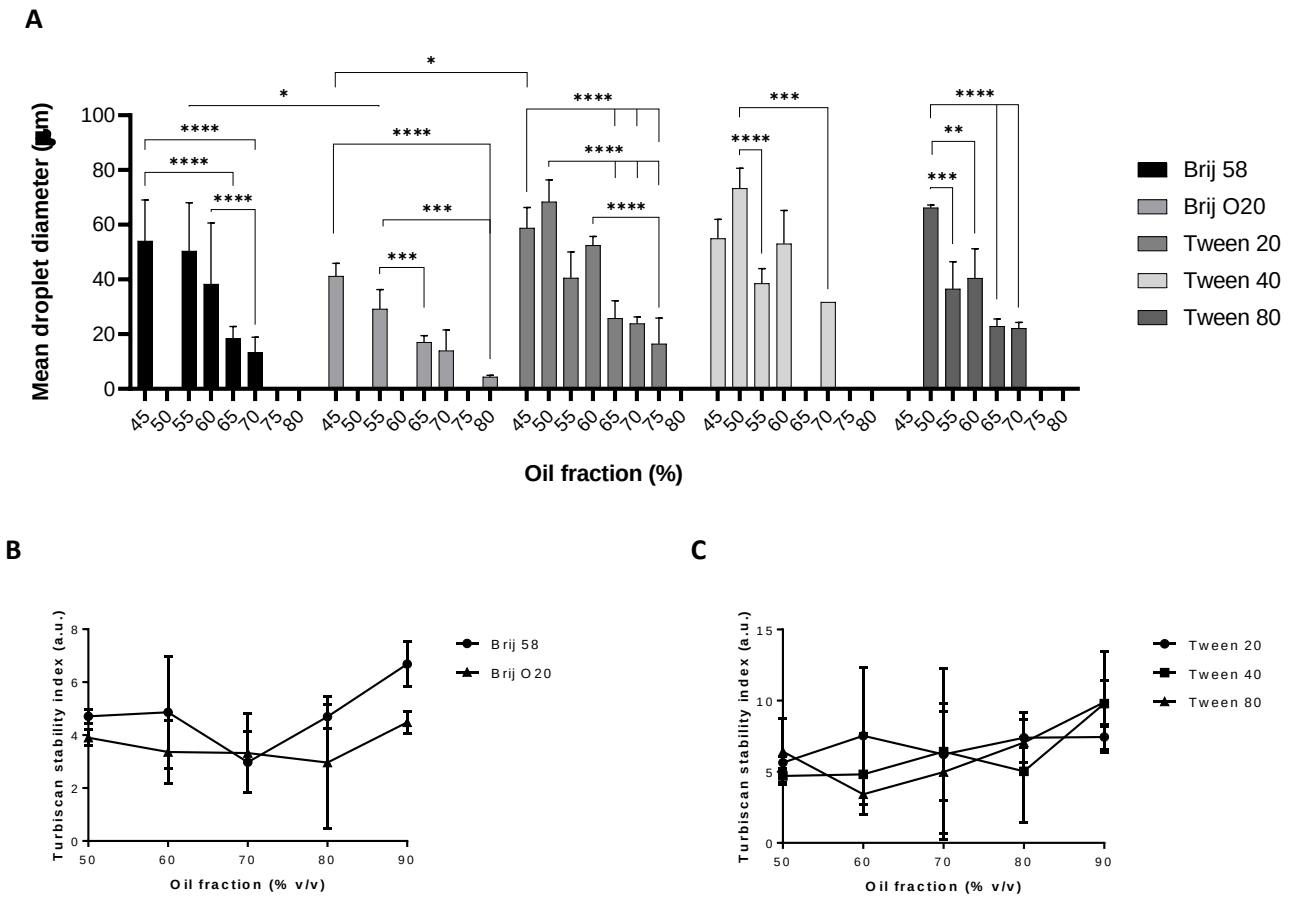

Fig. 8: Effect on emulsion stability of surfactants with 20 POE repeat head group units. Emulsions were prepared with 0.1% (v/v) surfactant and oil fractions from 45% to 80% (v/v). Subset graphs show the same data, split by surfactant family, over a range of oil fractions: **[B]** Brij 58 and Brij O20; **[C]** Tween 20, 40 and 80.

Of the surfactants studied, all Tweens and two of the Brijs had head groups with 20 repeat POE units. Stability was compared within and across these surfactant families with equal head group. Brij molecules are fairly simple and linear, whereas Tweens are much bulkier with the hydrophilic head group comprising four branches of variable length. The distribution of POE around the Tween molecule is therefore significantly different to that with Brij.

While Brij surfactants were more effective stabilisers in the test emulsion system, the five surfactants displayed similar patterns in stability across increasing oil fractions below and in the HIPE regime (fig. 8A).

Brij 58 and Brij O20 (16- and 18-carbon hydrocarbon tails; HLB 15.7 and 15.0 respectively) both showed intermediate emulsion stabilisation below the HIPE regime (fig. 8B). Brij 58 has an OCC of 70% oil fraction and stability reduced above this oil fraction. Brij O20 displayed good stability between 70% and 80% oil fraction, with OCC 80% v/v oil.

The Tween mixtures displayed poor stability, failing to emulsify completely and then rapidly decaying after mixing (fig. 8C). Tween 20 (HLB 16.7) conferred slightly better stability than either Tween 40 (HLB 15.6) or Tween 80 (HLB 15.0, equal to Brij O20).

This again shows a problem with overreliance on the HLB system for surfactant selection, as the highest HLB Tween gave best stability, but the lower HLB Brij (O20) was more effective and had high OCC, despite a difference of 1.7 HLB between the two.

Effect of branching vs straight chain surfactants

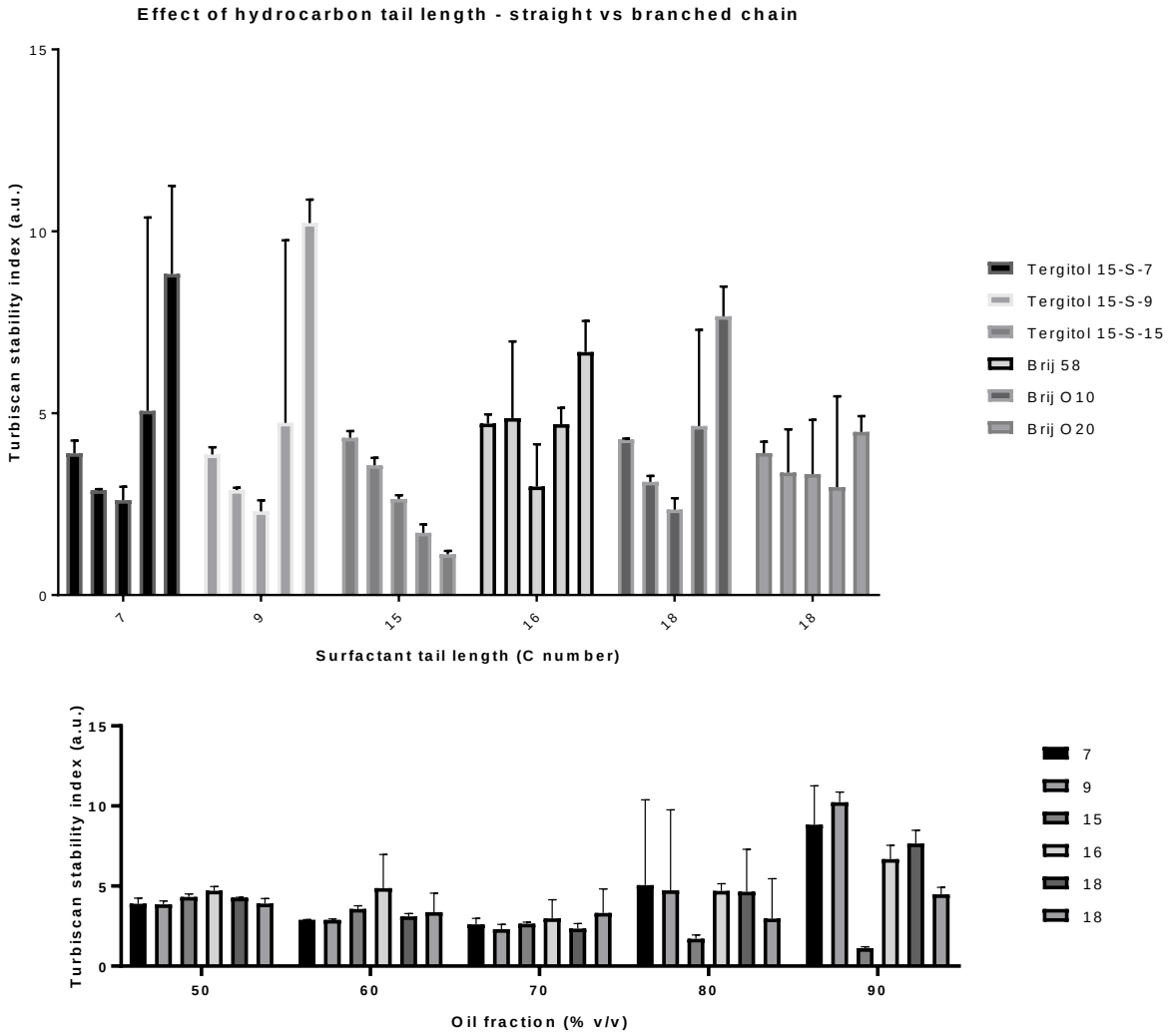

Fig. 9: Effect of surfactant hydrocarbon tail chain length on emulsion stability between straight chain (Brij) and branched chain (Tergitol) surfactants. Stability measurements were recorded 15 minutes after mixing in each case.

Brij surfactants have straight hydrocarbon tails and Tergitol surfactants have two-branched tails (Table 2). Tergitol 15-S-15 is approximately similar in size to the Brijs. The two smaller Tergitols (15-S-7 and 15-S-9) showed intermediate stability up to OCC, OCC at 70% oil, and then reduction in stability in the HIPE regime. The larger Tergitol, T-S-15, also has intermediate stability below the HIPE regime (TSI~3 at 70% oil fraction). Unlike the smaller Tergitols, stability continues to increase with increasing oil fraction into the HIPE range, with OCC at 90% oil. The behaviour is more typical of the bulkier Tergitols TMN-6, TMN-10, NP-10 (Table 3).

The straight chain surfactants of the same approximate size, Brij 58 and Brij O10, also showed intermediate stability below the OCC (70% oil fraction). Above the OCC, in the HIPE range, emulsions with Brij surfactants

reduced in stability such that TSI was higher than the equivalent increments below the OCC. Emulsions containing Tergitol had less of a decrease in stability away from the OCC, possibly due to stabilising effect of the longer hydrocarbon tail.

There may be a critical chain length for stability before the branching effect of the Tergitols has any enhanced stabilising effect in very high oil fraction emulsions. Tree roots, which are only effective anchors if they are deep enough in soil, are a useful analogy. Once they are deep enough, lateral spread will further improve anchoring. Surfactants may require a hydrophobic tail long enough to provide 'anchorage' in dispersed oil before hydrophilic head group size has a significant effect on emulsion stability.

Effect of standard vs reduced surfactants

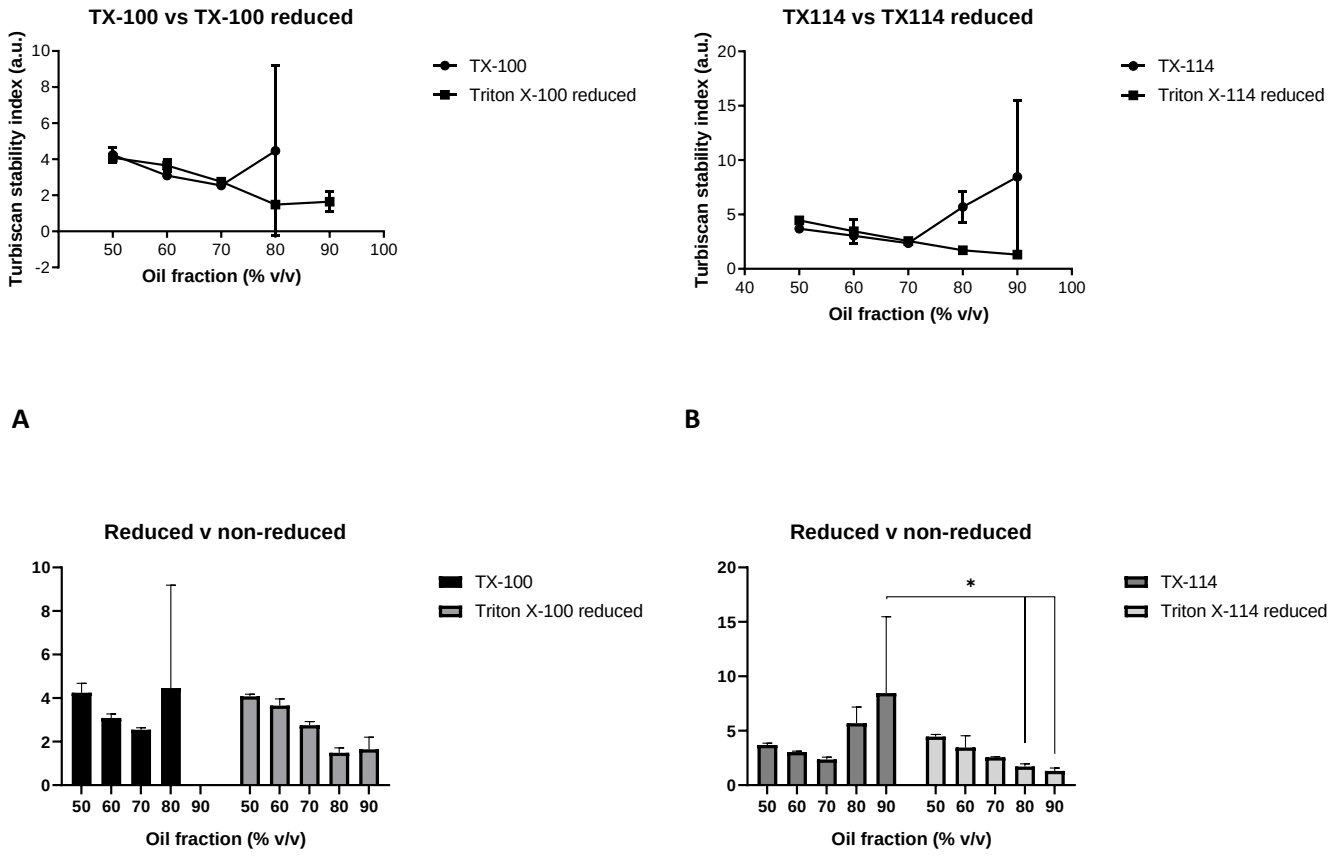

Fig. 10: Emulsion stability with standard and reduced surfactants at increasing oil fractions. [A] Triton X-100 (OCC= 70% oil) and Triton X-100 reduced (OCC= 80% oil); **[B]** Triton X-114 (OCC= 70% oil) and Triton X-114 reduced (OCC ≥ 90% oil).

Effect of conventional vs reduced surfactants

Triton X-100 and Triton X-114 are conventional surfactants (Table 2) and are also available in equivalent reduced forms (table 3), though these are less widely used. The reduced forms differ in that the reduced forms differ in that the head group of non-reduced surfactants is benzene-based, whereas in reduced surfactants it is cyclohexane-based (Tables 2 and 3). Both reduced surfactants displayed improved stability compared to the non-reduced form.

Below their respective OCC, reduced and non-reduced Triton X-100 standard form showed very similar stability, with only a slight deviation at 60% oil fraction (fig. 10A). With TSI between 3 and 4, both surfactants formed and stabilised emulsions for short periods of time. In the HIPE range, emulsion stability varied between the two surfactants. Triton X-100 showed greatest stability (OCC) at 70% oil fraction, below the HIPE range (≥74%, whereas the reduced form had OCC at 80%. This differs from the other 'alternative' surfactants which had OCC at 90% oil fraction, the highest internal volume fraction tested. The mechanism of action of the reduced surfactant may be suppression of instability, rather than promotion of stability at the oil/aqueous interface. The reduced surfactant still showed excellent stability at 90% oil fraction, however. Triton X-100 mixtures did not emulsify at 90% oil fraction and so are not presented.

Triton X-114 and the X-114 reduced behave similarly. 90% emulsions formed with Triton X-114 but stability was poor; in the HIPE range above 74% oil emulsions destabilised quickly within the 15-minute analysis window. As with the Triton X-100/reduced pairing, Triton X-114 and the reduced equivalent showed very similar TSI measurements up to 70%. In all cases, stability was good with TSI<5. Above 70%, stability continued to increase in the reduced surfactant emulsion system with OCC 90%. The actual oil carrying capacity may be greater, but the Turbiscan is limited to analysing emulsions with internal volume fraction ≤95%.

Although the reduced surfactants form more stable emulsions than their non-reduced counterparts, the stability approaching extremely high oil fraction (90% v/v) increased more slowly than other unconventional surfactants, such as Ecosurf or Tergitols (table 3). However, HIPEs can have extremely high viscosity which can impart a physical, as well as chemical, component to resist emulsion breakage. In scenarios where short-term emulsification is required (i.e. templating, where in the internal phase is removed, or transport, where is the internal phase must be recovered efficiently) this could be beneficial. The emulsion could be tuned to have good stability at the desired oil fraction over a particular timeframe, and then destabilise when the emulsion is no longer required and the internal phase needs to be removed.

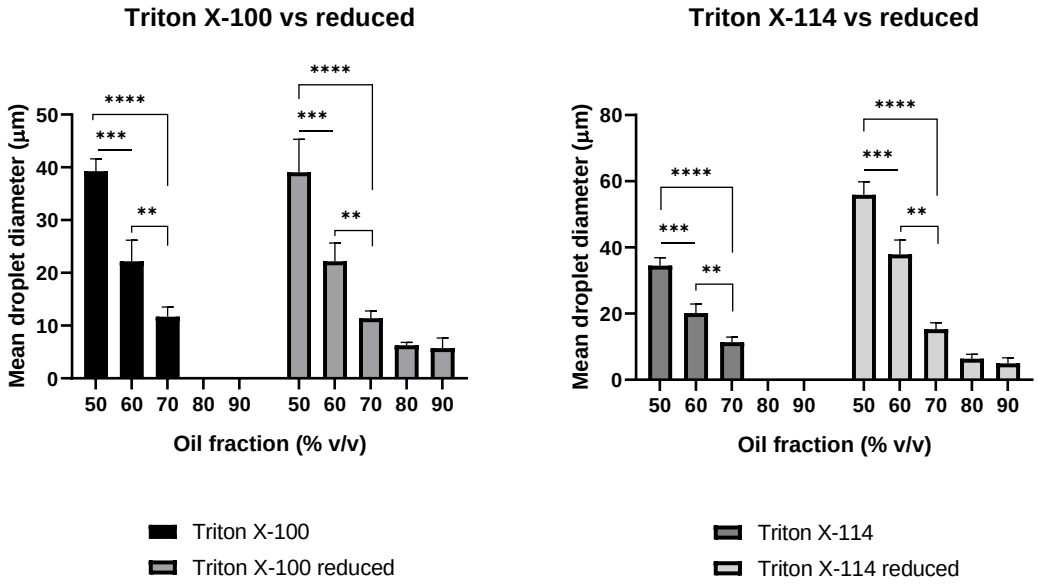

Fig. 11: Particle size of emulsions containing reduced and equivalent non-reduced surfactants at increasing oil fractions. Particle size was calculated in Turbisoft software based on backscattered and transmitted light data and refractive indices of the continuous and dispersed phases. **[A]** Triton X-100 (OCC= 70% oil) and Triton X-100 reduced (OCC= 80% oil); **[B]** Triton X-114 (OCC= 70% oil) and Triton X-114 reduced (OCC ≥ 90% oil).

CONCLUSIONS

The vast range and number of surfactants available makes selection of appropriate surfactants a lengthy and time-consuming task. Commercial protocols like the ICI Guidelines suggest screening surfactants by HLB. However, as demonstrated here and reported elsewhere in the literature, there are many other surfactant attributes which contribute to their efficacy in a given emulsion system.

The HLB metric for surfactant selection is an accessible tool but has limited practical use in selecting surfactants for optimum emulsion stability. Identifying surfactants with appropriate HLB for the oil in the emulsion pre-selects a group of surfactants but within this group, surfactants will display a wide range of stabilising capability. Currently, this can only be determined experimentally.

Emulsion stability is the result of the complex interplay between surfactant structure; method and speed of mixing; salinity and molarity of the aqueous phase; and the density and viscosity (empirical and differential) of the aqueous and the oil phases. No one metric is likely to be powerful enough to adequately describe all the contributing factors. However, a number of tools may be used concurrently to identify and select a number

of candidate surfactants which may then be tested thoroughly to assess practical emulsion stabilising capability in a given system.

The ability to identify the oil carrying capacity, the volume fraction of the internal phase at peak emulsion stability, is a useful tool in emulsion design. It may either be used to select surfactants where a particular oil volume fraction is required, or it may be used to optimise the oil volume fraction for a given surfactant.

Further work is required to elucidate the reasons for the different behaviours of the two classes of surfactant identified here (fig. 2), enabling easier identification of surfactants into one of the two classes of surfactant by OCC behaviour.

ACKNOWLEDGEMENTS

Thanks to Dr. Julian Fells and Prof. Steve Elston of the Department of Engineering Science at the University of Oxford for their assistance with the refractometer.

3.1 APPENDIX

Particle size data

Emulsions were initially analysed using single particle optical sizing (SPOS) using an Accusizer 780 (NICOMP Particle Sizing Systems, Santa Barbara, CA, USA). However, this technique required sample dilution which is not suitable for analysing highly concentrated HIPE oil-in-water emulsions.

Particle size was then determined computationally using Turbiscan results, using a combination of backscattering and transmission data, and the refractive indices of the continuous and dispersed phases. Sizing results for each surfactant family are shown below.

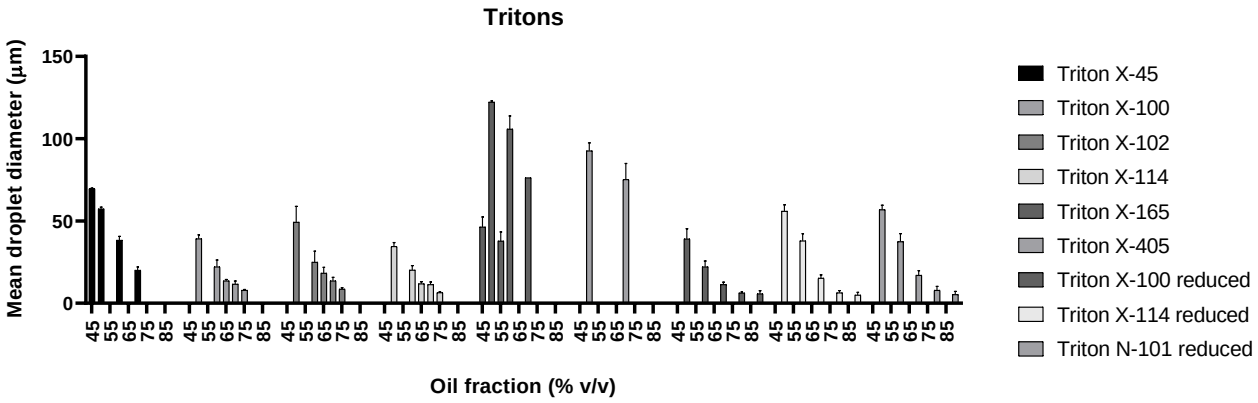

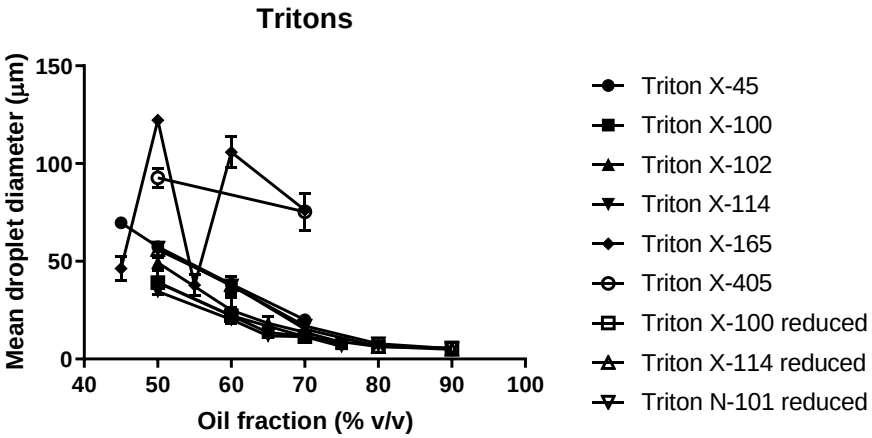

With the exception of emulsions containing Triton X-165, all emulsions showed reducing droplet size with increasing internal phase volume fraction. This effect may be directly attributed to the surfactant as mixing method and rate was common to all samples.

Tweens also showed a general reduction in particle size with increasing oil fraction. This is somewhat counterintuitive given that increasing oil fraction also correlated with reduced emulsion stability which commonly occurs by droplet growth.

The measurement of the very small droplets, smaller than those detected in Triton emulsions, may arise from residual, isolated droplets in the central measurement region after phase separation causing emulsion breakage and clearing.

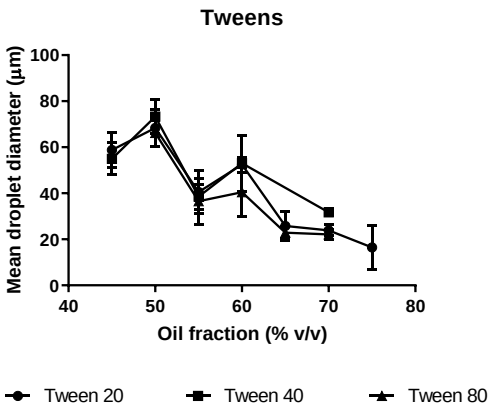

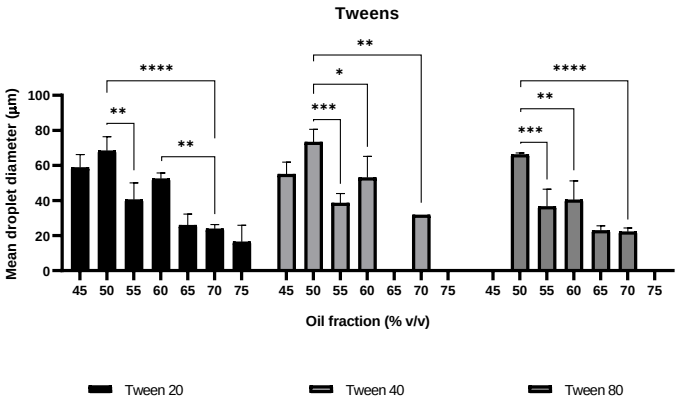

As with other surfactant families, Brij emulsions showed a general reduction in particle size with increasing oil fraction. The larger droplets measured in the 65% oil Brij O10 emulsion (5% below OCC) is likely a genuine measurement, with larger droplets arising from a homogenous and stable emulsion with low tendency to separate during the test period.

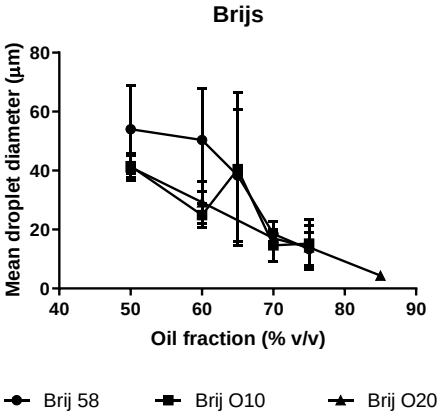

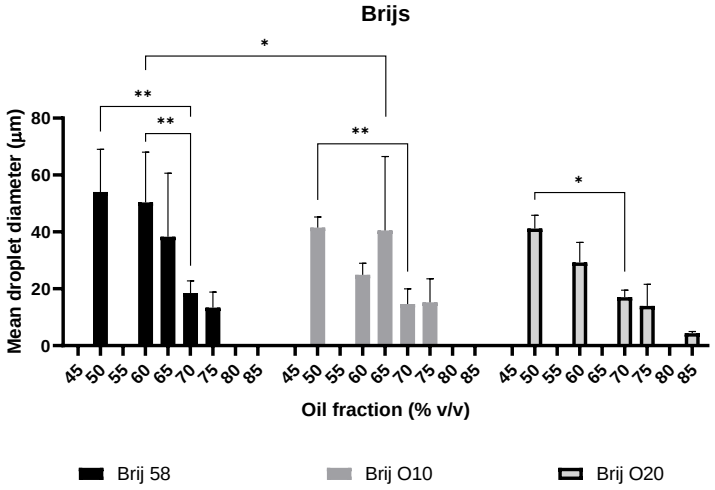

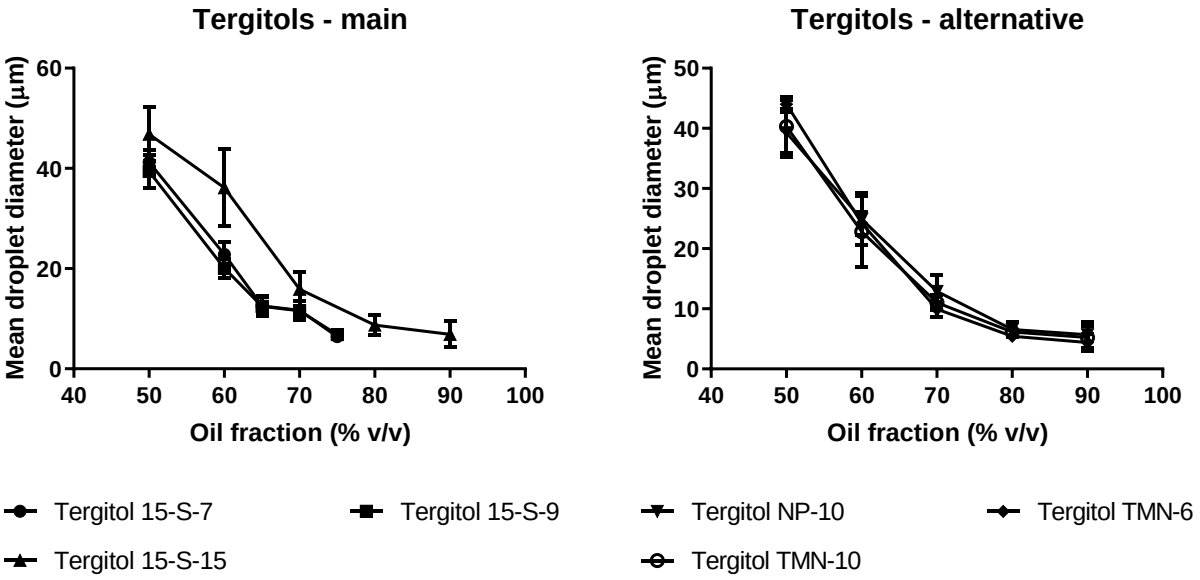
Tergitols - main
Mean droplet diameter (µm)
Oil fraction (% v/v)
Tergitols - alternative
Mean droplet diameter (µm)
Oil fraction (% v/v)
Tergitol 15-S-7
Tergitol 15-S-9
Tergitol NP-10
Tergitol TMN-6
Tergitol 15-S-15
Tergitol TMN-10

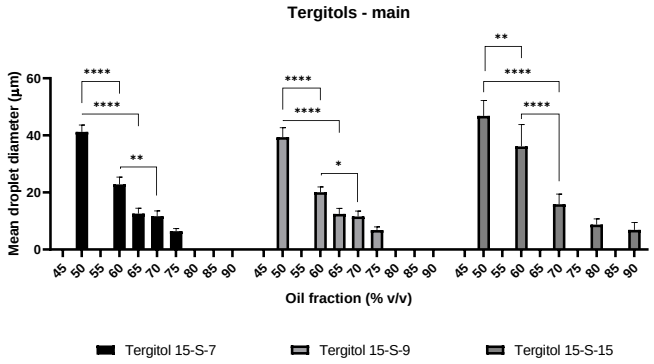
Tergitols - main
Mean droplet diameter (µm)
Oil fraction (% v/v)
Tergitol 15-S-7
Tergitol 15-S-9
Tergitol 15-S-15

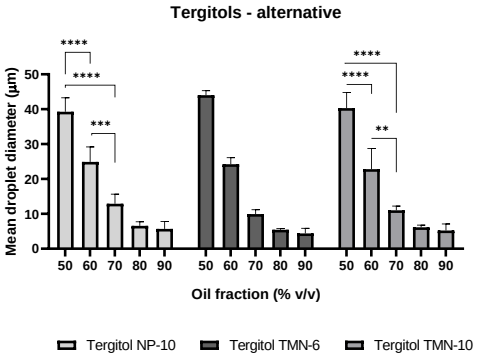
Tergitols - alternative
Mean droplet diameter (µm)
Oil fraction (% v/v)
Tergitol NP-10
Tergitol TMN-6
Tergitol TMN-10

3.2 Formulation and characterisation of oil-in-water emulsions to template highly porous protein structures

ABBREVIATIONS

DMEM	Dulbecco's Modified Eagle's Medium	O/W	oil-in-water emulsions
ECM	extracellular matrix	OCC	oil carrying capacity
ETPM	emulsion templated fibrin scaffold	PM0	foamed fibrin scaffolds
FBS	foetal bovine serum	polyHIPE	scaffold templated from HIPE
GTA	glutaraldehyde	PS	penicillin-streptomycin
HIPE	high internal phase emulsion	PVA	poly vinyl alcohol
HLB	hydrophile-lipophile balance	SEM	scanning electron microscope/graph
MES	2-(N-morpholino) ethane sulfonic acid	TSI	Turbiscan® Stability Index
MSC	mesenchymal stem cell	UTS	Ultimate tensile strength

ABSTRACT

Emulsion templating is a versatile technique for creating porous materials. Emulsions can be used to create range of porous biocompatible materials such as polylactic acid, polymethyl methacrylate and polycaprolactone. These porous biomaterials have precise micro- and macro-architectures dictated by the emulsion template but have limited biologically relevance. Subsequent processing steps, such as surface treatment or functionalisation, may be required.

The use of proteins (e.g. gelatin, collagen and fibrin) as the polymeric material allows the introduction of physiologically relevant chemistries to the construct. However, the surfactants needed to stabilise emulsions for templating are often aggressive and denaturing at the concentrations required, which can affect the macro-molecular structure.

In this section, the manufacture of scaffolds by a facile emulsion templating process is described. Non-ionic surfactants were screened for their ability to stabilise emulsions at low concentrations (well below cytotoxic concentration). This was achieved by systematically increasing oil fraction of oil-in-water emulsions of decane and physiological buffer (MES/NaCl) and analysing short-term stability (in line with fibrin clot time) using static multiple light scattering. Oil fraction was gradually increased into the high internal phase system.

Surfactants capable of sustaining high internal phase emulsions (HIPEs) and therefore templating highly porous materials (polyHIPEs) were previously identified (Chapter 3.1). However, their biocompatibility was not assessed. Suitability of candidate emulsion systems was confirmed with templating. Fibrin scaffolds were found to have retained native fibrous structure, creating an intricate “basket weave” structure (confirmed with electron microscopy). Thromboelastometry confirmed no prohibitive effect of surfactant on fibrin formation. CCK-8 showed no evidence of cytotoxicity in either contact or leachable scaffold assays.

INTRODUCTION

Emulsion templating is a widely used method of creating biomaterial products, wherein two immiscible phases are mixed with surfactant to create a stable dispersion of spheroids. High internal phase (HIPE) emulsions, in which the dispersed phase comprises >74% total volume fraction (Cameron and Sherrington, 1996; Tai et al., 2001), have been used to create extremely porous materials for many years – most commonly using hydrophobic synthetic polymers in a continuous oil phase (Bokhari et al., 2007; Carnachan et al., 2006; Cui et al., 2010; Hentze and Antonietti, 2001; Musgrave et al., 2017; Owen et al., 2016; Quell et al., 2017; Zhang and Cooper, 2002). Some oil-in-water (o/w) HIPEs have been used to create hydrophilic scaffold materials, polyHIPEs; however, to date, protein polymers have not been templated using such emulsions (Franks et al., 2006; Sultana and Wang, 2008).

Proteins – particularly those found in native extracellular matrix such as collagen – are attractive scaffold materials as they are biocompatible, biodegradable and offer biochemical, mechanical, and structural properties in line with physiological requirements. Proteins are often processed to purify, sterilise, or stabilise them for use. These processes render them may reduce risk of contamination or immunogenicity but can denature the protein and destroy the native hierarchical structure. When native protein is required, it is important to optimise the type and extent of purification and sterilisation processing to preserve the structure and biochemical function of the molecule. For example, treatment with surfactants such as SDS (ionic) or Triton X-100 (non-ionic) has been found to have no effect on collagen content in native tissue (Gilbert et al., 2006; Song and Ott, 2011). Freeze drying, another method of sterilisation and stabilisation, has been shown not to alter the metabolic or biological properties of fibrinogen (Regoeczi and Stannard, 1969), though it is susceptible to degradation by enzymes and other means (Belew et al., 1978; Kopeć and Latallo, 1978).

The emulsion system presents a challenge in templating proteins as the type and choice of surfactant is imperative not only to emulsion stability but also to protein integrity. Insufficient surfactant limits the stability of the emulsion and/or the volume of fraction of the internal phase. Surfactants required to generate sufficient emulsion stability for proteins to assemble and consolidate can delay formation or even damage or the native structure, especially because both tend towards interfaces and so are concentrated in in a small space competing for the interface (Norde and Lyklema, 1991; Wilde et al., 2004).

The charge of surfactants can be disruptive to proteins (Moosavi-Movahedi, 2005; Otzen, 2011; Song and Ott, 2011), but even non-ionic surfactants, such as Tweens, are cytotoxic above a critical concentration as a result of the surface active/detergent properties. There are two ways to approach this problem. The first is to accept that the surfactant will denature the protein. This may be desirable in that the biochemistry of the protein is still present, but any fine structure/structural relevance to native ECM is lost. Additional top-down manufacturing steps, such as photo- or electron beam lithography, plasma treatment, or coating with adhesion proteins; or bottom-up approaches like self-assembly of copolymers on the scaffold surface, are required to add nanotexture to the scaffold (Viswanathan et al., 2012; X. B. Yang et al., 2001). These have been shown to enhance cell compatibility, migration and adhesion with the scaffold surface (Mann and West, 2002; Park et al., 2007; X. B. Yang et al., 2001).

The second is to use synthetic polymers, particularly those with proven biocompatibility and regulatory approval such as PLLA, PGA, PCL and polyanhydrides (Abedalwafa et al., 2013; Nair and Laurencin, 2007). However, solubility presents an issue. Organic solvents may be required, increasing the environmental cost of the manufacturing process. As with scaffolds of denatured proteins, the microstructure will be templated by the emulsion but fine textures and nanotextures will be lacking (fig. 1).

For this work, fibrin, a fibrous blood protein which forms blood clots in response to injury, was selected as the scaffold material (Chapter 2). To template fibrin scaffolds, its precursor molecule fibrinogen would be dissolved in the aqueous phase. Thrombin would then be added to catalyse conversion of soluble fibrinogen to insoluble fibrin fibres. The thrombin-fibrinogen system was interesting as previous work has shown that clot time and thrombin: fibrinogen ratio can affect the diameter and density of resultant fibrin (Blombäck et al., 1989; Blombäck and Okada, 1982). This offered an additional degree of control and ability to tune the scaffold material. However, clot time must be balanced against emulsion stability to ensure the fibrin templated the original emulsion with the intended droplet (pore) diameter and spacing.

Thrombin distribution was an area of concern. It was thought that late addition of thrombin, after initial dispersion of oil and water phases but before complete emulsification, would offer the best chance of effectively distributing the thrombin to produce homogeneous fibrin.

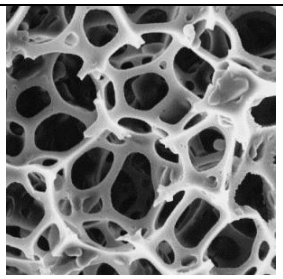	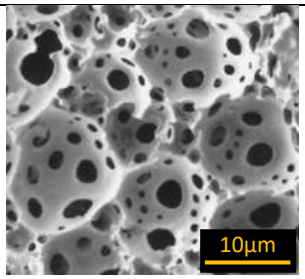	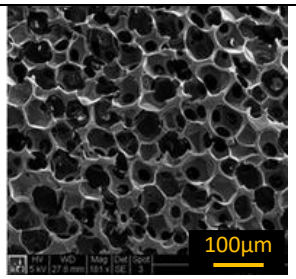
Styrene-DBV polyHIPE (Akay et al., 2004) *(no scale provided in source material)*	2-ethylhexyl methacrylate-DVB (90:10) polyHIPE (Sergienko et al., 2002)	NIPAM-based polyHIPE (Pickering emulsion with PMMA beads) (Kwon Oh, 2011)
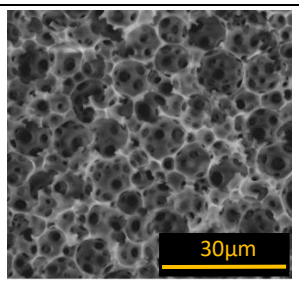	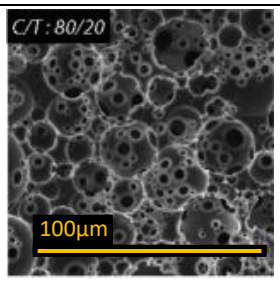	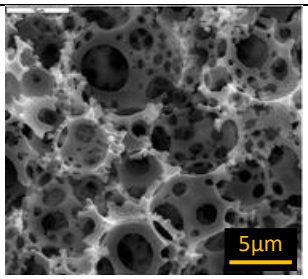
2-hydroxyethyl methacrylate polyHIPE (Paljevac et al., 2012)	Polycaprolactone methacrylate polyHIPE (80:20 chloroform: toluene) (Dikici et al., 2019)	VBC-DVB polyHIPE stabilised with Span 80 (Barbetta et al., 2000)

Fig. 1: Cross-sectional electron micrographs of emulsion templated scaffolds from literature. Scaffolds were templated via water-in-oil emulsions or Pickering emulsions (those stabilised with solid particle). High template fidelity creates scaffolds with close-packed spherical pores.

Once formed, the emulsion must remain stable for at least the time taken for fibrin to form. Having previously identified non-ionic surfactants that are capable of short-term stabilisation of high internal phase emulsions (Chapter 3.1), the effect of incorporating biological buffer, fibrinogen and thrombin was next evaluated. Suitable HIPE surfactants are those above in red line in fig. 2, below.

Another consideration was how the surfactant and protein might interact. Both have a tendency to assemble at the interface (Norde and Lyklema, 1991). In a HIPE system, surfactant and protein would be expected to be closely associated at the thin interfaces. This could potentially denature the protein or slow fibrin formation. Non-ionic surfactants with high "oil carrying capacity" were selected to allow their use in smaller concentrations to try to avoid or reduce this effect.

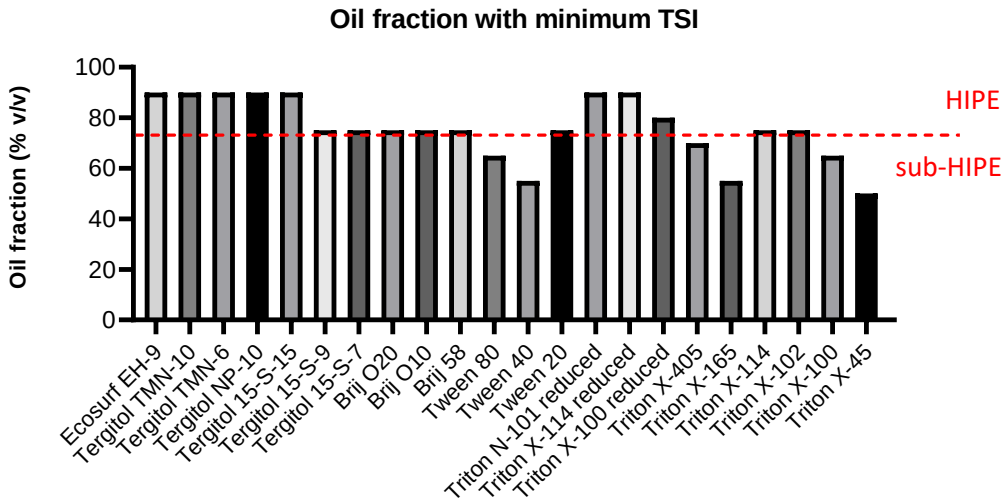

Fig. 2: Summary of oil carrying capacity of surfactants tested in previous experiments where the oil carrying capacity is the volume fraction of oil in the emulsion at which stability is greatest. Each emulsion contained 0.1% v/v surfactant and was tested in triplicate. Reported values represent stability at 15 minutes after emulsification. HIPEs are emulsions where the internal phase exceeds maximum spherical packing of the internal phase, i.e. 74% of the total volume.

The aim was to generate a high internal phase emulsion capable of maintaining a stable droplet arrangement of appropriate diameter and spacing for cell and blood vessel ingress (fig. 3). Further, the emulsion must not denature the fibrinogen or thrombin and allow their interaction to form a native-like fibrin network at the oil/water interface.

Emulsion stability was evaluated both macroscopically and using light scattering with a Turbiscan LAB analyser against increasing oil fraction. When translated to scaffold manufacture this produced high fidelity, highly porous scaffolds with close cell packing and even protein distribution, resulting in an interconnected structure with well-defined pores (confirmed by scanning electron microscopy). Droplet size was evaluated using light microscopy and was optimised for cell ingress and angiogenesis.

The ability to create protein polymeric materials with well-distributed, delicate protein microstructure is of significance in development of scaffold materials for tissue engineering. Currently, polyHIPE materials are largely restricted to a small number of available hydrophobic biomaterials available using water-in-oil emulsions. This work demonstrated the capability to design well-characterised emulsions to accurately template protein materials such as fibrin, collagen, and alginate, which are commonly used in tissue engineering scaffolds. This method allows hierarchical scaffolds to be created in which the native protein structure is preserved (not possible by other methods).

	Optimal	Achieved
Pore size	70 – 200 µm *Cell ingress* (Choi et al., 2013; Marshall et al., 2004)	50 – 200 µm
Interconnect size	25 – 35 µm *Angiogenesis* (Bokhari et al., 2007; Marshall et al., 2005)	20 – 40 µm
Porosity	≥ 74% *Exceeds perfect sphere packing*	Up to 95%

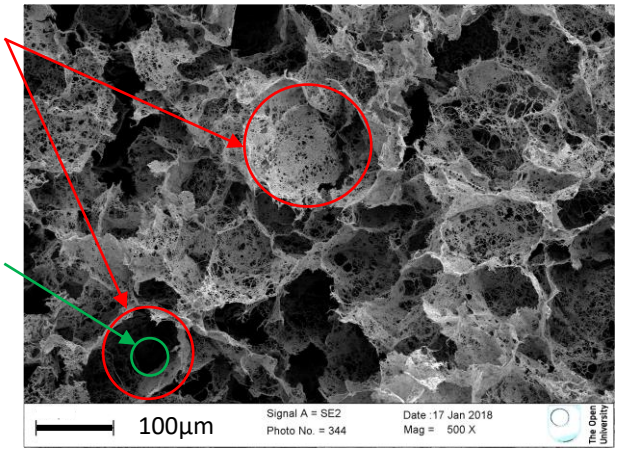

Fig. 3: Comparison of typical fibrin-based scaffold parameters with optimal values cited in the literature. The optimised scaffolds manufactured according to the method described in this report all meet (pore size; interconnect size) or exceed (achievable porosity) the cited values. Scale bar = 100µm.

N.B. Up to 74% is not an optimal figure for porosity; simply the limit achieved (i.e. sub-HIPE) by authors describing scaffolds using native proteins by comparable methods.

Initially, well-characterised common surfactants (including Tween-Span) were used to establish a working system with the relevant proteins and buffers. This was gradually modified by increasing oil fraction, moving to more efficient HIPE surfactants (fig. 2) when required. The emulsion systems were evaluated for stability and then protein- and cyto-compatibility. Volume fraction of oil was increased in a stepwise fashion from 50% v/v into the HIPE system up to 95% internal volume fraction. A systematic approach was used to achieve maximum oil fraction with minimum surfactant, while maintaining emulsion stability. The effects of mixing speed and method were evaluated as well as surfactant type and concentration. Non-ionic surfactants were used throughout as these were supposed to have a less denaturing effect on the structure and function of proteins compared to ionic surfactants.

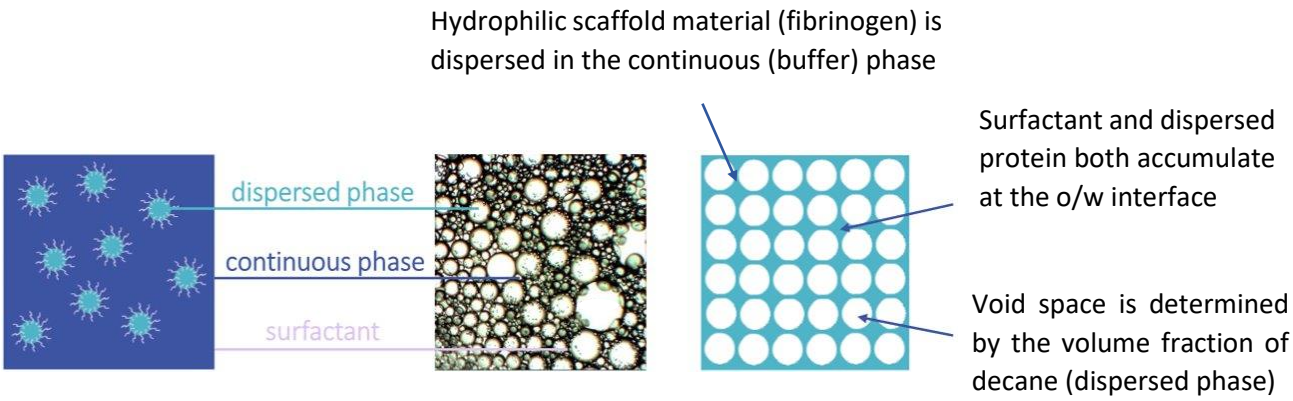

Fig. 4: Arrangement of the dispersed (internal) phase, continuous (external) phase and surfactant in an oil-in-water (o/w) emulsion. Monomers in the continuous phase polymerise to create a solid continuous matrix. The light micrograph shows a surfactant-stabilised o/w emulsion in a monolayer on a glass slide.

EXPERIMENTAL PROCEDURES

Materials

All water and buffers were autoclaved or sterile filtered, as appropriate, prior to use. All preparatory and formulation work was undertaken in a laminar flow hood to minimise risk of contamination. 2% bovine fibrinogen (w/v of clottable protein) and 5% w/v polyvinyl alcohol (PVA) (M_w 31,000-50,000 g/mol, 87-97% hydrolysed) were prepared by dissolving in MES/NaCl buffer (25 mM/150 mM, pH 7.4) at 37°C. 1 M calcium chloride solution was prepared in distilled water. Thrombin (pre-dialysed; frozen aliquots) was warmed to 37°C before use.

Decane and surfactants (Tween 80; Span 80; ETOCAS 35-MH, ETOCAS 35 RB; Triton X-100, X-102, X-114, X-165, CG-110; Brij O10) were used as purchased. Tween 80 and Span 80 were also mixed in various proportions to generate surfactant blends with appropriate required HLB to match decane (Table 1).

Volume fraction		HLB (hydrophilic mixtures)
Tween 80	Span 80	
55	45	10.185
60	40	10.72
65	35	11.255
70	30	11.79
75	25	12.325
80	20	12.86
85	15	13.395
90	10	13.93
95	5	14.465
100	0	15

Table 1: HLB of different blends of Span 80 (HLB 4.3) and Tween 80 (HLB 15). Only hydrophilic blends (HLB >10) are shown as the intended use was o/w emulsions. The highlighted blends were found to have best stability and were included in early templating trials.

Emulsion preparation

Oil and aqueous phase were prepared as previous. Initial tests were performed according to ICI guidance (ICI Americas, Inc., 1984) and used 50% decane (v/v) and 1% (v/v) Tween 80/Span 80 in varying proportions to elucidate required HLB. Decane, buffer and surfactant were mixed at 5000 rpm using a high shear mixer with impeller blades (Caframo Ultra Speed BDC6015, Caframo Lab Solutions, Georgian Bluffs, Ontario, Cn). Vortex (Fisherbrand WhirliMixer) and hand shaking were used as alternative methods of emulsification. Oil fraction was systematically increased by increments of 5%. Different surfactants were trialled, and surfactant concentration reduced stepwise (1, 0.5, 0.1% (v/v)). Only formulations resulting in emulsification were progressed to the next stage of testing.

Emulsion characterisation

Emulsion stability was evaluated as described in Chapter 3.1. 3 ml samples were scanned every 30 seconds for 15 minutes. Droplet size of the internal phase was evaluated by placing a sample of emulsion on a glass slide and imaging with light microscopy. Droplet diameter was measured using Fiji by Image J.

Scaffold preparation by emulsion templating

Formulations which successfully emulsified and had TSI≤3 were selected for emulsion templating. This was approached systematically, starting with 50% internal phase, and gradually increased as the quality of emulsions improved. Brijs, Tritons and Tergitols were used in HIPEs to template polyHIPE scaffolds. Surfactants capable of stabilising HIPEs were previously identified and are shown as those with oil fractions at peak stability above 74% v/v (fig. 2).

Briefly, the decane and surfactant were used as per the basic emulsion recipe. The MES/NaCl buffer aqueous phase (pH 7.4) also contained bovine fibrinogen (2% w/v clottable), thrombin and calcium chloride. The decane, surfactant, fibrinogen and calcium were mixed to emulsify before adding the thrombin and mixing for a further 30 seconds. Emulsification of early compositions was performed using the Caframo Ultra Speed BDC6015 impeller mixer.

Emulsions were then transferred to 5x5 cm square weighing boats and incubated for 1 hour at 37°C. Scaffolds were cross-linked 1 hour each side with 0.2% glutaraldehyde solution, washed five times with 0.1% sodium borohydride and four times with deionised water. Some scaffolds were washed on each side in dilute excipient (0.2% w/v PVA, 1% w/v Tween, 1 M sorbitol or Tween/sorbitol). Scaffolds were then lyophilised overnight at -40°C under vacuum (VirTis Genesis 25ES, SP Scientific, Warminster, Pennsylvania, USA).

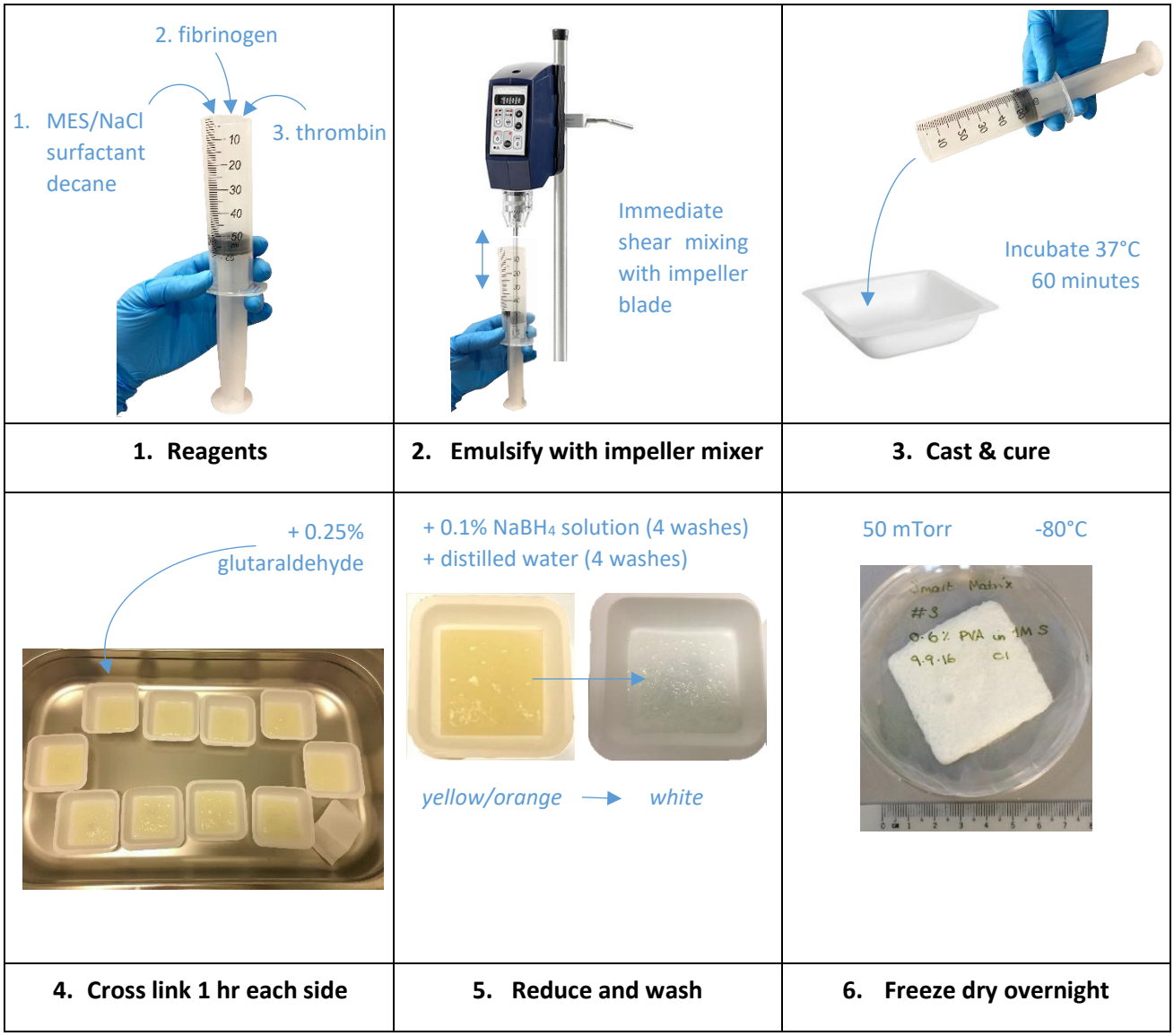

Fig. 5: Overview of scaffold templating method during early development. The basic emulsion components (decane, aqueous buffer and surfactant) were added to a 50 ml syringe body with the tip removed and briefly pre-mixed before adding fibrinogen solution. The reagents were mixed until emulsified, by slowly raising and lowering the syringe while keeping the mixer blades submerged. Scaffolds were cast into weighing boats and incubated to allow fibrin to form before cross-linking. Sodium borohydride solution was used to remove excess glutaraldehyde solution and then removed with successive water washes. Scaffolds were stabilised with freeze drying before imaging.

Thromboelastometry

Thromboelastometry was assessed using a Stago STartMax coagulometer. All testing was performed at 37°C using pre-warmed reagents. Surfactants were added to fibrinogen solutions (2% clottable protein in MES/NaCl) at 0.1, 0.2, 0.5, 1.0 or 2.0% (v/v). 2 ml each solution was placed into a cylindrical cuvette containing a small steel ball bearing. The cuvettes were situated over the magnetic region of the coagulometer so that the ball bearings rotated around the base. 50 µl thrombin was then added to each sample and the time taken for a fibrin clot to form recorded. The clot time was determined as the point at which the viscosity had increased sufficiently to hold the ball bearing at a fixed position in the fibrin gel and resist the magnetic force applied. All samples were tested in triplicate.

RESULTS AND DISCUSSION

Emulsion templating below the HIPE regime

The ICI Americas guide suggests beginning emulsion formulation with a blend of Tween 80 and Span 80, widely used and well-characterised surfactants, to elucidate required HLB of the oil phase (ICI Americas, Inc., 1984). The required HLB, and most suitable Tween/Span blend (70:30 by volume, HLB 11.79) was previously identified (Chapter 3.1).

The same strategy was applied to early attempts to template scaffolds with the decane/buffer system. Instead of varying surfactant, oil fraction was increased stepwise (fig. 6) to give a proof of concept and to test the bounds of the template method.

Calcium chloride solution was added to fibrinogen and alginate (adapted from a confidential in-house method) dissolved in MES/NaCl buffer (pH 7.4). This was mixed with decane and the Tween/Span surfactant mixture in a 50 ml syringe body (fig. 5). Immediately on the addition of thrombin, the mixture was emulsified using an impeller mixer. The emulsion was cast into a flat-bottomed weighing boat, incubated to allow fibrin formation, cross-linked, washed and dried. The micrographs below (fig. 6) show cross-sections of the freeze-dried scaffolds under scanning electron microscope.

These early scaffolds are characterised by thick, dense fibrin fibres and thick pore walls with few interconnects. This occurred partly because of the relatively low oil fractions (50%, 60%) and partly because of the poor stability afforded by Tween/Span in this system at 70% oil, close to the HIPE regime. The amount of surfactant was doubled to 0.2% in an attempt to improve stability, but this was unsuccessful. While fibrin formation appeared unaffected by the increase in surfactant concentration, the emulsion still destabilised rapidly and gave rise to a dense material with low porosity.

At 50% oil fraction, discrete pores left by the oil droplets are visible, indicating the template was effective and the emulsion was stable during the time taken for fibrin to form at the interface. However, the low oil fraction gave less than optimal spheroid packing, producing thick mats of fibrin which would not permit ingress of cells. Additionally, the droplets at this oil fraction were quite large, producing pores ranging from 100 µm in diameter up to 500 µm and beyond.

At 60% oil fraction, the porosity increased and droplet size reduced. The fibrin walls were thinner and separate fibres were distinguishable at high magnification. Thicker regions, such as the curved diamond at the furthest space between pores, comprised fibrin bundles rather than the mats observed at the thinner points. There was some evidence of interconnection between pores and much greater diffusional space between fibres. However, pores were less distinct, probably due to reduced emulsion stability giving less time for fibrin to form around the oil droplets before they destabilised.

Microstructure of initial templated fibrin scaffolds

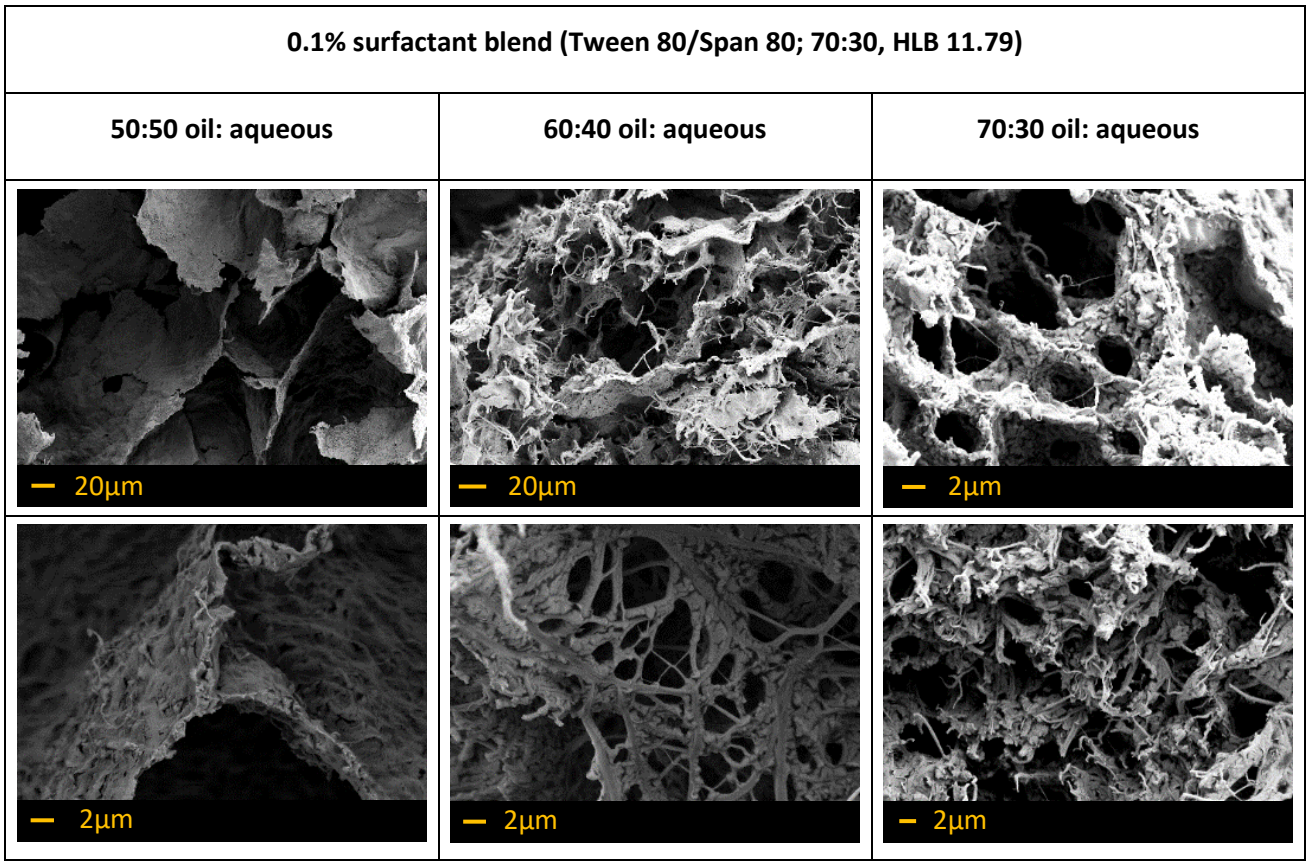

Fig. 6: Cross-sectional electron micrograph images of emulsion-templated fibrin-based scaffolds with increasing porosity. The micrographs show magnified images (top row 2,500x; bottom row 10,000x) of scaffolds produced with 50% oil, 60% oil, and 70% oil by volume fraction in the emulsion. This translates to approximately the same porosity in the templated scaffold. 70% oil emulsions were not stable throughout initial scaffold incubation, so surfactant concentration was increased to 0.2% v/v.

The same properties were observed in the scaffold templated from a 70% oil fraction emulsion with the same concentration of surfactant (0.1%). Pore size reduced further but the emulsion stability was poor, resulting in separation of oil before the fibrin formation and scaffold consolidation had completed. This negatively impacted pore spacing and therefore wall thickness, as the emulsion decayed by particle migration and coalescence. Distinct fibrin fibres were visible, but they were clumped together owing to the rapid separation of the oil and aqueous phases.

At low internal phase volume fractions, pore size and wall thickness were not adequate. At high oil fractions the emulsions were not sufficiently stable to maintain a template for fibrin formation.

Effect of increasing surfactant concentration on microstructure

Surfactant concentration was increased in an attempt to improve emulsion stability. This was intended to promote the formation of smaller, more stable droplets and delay the onset of instability in higher oil fraction emulsions to allow time for fibrin formation around the oil droplets.

Decane-MES/NaCl (70:30 by volume) emulsions were prepared as previously, with either 0.1% or 0.2% (v/v) Tween 80/Span 80 surfactant mixture added to stabilise.

However, microstructural evaluation of cross-sectional freeze-dried samples showed no improvement in porosity, interconnectivity, or fibrin fibre arrangement in the 0.2% system (fig. 7). Conversely, scaffolds prepared with 0.2% Tween/Span showed equal or reduced porosity and minimal diffusional space. Fibrin fibres were evident but had amassed in dense sheets rather than a looser interwoven structure.

With 0.1% surfactant, porosity was similarly low, suggesting that a similar volume of oil was held in the aqueous phase during templating. Emulsion separation by creaming was therefore unlikely. Fibrin fibres again formed in sheet-like structures, but individual fibres were visible within the sheets. This may suggest that the higher surfactant concentration (0.2%) slightly denatured the protein at the interface; however, both concentrations remained extremely low so this is unlikely.

It was evident that increasing oil fraction would greatly improve the porosity, wall thickness and interconnectivity. Evidence of individual fibrin fibres at the thinnest parts of the pore walls (fig. 6, fig. 7 bottom left) showed that the fibrin sheet could be improved by templating from an emulsion with more closely packed oil droplets. Increasing oil fraction beyond the oil carrying capacity of the surfactant would lead to reduced emulsion stability and poorer template fidelity. Increasing surfactant concentration further could slightly improve stability, though previous work suggested the choice of surfactant was more important than the concentration (Chapter 3.1). Additionally, higher concentration of surfactant at a smaller interface (caused by closer packing of droplets in an emulsion with greater internal volume fraction) carries a higher risk of denaturing protein at the interface and either preventing fibrin formation or adversely affecting the native fibrous structure.

	Surfactant concentration (v/v)	
Magnification	**0.1%**	**0.2%**
500 x	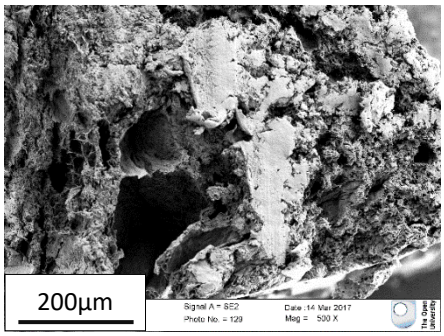	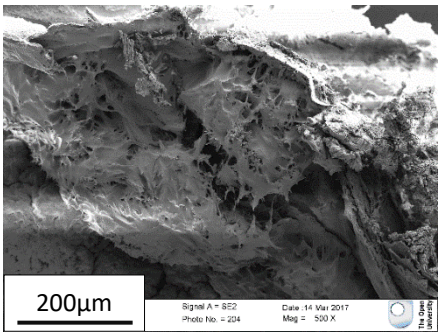
1000 x	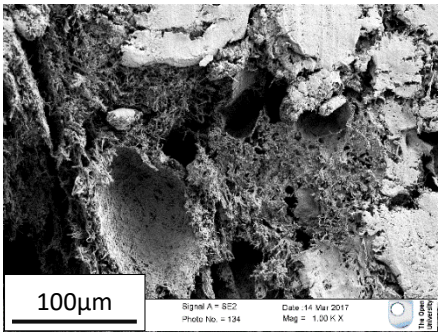	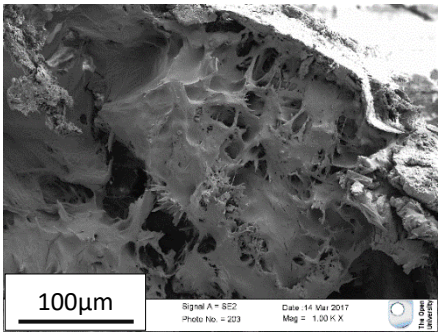
5000 x	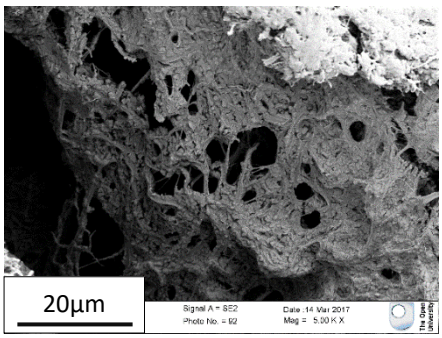	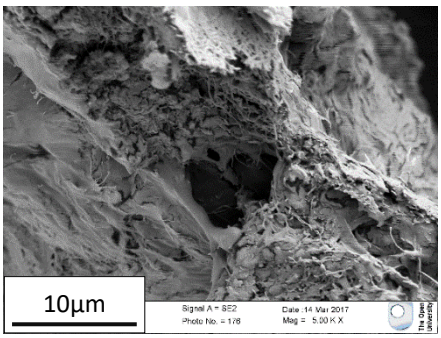
10,000 x	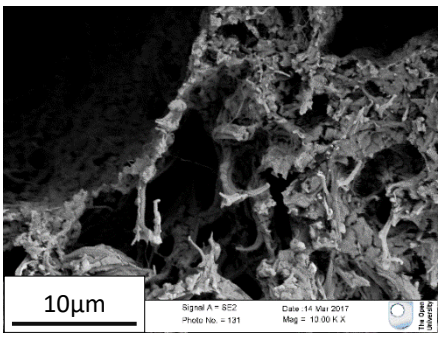	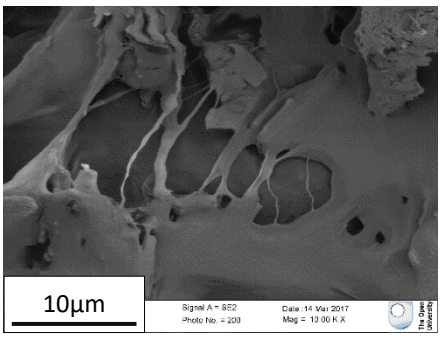

Fig. 7: Cross-sectional electron micrographs of fibrin-based scaffolds templated with emulsions containing 0.1% or 0.2% v/v surfactant. Emulsions and templated scaffolds were prepared as previously described. Emulsions contained 70% oil fraction and either 0.1% or 0.2% v/v Tween 80/Span 80 surfactant blend in a ratio of 70:30 to give an HLB of 11.3.

Effect of PVA and alginate copolymers on microstructure

	PVA	Alginate
50%	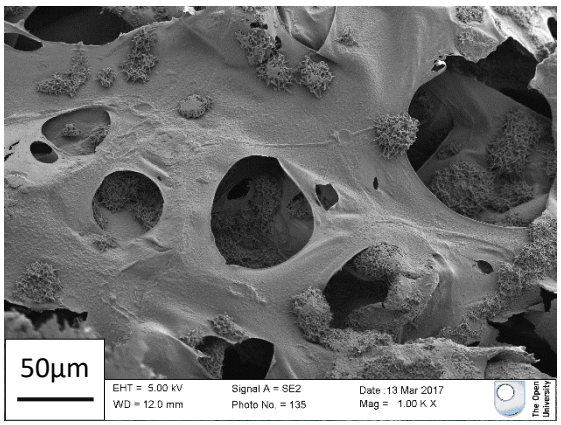	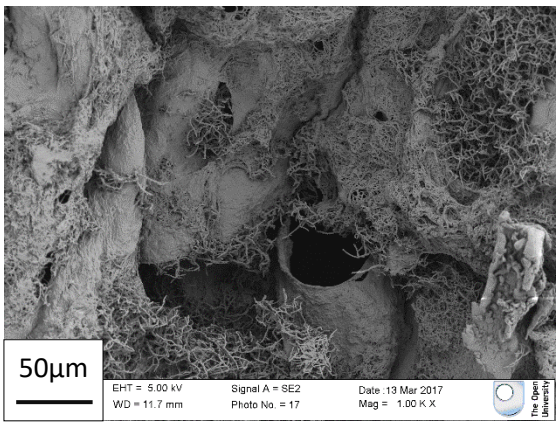
60%	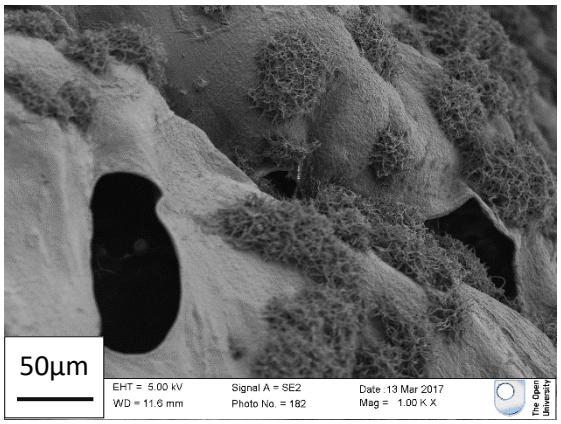	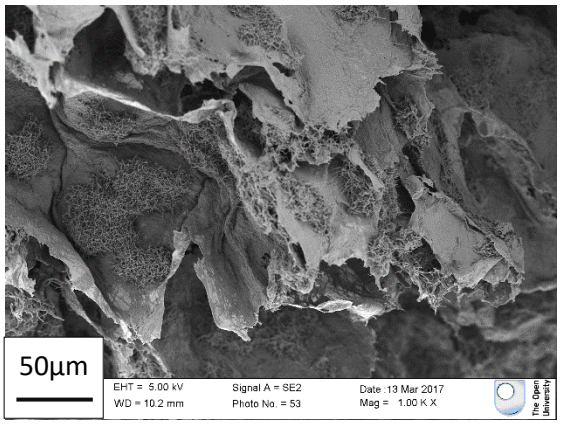
70%	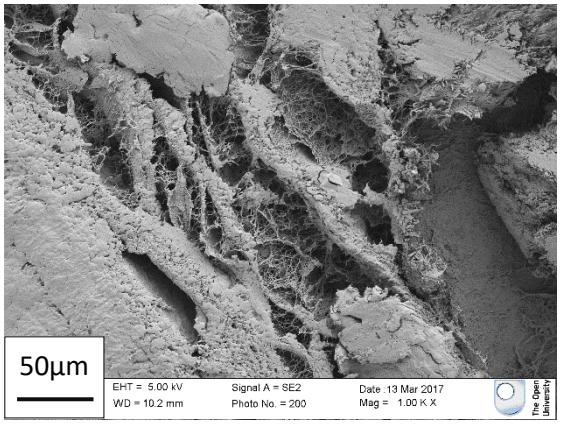	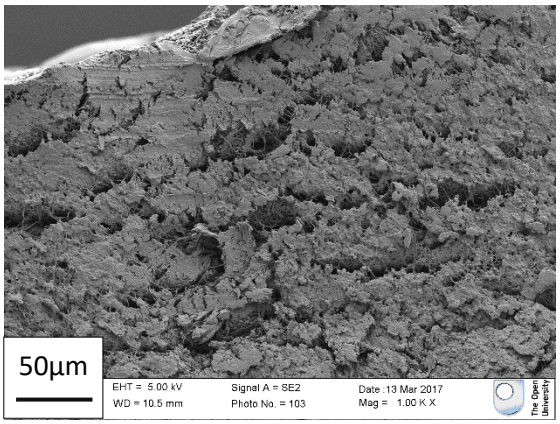

Fig. 8: Cross-sectional electron micrograph images of emulsion-templated fibrin-based scaffolds with increasing porosity containing either PVA or alginate (1:2 copolymer: fibrin). Scaffolds were produced in triplicate; representative images are shown.

An existing in-house method for preparation of fibrin scaffolds via a foaming method (confidential) used alginate as a copolymer and bulking agent. This served to improve the bulk strength and handling of the scaffold and provide stability especially between foaming and formation of a consolidated fibrin network.

The same alginate was added to the templated scaffolds for the reason, to provide stability and increase integrity of the friable scaffold. Alginate is biocompatible and has a long history of use in the biomedical industry. Being significantly cheaper than fibrin, it is also an economically attractive option.

However, while foamed scaffolds produced with fibrin-alginate have a delicate fibrous structure, the equivalent recipe produced thick, dense sheets when templated (fig. 8). After preliminary drying the scaffold had a gum-like texture, perhaps due to difficulty in removing liquid effectively. Examination of the microstructure shows extremely low porosity and almost no diffusional spaces. At 60% oil fraction and to some extent 50%, a small number of pores are visible. However, it is clear that the emulsion was not templated effectively. The alginate did not improve emulsion stability. At higher oil fraction (70%) there are no pores visible. In all cases, fibrin fibres were only visible in the thick walls where they had been exposed by a scalpel blade during sample preparation for microscopy. The alginate appeared to cloak the fibrin and form dense mats with low permittivity, rather than associated with individual fibres as intended.

When alginate was substituted with the same amount of PVA, scaffolds at 70% oil fraction appeared superficially very similar to the equivalent fibrin-alginate scaffolds. However, instead of a gum-like texture the bulk scaffold was robust and springy to touch, suggesting promising viscoelasticity that would reduce brittle fracture of the dried scaffolds.

At lower oil fractions, the scaffolds again displayed impermeable sheet-like pore walls with PVA coating the fibrin fibres. This could be suggestive of an imbalance between the PVA and fibrin. Some pores were visible, and some interconnects where the fibrin had not formed walls at the closest contact point to the adjacent pore.

The low oil fractions used produced emulsions with fewer, larger droplets. The spacing between droplets was therefore greater than optimal, leaving space for thick walls to form. Given that alginate did not coat fibrin fibres in this way in comparable scaffold produced by foaming, it could be assumed that the coating and resultant sheet formations occurred either because of the excessive pore spacing, the tendency for polar molecules (i.e. alginate), zwitterions like proteins and amphiphilic polymers (PVA) to assemble at the oil-water interface – theoretically with a higher interfacial affinity than fibrin – or a combination of the two. Poor stability of the emulsion at greater oil fractions created faster breakage (for example, by creaming or coalescence) which would serve to further increase spacing between droplets.

More stable emulsions of greater oil fraction, above 74% (in the HIPE regime), were required to produce effective porous materials.

Different surfactants were trialled for improved stability at higher oil fractions (Chapter 3.1). Briefly, Brijs, Tritons and Tergitols were more effective than the Tween/Span mixture at stabilising emulsions at and above 70% oil fraction. Having established proof of concept with this system, future work replaced Tween/Span with more effective surfactants.

Effect of mixing speed on emulsion stability

Increasing mixing speed increases shear, producing smaller droplets and improving stability by imparting more energy into the system. Particle size was previously investigated using Turbisoft software in conjunction with the Turbiscan™ static multiple light scattering analyser (Chapter 3.1).

Fibrin scaffolds were manufactured as previously but with alginate removed and replaced with equal volume of MES/NaCl buffer, and Triton X-165 in place of Tween/Span to enable better stability. The mixtures were emulsified using either the impeller mixer (Caframo Ultra Speed BDC6015, Caframo Lab Solutions, Georgian Bluffs, Ontario, Cn) or vortex (Fisherbrand WhirliMixer) to emulsify immediately after addition of thrombin. The impeller mixer was used at maximum speed, 5000 rpm, to create the highest shear rate. The vortex mixing rate was not quantified but is constant with the mixing vessel is applied at fixed pressure. It is significantly greater than the highest mixing speed possible by the impeller mixer.

After manufacture, scaffolds were freeze dried and the cross-sections examined under electron microscope. Void diameter was quantified in Image J (fig. 9). Each graph represents cumulative void diameter from three sample. Voids were determined as any resolvable gap visible in a 1000x magnified SEM image. Voids therefore include pores at the largest end of the scale (10s-100s µm), interconnects (typically 10s µm) and diffusional space (nm-µm).

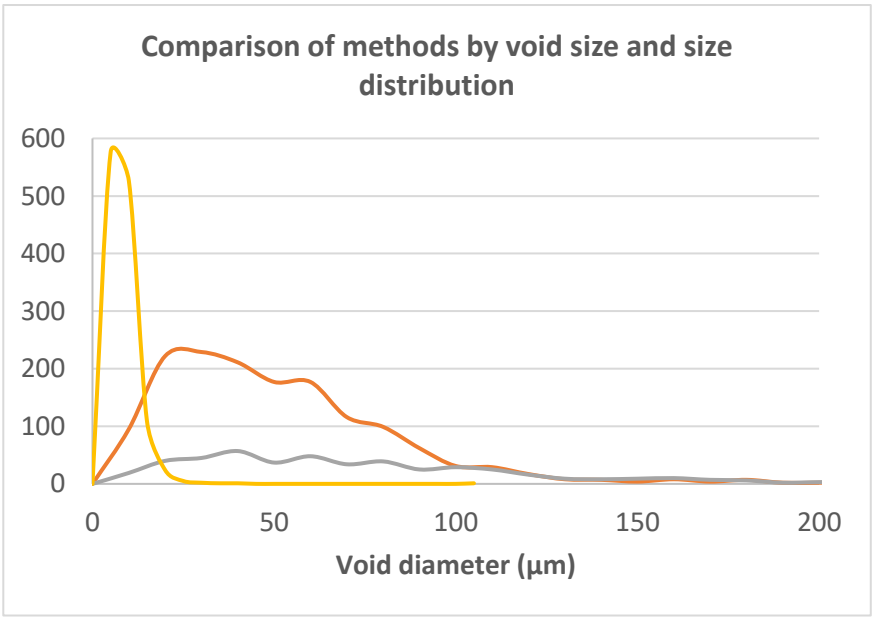

Fig. 9A.

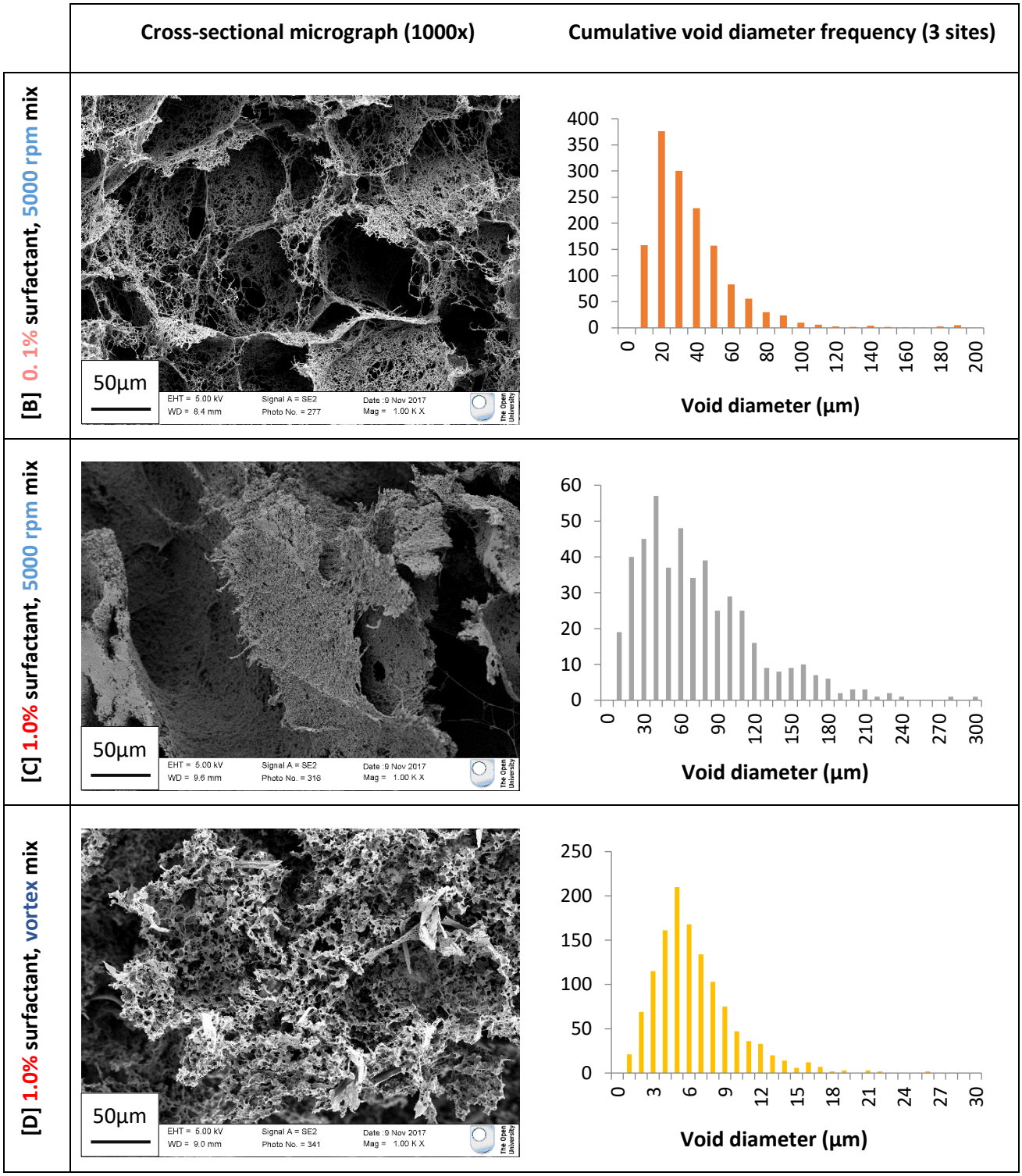

Fig. 9: Effect of increasing surfactant concentration and mixing speed on microstructure and pore geometry of fibrin-based scaffolds. [A] void diameter frequency distribution of scaffolds made with different mixing speed and surfactant (Triton X-165) concentration showed that **[D]** vortexing created a very high number of small diffusional voids compared to **[C]** lower rate mixing, whilst reducing surfactant **[B]** maintained comparable porosity but greatly increased the number of interconnects and diffusional spaces.

The scaffold made with 0.1% Triton X-165 surfactant and mixed at 5000 rpm (fig. 9B) describes the typical manufacturing case. The scaffold had a porosity of 90% with well-distributed fibrin fibres creating a basket-weave structure. Pores were rounded and tightly packed and had a small size distribution. The smaller, more frequent voids recorded on the histogram include diffusional gaps (<20 µm) and interconnects (20-60 µm). The large number of these voids indicate a highly permeable, open-pored structure.

Increasing surfactant concentration tenfold to 1% (v/v) showed a dramatic effect on both microstructure and pore geometry (fig. 9C). The oil fraction was maintained at 90% so nominal porosity was equal to [A], but the void size distribution was much greater with a small number of very large pores. These were beyond the scale useful to cells for signalling and environmental signalling and are not desirable. Additionally, the reduced internal surface area created dense, thick fibrin walls with reduced texture and greatly reduced interconnectivity and number of diffusional gaps. chemistry. These modifications and their modification are described in Chapter 3.3.

Theoretically, increasing the mixing speed will reduce the droplet size to a fixed minimum for each emulsion system, and the energy input will enable the emulsion to reach the most thermodynamically favourable state. Therefore, the higher surfactant system was trialled with increased mixing speed to try and reduce the number of very large pores. Indeed, mixing by vortex did dramatically reduce void size and created a normal distribution of void diameters (fig. 9D). However, the emulsion produced was extremely fine and average pore diameter was below the threshold for useful interconnect size (fig. 3). The pores were too small to support either cell migration angiogenesis. Additionally, the high-speed vortex damaged the protein and destroyed the fibrous structure. The fibrin formed in smooth sheets rather than fibrous meshes, reducing diffusional gaps.

Together, these histograms highlight the reduction in porosity and increase in pore size distribution to include very large outliers when surfactant concentration is increased (fig. 9A). Increasing mixing speed to vortex showed a dramatic shift to the left, with a very large number of pores with diameter about 5 µm and almost all pores in the range 1-15 µm. These were all in the diffusional gap range (fig. 3) and had little other function as they were too small to allow ingress of cells or blood vessels.

A more moderate increase in mixing speed may be useful; however, this is below the upper range of the impeller mixer. It is not possible to reduce the rate of the vortex in a controlled or reproducible manner.

Mixing speed was investigated in more detail using only the impeller mixer. Brij O10, Triton X-100 and a mixture of Tween 80/Span 80 (75:25) were used as stabilising surfactants at three different oil volume fractions: below, close to and above the HIPE transition of 74% internal volume fraction (Table 2).

sub-HIPE *HIPE*

Mixing speed (rpm)	Oil fraction (% v/v)					
	70			75		80
	Brij O10	Triton X-100	T-80/S-80*	Brij O10	Triton X-100	Triton X-100
1000	11.30	3.189	6.424	14.24	3.571	2.483
2000	2.945	2.758	3.686	13.67	2.601	2.225
3000	3.013	8.763	6.146	8.677	2.723	2.493
4000	4.266	3.637	5.860	2.440	3.213	9.886
5000	2.886	2.705	2.801	8.341	2.398	5.128

Table 2: Turbiscan stability index (TSI) of emulsions containing 0.1% (v/v) surfactant and either 70% (sub-HIPE) or 75% (HIPE) decane (v/v) 15 mins after mixing. Surfactant, buffer and decane were mixed in the body of a 50 ml syringe with a Caframo impeller mixer. Surfactants tested were Brij O10 (HLB 12.4); Triton X-100 (HLB 13.4); Tween 80/Span 80 (75:25) (HLB 12.33). TSI is given to 4 significant figures.

Stability was measured using the Turbiscan™ static multiple light scattering analyser and expressed using the Turbiscan stability index (TSI) which reflects the change in transmitted and backscattered light across the height of a sample over a period of time (Chapter 3.1). A higher value of TSI reflects poorer stability; a lower value reflects greater stability. However, because TSI measures rate of change, emulsions which break instantly after mixing ceases can display low TSI values.

Below the HIPE regime, at 70% oil fraction, emulsions containing Brij O10 demonstrated very poor stability when mixed at 1000 rpm but significantly improved in stability from 2000 to 5000 rpm mixing speeds (Table 2, fig. 10). The significant change ($p<0.0001$) in stability between emulsions mixed at 1000 rpm and those mixed at all other speeds suggests that above 1000 rpm, the shear rate imparts sufficient energy to the system to emulsify effectively and produce an even dispersion of droplets more resistance to breakage by migration or aggregation.

When oil fraction increased to 75%, just above the HIPE transition, emulsions containing Brij O10 gradually increased in their stability from 1000 to 3000 rpm (Table 2, fig. 11). At 4000 rpm peak stability was achieved. Interestingly, the stability then reduced at 5000 rpm. Samples were only mixed for 1 minute in order to make effective comparison between conditions and repeats. It is therefore possible that mixing speed was sufficient

to produce a stable emulsion, but mixing time was not. This is a feature of HIPE systems where the oil is emulsified gradually. The first part to emulsify is dense and sinks, making further emulsification more difficult.

Brij O10 did not emulsify mixtures containing 80% v/v oil phase.

Mixtures containing Tween 80/Span 80 only emulsified at 70% oil fraction (Table 2). Stability was better when mixed at 5000 rpm but there was no clear trend with mixing speed from end point TSI. However, the stability data over time (fig. 10) showed very similar profiles for all samples in the first five minutes after mixing. By 15 minutes, samples mixed at 2000 rpm and 5000 rpm showed lower TSI than those mixed at 1000, 3000 or 4000 rpm. Macroscopic evaluation of the sample cuvettes. Showed that the emulsion prepared at 2000 rpm had broken during analysis. However, whereas the other samples broke by coalescence in a homogeneous manner, the 2000 rpm samples only partially separated by creaming. The emulsion underneath the separated oil remained, and so TSI reduced rapidly then plateaued when the emulsion adjusted after creaming. For this reason, it is important to consider TSI only one tool to measure emulsion stability. It should not be considered without macroscopic observation and raw transmission and backscattering data to show the method and extent of destabilisation.

Emulsions containing Triton X-100 formed at 70, 75 and 80% oil fraction. At 70% oil fraction, stability was generally good and comparable at all mixing speeds except 3000 rpm. As with Brij O10, this can be explained by the fact that mixing speed may be sufficient while mixing time is not. This was supported by macroscopic evaluation of the sample in the cuvette. However, in both cases it is interesting that this occurred at an intermediate mixing speed.

At 75% oil fraction, just into the HIPE regime, all Triton-containing samples emulsified easily and remained macroscopically stable throughout analysis (Table 2). Turbiscan™ analysis showed a small change in stability (fig. 11) but this was not sufficient to cause visible change to the turbidity or extent of the emulsion.

At 80% oil fraction, Triton-containing samples mixed at 1000, 2000 and 3000 rpm failed to emulsify and rapidly separated after mixing. This produced misleadingly low TSI values (Table 2). At 4000 rpm, an emulsion did form but degraded rapidly. A more stable emulsion formed on mixing at 5000 rpm. However, this did not match the stability achieved at lower volume fractions.

This experiment suggested Tritons as an interesting candidate surfactant family for this emulsion system. The ability to stabilise HIPEs showed promise. Three possible barriers to effective emulsification were proposed: inadequate mixing time, inappropriate mixing method and choice of surfactant.

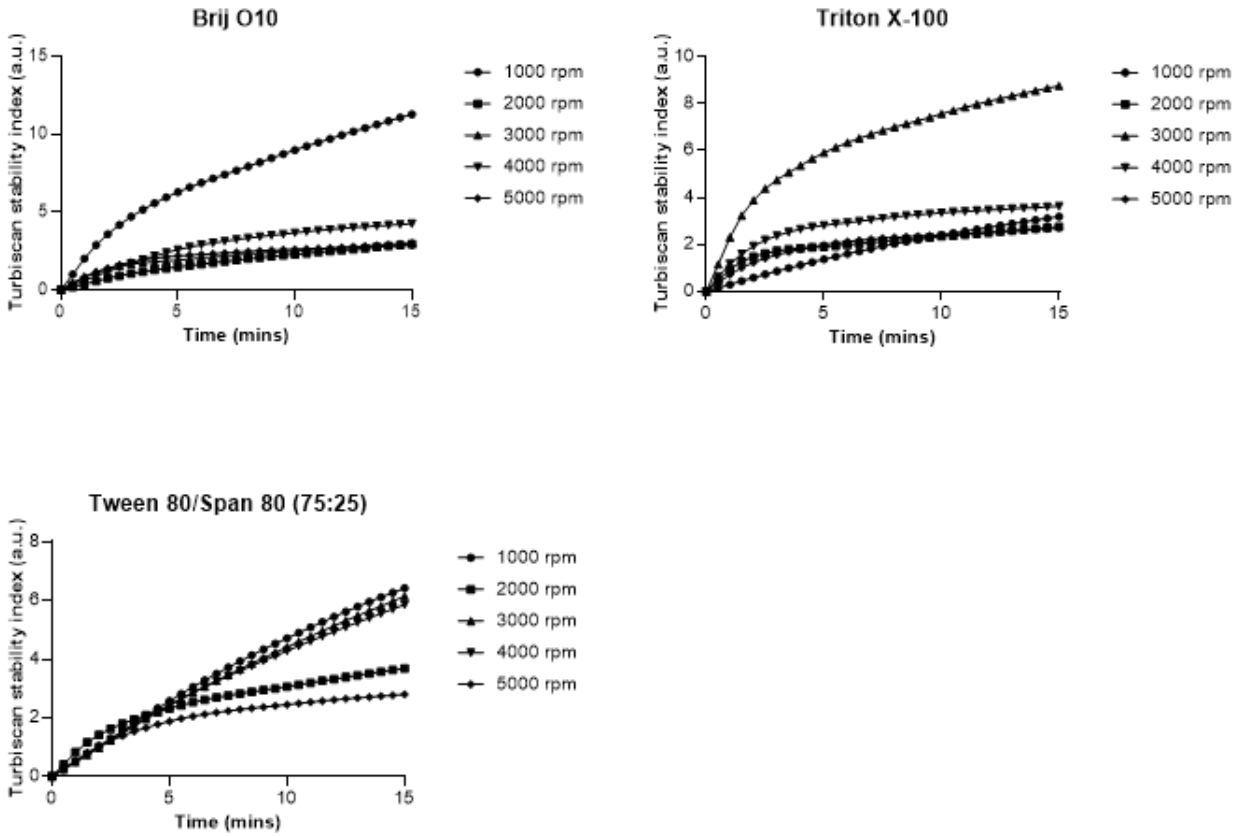

Fig. 10: Stability profile of emulsions stabilised with [A] Brij O10, [B] Triton X-100 and [C] Tween 80/Span 80 at different mixing speeds. Emulsions contained an oil fraction of 70% decane and 0.1% v/v surfactant. Tween 80/Span 80 were used in a ratio of 75:25 (HLB ~12.3), the optimal ratio for stabilising decane/buffer solutions based on previous experimentation. Emulsion samples were scanned every 30 seconds for 15 minutes after preparation and mixing. Mean results are plotted for each time point; n=3. One-way ANOVA showed significant effect of mixing speed on emulsion stability with each of the three surfactants (****, $p<0.0001$).

Mixing time was set at 1 minute for these tests for ease of comparison between samples. For basic formulation, mixing was performed until emulsification was achieved to resolve this problem.

Using the impeller mixer was an efficient and reproducible method of mixing; however, for HIPEs which emulsify in parts, it is not an appropriate method. Once emulsification begins, the initial dense emulsion at the bottom of the mixing vessel is difficult to reintroduce without losing oil through the top of the vessel. Instead, high shear mixing was achieved by placing the constituent emulsion materials in a small lidded container and shaking vigorously. Collision with the container walls at close confines effectively distributed the oil throughout the container. This facilitated better and faster emulsification of the remaining oil.

The Triton family of surfactants comprises many similar surfactants with increasing hydrophilic chain size. Given that Triton X-100 was an effective emulsifier at the HIPE transition, it was posited that a more hydrophilic Triton surfactant may be more effective at stabilising HIPEs with higher volume fraction.

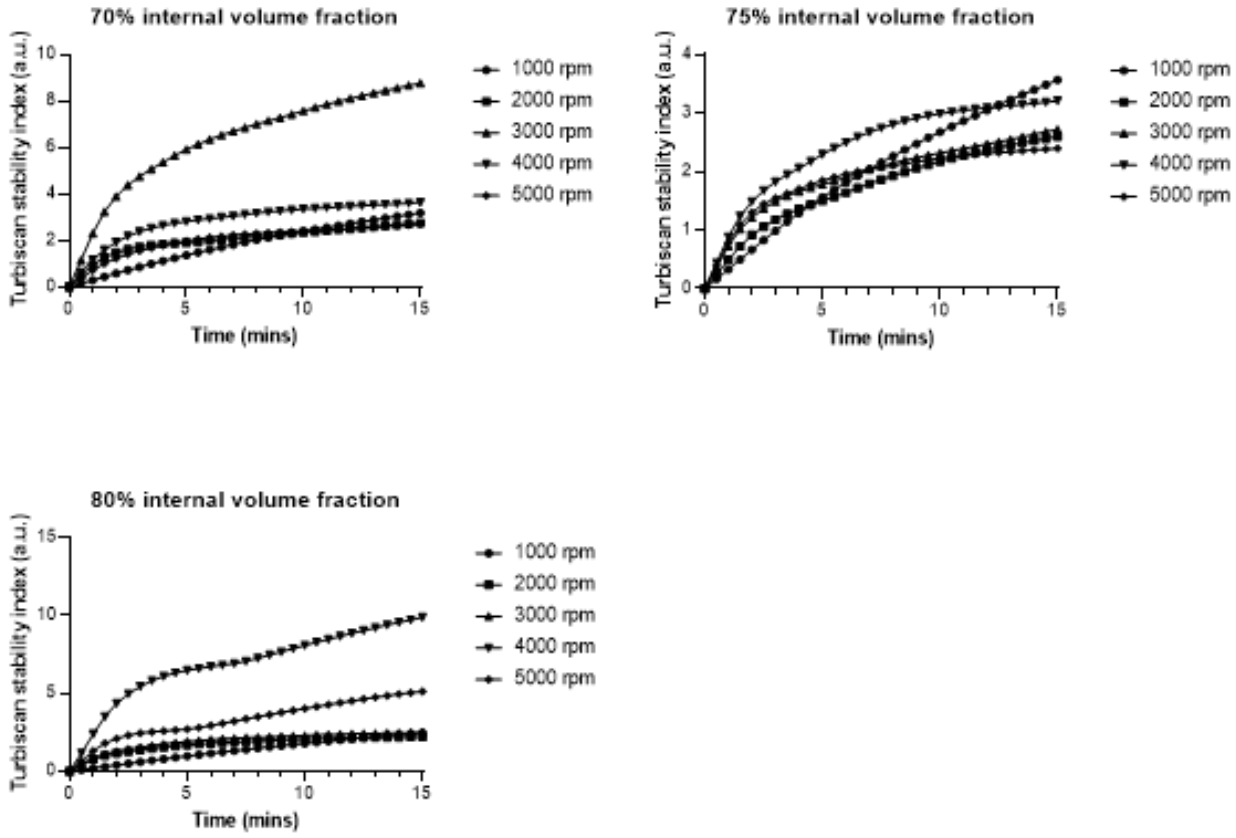

Fig. 11: Stability profile of emulsions with variable decane/buffer composition at different mixing speeds. Emulsions all contained 0.1% v/v Triton X-100 and were prepared with an impeller mixer to emulsify. Turbiscan measurements were taken every 30 seconds for 15 minutes after mixing. Emulsions containing 75% and 80% (v/v) decane are HIPE systems. Mean results are plotted for each time point; n=3. One-way ANOVA showed highly significant effect of mixing speed on emulsion stability above and below the HIPE transition (74%), at 70% and 80% oil fractions (****, $p<0.0001$) and a slightly significant effect close to the HIPE cut-off (75% oil fraction) (*, $p=0.0129$).

Effect of the addition of PVA on emulsion stability

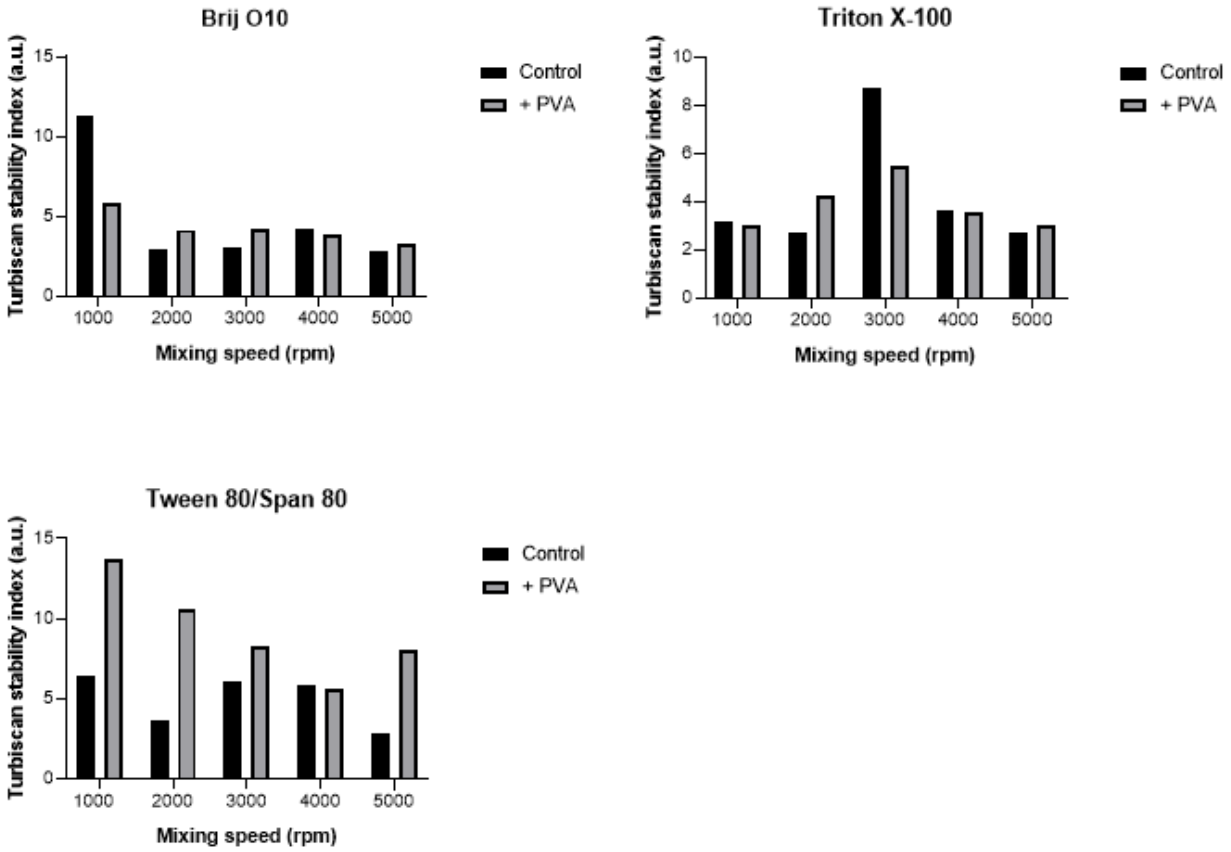

Fig. 12: Stability of emulsions stabilised with [A] Brij O10, [B] Triton X-100 and [C] Tween 80/Span 80 at different mixing speeds, with and without PVA. 5% stock PVA solutions (in MES/NaCl buffer) were added to give an overall concentration of 0.1% in the emulsion. Surfactants were added at 0.1% (v/v) with respect to the total emulsion volume. TSI is reported for stability of emulsions measured 15 minutes after mixing.

PVA demonstrated interested mechanical properties when added to the fibrin scaffold. When added in low concentrations it had no detrimental effect on the microstructure (Chapter 3.3). However, early trials with PVA showed a tendency to form sheets at the interface and coat the open fibrous structure created by the fibrin (fig. 8). PVA is an amphiphilic molecule and will therefore tend towards accumulation at an interface. It was thought that the addition of PVA to the aqueous phase, as well as improving scaffold properties, may have an additional stabilising effect on the emulsion.

This was not the case in Tween/Span emulsions. Samples with and without PVA failed to emulsify when mixed below 4000 rpm. At 5000 rpm, the PVA did improve stability (not reflected in the TSI data because, as previously described, TSI is misleadingly low for very unstable emulsions).

For emulsions containing Brij O10, which did emulsify, the addition of PVA showed no significant change in emulsion formation time or stability. This was also the case for emulsions containing Triton X-100.

These results demonstrate that PVA would not significantly affect stability of the emulsion, which must be adequately stabilised by a combination of non-ionic surfactant and mixing speed and method. However, they also show that there would be no deleterious effect if PVA was added in order to improve properties of the templated scaffold.

Effect of surfactant concentration on fibrin formation time

Thromboelastometry testing was preformed to ensure the choice and concentration of surfactant in the emulsion would not adversely affect fibrin formation from fibrinogen and thrombin. The time taken for a fibrin clot to form from fibrinogen (2% w/v clottable protein in MES/NaCl) and thrombin in the presence of Ca2+ ions and surfactant at various concentrations was measured using a thromboelastometer (Stago STartMax). The fibrinogen: thrombin (4:1) ratio used was the same as for standard scaffold manufacture. The clot time is determined as the point at which the fibrin gel forming becomes sufficiently firm to resist the movement of an embedded steel ball bearing in a magnetic field. A sample containing no surfactant was used as a negative control. Each combination was tested in duplicate.

The surfactants used vary in HLB (Brij O10=12.4, Triton X-100=13.4, Triton X-165=15.5, Tween 80=15). The Tritons and Brijs are capable of stabilising decane-based emulsions; the Tween is not an adequate surfactant for this system but was tested as it has documented cytotoxic effects at higher concentrations.

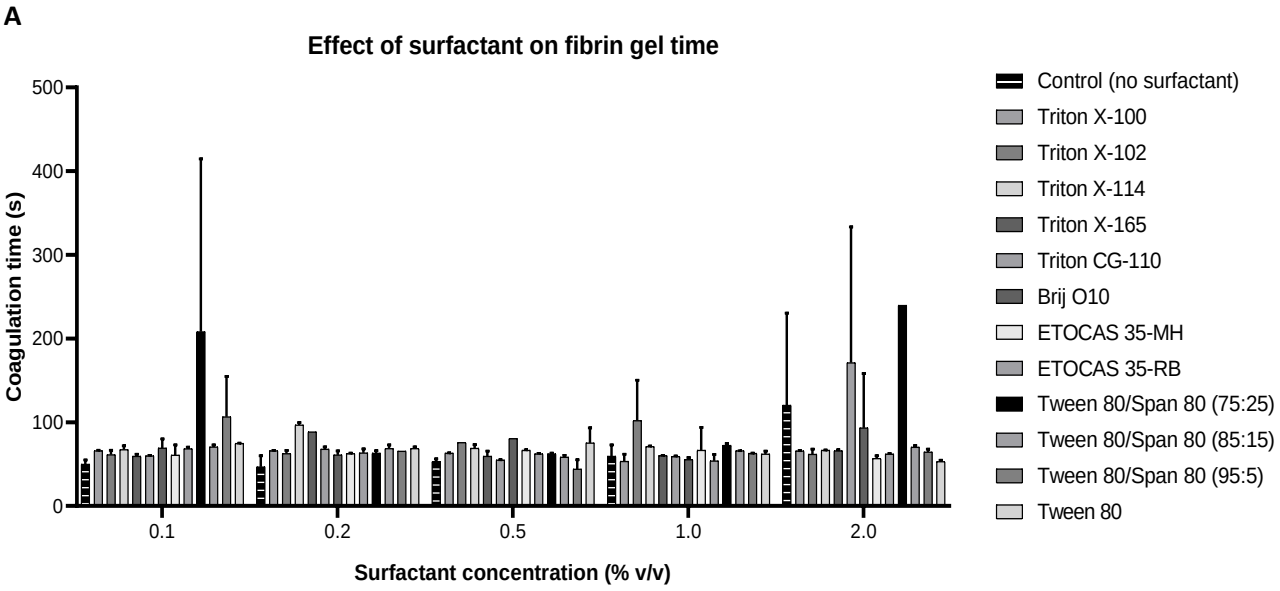

Fig. 13: Effect of surfactant and surfactant concentration on coagulation time of fibrinogen/thrombin. Neither presence nor choice of non-ionic surfactant was found to have any significant effect on fibrin gel formation time. Tween 80/Span 80 in a ratio of 3:1 (HLB 12.3) was the only formulation with significantly reduced gel time compared to the control (0.1% **) or other surfactants (*).

Below: Cuvettes showing the steel ball bearing held in a fibrin gel. **[B]:** Less stable emulsions, or systems with a slow clot time, separated in the cuvette. The lower section was denser and more opaque. **[C]:** in more stable emulsions, less separation occurred and the resultant gel was less dense but comprised a greater portion of the total test volume. The gel appeared cloudy, rather than translucent (fig. 13B) because the gel in the stable emulsion system trapped oil droplets which increase backscattering of incident light.

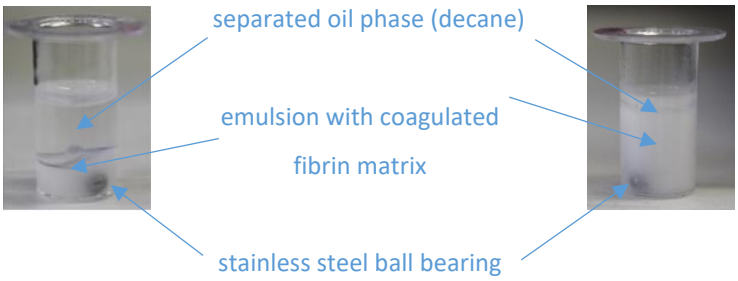

B **C**

Less stable emulsions tended to separate before the fibrin clot formed (fig. 13B). This was clearly distinguishable by the appearance of a transparent layer of oil at the top of the cuvette. The denser aqueous phase, containing fibrinogen and thrombin, sank to the bottom and formed the fibrin clot. Depending on the rate of destabilisation and the fibrin clot time, the two phases could separate completely, as shown above, or partially, giving rise to a gradient of gel strength. In this case, fibrin clots were densest at the bottom of the cuvette, close to the ball bearing.

In more stable emulsions, the oil phase remained dispersed during fibrin formation. The clot was therefore dispersed throughout the cuvette instead of accumulating in a dense gel at the base. The coagulometer works by timing gel formation until it is sufficiently strong to resist and stop the movement of a circulating ball bearing. The different fibrin densities formed in stable and unstable emulsions were therefore a concern for quantifying clot time; however, even the diffuse gels were able to slow the movement sufficiently to trigger the coagulometer. However, the pitfalls of this test highlight the importance of considering a range of data (clot time, mechanical strength, microstructure) in conjunction when evaluating scaffold design parameters.

Surfactants are key to forming stable emulsions with a specified mean droplet diameter. Ionic surfactants can interact with proteins and denature them, impairing or destroying the native structure. Even non-ionic surfactants display a degree of cytotoxicity. There are two factors at play: one being the surfactant concentration and the other being the HLB. The concentration must be sufficiently high to stabilise the emulsion, but low enough to avoid protein interference or degradation. At optimal HLB, the surfactant will display equal affinity for the aqueous and oleic phases of an emulsion. In a perfect system, the surfactant will

be fully engaged at the interface and will not interact with protein. Selecting a surfactant that displays slightly more lipophilicity may further reduce risk of protein interaction by physically moving the surfactant deeper into the oil phase and away from the protein in the aqueous phase, but this would be detrimental to the emulsion stability.

In this case, all of the surfactants tested formed emulsions at all concentration. As previously discussed, the Tritons and Brij were selected for their superior stabilising power at higher oil fraction. Tween was used as a useful back-reference and because it is a well characterised, commonly used commercial surfactant. None of the surfactants tested, at any concentration, increased the coagulation time beyond a reasonable length of time (i.e. coagulation always occurred within 2 minutes which is well within the stability time of the emulsion and thus template). There were no clear patterns between concentrations or surfactants.

CONCLUSIONS

As an adherent protein key to the wound healing process, fibrin is an excellent candidate material for a skin tissue engineering scaffold. It self-assembles into strong fibres from fibrinogen and thrombin. Varying their ratios allows tunable fibre diameter and mesh density. Artificial cross-linking of fibrin (in this case, with glutaraldehyde) imparts mechanical strength to the scaffold and also prolongs its residence in vivo by resisting proteolytic degradation. This enables the scaffold to persist for a clinically useful timeframe while the regenerating and remodelling tissue gradually takes over the mechanical and structural contributions from the scaffold. Fibrin fibres form the base of the hierarchical structure and differentiate the scaffold from other materials. If the protein's native structure is damaged (due to artificial processing, or accidental or incidental denaturation) the structural functionality is lost.

Emulsion templating was selected as a method of producing tightly prescribed and reproducible three-dimensional scaffolds while retaining fibrous fibrin structure. Emulsion templating offers advantages over other methods of creating porous materials. Unlike foaming, control over porosity, pore size, pore size distribution and wall thickness are possible. The structures generated are more organic in shape than those typically created by additive manufacturing, where a simple pattern is often repeated to build the structure. Electrospinning offers a method of generating spun fibres down to the nanoscale with good control, but the use of high voltages and aggressive solvents limits the use of native proteins as a scaffolding material. Additionally, creating complex and controlled 3D structures is not possible by this method alone. Melt moulding requires high temperatures which denature proteins, removing native structures. Use of particle leaching creates tightly packed, highly porous structures with small size distribution and good control over pore size, but removal of the porogens often requires complex or aggressive post-processing that again precludes the use of native proteins.

While emulsion templating is a commonly used process and has been widely used for a long time, the most common methods use an inverse water-in-oil emulsion. The chemicals and processing conditions used are aggressive and better suited to synthetic polymers rather than proteins. Oil-in-water emulsions stabilised with ionic surfactants, or surfactants at high concentrations, are similarly denaturing and preclude the use of proteins in their native form. To our knowledge, the method described above is unique in allowing for HIPE templating of a protein in its native form (≥74% porosity). Furthermore, owing to the limitations of other methods described here, our technique may be the only method for producing such high porosity materials with native proteins.

In the work presented, emulsions were refined to produce homogeneous emulsions with stability in excess of fibrin clot time. This allowed the fibrin network to consolidate around the oil droplets at optimal diameter and dispersion. Surfactants were screened for their ability to stabilise high internal phase emulsion (>74% v/v) up to 95% oil fraction, enabling generation of very highly porous scaffolds. Droplet packing was very tight in the HIPE regime, so pore walls were thin and improved diffusional and interconnection voids.

Identifying suitable surfactants with high oil carrying capacity allowed their use at lower concentrations (0.1% v/v). At this concentration, no detrimental effect on fibrin formation time or microstructure was observed. The density of droplets in the dispersed phase is varied by changing the ratio between the continuous and dispersed phases. Here, dispersed phase ratio was increased in small increments, using different surfactants to maintain stability at higher oil fractions. In this way, oil phase was gradually increased from 50% (fig. 6) to 90% (fig. 9).

Mixing speed was optimised to obtain oil droplets and thereby pore sizes conducive to cell and blood vessel ingress (fig. 3). Emulsion droplet size can be controlled and varied by altering the interfacial tension between the oleic and aqueous phases. Homogenisation of an emulsion system, for example by shear mixing, reduces droplet size to a minimum after which no further decrease is observed. The smallest droplets are achieved by mixing at the highest speed for the shortest time, until the theoretical minimum droplet size is achieved, then the mixing time has no further effect (Prinderre et al., 1998; Solans et al., 2005). However, mixing by vortex was shown to destroy fibrin structure and produce pores too small to allow cell ingress. Instead, mixing at 5000 rpm with an impeller mixer produced a narrow range of droplets of optimal diameter.

The minimum droplet size is governed by interfacial tension and the availability of surfactant in the emulsion system. Homogenisation promotes droplet formation by distributing surfactant throughout the system to enable assembly around a greater number of interfaces. This can also be achieved by, or in conjunction with, increasing the concentration of surfactant.

This work enabled creation of a prototype fibrin-based scaffold with appropriate microstructure (porosity, interconnectivity, wall thickness) from a stable, non-denaturing emulsion. Successful drying and subsequent

storage of the scaffolds confirmed that the oil phase was successfully removed from the scaffold during the washing process. This is important for prolonging shelf life and ensuring cytocompatibility.

As a result of the experiments described here, a final scaffold composition of 2:1 fibrin:PVA, templated from a 90% oil fraction emulsion containing 0.1% Triton X-165, was selected. With the emulsion composition optimised and confirmed, further refinements to the scaffold were made without the need to revise emulsion formulation.

ACKNOWLEDGMENTS

This work was funded by The Open University, Cells for Cells and Consorcio Regenero. The project is hosted by the tissue engineering group at the Institute of Biomedical Engineering, University of Oxford (Cui group). The authors would also like to thank Gordon Imlach (The Open University) for providing SEM training.

GFP-MSC-hTERT were kindly provided by Dr. James Li (Dept. Paediatrics and Adolescent Medicine, LKS Faculty of Medicine, University of Hong Kong.

3.3 Manufacture and characterisation of novel fibrin-based hierarchical polyHIPEs

ABBREVIATIONS

CCK-8	cell counting kit	MMP	matrix metalloproteinase
DMEM	Dulbecco's Modified Eagle's Medium	O/W	oil-in-water emulsion
ECM	extracellular matrix	PBS	phosphate buffered saline
EtOH	ethanol	PEG	polyethylene glycol
ETPM	emulsion templated fibrin-based scaffold	PM0	foamed fibrin-based scaffold
		polyHIPE	scaffold templated from HIPE
FBS	foetal bovine serum	PS	penicillin-streptomycin
GFP-MSC	fluorescently labelled mesenchymal stem cell	PVA	polyvinyl alcohol
		SEM	scanning electron microscope/graph
GTA	glutaraldehyde	UTS	ultimate tensile strength
HIPE	high internal phase emulsion	W/O	water-in-oil emulsion
MES	2-(N-Morpholino) ethanesulfonic acid		

ABSTRACT

Emulsion templating is a versatile technique for creating porous materials with well-defined porosity, pore diameter, pore size distribution and the degree of interconnectivity between these pores. Hydrophilic or hydrophobic monomers may be dispersed into the aqueous or oleic phase, respectively. Synthetic biocompatible polymers such as PMMA, PLLA and PCL can be templated using water-in-oil emulsions. The resultant porous biomaterials have precise micro- and macro-architectures arising from the emulsion template but lack biologically relevant structures. These may be added in subsequent manufacturing steps. Using proteins (gelatin; collagen) as the polymeric material allows the introduction of physiologically relevant chemistries to the biomaterial. However, the surfactants required to stabilise emulsions for templating are aggressive and denaturing for proteins, altering their structure.

This experimental section describes scaffolds manufactured by a facile emulsion templating process that does not use organic solvents and minimal non-ionic surfactant (well below cytotoxic concentrations). Template fidelity is good, allowing repeatable small batch manufacture of scaffolds with tuneable porosity, pore size and pore size distribution. Electron microscopy of the scaffolds reveal the fibrous protein structure is preserved, creating an intricate "basket-weave" structure down to the nanoscale and removing the need for subsequent processing. Further, the scaffolds show mechanical properties, cyto-compatibility and angiogenic potential in line with market-leading scaffold products.

INTRODUCTION

Emulsion templating is a widely used and highly versatile method of introducing porosity (Kimmins and Cameron, 2011; Zhang and Cooper, 2005) whereby immiscible phases (typically oleic and aqueous-based) are mixed to form a dispersion of droplets (the dispersed phase) in a continuous phase (Hentze and Antonietti, 2001; Tadros, 2013). An amphiphilic molecule, such as a surfactant, may be added to promote stability of the emulsion (Hentze and Antonietti, 2001).

A water-in-oil emulsion (w/o) has oil droplets dispersed in an aqueous continuous phase. An oil-in-water emulsion (o/w) has aqueous droplets dispersed in an oleic continuous phase (Tadros, 2013). Hydrophobic polymers, such as the commonly-used styrene/divinylbenzene co-polymer system, dissolve in the oil phase to form a scaffold matrix around the dispersed aqueous phase in 'inverse' w/o emulsions (Silverstein, 2014).

Alternatively, the polymer may be dissolved into the dispersed phase (i.e. a hydrophobic polymer in an o/w emulsion) to form micelles or template microbeads. These polymer microbeads may be used to deliver a variety of substances *in vivo*, such as proteins, drugs and DNA/RNA (Ho et al., 1994; Kulkarni et al., 2011; Tessmar and Göpferich, 2007).

High internal phase emulsions (HIPEs) allow greater yield of templated beads (if the polymer forms in the dispersed phase), or highly porous templated scaffolds (where the polymer forms in the continuous phase). Additionally, the interfacial nature of the HIPE phase gives stability to the formed structure (polyHIPE) during the manufacturing process.

Some oil-in-water polyHIPEs have been used to create hydrophilic scaffold materials, including some protein biomaterial scaffolds. However, these use processed or denatured proteins (such as gelatin) as a base material (Barbetta et al., 2005). To date, native-structured protein polymers have not been templated using polyHIPE. This section focuses on emulsion templating using o/w emulsions with hydrophilic materials in the continuous phase.

The emulsion system presents a challenge in templating proteins: surfactants required to generate sufficient emulsion stability to support the protein framework during consolidation can denature proteins and hinder this process.

In the work presented, protein polyHIPE emulsions were manufactured and characterised using an optimised emulsion system. A range of surfactants (Brijs, Tritons, Tweens, Spans and Tergitols) were studied for emulsifying decane (dispersed phase) in physiological buffer. Emulsion stability was evaluated using light scattering with a Turbiscan LAB analyser against increasing oil fraction. Internal phases of up to 95% volume fraction were achieved in an optimised system. When translated to scaffold manufacture this produced high fidelity, highly porous scaffolds with close cell packing and even protein distribution, resulting in an

interconnected structure with well-defined pores (confirmed by scanning electron microscopy). Droplet size was optimised for cell ingress and angiogenesis.

Iterative design and characterisation of the emulsion system allows control of the diameter, number and packing of droplets within the dispersed phase. This approach offered a rapid and effective screening method for protocol design for templating of protein polymeric materials.

Fibrin has been widely investigated as a scaffold for a diverse range of tissue engineering applications including engineering of small blood vessels and heart valve prostheses; cartilage; bone and skin, as well as a carrier for transplanted stem cells (Bensaïd et al., 2003; Geer et al., 2002; Jockenhoevel et al., 2001; Perka et al., 2001; Swartz et al., 2005; Yasuda et al., 2009). The use of fibrin composite tissue engineering constructs, with materials such as fibrin-agarose, fibrin-collagen, fibrin-alginate, fibrin-PCL, fibrin-PLLA-PLGA and fibrin-polyurethane has also been described (Carriel et al., 2012; Collen et al., 2003; S. B. Lee et al., 2003; Lesman et al., 2011; Levenberg and Lesman, 2014; Ma et al., 2012, 2003; Schagemann et al., 2010; Serbo and Gerecht, 2013; Shikanov et al., 2009; Swieszkowski et al., 2007; Weinberg, 1989).

The strength of fibrin adhesion derives from its ability to bind to cells (de la Puente and Ludeña, 2014) either directly, via integrin receptors, or indirectly via ECM proteins such as fibronectin (binding to fibroblast and phagocyte receptors) (Makogonenko et al., 2002) and vitronectin (binding to collagen and endothelial cell receptors) (Preissner and Jenne, 1991).

Fibrin has been used as a haemostatic agent for over 100 years (Loeb, 1909). Its therapeutic use was inspired by its native action in the coagulation cascade, and it is used to rapidly seal a wound and prevent blood loss in extreme scenarios, such as battlefield injuries (Borst et al., 1982; Granville-Chapman et al., 2011; Vournakis et al., 2003). This versatility in application may derive from the characteristic structure of fibrinogen, and the different ways of producing fibrin from fibrinogen (using autologous, allogeneic, xenogenic or recombinant fibrinogen and polymerising with thrombin or snake venom (Linnes et al., 2007; Stocker et al., 1982).

In normal physiology, the persistence of fibrin constructs – blood clots – is regulated by the interplay between the coagulation and fibrinolysis cascades (Clark, 2003; Standeven et al., 2005). Regulation of artificial fibrin scaffolds is likewise tuneable by mechanical, chemical, or enzymatic means. The number, diameter and density of fibrin fibrils affects degradation rate; as does the biochemical environment, including proteolytic enzymes.

One problem with the use of fibrin for implantable biomaterials is its rapid degradation *in vivo*. Protease inhibitors like aprotinin or tranexamic acid can delay proteolytic degradation, prolonging the persistence of implanted fibrin constructs as required to support the repairing tissue (de la Puente and Ludeña, 2014; Jockenhoevel et al., 2001).

Having identified and evaluated a number of surfactants capable of stabilising a high internal phase emulsion (Section 3.1) at sufficiently low concentration to avoid denaturation of fibrinogen in the aqueous phase

(Section 3.2), the next step was to fine-tune the emulsion to generate desirable properties in the templated scaffold. The optimised method developed preserves fibrin's hierarchical fibrous structure and differentiates the scaffold from other protein scaffolds where native structural functionality is lost during processing.

The fibrin fibres around the oil-templated pores form a connected series of niches for cell residence. The size of these pores is critical to permit cell and blood vessel ingress. Good interconnectivity – a consequence of the basket-weave structure as well as high porosity and very close pore packing – enables cell migration and communication and also supports angiogenesis. This is vital for the development and survival of the regenerating tissue. Rapid angiogenesis will help accelerate the cellular response. Scaffold structure and pore size is dependent upon the size and packing of oil droplets in the precursor emulsion. A key objective was to ensure template fidelity from the optimised emulsion and the resultant scaffold by balancing emulsion stability with unimpaired fibrin formation.

Initial templated scaffolds (fig. 3, Section 3.2) suffered insufficient porosity, giving rise to large, unconnected pores and thick pore walls. Excessive fibrinogen concentration also produced thick walls between pores, and densely packed fibres will few diffusional spaces. Scaffolds with higher porosity were difficult to manipulate and often tore during manufacture. A secondary aim was to improve mechanical properties of highly porous scaffolds to allow thinner pore walls with more diffusional space. It was hypothesized that addition of another polymer with viscoelastic properties could act to support lower density fibrin fibres and promote bulk elasticity of the scaffold to improve handling.

The ability to create protein polymeric materials with well-distributed, delicate protein microstructure is of significance in development of scaffold materials for tissue engineering. Currently, polyHIPE materials are largely restricted to a small number of available hydrophobic biomaterials available using water-in-oil emulsions. This work demonstrated the capability to design well-characterised emulsions to accurately template protein materials such as fibrin, collagen and alginate, which are commonly used in tissue engineering scaffolds. This method allows hierarchical scaffolds to be created in which the native protein structure is preserved (not possible by other methods).

EXPERIMENTAL PROCEDURES

Materials

All water and buffers were autoclaved or sterile filtered, as appropriate, prior to use. All preparatory and formulation work was undertaken in a class I HEPA filtered laminar flow hood to minimise risk of product contamination. 2% bovine fibrinogen lyophilised powder (w/v of clottable protein) was prepared by dissolving in MES/NaCl buffer (25 mM/150 mM, pH 7.4) at 37°C with minimal agitation to prevent foaming. Calcium chloride solution (1 M in distilled water) and stock polyvinyl alcohol (PVA) (M_w 31,000-50,000 g/mol, 87-97% hydrolysed) solution (5% w/v in MES/NaCl, dissolved overnight at 37°C with periodic agitation) and thrombin (pre-dialysed, in frozen aliquots) were warmed to 37°C before use. Decane and surfactants were used as purchased. 0.8% (v/v) glutaraldehyde solution was prepared by adding 8 ml Grade I glutaraldehyde (25% in H_2O; Sigma Aldrich) to 800 ml absolute ethanol and 200 ml 0.1 M MES (aqueous solution, sterile filtered, pH 7.4). Glutaraldehyde solution was prepared freshly for each of the two washes, no more than 10 minutes before use.

Suitable surfactants include Triton X-100, X-102, X-114, X-165, X-100 reduced, X-114 reduced, N-101 reduced; Brij 58, O10, O20; Tergitol 15-S-7, 15-S-9, 15-S-15, TMN-6, TMN-10, NP-10; Ecosurf EH-9.

MES monohydrate crystals were purchased from Fisher Scientific (Loughborough, UK); all other materials were purchased from Sigma Aldrich, Inc. (Gillingham, Dorset, UK).

Emulsion preparation

Emulsions were prepared separately for each 5x5 cm scaffold; each with a volume of 22 ml. Decane formed the oleic phase (90% v/v). The aqueous phase (10% v/v) comprised fibrinogen, thrombin (in a 4:1 ratio), calcium chloride and PVA all dissolved in a MES/NaCl buffer solution (pH 7.4). For each scaffold, 20 µl surfactant was dispersed in 20 ml decane in a 50 ml universal tube. 5 µl calcium chloride solution, 625 µl MES/NaCl buffer and 100 µl 5% PVA solution were added and shaken vigorously. 1 ml warmed fibrinogen solution was added, and the tube was shaken vigorously until the contents emulsified fully (determined by dramatic change in viscosity and opacity). 250 µl warmed thrombin was added and the mixture was shaken immediately and vigorously for 30 s.

Scaffold manufacture

The final emulsion was poured into a square-edged weighing boat which was tapped to remove air bubbles. The weighing boat was covered to reduce evaporation and incubated for 1 hour at 37°C.

The scaffold was incubated for 1 hour at room temperature with 25 ml cross-linking solution (abs. ethanol, 0.1 M aqueous MES solution (pH 7.4) and glutaraldehyde (25% aqueous solution) in a ratio of 100:25:1). The

scaffold was flipped over the process repeated for another hour with fresh cross-linking solution. During cross-linking the scaffolds turn from white to yellow (colour intensity is dependent on concentration of glutaraldehyde and fibrinogen present). Residual glutaraldehyde was consumed by a series of 5 reducing washes using 0.1% sodium borohydride in distilled water. The solution was changed and the scaffold flipped over after each wash. This process was repeated for a further four washes with distilled water, flipping the scaffold and replacing with fresh water each time. The scaffolds were then washed in 0.2% aqueous PVA solution (w/v) for 5 minutes each side before draining. Scaffolds were then lyophilised overnight at -40°C under vacuum, (VirTis Genesis 25ES, SP Scientific, Warminster, Pennsylvania, USA).

Characterisation methods

Microstructural evaluation

Three scaffolds per condition, and three samples per scaffold were tested (nine samples per condition). The scaffold samples were cut to approximately 8x3 mm, mounted in cross-section and sputter coated on stubs. Micrographs were taken with a Zeiss Supra 55 VP scanning electron microscope (aperture 20 µm; current 5 kV). Each sample was imaged at three different sites. Void size and size distribution (including all measurable voids) was evaluated using the measure function in Image J. The images used for analysis were all 1000x magnification micrographs, as these images contain clear resolved structures of interest at both pore and interconnect level.

Pore and interconnect sizes are measured manually from SEM micrographs using Image J. The largest round shapes that can be resolved as assigned as ‘pores’; the smaller structures within these are assigned ‘interconnects’. Immeasurably small distances (using this method, at appropriate magnification to resolve pores) are designated diffusional gaps (space between fibrin fibres as opposed to templated structures) and are not recorded owing to their small size and high frequency.

Cyto-compatibility

Cylindrical samples were cut with an 8 mm biopsy punch (n=3) were cut from two scaffolds (six samples per condition). These were washed twice with 70% EtOH, twice with PBS and once with DMEM. GFP-MSC-hTERT* were seeded (p12, 50,000 cells/well) onto the hydrated scaffolds and a plate control with 150 µl DMEM+FBS+PS. At 24 h (acute response time) and 120 h (chronic response time), 300 µl DMEM/CCK-8 (10:1) was added and incubated for 4 hours at 37°C before reading absorbance at 450 nm.

Mechanical testing

Cyclic compressive testing was performed on bulk hydrogels of the same composition as the aqueous phase of the fibrin-PVA scaffolds. Each gel was formed into a disc of approximately 1 cm in diameter and 3 mm deep. Testing was performed on an Instron UTM 5942 using a 5 N load cell for a total of five cycles.

Freeze-dried scaffolds were cut to 10 mm wide strips (approximately 50 mm long and 3 mm wide). Small pieces of dry paper towel were folded over either end to provide additional grip and prevent slippage. The ends of the scaffold were secured leaving a gauge length of 40 mm. Testing to failure was performed in triplicate for each scaffold using an Instron UTM 5582 (100 N load cell, crosshead speed 8 mm/minute).

Scaffold degradation (hydrolytic and enzymatic)

6 mm discs were cut from each scaffold. To measure hydrolytic degradation, scaffold samples were incubated at 37°C in sterile PBS. Enzymatic degradation was measured by incubating scaffold discs at 37°C in PBS with a) 0.25% trypsin, b) 0.125 U/ml plasmin and c) MMP-1, MMP-2, and MMP-9 (each 0.2 μg/ml). Each of the solutions for the enzymatic degradation assay were changed daily. For both enzymatic and hydrolytic assays, discs were removed and freeze-dried at the following time points: 7, 14, 21 and 28 days (hydrolytic) and 1, 3, 5, 7, and 10 days (enzymatic). Each test was performed in triplicate. Degradation was reported as percentage change in mass from day 0 to the time point.

$$\Delta \text{ mass } (\%) = 100\ (W_0 - W_t W_0) \qquad \text{(eq.1)}$$

Equation 1 (from Grizzi et al (26)) expresses the change in mass over time where W_0 is the initial dry mass and W_t is the mass of the same sample, removed from the test solution at time *t* and lyophilised before weighing.

Statistical analysis

Statistical analysis was performed using GraphPad Prism version 8.1.2. Significance was evaluated using one- or two-way analysis of variance (ANOVA), as appropriate, with Tukey's post-hoc multiple comparison tests. Levels of significance were assigned as follows – * where $p<0.05$; ** where $p<0.01$; *** where $p<0.001$ and **** where $p<0.0001$.

RESULTS AND DISCUSSION

Comparison of emulsion templated and foamed scaffolds of similar protein composition

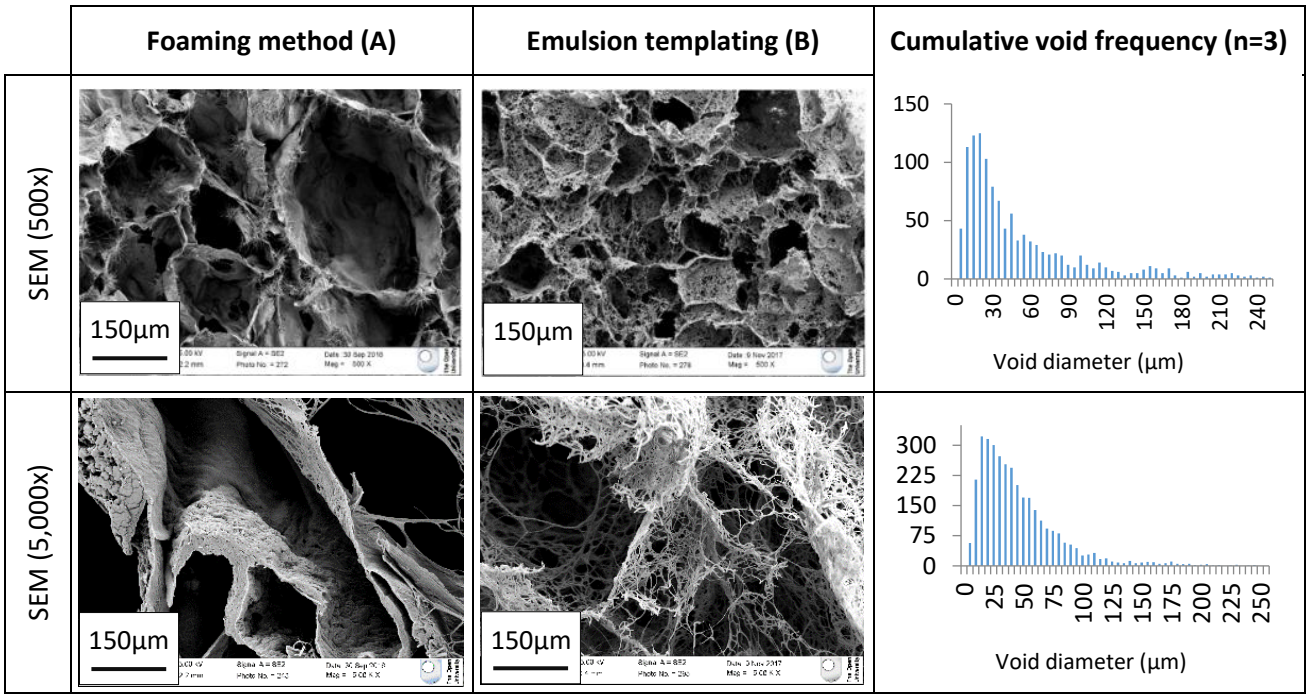

Fig. 1: Cross-sectional electron micrograph images and void diameter frequency charts of fibrin-based scaffolds produced by (A) foaming method and (B) emulsion templating. Foaming creates a high degree of porosity but offers no control over pore size or size distribution and therefore lacks reproducibility. Lack of pore size control is shown in the histogram with a wide distribution of void diameters recorded. Additionally, foaming can produce very dense regions of protein (shown in the higher magnification image). There are few interconnects or smaller voids. Emulsion templating offers more control over pore size, with a more uniform pore size distribution. Total void frequency is significantly higher in the templated scaffold owing to better interconnectivity and many more small voids ("diffusional gaps").

Emulsion templating offers better control over droplet size and wall thickness compared to other methods such as foaming (fig. 1). The foamed scaffold had regions of high porosity but was very heterogeneous. The foaming method created a somewhat interconnected network between the pores generated by coalescing bubbles. Variability in porosity and wall thickness were governed by dispersal of foaming agent through mixing homogeneity. If the foaming agent is not dispersed uniformly dense regions of material form. In vivo these would provide no functionality and may exacerbate the inflammatory response and could lead to M1 macrophage attack (reducing scaffold persistence) or fibrous encapsulation (Merritt et al., 1979; Sheikh et al., 2015; Šprincl et al., 1971).

Formation of hierarchically structured templated scaffolds

The pore size in templated scaffolds is governed by the size of oil droplets in the internal phase. With fixed surfactant type and concentration, oil and aqueous phases and energy of mixing, thermodynamics dictate that the same approximate size of droplets will form each time (Fontenot and Schork, 1993). Steric repulsion of the surfactants govern pore spacing, and fibrin(ogen) content prescribes the fibre density that will form around the pores. In the HIPE system, interfacial forces become dominant due to the border effect described by Plateau's laws (Kravchenko et al., 2018). An emulsion must be sufficiently stable to maintain droplet size and spacing during the fibrin formation time. The curved triangular spaces between droplets, which may be approximated to I-beams, confer compressive strength to the emulsion and templated systems.

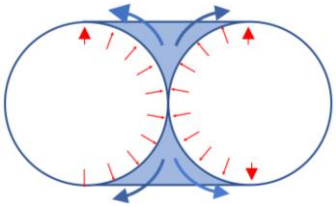

Fig. 2: Droplet proximity and internal pressure push scaffold material away from the point of contact. This becomes an interconnect.

In this case, template fidelity may be assumed. Porosity is therefore governed directly by the volume fraction of the oil internal phase and is also easily controlled. These features allow the emulsion templated scaffold to be faithfully reproduced within and across multiple batches.

Unlike porosity, interconnectivity is not directly governable but may be controlled to a degree. It arises from the closeness of the pores and the quantity of material forming the walls. The degree of interconnectivity is greater in scaffolds with tightly packed pores and the minimum material to support the structure. At the closest point of contact between two pores, the internal droplet pressure pushes the material to either side of the contact point and leaves a connecting space (fig. 2). The materials described here have varying interconnect diameters but consistently high degrees of interconnectivity, creating an open-celled structure within the scaffold (fig. 3).

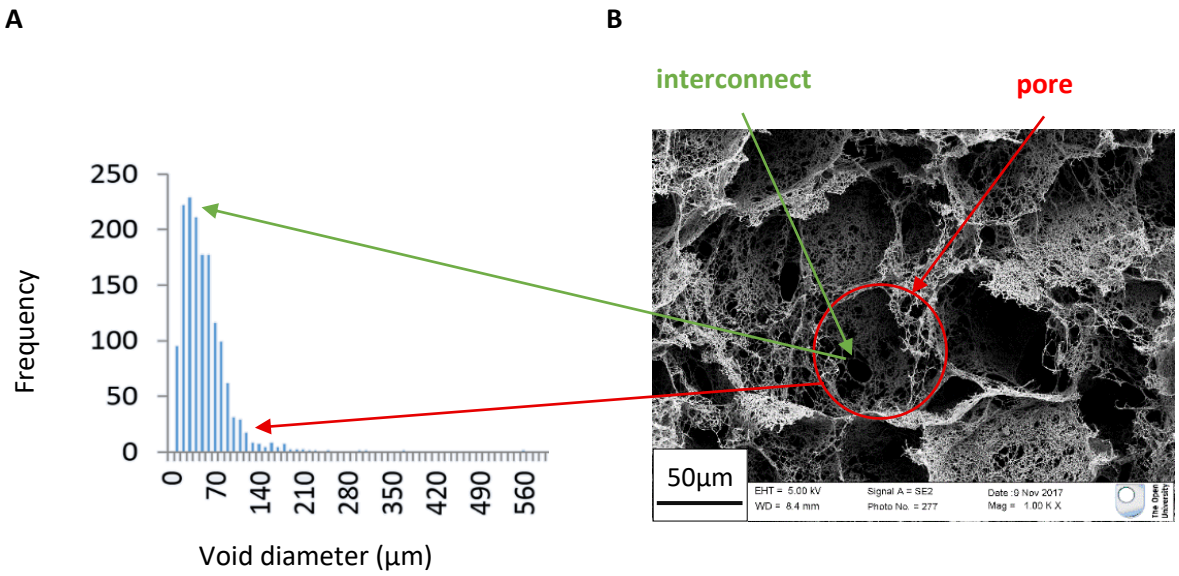

Fig. 3: Cross-sectional scanning electron micrograph showing geometry of optimised emulsion-templated scaffold. [A] Cumulative frequency from three sites analysed from the same scaffold. Mean pore size 102.35 µm, SD=74.83; mean interconnect size 35.05 µm, SD=15.34; mean diffusional void size 7.13 µm, SD=1.96. All measurable voids were quantified at the widest point using Image J (1000x micrograph). Pores were determined as the largest resolvable round structures on the image; interconnects are the smaller gaps within them. Very small gaps resulting from spaces between fibrin fibres, as opposed to template shape, were designated as diffusional gaps. Only the larger diffusional gaps were measured as most were too small to measure accurately by this method. Fig. 3(B) shows a typical cross-section of a freeze-dried scaffold (Zeiss Supra 55 VP; 5 kV, 1000x magnification).

Optimising fibrinogen concentration

Fibrinogen content in the aqueous phase was initially calculated based on an existing in-house method for manufacturing fibrin-based scaffolds by another method (not disclosed). This proved successful with sub-HIPE oil fractions (50-70% v/v; previously reported in Chapter 3.2) but at higher oil fractions produced dense polyHIPE materials which frequently tore during manufacture owing to excessive bulk.

The concentration of fibrinogen in the aqueous phase of the HIPE was halved, maintaining proportions of thrombin and calcium chloride, to produce more delicate structures (fig. 4(B)). Reducing the protein concentration resulted in thinner yet more robust scaffolds with excellent handling properties (wet and dry) as well as increased permittivity and interconnectivity as illustrated in the cross-sectional SEM images.

The precursor emulsion must contain sufficient fibrinogen to form fibrous networks around the largest of the pores that can adequately support their own weight when the template is removed. Fibrinogen solutions

become extremely viscous above 5% (w/v, clottable protein). 10% was found to be the highest useful concentration with the method and equipment described here.

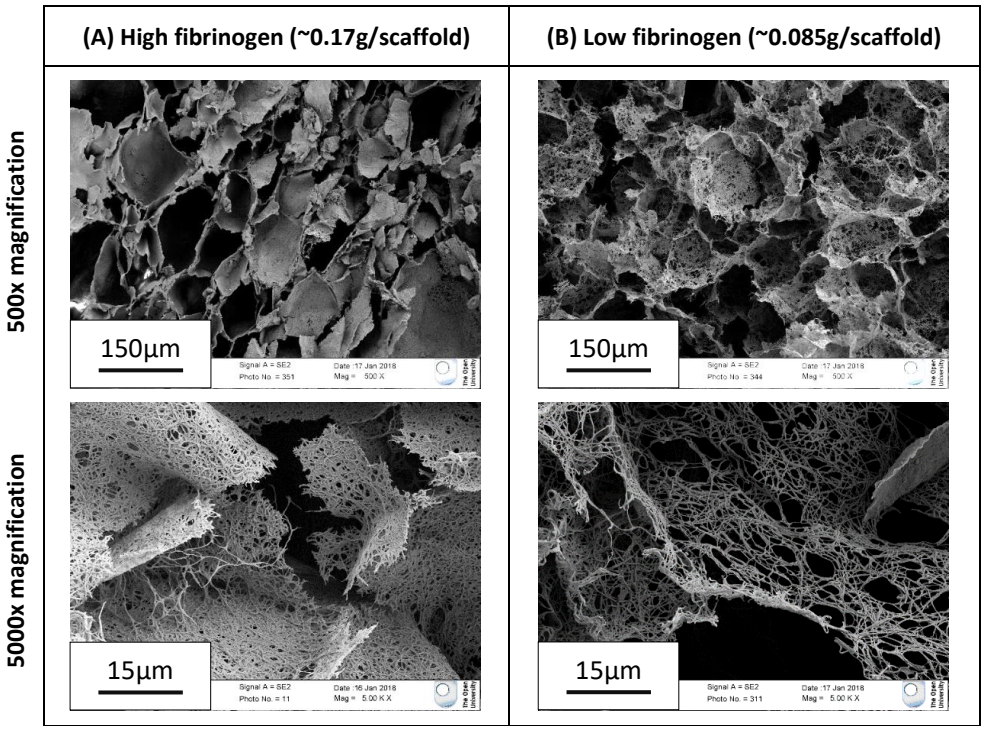

Fig. 4: Effect of fibrin concentration on scaffold architecture. A higher fibrinogen concentration results in the formation of a dense fibrous network of fibrin resembling a mat. Template fidelity is good at pore level, but there are few interconnects and diffusional gaps. Any additional materials such as co-polymers settle between the fibres and further reduce permeability (visible in 5000x image). At reduced fibrinogen concentration, template fidelity is preserved but the fibrin network is more diffusive and individual fibres are evident. Interconnectivity is greatly increased. Diffusional gaps are also far more prevalent.

The fibrinogen volume was limited by the total emulsion volume (i.e. the size of scaffold desired) and the volume fraction occupied by oil (i.e. the desired scaffold porosity) as well as any other materials to be included.

A higher fibrinogen concentration ensured more fibrin coverage around the oil droplets and better mechanical strength. Lower fibrinogen concentration gave a more diffusive, fibrous basket-weave structure which in turn gave better diffusivity, permeability, and pore interconnectivity These features are all important scaffold design considerations so fibrinogen content must be modulated to achieve the optimum balance.

The high-fibrinogen scaffold was easier to manufacture owing to the improved mechanical strength. Fibrin formed rapidly and was therefore more forgiving of emulsion instability. Template fidelity was good, with tightly packed pores of similar sizes in the region 50-200 µm. However, the walls were very dense, resulting in reduced interconnectivity and permeability. Additionally, with the fibrin fibres are so closely associated, the

PVA co-polymer tended to cover groups of fibres rather than individual strands and further closed up the diffusional gaps (fig. 4(A), 5000x).

When fibrinogen concentration was too low, the scaffolds collapsed during manufacture, suggesting the fibrin was insufficient to surround larger pores. These are not pictured as they could not be preserved through to drying. Reducing the fibrinogen concentration from the high concentration (10% w/v clottable protein) to 5% then 2% w/v produced a scaffold which was readily handleable throughout manufacture. Template fidelity was as good as in the high-fibrinogen scaffolds, with tightly packed rounded pores. The sparser distribution of protein around the interface resulted in a more open structure with much greater interconnectivity and more diffusional gaps for the same meso-porosity. Under higher magnification, individual fibrin fibres were clearly visible (fig. 4(B)). These were sufficiently closely arranged to impart strength, but well-spaced enough that the PVA co-polymer did not coat them and seal up the smallest voids.

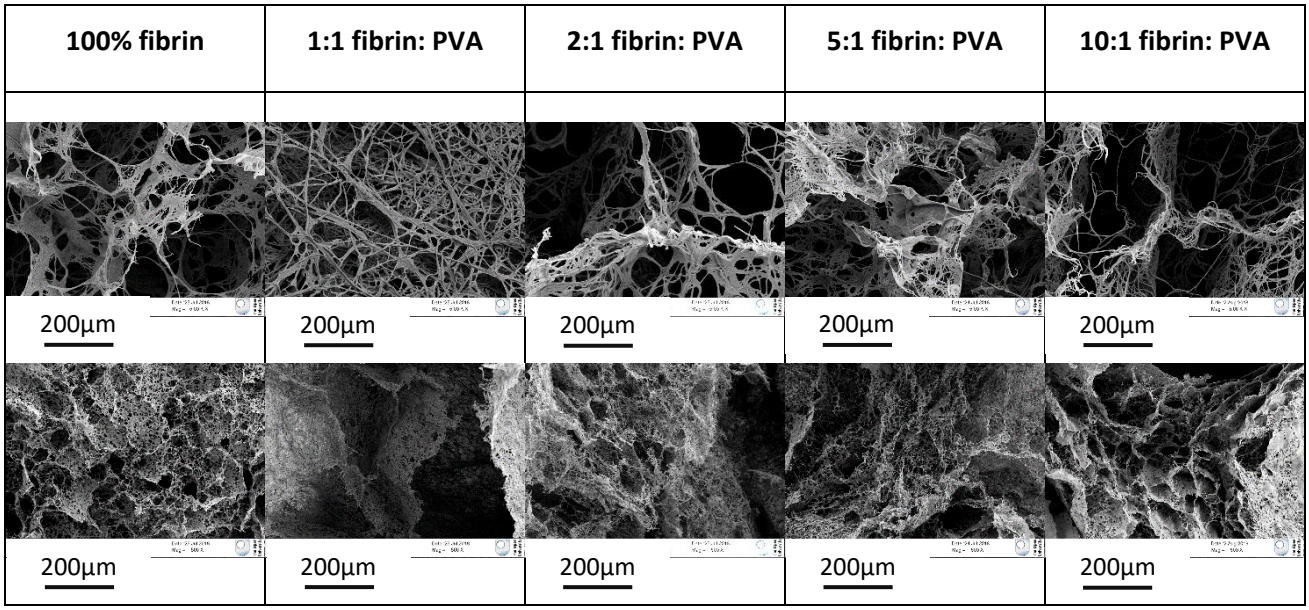

Fig. 5: Effect of fibrin: PVA ratio on scaffold micro-architecture. Fibrin scaffolds without PVA are fragile and brittle but have a delicate basket-weave hierarchical structure (5000x, top row; 500x, bottom row). Interconnectivity is high, with high permeability from diffusional gaps. 1:1 fibrin: PVA has greatly reduced interconnectivity and diffusional gaps. The PVA glues together neighbouring fibrin strands, reducing the hierarchical structure. At and above fibrin content of 2:1 fibrin: PVA the bundling of fibrin fibres by PVA is still present, improving resilience and handle-ability, but the underlying fibrous architecture is still visible.

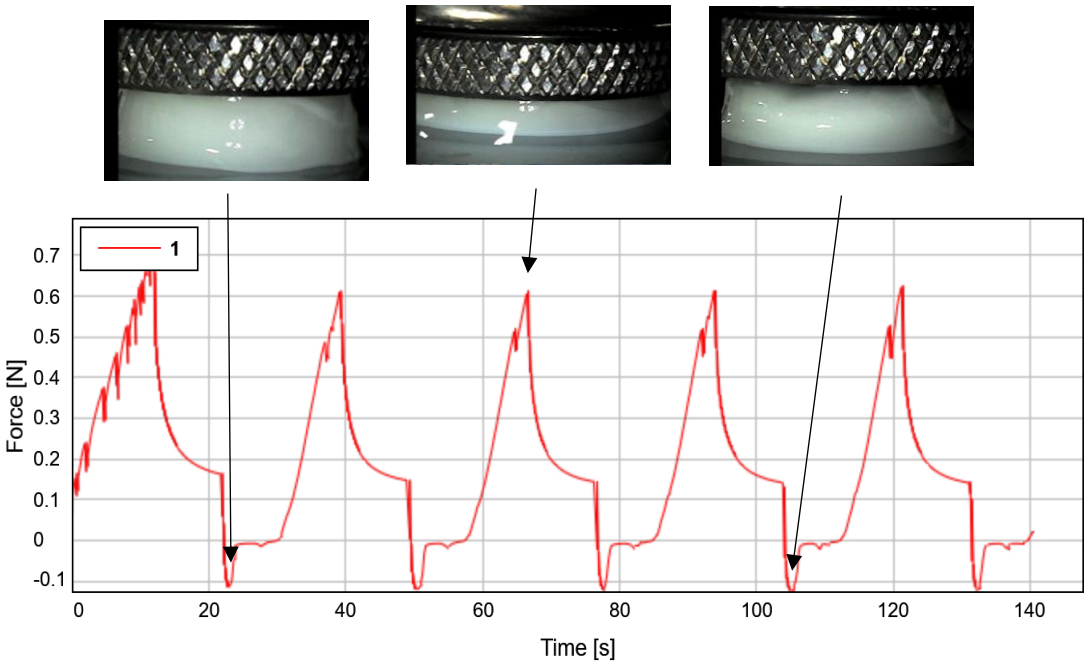

Fig. 6: Behaviour of bulk fibrin/PVA hydrogels under cyclic compressive loading. Bulk hydrogels of 2:1 fibrin: PVA show an elastic response with good recovery between loading. This testing is qualitative and is shown only for a single sample to demonstrate typical behaviour.

Addition of PVA to enhance elastic behaviour

Native fibrous fibrin produces scaffolds with optimal microstructure, but they behave in a brittle manner at macro-scale and can be fragile to handle. Scaffolds must be sufficiently robust to withstand manufacture, and to be cut, positioned, and stapled or sutured into place in clinical use. PVA was incorporated as a co-polymer to increase bulk elasticity of the scaffold. As previously described, aqueous component volumes are limited by the desired porosity and associated oil fraction, so a working solution of 5% w/v PVA was used. At 1:1 fibrin: PVA, the PVA was found to coat closely arranged fibrin fibres and draw them into thick bundles. While this did improve elasticity and handleability, it disrupted the microstructure by reducing nano-texturing and diffusional gaps. At meso-scale, reduced interconnectivity and diffusivity were evident (fig. 5).

Halving the PVA ratio to 2:1 gave a comparable improvement in elasticity but with less detriment to the microstructure. Although there was some association of fibrin fibres, diffusional gaps and interconnects remained evident. The structurally and biologically relevant hierarchy remained but the mechanical behaviour was much improved, so the 2:1 composition was deemed optimal.

At 5:1 and 10:1 fibrin: PVA, the microstructure was not significantly affected by the addition of PVA. However, the macro-scale mechanical properties were similarly unaffected so there was no benefit of PVA addition at these levels.

2:1 fibrin: PVA represents a concentration of 0.2% w/v PVA in the emulsion mixture. Even at this level, elasticity of the scaffold was increased. Bulk hydrogels of 2:1 fibrin: PVA, in discs of approximately 10 mm x 3 mm, were tested in their hydrated state under cyclic compression. The 2:1 material showed excellent recovery between each cycle, with closely similar stress-strain and recovery curves being produced each time (fig. 6). The linear slope on the ascending side is characteristic of elastic behaviour. The descending slope of each cycle represents the viscous component and is likely associated with the displacement and re-association of water with the hydrogel. The displaced water is visible in the second image of the compressed gel, and just visible drawing up the left edge of the right-hand image where compressive force has been released.

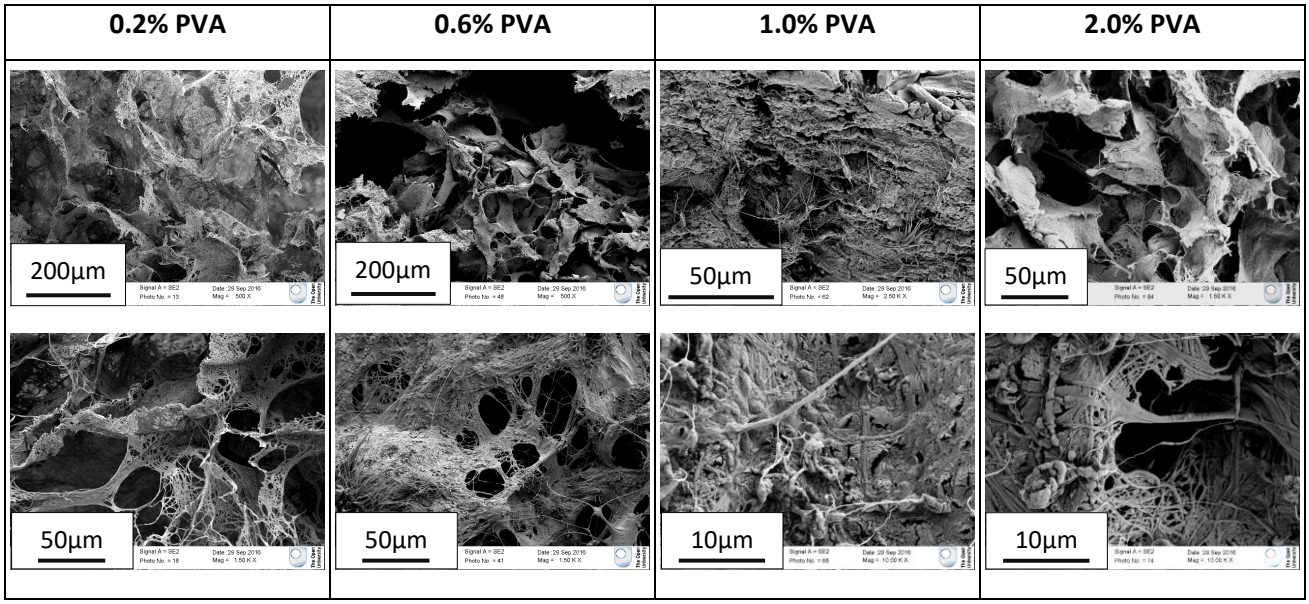

Fig. 7: Effect of PVA on scaffold micro-architecture when used as an excipient. Fibrin-based scaffolds washed with aqueous solutions of PVA (M_w 31,000-50,000 g/mol, 87-97% hydrolysed) were freeze-dried and imaged in cross-section. 0.2% v/v PVA supports the scaffold structure during freeze-drying, with hierarchical void diameter and individual fibres visible. Interconnects, diffusional gaps, and fine fibrous structure are reduced in scaffolds washed with 0.6% v/v PVA. The effect intensifies at and above 1.0% PVA where the PVA coats and masks the underlying protein structure.

Incorporating PVA as an excipient (0.2% w/v aqueous solution) prior to lyophilisation was initially used to protect the delicate microstructure under drying pressure (50 mTorr). Although not required for this purpose, it was found improve elasticity and general handling of both the dried and re-hydrated scaffold. The effect was comparable to when PVA was added to the emulsion mixture. When used as an excipient, the PVA is not an integral part of the scaffold and is likely to be washed out during rehydration and sterile washing before placement on a wound. However, it could improve handling by clinicians up to that point, allowing it to be positioned over a wound and cut to shape more easily.

Cross-sectional micrographs show that the microstructure was unaffected by washing with PVA at 0.2% w/v, determined as the optimal concentration for improving mechanical behaviour without detriment to the microstructure (fig. 7). The basket-weave structure, interconnectivity and diffusional gaps were clearly evident. Increasing the concentration to 0.6% w/v gave a comparable improvement in elasticity and handling, but the PVA closed up the fine microstructure by forming sheet-like structures over the fibrin. At 1% and 2% this was worsened with thicker deposition, even causing the formation of artefacts like globules and thick strands of PVA.

Scaffold cyto-compatibility

Two identical scaffolds (D3, D4) from different manufacturing batches (0.1% surfactant, 90% porous, 2:1 fibrin: PVA, 2% fibrinogen) were tested with triplicate samples from each. A scaffold ("PM0") with the same wall material and comparable porosity and pore size, manufactured via a foaming method (confidential), was used as a 3D control. This material is known to be non-cytotoxic, verified with both in vitro and in vivo assays. Surfactant (in this case, Triton X-165) was added to the same volume of media to give a concentration of 0.1% v/v, equivalent to the concentration used in the emulsion to template the scaffold. This was used to test inherent surfactant cytotoxicity.

At 24 hours in culture, cell count was comparable between the two scaffolds but 3/5 the count on the 2D plate control. 24 h was selected as a time-point relevant for acute toxicity. However, by 120 h cell count on the scaffold had increased to be comparable with the 2D plate control. This would suggest there was no toxic response as cell numbers would not be expected to recover to such a degree. It is possible that the reduced cell population in the scaffolds at 24 h is due to the cells expending energy exploring and colonising the 3D environment rather than proliferating.

The difference in absorbance between the templated scaffolds (D3, D4) and the foamed scaffold (PM0 e) in the 24 h leachable assay was not significant.

In the contact assay, there was no significant difference between the two templated scaffolds at either 24 or 120 h. However, the reduced absorbance of the templated scaffolds compared to the foamed scaffold was significant at 24 h (D3*; D4**). The difference in absorbance between the unbound surfactant and all scaffolds was highly significant (****), suggesting that the surfactant used for templating, although cytotoxic in itself, is largely removed during washing and poses low risk of cytotoxicity during application.

This initial result suggests no cyto-toxic response at either acute (24 h) or chronic (120 h) exposure time.

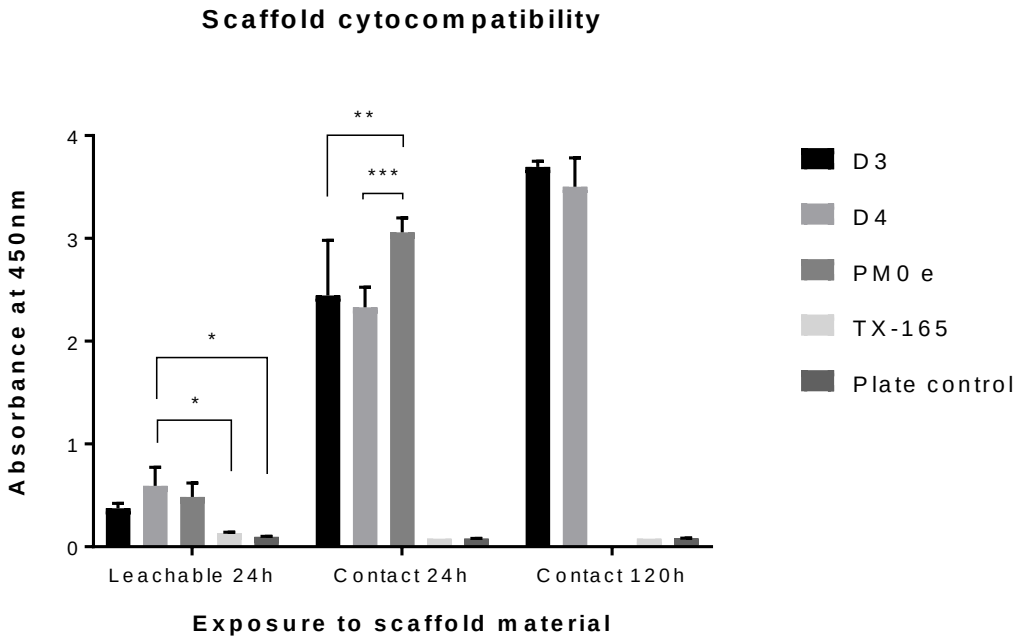

Fig. 8: Cyto-compatibility of fibrin-based scaffolds based on 120 h culture in direct contact. Cell number was calculated from a standard curve, based on fluorescence of CCK-8 (1:10 dilution in DMEM) at 450 nm. PM0e is a foamed fibrin-based scaffold of comparable composition to D3 and D4. 0.1% Triton X-165 in DMEM was used as a control well ("TX-165"). Both (identical) emulsion-templated fibrin-based scaffolds (D3, D4) showed reduced cell count after 24 h in culture compared to the plate control. However, by 120 h cell numbers on the scaffolds had recovered close to plate control. Cell count increased on the ETPM (D3, D4) 116% and 131% between 24 h and 120 h. Increase in cell count on the plate control in the same timeframe was 57%.

Mechanical testing

The additional strength provided by cross-linking fibrin makes the scaffolds more robust and easier to handle. It also brings the soft gel closer in strength to native skin tissue. It is widely reported that cells can sense and respond to the substrate stiffness. The mechanical properties of a scaffold can influence both stem cell differentiation and morphology, so it is important to match closely with native tissue (Freed et al., 2009; Hollister et al., 2002; Hutmacher, 2001). Matching scaffold strength to the native tissue also helps promote integration, as the implant will behave in a more contiguous manner. Cross-linking also increases resistance to proteolytic degradation so the scaffold can persist in vivo for a clinically useful timeframe.

In vivo, cross-linking of newly-formed soluble fibrin fibrils by activated coagulation factor XIII stabilises the fibrils to form a strong, elastic insoluble clot (Standeven et al., 2005). The same effect may be achieved in artificial fibrin constructs by chemical cross-linking with reagents such as genipin (Dare et al., 2009; Linnes et

al., 2007), glutaraldehyde (McManus et al., 2006) or carbodiimides such as EDC in NHS buffer (Grasman et al., 2012); or by photo crosslinking with the aid of a ruthenium catalyst (Bjork et al., 2011).

It was expected that increasing glutaraldehyde concentration would increase Young's modulus (and ultimate tensile strength in line with this as the material is elastic). However, there was little difference in modulus between 0.2% and 0.4% v/v glutaraldehyde. 0.8% v/v produces significantly higher Young's modulus, but higher concentrations showed modulus reducing to very low values. UTS showed a slightly different trend, but in both cases 0.8% glutaraldehyde concentration was optimal (fig. 9).

Cross-linking creates shorter length bonds between fibrin molecules, resulting in contraction of the bulk scaffold. It was hypothesised that more cross-linker would result in more contraction, so scaffolds were measured along the x and y axes after the first and second cross-linker washes and then again after the scaffolds were reduced, washed, and freeze-dried. Generally, the scaffolds did contract between the first and second cross-link.

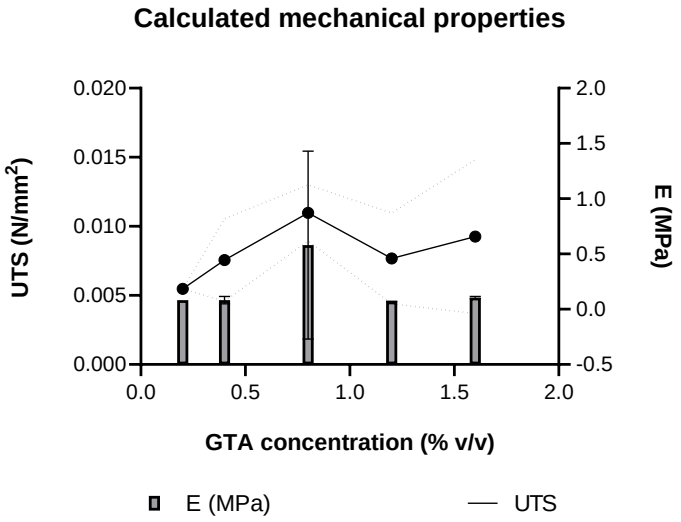

Fig. 9: Tensile behaviour of fibrin-based scaffolds cross-linked with glutaraldehyde at various concentrations. Tensile testing of rectangular strips of freeze-dried scaffold samples showed an intermediate (0.8% v/v) glutaraldehyde concentration gave highest ultimate tensile strength (UTS) and Young's modulus compared to higher or lower concentrations. The large error bar arose from sample slippage in the vertical testing clamps.

Interestingly, the contraction from 'as cast' (5x5 cm) reduced after freeze drying to a very small decrease. It is possible that the reduction in the hydrated state is not due to cross-linker so much as hydrostatic pressure from the surrounding solution. Scaffold shrinkage showed no dependence on cross-linker concentration except at 1.6%, and reduction in the final dried scaffold was minimal (fig. 10(B)).

Tensile testing of scaffolds cross-linked with 0.8% glutaraldehyde showed elastic behaviour to failure (indicated by the straight ascending slopes on the graph). All three repeats failed at the same strain (~1.7). Stress varied between sample, with the first replicate exhibiting more soft behaviour than the second, but these were broadly in agreement (fig. 10(A)). This could suggest that the lowest glutaraldehyde concentration is sufficient to crosslink the fibrin, or that most of the mechanical strength comes from the fibrin and not the additional crosslinking. The tension imparted from the HIPE structure itself – where the interfaces may be approximated as I-beams, or a classical honeycomb structure – may also contribute to mechanical strength as reduce the role played by glutaraldehyde crosslinking (Kravchenko et al., 2018).

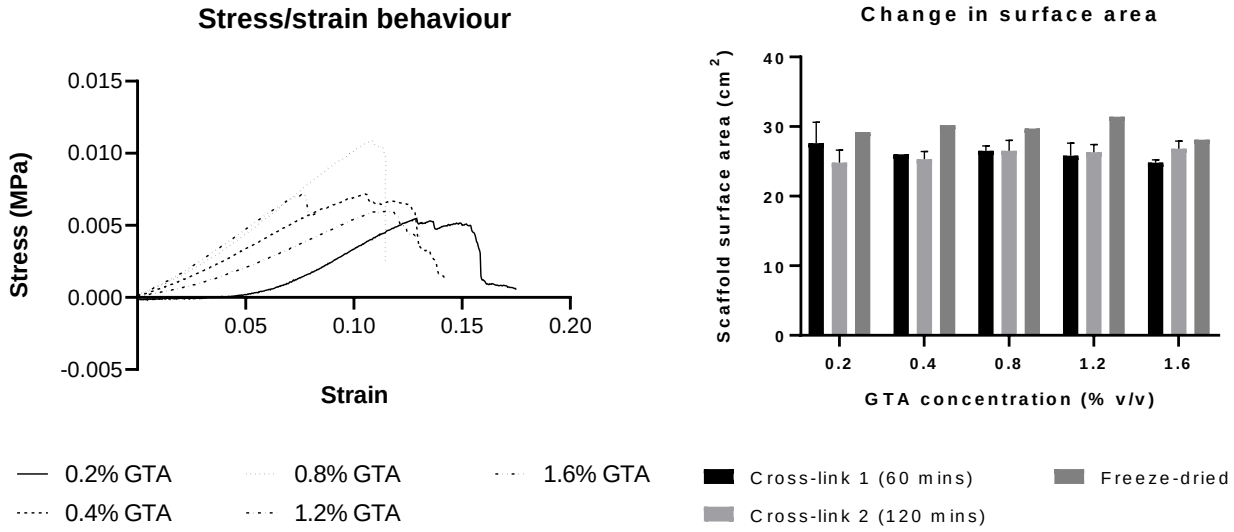

Fig. 10: Effect of glutaraldehyde cross-linker concentration on (A) tensile strength and (B) surface area of fibrin-based scaffolds. Young's Modulus is consistently low (~0.1 MPa) for all cross-linking concentrations except 0.8% glutaraldehyde (GTA). Ultimate tensile strength (UTS) increases with glutaraldehyde concentration up to 0.8% GTA but then reduces. Glutaraldehyde cross-linking causes moderate shrinkage at all concentrations **(fig. 10 (B))**; however, the reduction in area from as-cast dimensions is much less notable after the scaffolds have been freeze-dried.

Hydrolytic degradation

The scaffolds are likely to be washed in PBS before application to a wound. Once applied and secured to the wound, the scaffold will be hydrated with plasma and wound exudate. Wet degradation studies were performed to assess the predicted longevity of the scaffolds when used in vivo. In order to be useful as surgical skin scaffolds, the materials must be a) robust and handleable when hydrated to facilitate placement on the wound, and b) able to retain structure for a clinically useful timeframe. This must be at least 3 days, while growth factors recruit dermal cells and circulating monocytes to the wound (Falanga, 2005, 2004;

Kourembanas et al., 1990), but the scaffold should persist for several weeks in order to provide structural support during remodelling to promote regeneration rather than scarring (Gurtner et al., 2008).

The first, simpler test used sterile buffered PBS. With physiological pH and no enzymes present, any degradation was attributable to hydrolysis. Triplicate samples from various scaffolds were incubated in PBS at 37°C. Samples for each time point (1, 4, 7, 14, 21, 28 days) were removed, dried, and weighed. Change in mass was compared to the original dry mass of each sample. Scaffolds with different composition were formulated with the same standard emulsion (90% v/v decane, 0.1% v/v Triton X-165 surfactant) but with either only fibrin or 2:1 fibrin: polymer. Matriderm® (bovine collagen/elastin; Dr. Suwelack Skin & Health Care, Billerbeck, Germany) and Integra® Dermal Regeneration Template (shark glycosaminoglycans and bovine collagen; Integra LifeSciences, Plainsboro, NJ, USA) were used as commercially available and widely used control materials.

Of the materials tested, the two collagen-based materials were the only ones to lose mass over time. Integra®'s silicon backing was removed for the degradation test. Without it, the collagen matrix degraded within 24 hours. No material was recoverable to dry and weigh for any time point.

Matriderm® remained intact and handleable but consistently reduced in mass between each time point. The reduction in mass was significant compared to the porous fibrin scaffold (day 1, $P=0.0460$; day 4, $P=0.0180$; day 14, $P=0.0008$; day 21, $P=0.0479$; day 28, $P=0.0049$).

All the fibrin-based scaffolds behaved very differently. The appearance and handling were unchanged throughout the study. Dry mass increased in many cases, suggesting that the PBS hydrated rather than hydrolysed the scaffold (fig. 11).

No materials showed significant change in mass between consecutive time points.

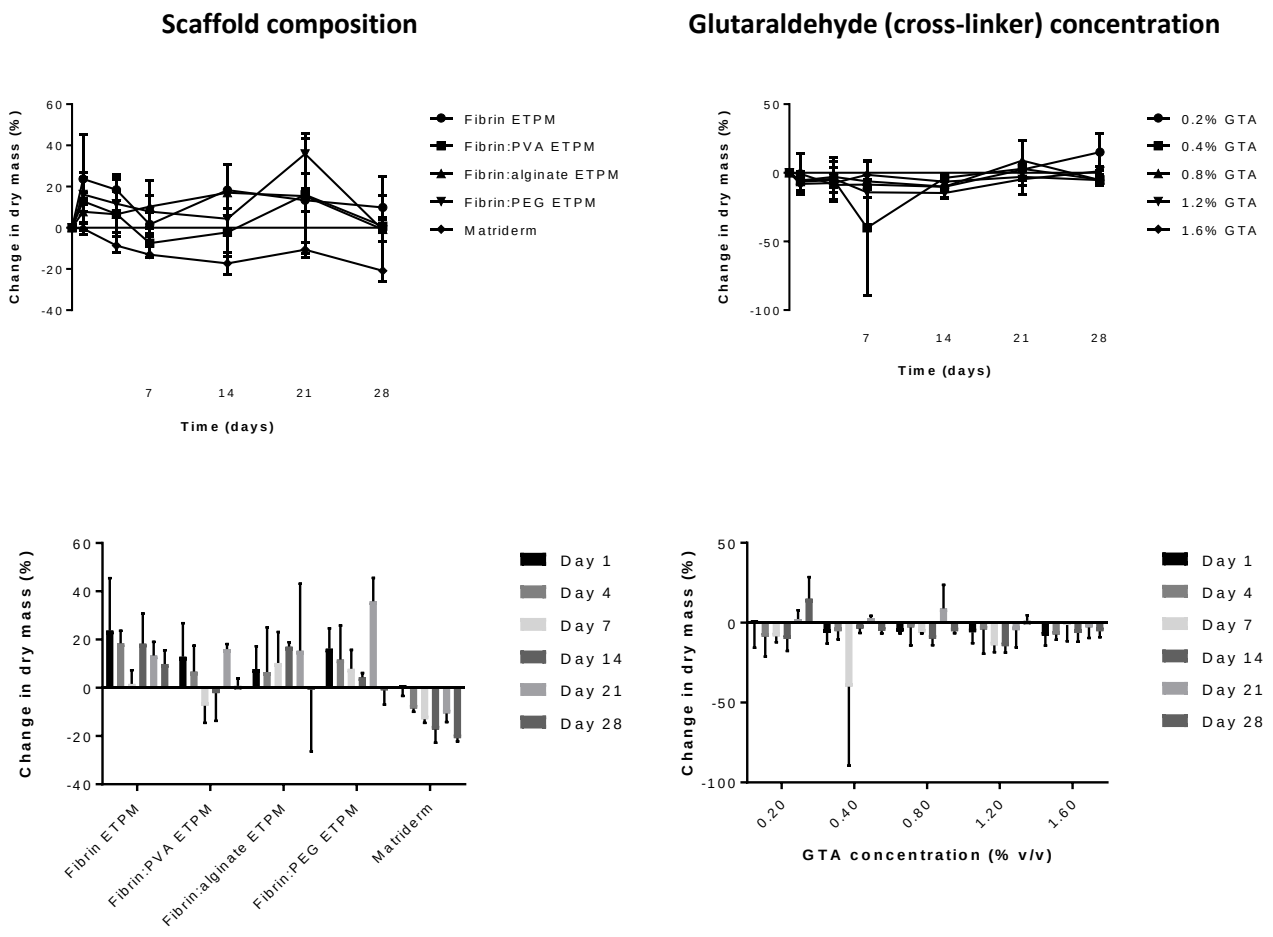

Fig. 11: Change in mass of scaffolds of various compositions incubated for 28 days in sterile PBS. The assay was adapted from ASTM 1635. Triplicate samples were made for each time point and the mass taken of the dried scaffold. (A) 90% porous emulsion-templated fibrin scaffolds alone or with PVA, alginate or PEG added to the aqueous phase of the emulsion were compared with commercial products Matriderm® and Integra®. Integra® dispersed before the first time point and could not be recovered for weighing. (B) Glutaraldehyde cross-linking density for 2:1 fibrin: PVA scaffolds showed no significant difference between 0.2% and 1.6% v/v.

A similar study was performed for 2:1 fibrin: PVA scaffolds manufactured as previously but with different cross-linker concentrations. The starting glutaraldehyde concentration was 0.8% v/v, taken from an existing in-house protocol for fibrin formation. It was expected that increasing cross-linker concentration would prolong scaffold longevity and reduce hydrolytic degradation. However, while most samples in this study did lose dry mass over time, the difference in degradation between the cross-linker concentrations was not significant at any time point except Day 7 (0.4% and 0.8% GTA*, P=0.0308; 0.4% and 1.6% GTA*, P=0.0103). Cross-linker concentration in this case can therefore be selected to optimise mechanical properties (fig. 9) rather than stability.

Enzymatic degradation

The different fibrin-based scaffolds were tested with Matriderm® and Integra® in a second study, in which various enzymes were added to the PBS to better represent the wound environment during the healing and remodelling processes. Non-specific enzymes were used owing to the different materials used in each scaffold (i.e. collagenase would be expected to degrade collagen-based Matriderm® and Integra® more efficiently than fibrin-base scaffolds). Concentrations of these enzymes were based on values reported in the literature (Lim et al., 2018; Lobmann et al., 2002; West and Hubbell, 1999).

MMPs, secreted by fibroblasts in the wound, are actively involved in the degradation of the wound bed and then of scar matrix components throughout healing and remodelling (Rohani and Parks, 2015; Tarnuzzer and Schultz, 1996). MMPs are consistently reported to be increased in chronic wounds and are therefore an interesting and relevant enzyme to explore for scaffolds intended for treating ulcers (Lobmann et al., 2002).

Degradation in Trypsin (fig. 12 (A))

Matriderm® degraded rapidly in the trypsin solution and was only recoverable on day 1. On day 1, Matriderm® had degraded significantly more than Integra®, the other collagen-based scaffold ($P=0.011$) and the fibrin-based scaffolds ($P\leq0.0001$).

Unlike in PBS alone, Integra® retained some integrity over the course of the study. However, mass loss was the greatest of any of the scaffolds across all enzymes tested. Given the hydrolytic degradation results, this may have arisen from interaction with the PBS rather than being specifically attributable to the enzymes. All other scaffolds showed a modest reduction in dry mass over time. The loss in mass between day 0 and days 1, 4 and 10 was highly significant ($P\leq0.0001$). Integra® degraded significantly more than all the fibrin-based scaffolds at all time points, with the most dramatic difference in mass lost occurring on day 1 ($P\leq0.0001$ compared to all fibrin-based materials).

The degradation of all the fibrin-based scaffolds was comparable across all time-points. The addition of either PVA, PEG or alginate made no significant difference to the scaffold longevity in this test.

Degradation in MMP mixture (fig. 12 (B))

As before, Integra® showed the most dramatic loss in mass over time ($P\leq0.0001$ compared to all other scaffolds at all time points). Again, this degradation may be hydrolytic in nature rather than enzymatic.

Matriderm® performed much better in the MMP solution compared to Trypsin. While mass was lost consistently day-on-day, the samples were retrievable and measurable at the end of day 10. The degree of degradation was higher than for the fibrin-based scaffolds, particularly the 2:1 fibrin: PEG scaffolds (day 7, $P=0.0213$; day 10, $P=0.0015$).

Change in mass was variable for the fibrin-based scaffolds, with material blend giving loss and gain in mass at various time points. There was no significant difference between any of the fibrin-based scaffolds. The only material that showed no significant change in mass at any time point was fibrin: PVA. Samples were moved to a desiccator for 24 h and re-weighed to ensure all water was removed from the samples but the results were unchanged and so appear to be genuine.

Degradation in plasmin (fig. 12 (C))

In the plasmin solution, samples of the fibrin-only scaffold generally gained mass over time. The other fibrin-based scaffolds showed significant changes in mass over time, mainly due to the fact that in some cases mass gain was recorded. Again, this was verified with re-weighing following 24 h in the desiccator.

Matriderm® and Integra® behaved in a more expected manner, both consistently losing mass over time with a time-dependent response. Matriderm® was slightly slower to degrade, with no significant loss of mass on day 1, but loss on subsequent days was much greater (P≤0.0001, 0.0003, 0.0002 respectively).

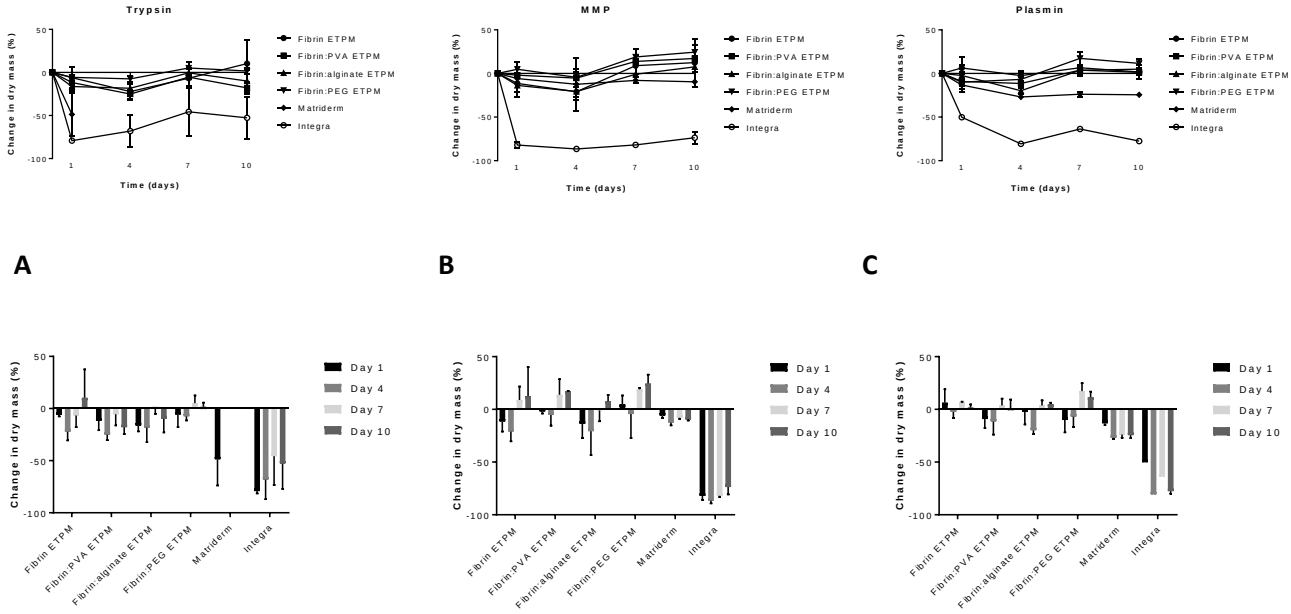

Fig. 12: Change in mass of scaffolds of various compositions incubated for 28 days in [A] 0.25% trypsin, [B] MMP cocktail and [C] 0.125 U/ml plasmin. The MMP mixture comprised 0.2 µg/ml of each of MMP-1, MMP-2, and MMP-9. Graphs show mean and standard deviation; n=3. All ETPM scaffolds containing other polymers were in a ratio of 2:1 fibrin: polymer. The change is mass was largely insignificant. In many cases the dry mass increased over time, possibly as a result of the polymers retaining water from the degradation solutions. No bulk degradation was noted in any of the fibrin-based scaffolds. Integra® scaffolds degraded rapidly in all conditions. Matriderm completely disintegrated in Trypsin [A] within 3 days but degraded more slowly in MMP and plasmin solutions.

As in the other solutions, Integra® degraded the most at all time points, with a large reduction in mass at each ($P \leq 0.0001$).

Given the variable results with fibrin-based scaffolds, it is difficult to draw specific conclusions about proteolytic stability. The test could be repeated with larger samples and more concentration enzyme solutions. With Integra® and Matriderm®, it is clear that these collagen-based materials were robust in PBS, but again enzymatic activity was less clear. The test could be repeated with a buffered solution in which these scaffolds are more stable.

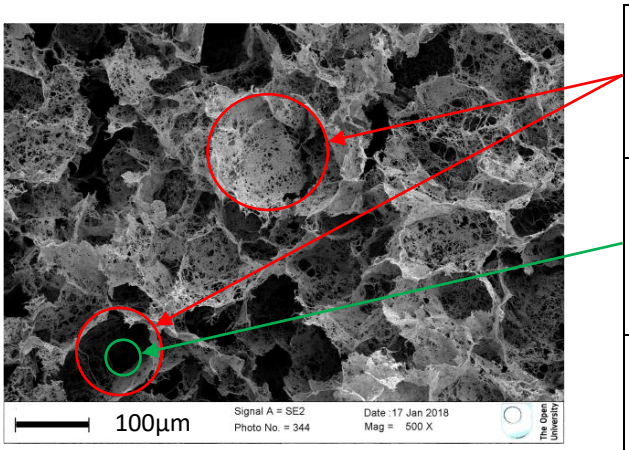

	Optimal	Achieved
Pore size	70 – 200 µm *for cell ingress* (Choi et al., 2013; Marshall et al., 2004)	50 – 200 µm
Interconnect size	25 – 35 µm *for angiogenesis* (Bokhari et al., 2007; Marshall et al., 2005)	20 – 40 µm
Porosity	≥ 74% *Exceeds perfect sphere packing*	Up to 95%

Fig. 13: Comparison of typical fibrin-based scaffold parameters with optimal values cited in the literature. The optimised scaffolds manufactured according to the method described in this report all meet (pore size; interconnect size) or exceed (achievable porosity) the cited values.

CONCLUSIONS

Emulsion templating offers advantages over other methods of creating porous materials such as electrospinning, foaming or other gas-based methods. Control over the critical design parameters - porosity, pore size, pore size distribution and wall thickness - is achievable. The structures generated are more organic in shape than those typically created by additive manufacturing, where a simple pattern is often repeated to build the 3D structure.

High internal phase emulsions (≥74%) allow for creation of highly porous structures at ambient or physiological temperatures, depending on the system design. Use of non-ionic surfactants at low concentrations avoids damage or denaturation of proteins, allowing the templated scaffold to retain native protein structure and properties. Some surfactants are more suited than others to this particular application (addressed in a separate report).

Retaining native protein properties is intended to offer biological recognition when implanted in vivo, particularly when using ECM proteins such as fibrin or collagen. They are recognisable by cells and readily and safely metabolisable.

Moreover, the thin fibres forming the hierarchical structure provide traction rails for migrating cells in the same way that electrospun fibres do. Templating also provides an engineered hierarchical 3D structure which is lacking in aerated scaffolds formed by foamed or gas bubbled or electrospun scaffolds. This level of control is possible by a methodical approach, first designing an emulsion of appropriate internal phase volume fraction, droplet size and stability before optimising scaffold materials and their concentrations. In this way, protein fibre density, pore size and interconnect density are easily tunable and reproducible between batches.

While operating parameters in aeration and spinning methods can be modified to influence air bubble number and diameter, or fibre diameter, porosity and spacing are ultimately determined by processes which cannot be controlled. In contrast, HIPEs have droplet sizes that can be controlled by mixing speed, oil fraction and surfactant choice. Thermodynamics dictate that spacing and diameter will be reproducible under the same conditions. If the emulsion is stable, the scaffold will be templated by the emulsion and therefore have a controllable and reproducible structure.

The method described here achieves the high porosity and interconnectivity of HIPE templating with the nanostructure of the native protein preserved in the final scaffold. This is an advantage over current methods where the HIPE regime limits material choice to synthetic materials or denatured proteins.

Additional processing steps are required in both cases to create fine nano-structured surfaces to enhance cell interaction, for example creating engineered structured topographies by microcontact printing or various lithography strategies; unstructured topographies by chemical etching or phase separation, or surface treating by plasma deposition (Chandrasekaran et al., 2011; Dalby et al., 2007; Norman and Desai, 2006; Viswanathan et al., 2012b). Materials like gelatin have poor mechanical integrity but contains an amino acid sequence (Arg-Gly-Asp) which promotes cell migration and adhesion. Surface deposition of such materials on a scaffold substrate combines the structure and mechanical integrity of the substrate material with the biological properties of the protein coating at the surface where cells interact with the material (Chandrasekaran et al., 2011). However, this second processing steps adds to the duration, cost, and complexity of manufacture.

This method also greatly increases the porosity and reduces the density achievable with native protein-based scaffolds. Typically limited to hydrogels, we present the possibility of engineering complex highly porous scaffolds. To our knowledge, the method is unique in allowing HIPE templating of a protein in its native form. Furthermore, owing to the limitations of other methods described here, our technique may be the only method for producing such high porosity materials with native proteins and the necessary control and repeatability for commercial application and regulatory approval. The method described in this report is robust and repeatable and generates scaffolds with properties in line with the requirements widely reported in the literature.

ACKNOWLEDGMENTS

This work was funded by The Open University, Cells for Cells and Consorcio Regenero. The project is hosted by the tissue engineering group at University of Oxford IBME (Cui group). The authors would also like to thank Gordon Imlach (The Open University) for providing SEM training and Igor Dyson (University of Oxford) for allowing use of the Instron UTS machine.

GFP-MSC-hTERT were kindly provided by Dr. James Li (Dept. Paediatrics and Adolescent Medicine, LKS Faculty of Medicine, University of Hong Kong).

3.4 Assessing scaffold angiogenic potential using the chick chorioallantoic membrane (CAM) assay

ABBREVIATIONS

CAM	chick chorioallantoic membrane	PVA	poly vinyl alcohol
ETPM	emulsion templated scaffold	REM	rapid eye movement
H&E	haematoxylin and eosin	SEM	scanning electron microscope
HH	Hamburger-Hamilton	Three Rs	Reduction, refinement, and replacement of animals in research
PBS	phosphate buffered saline		

ABSTRACT

Biomaterial scaffolds must be evaluated for their cytotoxic, functional, and proliferative effects on cells. Some of this can be performed in *in vitro* studies with cultured cells, but these models are limited and cannot adequately replicate complex features of *in vivo* models (notably blood supply and immune/inflammatory response). *In vivo* studies carry economic and ethical burden as well as increased variability between repeats. The chick chorioallantoic membrane (CAM) assay, which exploits the rapidly developing capillary plexus of a fertilised egg in the early stages of embryonic development, offers a compromise between the *in vitro* and *in vivo* systems.

Frequently used to study tumorigenesis and evaluation of angiogenic growth factors, the CAM assay may also be used to compare angiogenic potential of biomaterial scaffolds. While results are reported in the literature, detailed methods and protocols are frequently withheld.

Here, the CAM assay was used to evaluate angiogenic potential of fibrin-based polyHIPE scaffolds compared to commercial scaffolds Matriderm™ and Integra® Dermal Regeneration Template. Fibrin, fibrin-PVA and fibrin-alginate scaffolds with 90% porosity were also evaluated against non-porous films of the same composition to examine the materials' structural contribution to angiogenesis. Blood vessel development was monitored throughout the study and Drabkin's haem count used to assess haem in the excised scaffolds at the conclusion.

Assay method development and the merits of the various protocols available are also discussed in this experimental section.

INTRODUCTION

Even with scaffolds that are biocompatible and facilitate the migration of cells into and though the construct, the longevity of these exploratory cells is not guaranteed. Residence time is dictated by the availability of nutrients and oxygen, as well as removal of waste. This is especially true of a wound environment where high proliferation and differentiation rates are required. A rapidly forming and robust vasculature throughout the scaffold is essential to support the cells from an early stage and ensure the continued performance of the implanted scaffold. Impaired graft vascularisation may lead to infection, localised necrosis or rejection of the implanted material (Hendrickx et al., 2010; Sahota et al., 2004).

Historically, cell and vascular penetration of biomaterial scaffolds has been restricted to a couple of millimetres, which is therefore a limiting design factor on scaffold dimensions but also on the application of the material. A thin construct has limited use for replacement of repair of thick, dense tissues which is why many commercial materials are focussed on dermal replacement (the dermis is only 0.6-0.7 mm thick (Chopra et al., 2015; Oltulu et al., 2018) so the materials could conceivably replace the full thickness).

Successful graft materials must provide a framework for new and repairing vasculature (Oliver et al., 1983). Porous materials are highly desirable as skin scaffold. Their interconnected cavities provide space for neovascularisation and angiogenesis as well as aiding supply of nutrients and chemical stimuli, and removal of waste from the regenerating tissue (Busby et al., 2001; Thomson et al., 1995; Whang et al., 2000). A highly porous material further allows increased and more uniform infiltration of cells (Brauker et al., 1995; Carnachan et al., 2006; Glowacki et al., 1983; Klawitter and Hulbert, 1971; Lu et al., 2012; Mooney et al., 1991; Nade et al., 1983; Whang et al., 2000).

To support vascularisation, fibrin scaffolds must have pores with appropriate pore- and interconnect diameter were found to allow existing capillaries to penetrate and newly formed tips to further invade (Linnes et al., 2007). The literature cites a wide range of 'optimal' pore diameters which appear to be very specific to the particular material and application in each case. Marshall et al found that poly (2-hydroxyethyl methacrylate) scaffolds with pores of 35 μm diameter, implanted in mouse skin, showed enhanced angiogenesis compared to comparable scaffolds with either smaller or larger pores (Marshall et al., 2005). However, a year earlier the same group had stated that pores of 70 μm diameter were more effective at promoting vascularisation throughout the scaffold (Marshall et al., 2004). PLGA scaffolds with very large pore diameter, ≥200 μm, have been shown to promote the formation of low density networks

of larger blood vessels whereas smaller pore diameter (<200 μm) promotes the formation of high density networks of smaller blood vessels following implantation in nude mice (Choi et al., 2013).

Interconnectivity and interconnect diameter is equally important as this facilitates the passage of blood vessels through the scaffold. Indeed, interconnect diameter may be more important than pore diameter for vascularisation by promoting the proliferation, adhesion, and migration of endothelial cells through the scaffold. This has been demonstrated using HUVECs cultured in β-tricalcium phosphate (β-TCP) discs (Xiao et al., 2015). B-TCP scaffolds with larger interconnect diameters have been shown to exhibit improved vascularisation over those with smaller interconnect diameter, up to a maximum of 400 μm beyond which no significant difference is observed (Bai et al., 2010). The collective evidence suggests a minimum cut-off diameter for angiogenesis, possibly dictated by the diameter of endothelial cells which assemble to form new blood vessels (approximately 5-20 μm, dependent on location) (Garipcan et al., 2011). Above this critical diameter, the blood vessels have room to mature into thicker, more robust capillaries which are likely to occur at lower density.

In addition to ensuring biocompatibility and microstructure are conducive to vascularisation, biological strategies may be employed in tandem to further improve blood vessel ingress into the scaffold. This may be achieved with cells or biochemical or pharmacological agents. Scaffolds can be dosed with growth factors or gene vectors which are released into the wound as the polymer carrier degrades. Scaffolds may be seeded with vessel-forming endothelial cells prior to implantation so that the building-blocks for neovascularisation are already in place (Frueh et al., 2017). Disadvantages to biological vascularisation strategies include the increased cost and processing time created by added complexity, as well as increased challenge in safe storage and transportation of the prepared materials. The biological component is also likely to increase the risk-based class of the scaffold and change its designation to a combination product, which makes the regulatory approval process more convoluted.

There are two methods by which new blood vessels form: angiogenesis and vasculogenesis. Vasculogenesis describes the direct formation of blood vessels by differentiation of angioblastic precursor cells *in situ*. Angiogenesis describes the formation of new blood vessels from pre-existing ones (i.e. sprouts from existing capillaries and venules) (Risau, 1997). In this case, the scaffolds are intended for use as dermal skin templates where they would be placed into fresh wound beds. The wound bed already has established blood vessels with sprouting ends, so in this environment neo-vascularization would be expected to occur via angiogenesis.

Rapid vascularisation of a potential skin scaffold material is therefore essential to its success. Assessment of the angiogenic potential of candidate materials is an important criterion during scaffold development. Here, the chick chorioallantoic membrane (CAM) *in vivo* 'bridge' assay was used as a high-throughput technique for assessing angiogenesis in a 3D functional capillary bed.

CAM development and relevance

The CAM assay provides a useful bridge system between *in vitro* and *in vivo* models for investigating blood supply in biomaterial structures. *In vitro* models lack endothelial structures and 3-dimensional complexity, while *in vivo* models are overly complex with many extraneous variables when testing for a specific response (here, angiogenesis). There is also a risk of a lack of consistency and reproducibility between animals (Moreno-Jiménez et al., 2016). Finally, some animals may not tolerate implantation with materials designed for human use and bias the test with an immune response that would not be seen in human models.

The CAM is a respiratory organ that fuses with the shell and provides gaseous exchange with the outside environment to support the developing embryo. Importantly, the CAM is very highly vascularised, containing a dense plexus of capillaries, and highly branched blood vessels of many sizes. The largest of these are latterly accompanied by an extensive lymphatic network (Taizi et al., 2006). Rapid capillary proliferation continues until day 11 post-fertilisation and then progresses slowly until final vasculature arrangement is reached on day 18 (Ausprunk et al., 1974).

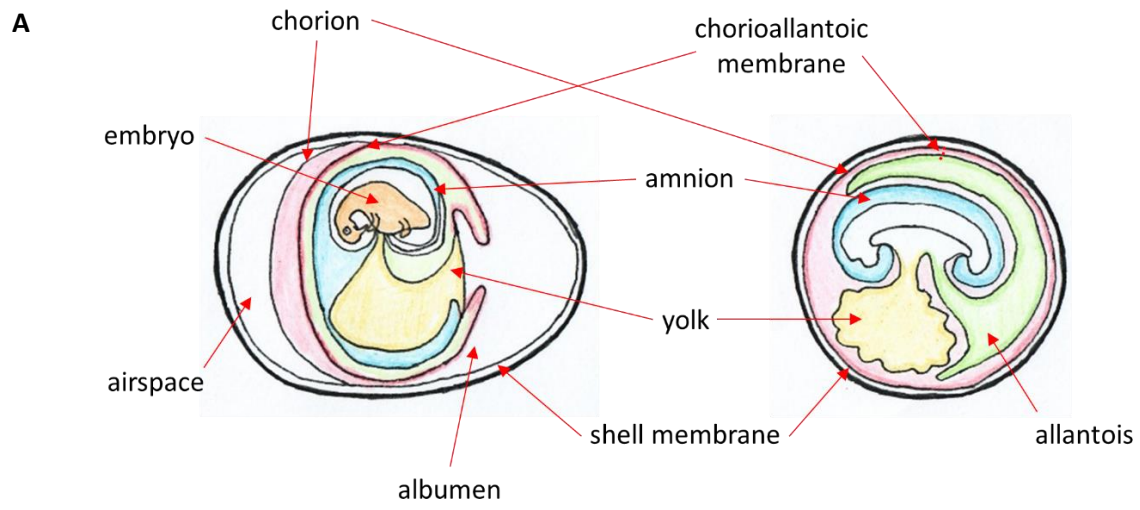

Fig. 1: Schematic diagram of a fertilised chicken egg showing the location of the chorioallantoic membrane in (A) longitudinal and (B) transverse view. The chorioallantoic membrane forms by the fusion of the chorion and the allantois on day 4 or 5 post fertilisation (Fuchs and Lindenbaum, 1988). Images adapted from (Gabrielli and Accili, 2010; Valdes et al., 2002).

The allantois emerges from the ventral wall at about 3.5 days after fertilisation. It grows rapidly from day 4 until day 10, during which time it fuses with the adjacent chorion to form the chorioallantoic membrane (CAM). The CAM is only fully differentiated on day 13 (Hamburger and Hamilton, 1992; Moreno-Jiménez et al., 2016; Nowak-Sliwinska et al., 2014). In order to capture the entire duration of angiogenesis and blood vessel maturation in the growing CAM, CAM assays for the study of biomaterials typically coincide with days 4 – 14 of development. However, on about day 14 of development the embryo makes complex movements to get into position for hatching. For this to happen the central nervous system has to be highly developed, by which time the embryo would be sensate. The assay was therefore designed to terminate at the end of day 13 or at the very latest early on day 14, in line with ethical guidelines to terminate before two-thirds gestation (Tong et al., 2013).

Chick embryos lack a functional immune system until approximately day 15 of development (Ribatti, 2010). The lymphoid system is not fully developed until the late stages of incubation (leading up to hatching on or around day 21 post-fertilisation), and bursal lymphocytes do not appear until between days 12-15 of embryonic development (Glick, 1979). IgM, which also originates in the bursa, is not identified until day 14 of development (Kincade and Cooper, 1971). This is the first immunoglobulin expressed during chicken development, so the embryo cannot form even a weak immune response prior

to day 14 of development (Tîrzui and Seres, 2010).

Thus, the CAM is a naturally immune-deficient host system when used in the early stages of development. After this time, the foreign test samples may incite an inflammatory response which may be detrimental to the wellbeing of the embryo; and secondly, the inflammatory response may provoke angiogenesis, making it difficult to assign vascular development confidently to material or inflammatory response (Nowak-Sliwinska et al., 2014; Ribatti, 2012). Before day 15, biomaterials and/or cellular materials can therefore be implanted and tested without species-specific restrictions (Dohle et al., 2009).

The CAM assay

The CAM assay makes use of the early rapid vessel formation. Substances to be tested are placed on the CAM and the interaction and infiltration of the new vessels with the materials is observed. Increased angiogenesis would indicate a more angiogenic material; more infiltration further suggests that number, size, and spatial arrangement of pores in the material is conducive to angiogenesis. This information is extremely useful in biomaterial scaffold design and suggests whether prototype materials would be capable of supporting cell *in vivo* or whether redesign is required.

In the CAM assay, a fertilised egg develops blood vessels that are easily visualised, accessed and manipulated (Dohle et al., 2009). The superficial layers of the CAM are transparent to most visible wavelengths, so the vasculature can be visualised by light and/or fluorescent microscopy (Nowak-Sliwinska et al., 2014). The small window cut into the shell in the established *in* ovo method can obstruct visualisation of the whole CAM. Visualisation can be further improved using an *ex ovo* method where the egg is displaced from the shell into a petri dish, allowing unimpeded viewing. *Ex ovo* culture has been associated with low embryo viability as the yolk typically ruptures either on cracking the egg, or during culture (as a result of excessive distension of the yolk on a flat surface) (Auerbach et al., 1974; Nowak-Sliwinska et al., 2014; Ribatti et al., 2000). Most loss occurs during the first three days in *ex ovo* culture, after which survival rates dramatically improve (Auerbach et al., 1974).

Test substances (in this case, small scaffold samples) are placed carefully around the capillary plexus at the start of embryo development. As the CAM grows and matures, it rapidly vascularises. The interaction with these blood vessels and the various test materials over time is observed. A more angiogenic material has greater interaction with the capillary plexus (more blood vessels resident, more branch points etc.).

As the assay is hosted in a developing organism, the stage of development must be carefully monitored during progression of the assay to avoid causing any undue disturbance. A timeline of assay progression is shown against Hamburger-Hamilton stages for chick embryo (fig. 2).

There are various protocols described, with varying levels of detail, in the literature. In the work described here, these protocols were evaluated, and aspects of several protocols were adopted and trialled during method development. The relative merits of these approached are discussed later.

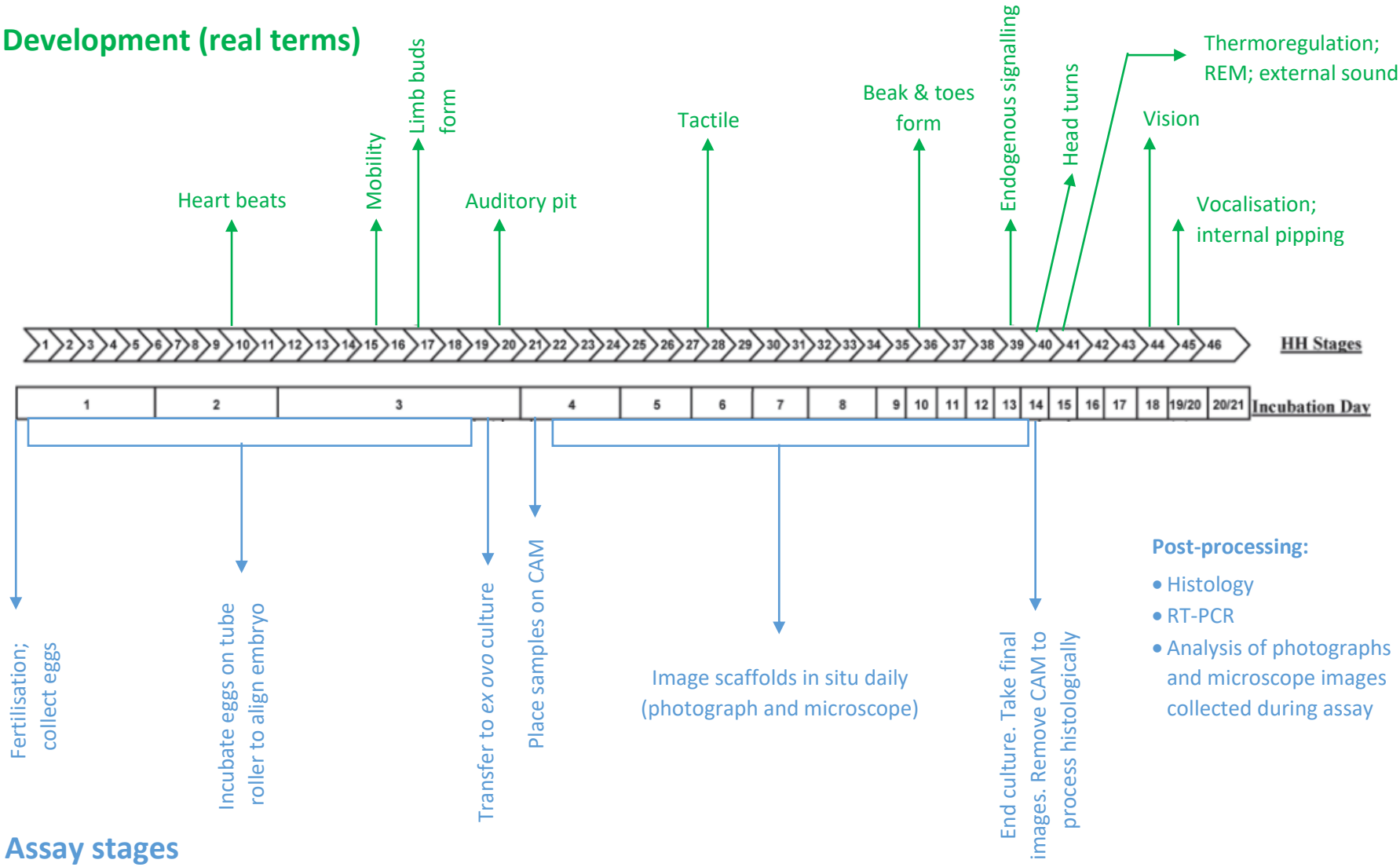

Fig. 2: Timeline of chick embryo development, based on Hamburger-Hamilton stages (Hamburger and Hamilton, 1992), alongside key stages from the CAM assay protocol. Figure adapted from Tong et al (Tong et al., 2013). The stages before Hamburger-Hamilton (HH) 2, in which an embryo forms from a germ, are described by Eyal-Giladi and Kochav (Eyal-Giladi and Kochav, 1976).

EXPERIMENTAL PROCEDURES

Materials

36 white eggs (*Gallus gallus domesticus*, Dekalb white) were purchased from Henry Stewart & Co. Ltd. (Norfolk, UK). Eggs were refrigerated until required. Mean weights per batch were 63.05g ± 0.62, 59.24g ± 2.96 and 58.98g ± 2.83.

Emulsion templated scaffolds ("ETPM") were manufactured according to the method described previously. All emulsions comprised 90% (v/v) decane and 0.1% (v/v) Triton X-165 surfactant. Fibrinogen: thrombin ratio was 4:1. Fibrin scaffolds with alginate or PVA contained 2:1 fibrin: copolymer.

Films were produced with the same polymer composition as each of the ETPM scaffolds (fibrin only, and fibrin-PVA and fibrin-alginate in a ratio 2:1). These were prepared in the same way as the aqueous phase of emulsions for the ETPM with the same order and timing of reagent addition and same method and duration of mixing. The films were cast in 5 cm^2 weighing boats, tapped to remove air bubbles and freeze dried alongside the ETPM over a 16-hour cycle to 50 mTorr, -40°C (VirTis Genesis 25ES, SP Scientific). Scaffolds and films were manufactured in triplicate, in a 'clean' environment to reduce contamination. This entailed autoclave sterilisation of all solutions and sterile filtration of thermo-sensitive solutions, then conducting mixing and casting in a category I laminar flow cabinet.

Pronova UP VLVG alginate was purchased from NovaMatrix Ultrapure Biopolymer Systems. Matriderm™ (Dr. Suwelack Skin & Health Care, Billerbeck, Germany) and Integra® Dermal Regeneration Template (Integra Life Sciences, Plainsboro, NJ, USA) were purchased through Northwick Park Institute for Medical Research. All other reagents and consumables were purchased from Sigma Aldrich.

Ethical considerations

Chicken embryos are not considered protected species under current Home Office regulations; however, a series of measures were implemented in line with the 'three Rs' (refinement, reduction, and replacement) principles originally proposed by Russell and Burch in the 1950s (Balls and Straughan, 1996; Guhad, 2005).

Eggs were sourced from a DEFRA regulated supplier. They were either put into immediate use or refrigerated on receipt to retard development. Fertilised eggs may be safely refrigerated for up to one week before warming for use. During use, the temperature of the incubator must be tightly regulated.

The optimal span of temperature during incubation is very narrow to maintain healthy and viable embryos (Webb, 1987).

The use of *ex ovo* CAM allowed total visualisation of the whole organism. While monitoring blood vessel interaction with the scaffolds, chick development was simultaneously tracked according to the Hamburger-Hamilton stages (figure 2). Length of incubation in reared eggs and chicks is a function of the level and stability of incubation temperature (Reed and Clark, 2011). In this study, with a controlled common environment, all embryos were expected to develop according to the same approximate time frame. Visual development tracking by Hamburger-Hamilton staging corroborated expected development stage with assay progression.

Early gestational chick embryos are immune-deficient so introduction of extraneous materials (especially xenogeneic material) should elicit no immune response and have no adverse effect on the embryo (Dohle et al., 2009; Glick, 1979; Kincade and Cooper, 1971; Tîrzui and Seres, 2010). Additionally, samples were introduced onto the CAM before the embryos became tactile, and the assay concluded before embryos developed visual or auditory sensation. All embryos should therefore have no sensory awareness of any procedures taking place.

The embryo is innervated during the development stages covered by a typical CAM assay, but the CAM itself is not. With careful placement and manipulation of test samples, the embryo should experience no pain (Moreno-Jiménez et al., 2016).

All materials were sterilised with 70% ethanol/autoclaving (as appropriate) prior to use, to minimise the risk of contamination to the *ex ovo* embryo. Egg shells are partially permeable, and application of ethanol or detergents significantly reduces embryo viability (Dohle et al., 2009). The eggs were instead cleaned using chlorhexidine gel then cleansed with distilled water and dried thoroughly.

The scaffolds were manufactured under 'clean' conditions to reduce introduction of contaminants and/or endotoxin. Matriderm™ and Integra® are supplied sterile. Prior to use, all scaffolds were washed in 70% ethanol and then thoroughly washed with PBS to sterilise. Preliminary *in vitro* cultures with scaffolds prepared in this way showed no adverse response.

The size and positioning of scaffolds around the CAM were considered for statistical relevance (biological repeats) and reducing the number of eggs required, while ensuring the scaffolds were distinct and separate with no interaction between samples.

Measures were implemented throughout to minimise mechanical trauma to the embryos. Eggs were rotated for 3 days prior to evacuation from the shells. The embryo resists the rotation and migrates to the upper surface. The shell may then be fractured on the opposite surface to reduce the impact

experienced by the embryo (Dohle et al., 2009). Increased survival rates (more than 50% higher) are reported using this method. Scaffolds were placed around the edge of the CAM to avoid disturbing the embryo or rupturing capillaries.

Eggs were checked at least daily during incubation. Non-viable embryos (assessed by absence of foetal heartbeat) were immediately isolated and terminated in line with Home Office regulations to protect the remaining embryos. All embryos were terminated at the end of the assay early on day 13 of development (before Hamburger-Hamilton stage 40).

Finalised method

This protocol was initially based on the method described by Dohle et al. (2009) and modified iteratively.

On receipt, eggs were checked for hairline fractures, mechanically cleaned with dry paper towel, and refrigerated until required (up to one week). Before use, the eggs were cleaned with chlorhexidine gel and dried thoroughly before weighing. They were then positioned in the pre-conditioning incubators on their longitudinal axes and the upper surface marked. The eggs were incubated at 37.5°C, 60-62% humidity with the incubator (RCom KingSuro Max 20, Autoelex Co. Ltd., Juchon, Korea) rotating through 60° every hour.

After 72 hours each egg in turn was removed from the incubator and the underside (opposite the mark on the upper surface) was tapped sharply against a scalpel blade. Surgical scissors were inserted through the fracture and used to grow the incision through shell and membrane. Finger pressure contained the albumen in the shell. Holding the egg just above an octagonal-based weighing boat (cleaned with 70% ethanol), the egg was evacuated into the boat. Each boat was lidded with an inverted weighing boat, offset to expose the corners. Four kim wipes, folded in half, were placed in a 100 cm^2 square weighing boat, and sprayed with distilled water. The lidded weighing boat was placed in the larger weighing boat then immediately incubated at 37°C, 80-85% humidity (HERAcell VIOS 160i, Thermo Scientific).

The next day, all scaffolds and films were washed in 70% ethanol then three times in sterile PBS. All were equilibrated in fresh, sterile PBS at room temperature while eggs were examined. Non-viable embryos, determined by absence of heartbeat (at this stage only visible as a red pulse), were removed and destroyed. A sterile 8 mm biopsy punch was used to make circular samples of the hydrated films and scaffolds. Using a pre-determined matrix, four scaffolds per egg were positioned at the edge of the capillary plexus, equally spaced around the circumference. Two samples from each scaffold were

used, with three scaffolds per material condition. Each sample and egg were photographed after placement. Eggs were then returned to the incubator for a further 8 days.

All eggs were checked daily for viability. The kim wipes were sprayed with fresh water daily, or as required, to maintain overall incubator humidity of 80-85%. Each egg was removed and photographed on days 1, 3, 5, and 7. At each timepoint, the embryo and each sample were imaged at 7.5x magnification with a camera attachment (GXCAM-9, GT Vision Ltd. Stansfield, UK; Nikon SMZ745T stereomicroscope).

Early on day 9 after sample placement, eggs and scaffolds were imaged as previously. All accessible samples were gently excised with forceps, using a scalpel to remove excess albumen where necessary. Each sample was deposited into the well of a 24 well plate. Embryos were destroyed immediately after sample excision.

The haem content of the excised scaffolds was assessed by Drabkin's assay, using the protocol provided by the manufacturer (Sigma Aldrich, available online). Samples were not treated with anticoagulants or calibrated to take account for lipids, abnormal plasma proteins or erythrocyte stoma. Briefly, excised scaffolds were placed in 24-well plates and incubated with 2 ml Drabkin's reagent for 30 minutes at room temperature. Absorbance on the spectrophotometer was set to 0 using distilled water as the reference. The samples were removed before measuring the absorbance of each well at 540 nm. A standard curve was prepared using reconstituted human haemoglobin (100 mg/ml to 6.25 mg/ml).

Angiogenic potential of materials was assessed by counting blood vessels penetrating the samples on each imaging day using Image J analysis of light micrographs.

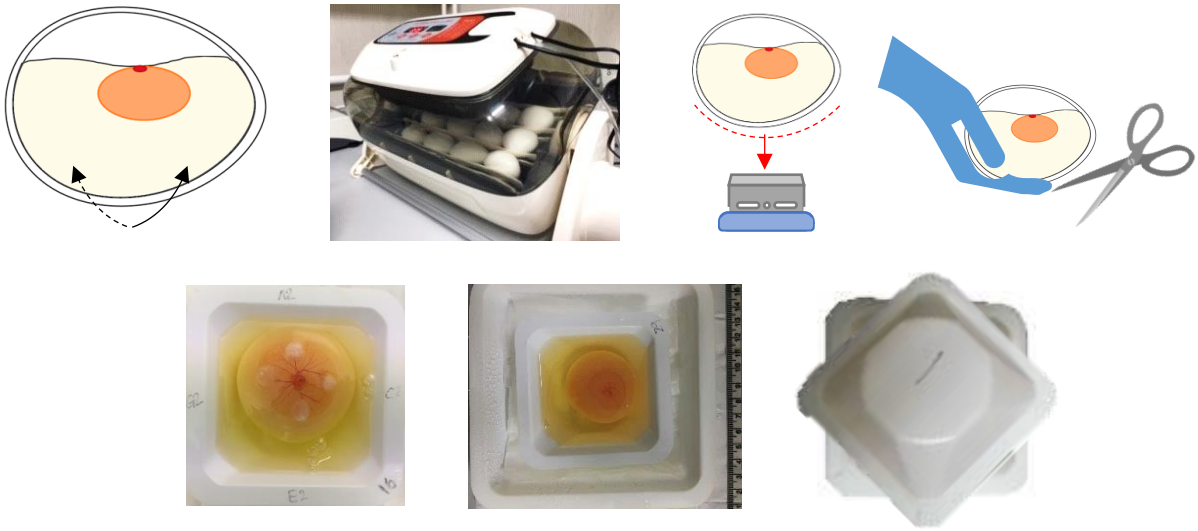

Fig. 3: Preparation of eggs for *ex* ovo culture in the CAM assay. Embryos were orientated to the upper surface of each egg over 72 hours in a rotating incubator. Each egg was cracked with a single tap to underside followed by propagation with surgical scissors, using finger pressure to contain the albumen. Eggs were then evacuated into octagonal-based weighing boats.

RESULTS

Of the eggs that were delivered fertilised and with shells intact, survival rate after transfer to *ex ovo* culture was over 70%. Some embryos died in the first 24 h of culture, typically those with rapid, shallow pulse immediately after evacuation. Viability in culture reduced over time, principally owing to yolks slowly leaking. Viability on days 1, 3, 5 and 7 after sample placement was 61.3%, 54.8%, 51.6% and 32.3% respectively. On the final day of the assay 29% of the batch remained viable. At all stages, embryos progressed as expected according to the Hamburger-Hamilton development stages.

The developing embryo shown in fig. 4 is characteristic of healthy embryos at each time point. At day 0 after cracking, the embryo was only visible by its pulse. The capillary plexus grew rapidly until it covered the air interface. At this point, capillaries began to mature, growing in diameter and interconnectivity. There was some evidence of remodelling during the maturation process. Scaffolds were initially positioned on top of the capillary network at the outer edge. However, the yolk distended as the embryo grew and consumed the contents, occasionally forcing the scaffolds off the edge of the plexus.

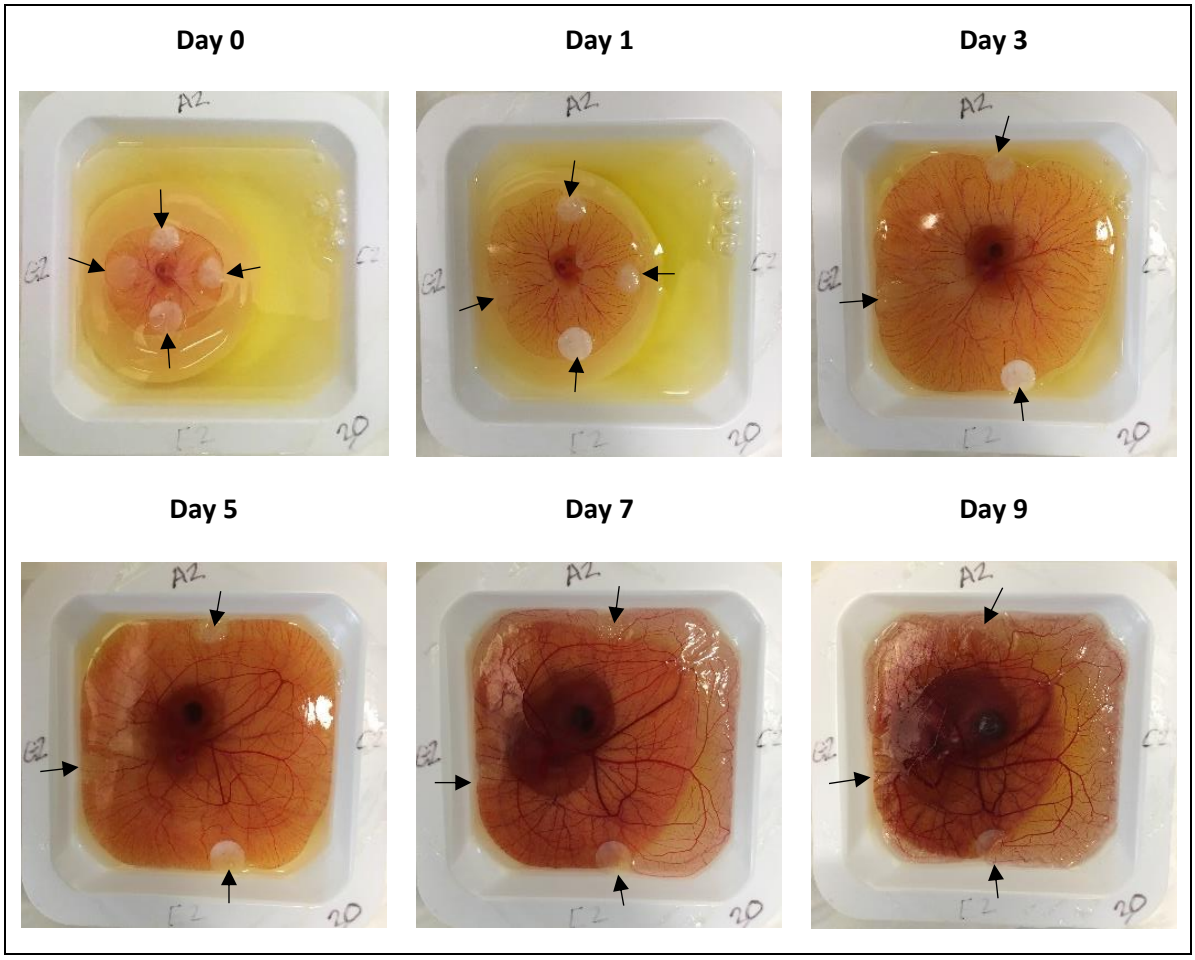

Fig. 4: CAM development at time points after sample placement. The yolk sac is displaced and consumed over time by the growing embryo. At day 0, the embryo was only detectable by its pulse. In the following 24 hours the head and spine became evident, and after 72 hours the head body and limbs were all visible. The thin capillary network grew rapidly in line with embryo development. After 5 days (incubation day 9; approximately HH stage 35) the capillary plexus reached full surface coverage and blood vessels matured in diameter, depth, and connectivity.

N.B. Scaffold C2 (right side of weighing boat) is not visible in the images from day 3 onwards. The sample adhered to the capillary plexus and was subducted into the albumen after the plexus covered the upper surface of the weighing boat.

Biomaterial interaction with capillaries over time

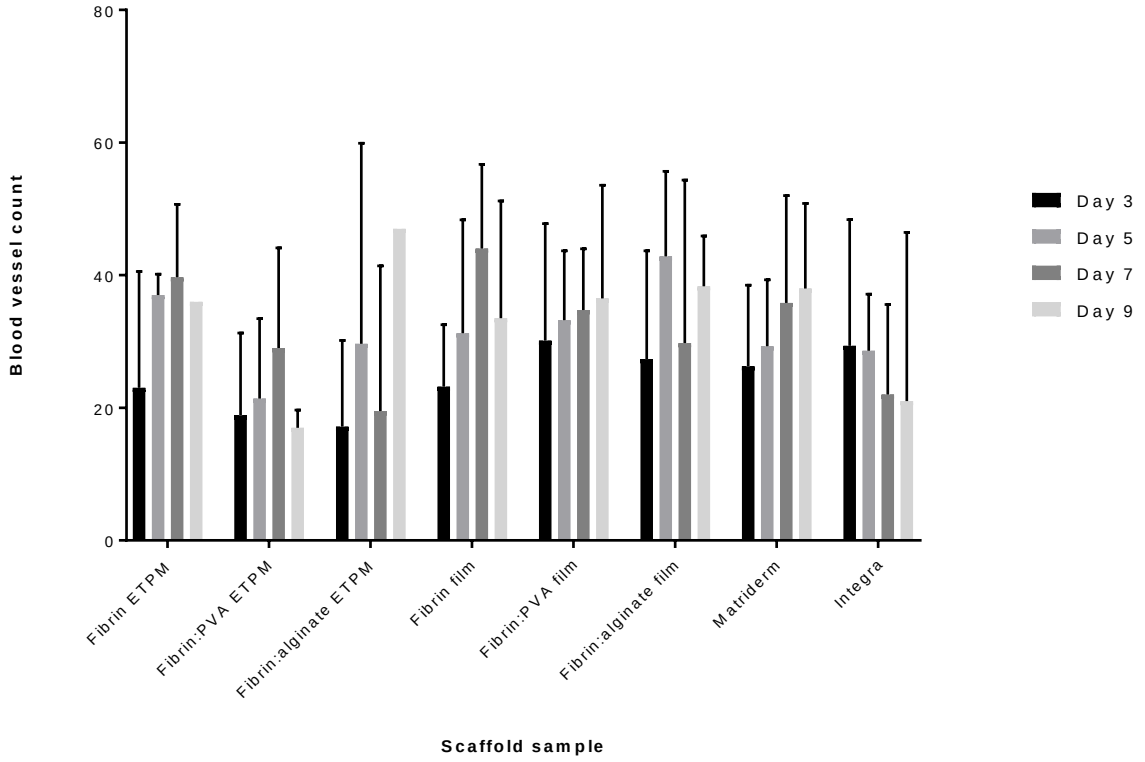

Fig. 5: Number of blood vessels interacting with scaffold samples. Each timepoint represents the number of days after sample placement on the CAM (incubation day -4). Interacting blood vessels were defined those entering and exiting around sample circumference. Mean values and standard deviations reported; *n* variable owing to loss of samples and embryos (as reported in Table 1). Two-way ANOVA showed no significant differences between samples or time points.

Most test materials perform comparably with the commercial comparators Matriderm™ and Integra®. The 90% fibrin ETPM scaffold performed particularly strongly, with greater blood vessel interaction than either commercial product on assay days 5, 7 and 9 (incubation days 9, 11 and 13). Prior to assay day 5, the capillary network in all cases was still growing; from day 5 onwards the entire surface of the culture dishes were vascularised and the capillaries moved from exploration and expansion to consolidation and maturation. In general, all samples showed increased blood vessel interaction over time. Some (fibrin ETPM, d9; fibrin-PVA ETPM, d9; fibrin-alginate ETPM, d7; fibrin film, d9; fibrin-alginate film, d7) showed a reduction at a single timepoint. Especially with the day 7 reduction, this result is likely to have arisen from the difficulty ascertaining which blood vessels were truly interacting

with the samples. The recovery in number at day 9 supports this theory. Another, less likely, possibility is that number of interacting blood vessels reduced due to conformational changes in the capillaries. This could occur with tortuous capillaries bending close to the perimeter of the sample.

Notably, Integra® was the only material to show consistent reduction in the number of interacting blood vessels across each time point. At day 3, the number of interacting blood vessels was the highest of all samples, but this declined over the course of the assay. The remaining blood vessels in the vicinity did not appear to have increased in diameter, suggesting the reduction in number was not offset by maturation of the major vessels.

In contrast, the number of blood vessels interacting with Matriderm™ samples increased day-on-day with the greatest increase occurring between days 5 and 7 after sample placement. This time point is of interest as it marks the change from exploratory blood vessel growth over the air interface to maturation. An increase in blood vessel interaction from day 5 onwards is therefore more likely to be indicative of a material influence rather than random growth.

Among the fibrin-based materials, there was no significant difference in the number of blood vessels counted either between the same materials at different timepoints, or different materials at the same timepoint. No advantage of any one material over another was apparent. The fibrin-only scaffold showed increased blood vessel interaction compared to fibrin-PVA and fibrin-alginate scaffolds, but the difference was not statistically significant. There was no discernible difference in the performance between the three different fibrin-based films. A slight reduction in interaction was expected in the alginate- and PVA- containing samples as these are not native blood proteins, like fibrin. It is possible that the response may be different or more pronounced for materials of human-origin fibrin in a human *in vivo* test, rather than bovine fibrin in a chick assay.

The fibrin films showed a greater number of blood vessels interacting compared to their 3-dimensional scaffold counterparts. However, this number is likely to be misleading as the films were more transparent and allowed greater visualisation, making it difficult to separate interacting vessels with non-interacting blood vessels below the sample. The results cannot therefore separate between material and structural contribution to angiogenic potential.

While the comparative results are not compelling, it should be noted that both Matriderm™ and Integra® have a long history of clinical use and have amassed a body of clinical and supporting academic evidence that suggests both *in vivo* efficacy and integration with host tissue. This would only be achievable with scaffold vascularisation.

		90% porous ETPM			Non-porous film			Commercial product	
		FIB	FIB-PVA	FIB-ALG	FIB	FIB-PVA	FIB-ALG	MatriDerm	Integra
Day 5	1	22, 32, 36	22, 32, 36	22, 32, 36	22, 32, 36	13	13	13	8, 13
	2	11				11		11	
	3	18	18			18	18		
Day 7	1								
	2								
	3			27	27			27	27
Day 9	1					21, 34	21, 34	21, 34	21, 34
	2	16, 30	19, 29	16, 30	19, 29	16, 30	19, 29	16, 30	19, 29
	3	7, 28	7, 28	17	17	28	7, 28	7, 17	17

Table 1: Explanted scaffolds per egg on culture days 5, 7 and 9. Samples were extracted at assay endpoint or after death of the embryo. Embryos that failed before the capillary plexus covered the surface of the culture well (incubation day 9, culture day 5) were destroyed without collecting scaffolds.

Quantification of haem present in explanted scaffold samples

Scaffolds were excised after the final blood vessel count on culture day 9 (incubation day 13) prior to termination. A Drabkin's assay was performed on these excised scaffolds to quantify haemoglobin present as a secondary output measure. In theory, any haemoglobin present in the samples must originate from embedded blood vessel fragments. Their presence confirms infiltration, unlike direct imaging which cannot distinguish between blood vessels interacting with samples from those simply passing underneath.

Both measures are useful to a degree, as vessels passing directing underneath the sample without penetrating may still be influenced in some way. The direction could be attributable to chemotactic properties of the material (positive response), or simply coincidental, or even a repulsive response by blood vessels eschewing the material but retaining their path by going above or below.

The Drabkin's assay revealed a low concentration of haemoglobin present in all samples. It should be noted that the assay is typically used to quantify haemoglobin concentration in whole blood samples,

and so concentrations at the low end of the manufacturer's suggested calibration range were expected.

Nonetheless, the results (fig. 6) are surprising for their discrepancy with the number of interacting blood vessel (fig. 5). Matriderm™ samples had among the highest number of interacting blood vessels at day 9. This is broadly in agreement with the result of the Drabkin's assay. However, the fibrin ETPM scaffolds, fibrin-PVA films and fibrin-alginate films which displayed similarly high levels of blood vessel interaction in the CAM assay were found to contain the lowest levels of haem by Drabkin's quantification (<0.07 mg/ml). This may be due to the difficulty in extracting the samples cleanly from the albumen. The fibrin-based scaffolds and films are all elastic in behaviour. Blood vessels are also highly elastic, and the albumen 'matrix' was highly viscous by the end of culture. There was resistance from all three components during sample harvesting. It is also possible that many of the blood vessels observed interacting with samples, particularly with the transparent films, were passing adjacent and below the samples. Films were retrieved largely intact without signs of tearing, which supports this supposition.

Although the fibrin-PVA and fibrin-alginate scaffolds showed reduced numbers of interacting blood vessels, the mean haem detected was greater than in fibrin only scaffold samples. It is difficult to draw positive conclusions from the results, but they do not show any detrimental angiogenic effect when PVA or alginate are used to replace some of the fibrin.

The addition of PVA, particularly, has been shown to significantly improve the mechanical properties of the fibrin-based scaffolds. PVA is similarly attractive from an economic stance: cost per gram is 175 times less than that of bovine fibrinogen and 290 times less than that of human fibrinogen. However, it is imperative that the *in vivo* performance is not compromised. Establishing equivalence in biocompatibility, cell interaction and angiogenic potential is essential. These early results are promising, but larger scale testing, as well as whole animal models, are required to confirm equivalent performance compared to fibrin-only scaffolds.

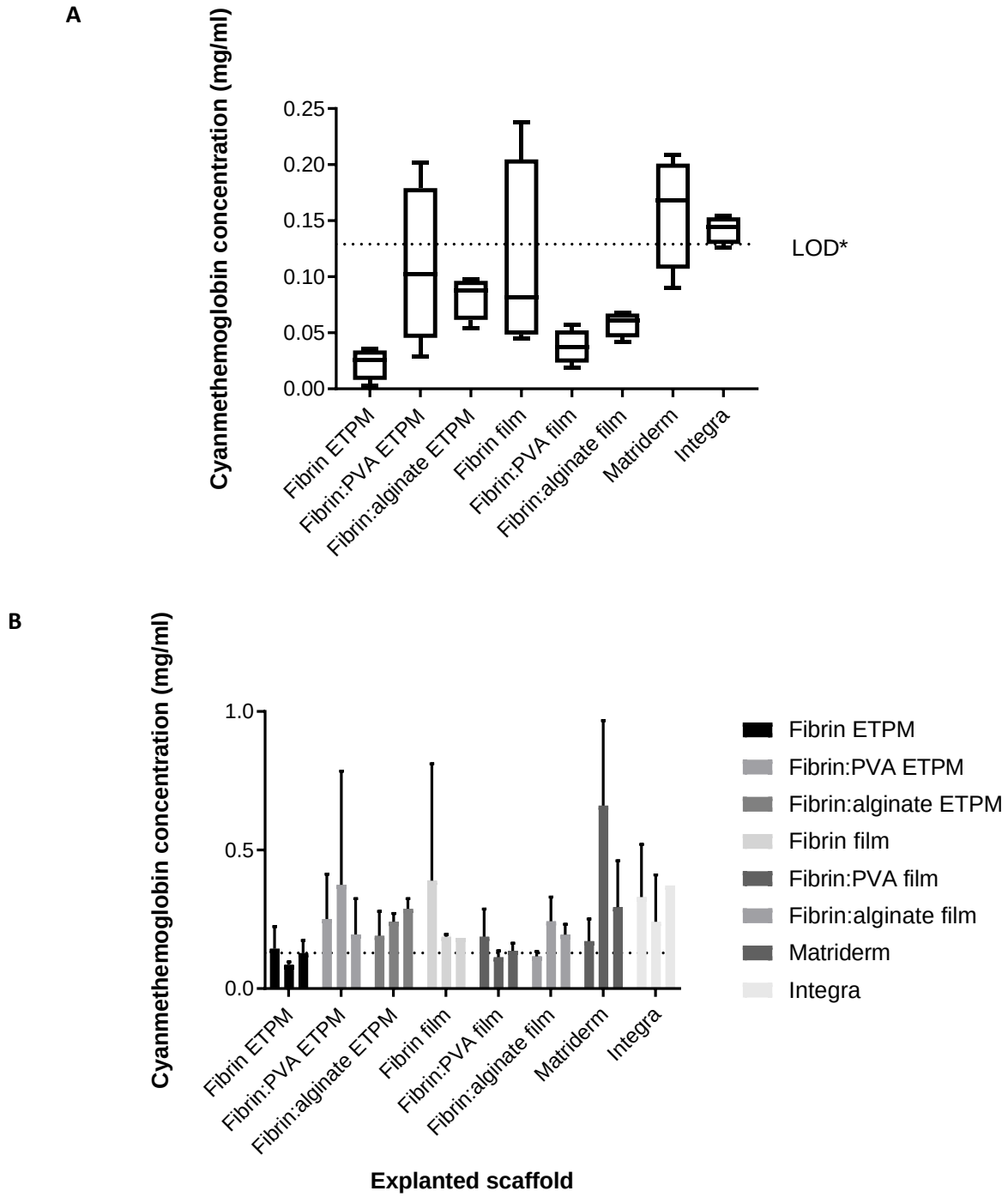

Fig. 6: Cyanmethemoglobin (mg/ml) detected using Drabkin's Reagent at 540 nm (R^2=0.9995). Scaffolds were excised with forceps immediately prior to termination to minimise risk of contamination with blood from neighbouring severed blood vessels. [A] box-and-whisker plot showing median, upper, and lower quartile and upper and lower values; [B] mean and standard deviation. Two-way ANOVA revealed no statistically significant difference between samples. *Dashed line shows limit of detection ($\mathrm{LOD} = \bar{x}_{\mathrm{b}_i} + S_{\mathrm{b_i}}$ where $\bar{x}_{\mathrm{b}_i}$ is the mean concentration of the blank and $S_{\mathrm{b_i}}$ is the standard deviation of the blank).

DISCUSSION

Biomaterial scaffolds of myriad materials and structures are reported in the literature. The importance of rapid vascularisation and angiogenic potential of these materials is equally well known. Insufficient vascularisation can lead to graft failure, rejection or necrosis (Hendrickx et al., 2010; Sahota et al., 2004). Confirming angiogenic potential of candidate biomaterials is therefore essential to their success. The fibrin-based scaffolds tested here went through an iterative design process to generate spatial structure parameters (porosity, interconnectivity, wall thickness, etc.) in line with reported literature values prior to evaluating angiogenic capacity.

The mouse aortic ring model and whole animal testing are alternative methods for testing biomaterial angiogenic potential. The CAM was selected as it offered a dynamic living system, mimicking the rapid physiological response during the wound healing cascade, but allowed higher throughput than use of animal models. Chick eggs are more readily available than research animals, and their lack of immune system and tactile sensation during scaffold placement ameliorate ethical concerns.

The CAM assay is widely used and reported for use studying tumorigenesis. However, methodologies are often sparse. Despite the large body of literature describing scaffold manufacture, the number of works reporting angiogenesis results is relatively small. This may go some way to explaining why products described as promoting rapid tissue integration fail to live up to clinical expectation.

Method development

The *ex ovo* CAM assay is well described in recent literature, and several groups describe the use of such culture for decades with degrees of success. It is generally accepted that *ex ovo* culture is more challenging than *in ovo* culture and embryo viability may be reduced. However, many groups describe various approaches that seek to attenuate this loss, and viability rates of ~70% have been cited.

The biggest losses consistently occurred, unavoidably, on delivery. Safely evacuating the eggs was the second barrier to survival. Whilst rotating the eggs did successfully orientate embryos to the upper surface of the egg, the yolk did not similarly migrate. Yolk rupture during cracking was the most common cause of mortality either immediately after cracking or during culture, depending on the extent and rate of the leak. The yolk solidified at the air interface, reducing the surface area for gaseous exchange.

Viability continuing to reduce throughout the assay (after transfer to *ex* ovo culture) was contrary to reported results (Reed and Clark, 2011). Attempts were made, with some success, to improve survival

rates by increasing ambient humidity and using alternative methods for evacuating embryos. Size of the embryo at evacuation was a strong indicator for survival. The largest carried a much higher mortality rate than smaller embryos with smaller and less developed capillary networks.

Despite reduced viability, *ex ovo* culture was selected for the larger test area, enabling the use of more scaffold samples per egg and a larger field of vision. Successful *ex ovo* culture is dependent upon a reliable method of extracting the egg contents intact and then recreating the shell environment in culture. The shell provides a partially permeable barrier, a calcium reservoir, and a structural support for the developing embryo. All three components must be replicated *ex ovo.* Here, embryos were not developed beyond Hamburger-Hamilton stage 40 so skeletal development was not a major concern and calcium supplements were not used. In place of a permeable membrane, embryos were incubated with tightly regulated humidity, temperature, and air supply. In terms of structural support, embryo viability is highly dependent on maintaining the shape of the yolk sac. In a flat culture dish, the yolk distends and ruptures, drowning the embryo. Some protocols suggest cracking the eggs into a hammock formed by securing film by the rim of a plastic cup (Cloney and Franz-Odendaal, 2015). This method effectively recreates the curvature of the intact egg, but the cups are not stable and are liable to fall.

The method used here was initially based on that described by Dohle et al. (2009), with some modifications. The Dohle group describe a tightly prescribed method for cracking the shell with a triangular pyramidal stirring bar in a defined and repeatable manner, which resulted in a 50% increase in embryo survival *ex ovo* (Dohle et al., 2009). This method was used during the pilot study, but the stirring bar was found to produce a small series of cracks that were insufficiently cohesive to create a neat fracture surface. In subsequent attempts, the stirring bar was replaced with a scalpel blade, followed by initial fracture with a scalpel blade followed by propagation with surgical scissors. This method proved most successful at piercing the shell and thick outer membrane and resulted in the greater viability (fewest egg yolks ruptured).

Most reported protocol cite an incubation humidity of 60-65%. Maintaining humidity is important to prevent the albumen and yolk drying out, however, excessive humidity may cause embryos to drown. In these experiments 65% humidity was found to be too low. 80-85% humidity improved embryo survival rates and visibly reduced drying and volume loss of the albumen. The use of damp kim wipes under each dish, suggested by Cloney and Franz-Odendaal (Cloney and Franz-Odendaal, 2015), proved successful at maintaining ambient humidity.

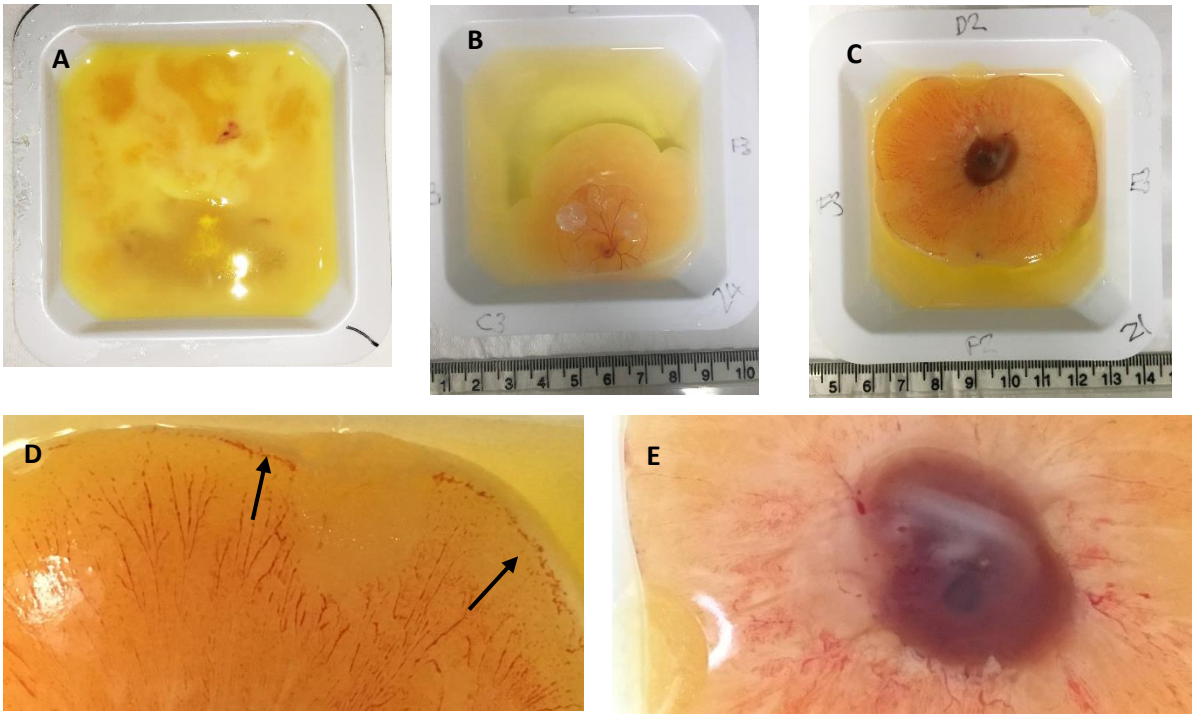

Fig. 7: Embryo mortality arising from **[A]** catastrophic yolk rupture, **[B]** slow rupture after 2 days in culture and **[C]** low humidity (60-65%). Mortality was detectable by [D] blood accumulating at the periphery of the capillary plexus, [E] whitening of the vessels and embryo. Images taken with iPhone, without magnification.

FUTURE WORK

In principle, angiogenesis should be enhanced in a cellularised scaffold compared to the same acellular scaffold because the resident cell would secrete their own cytokines and growth factors to enhance angiogenic potency (Frueh et al., 2017). In situ secretion of these factors is likely to have greater effect than dosing scaffolds with isolated growth factors as cell secretions would be more physiologically relevant and not suffer from loss of viability during manufacturing and processing or sterilisation techniques.

Additionally, if the implanted cells are endothelial or progenitor cells capable of differentiating into endothelial lineages, they may be able to form blood vessels in the scaffold interior. This could accelerate graft vascularisation compared to relying on vascularisation solely arising from existing vessels in the wound bed and periphery.

Implanting xenogeneous cells in an exogenous scaffold into a chicken egg is unlikely to be a useful model. The developing embryo is immune privileged over the course of the CAM assay so there would

be no inflammatory response but equally there would be no additional benefit. The immune response is an important consideration and should be included in output measures. Additionally, enhanced positive response possible from allogeneic or autologous cellularisation could not be monitored. It would therefore be more appropriate to study angiogenic potential of cellularised scaffolds during advanced animal clinical trials, after confirming efficacy with acellular scaffolds in the same model. The results of such a study would be a useful cost-benefit analysis to determine whether the added complexity, time, and cost of cellularising scaffolds translated to clinical benefit.

CONCLUSIONS

The CAM assay is a useful model for studying angiogenesis in biomaterial samples, allowing unimpeded real-time visualisation of the developing vascular network and material interaction. The assay allows higher throughput testing than conventional *in vivo* models. However, it is not without difficulties and egg viability is highly dependent on patience and experience. This may help explain the variability in protocols and parameters cited in the literature.

The CAM assay was intended to test three principal hypotheses:

1) use of a native blood protein, fibrin, would show greater angiogenic potential compared to similarly structured materials of heavily processed proteins (collagen/GAGs; Matriderm™ and Integra®);
2) reduction of fibrin content in favour of biocompatible but non-bioactive polymers (PVA) would reduce angiogenic potential;
3) 2-dimensional films would show reduced blood vessel interaction compared to highly porous (90%) 3-dimensional scaffolds of equivalent composition.

It was hypothesised that ETPM scaffolds would equal or exceed performance of commercial competitors owing to a combination of superior material and structural properties. Examination of the microstructures (reported previously) revealed ETPM scaffolds to have a much more open, interconnected structure than either Matriderm™ or Integra®. The results reported above could suggest that ETPM scaffolds behaved comparably with Matriderm™ and Integra® in terms of blood vessel interaction.

Surprisingly, there was no significant difference in blood vessel interaction between materials of different structure (3-dimensional scaffolds versus equivalent 2-dimenional films) or composition. Fibrin is a native blood protein, thought to have pro-angiogenic properties. *In vivo*, fibrin clots provide

a framework to promote capillary ingress during wound healing (Collen et al., 2003). The templating technique used to manufacture the fibrin-based scaffolds described here maintained the native protein structure and should preserve this functionality. PVA is not bioactive, so fibrin-PVA materials were expected to have less of an angiogenic response owing to reduced fibrin concentration.

However, the results are not sufficiently compelling to make firm conclusions. While the number of samples and eggs tested is sufficient for statistical significance, only one batch of eggs survived to assay completion, so no technical repeats were achieved.

The output measures could be improved to help refine data and increase confidence in the results. Counting blood vessels in a 3-dimensional model is complex and subjective. As the CAM develops, particularly beyond development day 8 (culture day 5), blood vessels remodel and develop in layers. It is difficult to determine whether vessels are interacting with the scaffold or passing underneath. Some protocols aim to counter this problem by only including vessels that are seen to enter and leave the scaffold, but unless the material is transparent this approach is not robust. The capillaries are dendritic and tortuous, so it is almost impossible to extrapolate with any confidence.

Locating the scaffolds during CAM growth and yolk consumption was also challenging. Scaffolds stick to the viscous albumen and thus move as the egg contents change conformation. This problem was slightly ameliorated with increased ambient humidity, as it prevented albumen drying at the interface. Some scaffolds subducted underneath the yolk sac as it flattened – particularly those where the initial capillary plexus was not central on the yolk at the time of scaffold placement. Additionally, the highly porous scaffolds became saturated with egg material (albumen, etc.) and became virtually indistinguishable over time. Imaging could be improved by use of contrast agents. Inks and dyes must first be trialled for biocompatibility to avoid biasing the study. Another option is fluorescent labelling of the scaffold during manufacture, for example, binding an agent like Alexa Fluor 594 to fibrinogen concurrently with thrombin addition.

Quantification of haem was intended as a more robust measure to supplement blood vessel count. It should help assess whether the blood vessels were active (some were observed to retract and remodel during the CAM assay) and consider capillary diameter and circulation capacity. However, precise extraction of the scaffolds was challenging and may have reduced the quality of the results. Scaffolds were removed with forceps. However, the high viscosity of the albumen at the end of the assay meant that vessels, which are elastic in nature, preferentially adhered to the albumen matrix rather than the scaffold. Surgical scalpels were used to cut away excess albumen around the edge of the scaffold, helping to keep blood vessel fragments in the excised scaffold. Some blood may have drained out of the vessels during this process. Fixing the tissue prior to excision was considered but discounted as

the Drabkin's assay is intended for liquid samples only. It may be possible to use some means of digesting the scaffold and albumen, perhaps by a mild acid digestion approach, but this would take extensive development and refinement to ensure homogenous samples with haem left intact for analysis.

Fixing the tissue would, however, be a useful approach to preserve capillary architecture. Sectioning and imaging samples, either staining with H&E or perhaps immunohistochemistry, would give a detailed 3-dimensional picture of the capillary plexus and its interaction with the scaffold. This would be particularly useful in conjunction with scaffold dyeing or other tagging as the scaffold would be clearly defined, making interaction by blood vessel count in and out of the scaffold a more robust measure. While labour intensive, this method would yield high-quality results and is highly recommended for future use.

ACKNOWLEDGEMENTS

Many thanks to Karen Evans, Agata Stramek, Iwona Bruna (BRU) and Igor Kraev, Brett Keith, Duncan Banks for their assistance sourcing and setting up equipment. Particular thanks to Agata Stramek for assistance with errant incubators, improving egg evacuation protocol and providing small animal training.

Matriderm™ and Integra® scaffolds were obtained through kind assistance of NPIMR (Northwick Park Hospital, Harrow, UK).

4. Conclusions

The aim of this project was to design and develop a skin tissue engineering scaffold, with particular application in the treatment of chronic wounds and serious burns. There are many products available that claim to promote healing of these wounds, and indeed there are many case studies of successful treatment with products such as Matriderm®, Integra® and Biobrane®. However, there remains an unmet clinical need for products which are able to 'regenerate' damaged skin; that is, to repair the appearance, composition, and function to equal surrounding undamaged skin.

Tissue engineering research has offered promising solutions in the shape of stem cell or gene therapy, or targeted delivery of growth factors, drugs, or extracellular vesicles. While targeted delivery may be achieved, retention in the wound environment is a challenge. Scaffolds offer an implantable 'niche' for cultured autologous cells or particular controlled doses of other therapies. The rate of release away from the immediate scaffold environment can be mediated by porosity and degradation rate. Emulsion templated allows creation of scaffolds with tunable, accurate and reproducible porosity and pore size. For the body of work described in this thesis, porosity was increased to 90% to maximise the internal area for cells and blood vessels while maintaining structural integrity and mechanical strength. Pore size was designed match values described in literature to encourage rapid colonisation by fibroblasts from the wound periphery and sprouting ends of neighbouring blood vessels to sustain resident cells.

Early results show cytocompatibility and the ability to support ingrowing vasculature, as demonstrated in the chick chorioallantoic membrane assay. Before clinical or commercial use the scaffolds should be tested more rigorously with higher throughput in vitro assays and large animal models to positively confirm biocompatibility, lack of immunogenicity and appropriate degradation profile.

Cell therapies are often prohibitively expensive and specialised for most healthcare providers. The scaffold produced here was designed will both outward migration of cultured cells and ingress of healthy native cells in mind. In all the experiments described, the scaffold was freeze-dried after manufactured and stored until use. This dramatically It is also a useful consideration for scaled-up commercial manufacture, as batches may be made in advance and stored until required. There is no need for cold-chain storage during shipment. However, heat treatment of the scaffolds was not tested so the fibrin may be sensitive to extreme heat (above 37°C; for example, in a shipping container).

The ability to retain cells or other therapeutic agents in the wound environment also improves the cost-benefit of such treatments by increasing the effective dose and reducing the need for several

successful treatments. Each of these is associated with hospital care, standard dressings and physical therapy and rehabilitation. Improving outcome with fewer surgeries would be hugely beneficial to patients by reducing the time spent in operative or postoperative care.

While the project was initially conceived as an exercise to design a scaffold for stem cell therapy – for the reasons outlined above – the engineering of the scaffold and the precursor emulsion itself was the focus of research. This decision was not consciously made but reflected available materials as well as expertise and research interests.

As the project evolved, formulation of an appropriate emulsion system became a larger area of research than anticipated. Significant time was spent trying to understand the factors contributing to emulsion stability and how to manipulate them without adversely affecting the protein scaffold. Oil carrying capacity was an unexpected discovery made during the systematic evaluation of surfactants. It proved a useful tool in accelerating surfactant selection for scaffold templating, but it has potential application in many other fields as well.

5. Future work

Scaffold design

Enhanced clot formation control

Alternative fibrinogen splicing, arising spontaneously in nature, produces an elongated γ-chain (γ'). This alternatively spliced variant normally circulates as γA/γ' (as opposed to γA/γA with conventional splicing). The γ' variant has been shown to exhibit looser protofibril packing and larger pores, together producing less stiff fibres. The fibres assemble in 3D networks differently, with more heterogeneity in diameter and spacing. Importantly, γA/γ' are more resistant to lysis (Allan et al., 2012; Domingues et al., 2016).

Cross-sectional SEM images of the scaffolds described in this project show structures more characteristic of the γA/γ' variant. However, this has not been confirmed. It would be interesting to do so and to attempt formation of scaffolds with structures characteristic of the γA/γA type. This should produce scaffolds with better mechanical strength but poorer resistance to hydrolytic degradation. The ability to tune γA/γA : γA/γ' for optimisation of mechanical and degradation properties would be very useful.

Thrombin concentration is widely known to impact clot strength as well as fibre diameter and density of the 3D mesh (Blombäck, 2000; Weisel, 2004). The concentration of thrombin used here was relatively low, producing fewer, thicker fibres with fewer branch points. It would be useful to increase thrombin concentration and investigate the effect of the change in fibre number, diameter, and number of branch points on the mechanical and degradative properties. The effect on cell adhesion and rate and extent of locomotion should also be studied. Fibre diameter and spacing in electrospun artificial membranes has been shown to affect the proliferation, orientation and integration of a variety of cell types with the scaffold, including fibroblasts, Schwann cells, neurons and dendrites, mesenchymal stem cells and smooth muscle and bone cells (Gupta et al., 2009; Jin et al., 2012; McCullen et al., 2007; Nam et al., 2007; Sun et al., 2007; Wang et al., 2013; Zhou et al., 2015). The same would be expected in a fibrin network. The fibrin scaffold poses a more interesting question as the electrospun membranes are commonly either 2-dimensional or very thin (50-200 μm, or 30 μm for single layer membranes)(Bhattarai et al., 2004; Pan et al., 2014; Pu and Komvopoulos, 2014; Riboldi et al., 2005).

Additional testing

***In vitro* assays**

Designing and characterising the emulsion system consumed a significant amount of project resources. In vitro tests were scaled back as a result. Although the final scaffold properties conform to values presented in the literature as being optimal for cell ingress and proliferation, this should be verified with culture of relevant cell types (dermal fibroblasts, endothelial microvascular cells, and mesenchymal stem cells). It would be useful to investigate the material and structural contributions of the scaffolds on metabolic activity (MTT; live/dead), adhesion and production of ECM components (immunofluorescence and colorimetric detection; qPCR; ELISA; Western blot analysis).

PVA, alginate and PEG were added to improve the mechanical properties of the scaffold and also to reduce the cost per unit area. Fibrinogen and thrombin are considerably more expensive that the other polymers, particularly when using the human proteins that would be needed for a clinical product. Inclusion of the other polymers makes the scaffold more economically viable. However, while the mechanical and structural effects of adding these materials were evaluated, the biological effects were not. Again, the effect on cell viability, adhesion, and differentiation (of primary MSCs) should be assessed for different material combinations at different ratios.

CAM assay repeats

The CAM assay was repeated multiple times owing to unexpected equipment failures and method fallibility. The final method worked well in our laboratory; however, the results obtained were inconclusive. It would be useful to repeat the assay with a technical repeat, as originally intended, as a larger sample size would give more confidence in the results.

Counting the number of blood vessels interacting with a small disc in a deep, translucent medium is difficult to perform accurately and objectively. Future assays, therefore, should use histology (H&E and immunohistochemistry) to give a better indication of blood vessel interaction with the scaffold.

Fixed samples would be much easier to handle without tearing either the scaffold or the vessels when removing from the viscous albumen. Sectioning to expose the scaffold would allow simple counting of blood vessels interacting with the material by eliminating the planes above and below (difficult to achieve by eye alone). H&E staining would increase contrast; immunohistochemistry could identify the new blood vessels from the ones made redundant during remodelling. Again, this is very difficult to do by eye as the colour contrast is very slight.

In vivo studies

In vitro assays are useful ways of predicting cell behaviour, particularly during the design and development stage, but are limited models of the complex whole animal system. Animal studies should form two stages: firstly, basic biocompatibility testing to ensure the fundamental safety of the material. Once this is confirmed, longer-term studies can assess the efficacy of the scaffolds at healing a) acute (surgical excision) and b) debrided full thickness burn wounds compared to current clinical products (Matriderm, Integra and Biobrane scaffolds). This two-stage procedure is similar to the testing process required by the FDA for testing safety and efficacy of implantable materials.

Using small animals allows a larger number of repeats, but less biologically relevant results for human use. Pig studies are more expensive, but more samples may be applied to a single animal and the pig is the best non-primate model for humans. Ultimately, the materials could be submitted for human clinical trials to be tested for safety and efficacy in healing surgical and burn wounds and chronic ulcers.

Preparation for commercial transfer

Batch size

The scaffolds described in this thesis have been optimised at lab scale, with a typical batch comprising 8-10 scaffolds, 5x5 cm^2. Scaffolds have been manufactured at 10x10 cm^2 (a typical commercial scaffold size), but batch size was reduced owing to size constraints of the fume hood and laminar flow cabinet.

To make the scaffolds commercially viable, the scaffolds must be manufacturable at 10x10 cm (or above) in larger batch sizes. The washing and drying stages are very time consuming and so the ability to produce a large number of scaffolds in a single batch would drastically improve the efficiency of the process and reduce operational costs.

Manufacturing time

Currently, all scaffolds are freeze dried prior to use. The freeze-drying process was shortened during process optimisation, but the complete freezing and drying cycle still takes 16 hours. For some freeze-dried products, the freeze drying is used as the mode of generating porosity and thus is an integral part of the process. In this case, the porosity is generated by the emulsion template and freeze drying is used simply to preserve the structure and to remove moisture, prolonging shelf-life. However, the results of the short-term hydrolytic degradation assay (*Chapter 3.3*) indicate that the scaffolds are stable in saline solution for at least one month. If the scaffolds remain stable in sterile buffered saline

for longer periods – for example, 1 to 2 years – it may be possible to eliminate the drying process completely and simply package the sterile scaffolds in a pouch with saline. Integra® Dermal Regeneration Template (Integra LifeSciences) is currently packaged in this manner. The long-term hydrolytic stability of the scaffolds in saline should be assessed, as should the bioburden after two years' storage in ambient conditions. The scaffold microstructure (e-SEM) and mechanical properties (tensile and compressive) of the non-dried scaffold should be compared to a typical freeze-dried scaffold that has been washed and rehydrated in saline as though for clinical application. If comparable, the freeze-drying step may be removed, reducing manufacturing time by half.

Process automation

Process automation would be a useful step towards commercialisation, freeing up labour time for characterisation and batch testing. The most obvious opportunity for optimisation is the emulsion mixing. Vortex mixing and shear mixing yielded inferior results to hand shaking for manufacture at lab scale. However, behaviour is likely to be different at larger scale owing to the increased distance between the mixer and the vessel walls changing the shear dynamics. Other methods of mixing should also be attempted. It may also be possible to generate a single large volume of emulsion from which a whole batch of scaffolds could be cast. This would certainly create good reproducibility within batches. If the emulsion mixing process was robust and repeatable then batch-to-batch variability could be minimised. This is an important point to prove during the regulatory assessment process.

The washing processes could also be at least partially automated. The rig shown below is a possible solution that would allow the wash timings and regular rotations of the scaffolds to be maintained.

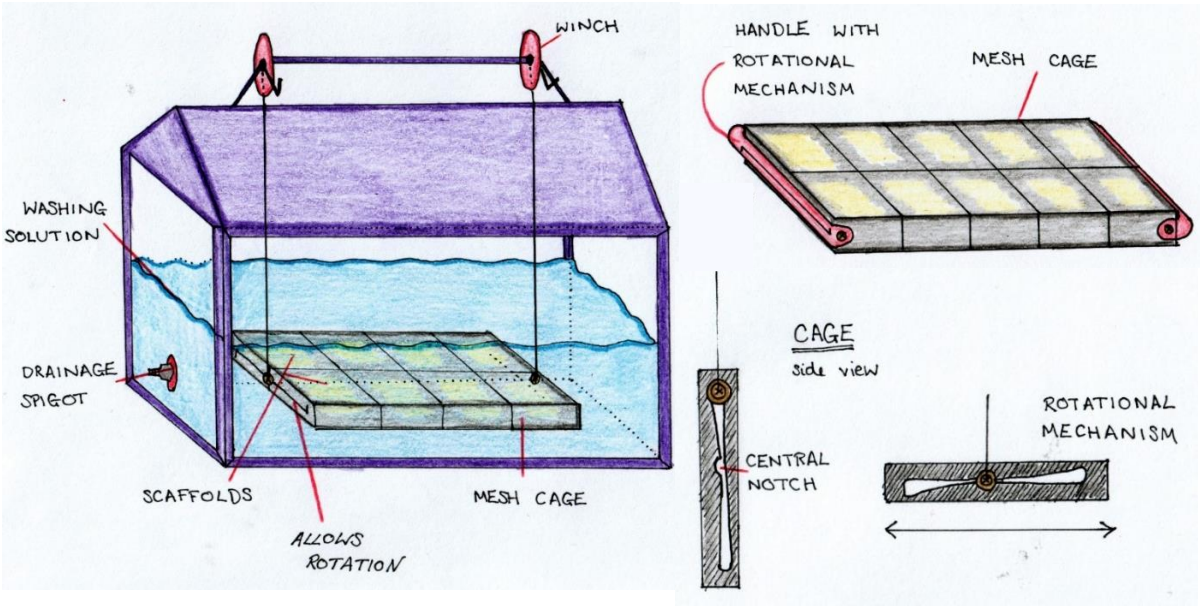

Fig. 1: Proposed rig for automation of the scaffold washing process. Automation has the potential to accelerate manufacture time, increase batch size capability and minimise handling. Reduced scaffold handling during manufacture decreases risk of damage to the scaffolds (increasing viable yield per batch) and risk of contamination introduced by laboratory personnel.

'Next generation' product modifications

Cellularised scaffolds

The scaffolds described here have thus far been characterised and discussed as an acellular product. Many of the commonly used clinical scaffolds are acellular; it is the ECM protein composition that gives some biological relevance. Adding cells adds significant cost, complexity (in manufacture, storage, delivery, safety, and regulation) and time to market. Autologous cells must be harvested then expanded and cultured in the scaffold. Transporting the cellularised scaffold from the lab to the patient while guaranteeing both sterility and viability is challenging. Clinical use of cellularised scaffolds is therefore likely to be limited to 'centres of excellence' where hospitals contain dedicated clean rooms and CL2 laboratories for cell culture and the surgical team is experienced with combination products.

The use of cellularised scaffolds must therefore be justified by in vitro and in vivo assays to confirm superiority over the acellular material. Increased rate of cell ingress and colonisation of the scaffold, particularly with rapid vasculature formation, would be extremely useful. Speed and penetration of

vasculature is a current limitation of tissue engineering scaffolds. If insufficient, any resident cells are likely to experience reduced viability.

Histology from in vivo implantation of acellular and cellularised (with autologous fibroblasts or mesenchymal stem cells) could be used to assess extent and maturity of vasculature at different time points. Histology would also reveal the presence of various ECM products secreted by cells and the organisation of these products in the wound. Cellularised scaffolds would be expected to show enhanced vascularisation, cell colonisation and ECM deposition owing to the contribution of the implanted cells in addition to wound periphery fibroblasts. This should be confirmed, and cost/benefit analysis performed compared to acellular materials.

Fibrin decoration

As evidenced from its physiological role as a clotting protein, fibrin is a naturally sticky protein. Unlike other biomaterials which must be treated with laminin or fibronectin to improve adhesion, fibrin may be directly decorated with therapeutic agents. Fibrin scaffolds are therefore an interesting vehicle for delivery of growth factors, extracellular vesicles, etc. to the wound environment. These could be used as additional biochemical cues to accelerate the wound healing response or to influence the type of healing. This could be a useful tool in promoting regeneration over scarring and less organised or less complete wound repair.

6. References

Abedalwafa, M., Wang, F., Wang, L., Li, C., 2013. Biodegradable poly-epsilon-caprolactone (PCL) for tissue engineering applications: A review. Rev. Adv. Mater. Sci. 34, 123–140.

Abismaïl, B., Canselier, J.P., Wilhelm, A.M., Delmas, H., Gourdon, C., 2000. Emulsification processes: on-line study by multiple light scattering measurements. Ultrason. Sonochem. 7, 187–192. https://doi.org/10.1016/S1350-4177(00)00040-7

Acharya, R., 2017. Chapter 3 - Interaction of waves with medium, in: Acharya, R. (Ed.), Satellite Signal Propagation, Impairments and Mitigation. Academic Press, pp. 57–86. https://doi.org/10.1016/B978-0-12-809732-8.00003-X

Ahmed, T.A.E., Dare, E.V., Hincke, M., 2008. Fibrin: A Versatile Scaffold for Tissue Engineering Applications. Tissue Eng. Part B Rev. 14, 199–215. https://doi.org/10.1089/ten.teb.2007.0435

Akay, G., Birch, M.A., Bokhari, M.A., 2004. Microcellular polyHIPE polymer supports osteoblast growth and bone formation in vitro. Biomaterials 25, 3991–4000. https://doi.org/10.1016/j.biomaterials.2003.10.086

Akhtar, S., Hasham, S., Abela, C., Phipps, A.R., 2006. The use of Integra® in necrotizing fasciitis. Burns 32.

Allan, P., Willige, S.U. de, Abou-Saleh, R.H., Connell, S.D., Ariëns, R. a. S., 2012. Evidence that fibrinogen γ′ directly interferes with protofibril growth: implications for fibrin structure and clot stiffness. J. Thromb. Haemost. 10, 1072–1080. https://doi.org/10.1111/j.1538-7836.2012.04717.x

Anderson, N.L., Anderson, N.G., 2002. The Human Plasma Proteome History, Character, and Diagnostic Prospects. Mol. Cell. Proteomics 1, 845–867. https://doi.org/10.1074/mcp.R200007-MCP200

Androutsos, G., Karamanou, M., Kostakis, A., 2011. Baron Guillaume Dupuytren (1777–1835): One of the most outstanding surgeons of 19th century. Hell. J. Surg. 83, 239–244. https://doi.org/10.1007/s13126-011-0044-z

Artz, C.P., 1970. Historical aspects of burn management. Surg. Clin. North Am., Surgery of Burns 50, 1193–1200. https://doi.org/10.1016/S0039-6109(16)39279-9

Arwert, E.N., Hoste, E., Watt, F.M., 2012. Epithelial stem cells, wound healing and cancer. Nat. Rev. Cancer 12, 170–180. https://doi.org/10.1038/nrc3217

Atiyeh, B.S., Costagliola, M., 2007. Cultured epithelial autograft (CEA) in burn treatment: Three decades later. Burns 33, 405–413. https://doi.org/10.1016/j.burns.2006.11.002

Atiyeh, B.S., Hayek, S.N., Gunn, S.W., 2005. New technologies for burn wound closure and healing - Review of the literature. Burns 31, 944–956. https://doi.org/10.1016/j.burns.2005.08.023

Auerbach, R., Kubai, L., Knighton, D., Folkman, J., 1974. A simple procedure for the long-term cultivation of chicken embryos. Dev. Biol. 41, 391–394. https://doi.org/10.1016/0012-1606(74)90316-9

Aulton, M.E., 1988. Pharmaceutics: The Science of Dosage Form Design. Churchill Livingstone.

Ausprunk, D.H., Knighton, D.R., Folkman, J., 1974. Differentiation of vascular endothelium in the chick chorioallantois: A structural and autoradiographic study. Dev. Biol. 38, 237–248. https://doi.org/10.1016/0012-1606(74)90004-9

Aust, L., Devlin, B., Foster, S.J., Halvorsen, Y.D.C., Hicok, K., du Laney, T., Sen, A., Willingmyre, G.D., Gimble, J.M., 2004. Yield of human adipose-derived adult stem cells from liposuction aspirates. Cytotherapy 6, 7–14. https://doi.org/10.1080/14653240310004539

Bai, F., Wang, Z., Lu, J., Liu, J., Chen, G., Lv, R., Wang, J., Lin, K., Zhang, J., Huang, X., 2010. The correlation between the internal structure and vascularization of controllable porous bioceramic materials in vivo: A quantitative study. Tissue Eng. Part A 16, 3791–3803. https://doi.org/10.1089/ten.tea.2010.0148

Bailey, K., Bettelheim, F.R., Lorand, L., Middlebrook, W.R., 1951. Action of Thrombin in the Clotting of Fibrinogen. Nature 167, 233–234. https://doi.org/10.1038/167233a0

Baldwin, S.P., Saltzman, W.M., 1996. Polymers for Tissue Engineering. Trends Polym. Sci. 6, 177–182.

Balls, M., Straughan, D.W., 1996. The three Rs of Russell & Burch and the testing of biological products. Dev. Biol. Stand. 86, 11–18.

Bannasch, H., Föhn, M., Unterberg, T., Knam, F., Weyand, B., Stark, G.B., 2003. Gewebeersatz (tissue engineering) von Dermis und Epidermis. Chir. 74, 802–807. https://doi.org/10.1007/s00104-003-0725-4

Barbetta, A., Cameron, N.R., Cooper, S.J., 2000. High internal phase emulsions (HIPEs) containing divinylbenzene and 4-vinylbenzyl chloride and the morphology of the resulting PolyHIPE materials. Chem. Commun. 221–222. https://doi.org/10.1039/A909060F

Barbetta, A., Dentini, M., Zannoni, E.M., De Stefano, M.E., 2005. Tailoring the porosity and morphology of gelatin-methacrylate polyHIPE scaffolds for tissue engineering applications. Langmuir 21, 12333–12341. https://doi.org/10.1021/la0520233

Belcaro, G., Cesarone, M.R., Errichi, B.M., Ledda, A., Di Renzo, A., Stuard, S., Dugall, M., Pellegrini, L., Gizzi, G., Rohdewald, P., Ippolito, E., 2006. Diabetic ulcers: Microcirculatory improvement and faster healing with pycnogenol. Clin. Appl. Thromb. 12, 318–323.

Beldon, P., 2010. Basic science of wound healing. Surg. Oxf., Perioperative management of co-morbid conditions 28, 409–412. https://doi.org/10.1016/j.mpsur.2010.05.007

Belew, M., Gerdin, B., Porath, J., Saldeen, T., 1978. Isolation of vasoactive peptides from human fibrin and fibrinogen degraded by plasmin. Thromb. Res. 13, 983–994. https://doi.org/10.1016/0049-3848(78)90227-X

Bensaïd, W., Triffitt, J.T., Blanchat, C., Oudina, K., Sedel, L., Petite, H., 2003. A biodegradable fibrin scaffold for mesenchymal stem cell transplantation. Biomaterials 24, 2497–2502. https://doi.org/10.1016/S0142-9612(02)00618-X

Bensouilah, J., Buck, P., 2006. Aromadermatology: Aromatherapy in the Treatment and Care of Common Skin Conditions. Radcliffe Publishing.

Bhardwaj, N., Chouhan, D., Mandal, B.B., 2017. Tissue engineered skin and wound healing: Current strategies and future directions. Curr. Pharm. Des. 23, 3455–3482. https://doi.org/10.2174/1381612823666170526094606

Bhattarai, S.R., Bhattarai, N., Yi, H.K., Hwang, P.H., Cha, D.I., Kim, H.Y., 2004. Novel biodegradable electrospun membrane: scaffold for tissue engineering. Biomaterials 25, 2595–2602. https://doi.org/10.1016/j.biomaterials.2003.09.043

Bjork, J.W., Johnson, S.L., Tranquillo, R.T., 2011. Ruthenium-catalyzed photo cross-linking of fibrin-based engineered tissue. Biomaterials 32, 2479–2488. https://doi.org/10.1016/j.biomaterials.2010.12.010

Blake, G.J., Ridker, P.M., 2001. Novel Clinical Markers of Vascular Wall Inflammation. Circ. Res. 89, 763–771. https://doi.org/10.1161/hh2101.099270

Blombäck, B., 2000. Fibrin formation in whole blood. Thromb. Res. 99, 307–310.

Blombäck, B., Bark, N., 2004. Fibrinopeptides and fibrin gel structure. Biophys. Chem., John D. Ferry Special Issue 112, 147–151. https://doi.org/10.1016/j.bpc.2004.07.013

Blombäck, B., Carlsson, K., Hessel, B., Liljeborg, A., Procyk, R., Åslund, N., 1989. Native fibrin gel networks observed by 3D microscopy, permeation and turbidity. Biochim. Biophys. Acta BBA - Protein Struct. Mol. Enzymol. 997, 96–110. https://doi.org/10.1016/0167-4838(89)90140-4

Blombäck, B., Okada, M., 1982. Fibrin gel structure and clotting time. Thromb. Res. 25, 51–70. https://doi.org/10.1016/0049-3848(82)90214-6

Bogdanov, S., 2004. Quality and standards of pollen and beeswax. Apiacta 38, 334–341.

Bokhari, M., Carnachan, R.J., Przyborski, S.A., Cameron, N.R., 2007. Emulsion-templated porous polymers as scaffolds for three dimensional cell culture: effect of synthesis parameters on scaffold formation and homogeneity. J. Mater. Chem. 17, 4088–4094. https://doi.org/10.1039/B707499A

Borst, H.G., Haverich, A., Walterbusch, G., Maatz, W., 1982. Fibrin adhesive: an important hemostatic adjunct in cardiovascular operations. J. Thorac. Cardiovasc. Surg. 84, 548–553.

Böttcher-Haberzeth, S., Biedermann, T., Reichmann, E., 2010. Tissue engineering of skin. Burns 36, 450–460. https://doi.org/10.1016/j.burns.2009.08.016

Boyce, S.T., 2001. Design principles for composition and performance of cultured skin substitutes. Burns 27, 523–533. https://doi.org/10.1016/S0305-4179(01)00019-5

Boyce, S.T., Kagan, R.J., Greenhalgh, D.G., Warner, P., Yakuboff, K.P., Palmieri, T., Warden, G.D., 2006. Cultured skin substitutes reduce requirements for harvesting of skin autograft for closure of excised, full-thickness burns. J. Trauma 60, 821–829. https://doi.org/10.1097/01.ta.0000196802.91829.cc

Boyce, S.T., Kagan, R.J., Meyer, N.A., Yakuboff, K.P., Warden, G.D., 1999. The 1999 Clinical Research Award: Cultured skin substitutes combined with Integra Artificial Skin* to replace native skin autograft and allograft for the closure of excised full-thickness burns. J. Burn Care Rehabil. 20, 453–461.

Boyce, S.T., Lalley, A.L., 2018. Tissue engineering of skin and regenerative medicine for wound care. Burns Trauma 6. https://doi.org/10.1186/s41038-017-0103-y

Boyce, S.T., Simpson, P.S., Rieman, M.T., Warner, P.M., Yakuboff, K.P., Bailey, J.K., Nelson, J.K., Fowler, L.A., Kagan, R.J., 2017. Randomized, Paired-Site Comparison of Autologous Engineered Skin Substitutes and Split-Thickness Skin Graft for Closure of Extensive, Full-Thickness Burns. J. Burn Care Res. 38, 61–70.

Boyd, J., Parkinson, C., Sherman, P., 1972. Factors affecting emulsion stability, and the HLB concept. J. Colloid Interface Sci. 41, 359–370. https://doi.org/10.1016/0021-9797(72)90122-1

Branski, L.K., Gauglitz, G.G., Herndon, D.N., Jeschke, M.G., 2009. A review of gene and stem cell therapy in cutaneous wound healing. Burns 35, 171–180. https://doi.org/10.1016/j.burns.2008.03.009

Brauker, J.H., Carr-Brendel, V.E., Martinson, L.A., Crudele, J., Johnston, W.D., Johnson, R.C., 1995. Neovascularization of synthetic membranes directed by membrane microarchitecture. J. Biomed. Mater. Res. 29, 1517–1524. https://doi.org/10.1002/jbm.820291208

Brennan, M., 1991. Fibrin glue. Blood Rev. 5, 240–244. https://doi.org/10.1016/0268-960X(91)90015-5

Broughton, G., Janis, J.E., Attinger, C.E., 2006. The basic science of wound healing. Plast. Reconstr. Surg. 117, 12S-34S. https://doi.org/10.1097/01.prs.0000225430.42531.c2

Brown, D.M., Barton, B.R., Young, V.L., Pruitt, B.A., 1992. Decreased Wound Contraction With Fibrin Glue—Treated Skin Grafts. Arch. Surg. 127, 404–406. https://doi.org/10.1001/archsurg.1992.01420040046007

Bryant, S.J., Cuy, J.L., Hauch, K.D., Ratner, B.D., 2007. Photo-patterning of porous hydrogels for tissue engineering. Biomaterials 28, 2978–2986. https://doi.org/10.1016/j.biomaterials.2006.11.033

Burke, J.F., Yannas, I.V., Quinby, W.C., Bondoc, C.C., Jung, W.K., 1981. Successful use of a physiologically acceptable artificial skin in the treatment of extensive burn injury. Ann. Surg. 194, 413–428.

Busby, W., Cameron, N.R., Jahoda, C.A.B., 2002. Tissue engineering matrixes by emulsion templating. Polym. Int. 51, 871–881. https://doi.org/10.1002/pi.934

Busby, W., Cameron, N.R., Jahoda, C.A.B., 2001. Emulsion-derived foams (PolyHIPEs) containing poly(ε-caprolactone) as matrixes for tissue engineering. Biomacromolecules 2, 154–164. https://doi.org/10.1021/bm0000889

Callam, M.J., Harper, D.R., Dale, J.J., Ruckley, C.V., 1987. Arterial disease in chronic leg ulceration: an underestimated hazard? Lothian and Forth Valley leg ulcer study. Br. Med. J. (Clin. Res. Ed.) 294, 929–931.

Cam, C., Zhu, S., Truong, N.F., Scumpia, P.O., Segura, T., 2015. Systematic evaluation of natural scaffolds in cutaneous wound healing. J. Mater. Chem. B 3, 7986–7992.

Cameron, N.R., Barbetta, A., 2000. The influence of porogen type on the porosity,surface area and morphology of poly(divinylbenzene) PolyHIPE foams. J. Mater. Chem. 10, 2466–2471. https://doi.org/10.1039/B003596N

Cameron, N.R., Sherrington, D.C., 1996. High internal phase emulsions (HIPEs) — Structure, properties and use in polymer preparation, in: Biopolymers Liquid Crystalline Polymers Phase Emulsion, Advances in Polymer Science. Springer Berlin Heidelberg, pp. 163–214. https://doi.org/10.1007/3-540-60484-7_4

Carnachan, R.J., Bokhari, M., Przyborski, S.A., Cameron, N.R., 2006. Tailoring the morphology of emulsion-templated porous polymers. Soft Matter 2, 608–616. https://doi.org/10.1039/B603211G

Carr, M.E., 1988. Fibrin formed in plasma is composed of fibers more massive than those formed from purified fibrinogen. Thromb. Haemost. 59, 535–539.

Carr, M.E., Gabriel, D.A., McDonagh, J., 1986. Influence of Ca2+ on the structure of reptilase-derived and thrombin-derived fibrin gels. Biochem. J. 239, 513–516. https://doi.org/10.1042/bj2390513

Carriel, V., Garzón, I., Jiménez, J.-M., Oliveira, A.-C.-X., Arias-Santiago, S., Campos, A., Sánchez-Quevedo, M.-C., Alaminos, M., 2012. Epithelial and Stromal Developmental Patterns in a Novel Substitute of the Human Skin Generated with Fibrin-Agarose Biomaterials. Cells Tissues Organs 196, 1–12. https://doi.org/10.1159/000330682

Catelas, I., Dwyer, J.F., Helgerson, S., 2008. Controlled Release of Bioactive Transforming Growth Factor Beta-1 from Fibrin Gels In Vitro. Tissue Eng. Part C Methods 14, 119–128. https://doi.org/10.1089/ten.tec.2007.0262

Cen, L., Liu, W., Cui, L., Zhang, W., Cao, Y., 2008. Collagen Tissue Engineering: Development of Novel Biomaterials and Applications. Pediatr. Res. 63, 492–496. https://doi.org/10.1203/PDR.0b013e31816c5bc3

Chandrasekaran, A.R., Venugopal, J., Sundarrajan, S., Ramakrishna, S., 2011. Fabrication of a nanofibrous scaffold with improved bioactivity for culture of human dermal fibroblasts for skin regeneration. Biomed. Mater. 6, 015001. https://doi.org/10.1088/1748-6041/6/1/015001

Chandrasekharan, J.A., Sharma-Walia, N., 2015. Lipoxins: nature's way to resolve inflammation. J. Inflamm. Res. 8, 181–192. https://doi.org/10.2147/JIR.S90380

Chang, C.-C., Kuo, Y.-F., Chiu, H.-C., Lee, J.-L., Wong, T.-W., Jee, S.-H., 1995. Hydration, Not Silicone, Modulates the Effects of Keratinocytes on Fibroblasts. J. Surg. Res. 59, 705–711. https://doi.org/10.1006/jsre.1995.1227

Chen, L., Tredget, E.E., Wu, P.Y.G., Wu, Y., 2008. Paracrine Factors of Mesenchymal Stem Cells Recruit Macrophages and Endothelial Lineage Cells and Enhance Wound Healing. PLOS ONE 3, e1886. https://doi.org/10.1371/journal.pone.0001886

Chen, Z., Wang, L., Stegemann, J.P., 2011. Phase-separated chitosan–fibrin microbeads for cell delivery. J. Microencapsul. 28, 344–352. https://doi.org/10.3109/02652048.2011.569764

Cheng, G., Youssef, B.B., Markenscoff, P., Zygourakis, K., 2006. Cell Population Dynamics Modulate the Rates of Tissue Growth Processes. Biophys. J. 90, 713–724. https://doi.org/10.1529/biophysj.105.063701

Cheng, N.-C., Wang, S., Young, T.-H., 2012. The influence of spheroid formation of human adipose-derived stem cells on chitosan films on stemness and differentiation capabilities. Biomaterials 33, 1748–1758. https://doi.org/10.1016/j.biomaterials.2011.11.049

Choi, S.-W., Zhang, Y., MacEwan, M.R., Xia, Y., 2013. Neovascularization in biodegradable inverse opal scaffolds with uniform and precisely controlled pore sizes. Adv. Healthc. Mater. 2, 145–154. https://doi.org/10.1002/adhm.201200106

Choi, Y.S., Hong, S.R., Lee, Y.M., Song, K.W., Park, M.H., Nam, Y.S., 1999. Studies on gelatin-containing artificial skin: II. Preparation and characterization of cross-linked gelatin-hyaluronate sponge. J. Biomed. Mater. Res. 48, 631–639. https://doi.org/10.1002/(SICI)1097-4636(1999)48:5<631::AID-JBM6>3.0.CO;2-Y

Chopra, K., Calva, D., Sosin, M., Tadisina, K.K., Banda, A., De La Cruz, C., Chaudhry, M.R., Legesse, T., Drachenberg, C.B., Manson, P.N., Christy, M.R., 2015. A comprehensive examination of topographic thickness of skin in the human face. Aesthet. Surg. J. 35, 1007–1013.

Chua, A.W.C., Khoo, Y.C., Tan, B.K., Tan, K.C., Foo, C.L., Chong, S.J., 2016. Skin tissue engineering advances in severe burns: review and therapeutic applications. Burns Trauma 4. https://doi.org/10.1186/s41038-016-0027-y

Clark, R.A.F., 2003. Fibrin Is a Many Splendored Thing. J. Invest. Dermatol. 121, xxi–xxii. https://doi.org/10.1046/j.1523-1747.2003.12575.x

Clark, R.A.F., Ghosh, K., Tonnesen, M.G., 2007. Tissue engineering for cutaneous wounds. J. Invest. Dermatol. 127, 1018–1029. https://doi.org/10.1038/sj.jid.5700715

Cloney, K., Franz-Odendaal, T.A., 2015. Optimised ex-ovo culturing of chick embryos to advanced stages of development. J. Vis. Exp. JoVE 95, 52129.

Collen, A., Hanemaaijer, R., Lupu, F., Quax, P.H.A., Lent, N. van, Grimbergen, J., Peters, E., Koolwijk, P., Hinsbergh, V.W.M. van, 2003. Membrane-type matrix metalloproteinase-mediated angiogenesis in a fibrin-collagen matrix. Blood 101, 1810–1817. https://doi.org/10.1182/blood-2002-05-1593

Cope, O., Langohr, J.L., Moore, F.D., Webster, R.C., 1947. Expeditious Care of Full-Thickness Burn Wounds by Surgical Excision and Grafting. Ann. Surg. 125, 1–22.

Cui, J., Wang, Y., Postma, A., Hao, J., Hosta-Rigau, L., Caruso, F., 2010. Monodisperse polymer capsules: Tailoring size, shell thickness, and hydrophobic cargo loading via emulsion templating. Adv. Funct. Mater. 20, 1625–1631. https://doi.org/10.1002/adfm.201000209

Cullum, N., Nelson, E.A., Fletcher, A.W., Sheldon, T.A., 2001. Compression for venous leg ulcers. Cochrane Database Syst. Rev.

Currie, L.J., Sharpe, J.R., Martin, R., 2001. The use of fibrin glue in skin grafts and tissue-engineered skin replacements: a review. Plast. Reconstr. Surg. 108, 1713–1726.

Curtis, C.G., Janus, T.J., Credo, R.B., Lorand, L., 1983. REGULATION OF FACTOR XIIIa GENERATION BY FIBRINOGEN*. Ann. N. Y. Acad. Sci. 408, 567–576. https://doi.org/10.1111/j.1749-6632.1983.tb23273.x

Cuttle, L., Kempf, M., Phillips, G.E., Mill, J., Hayes, M.T., Fraser, J.F., Wang, X.-Q., Kimble, R.M., 2006. A porcine deep dermal partial thickness burn model with hypertrophic scarring. Burns 32, 806–820. https://doi.org/10.1016/j.burns.2006.02.023

Dado, D., Levenberg, S., 2009. Cell–scaffold mechanical interplay within engineered tissue. Semin. Cell Dev. Biol., Regenerative Biology and Medicine: II and Patterning and Evolving the Vertebrate Forebrain 20, 656–664. https://doi.org/10.1016/j.semcdb.2009.02.001

Dagalakis, N., Flink, J., Stasikelis, P., Burke, J.F., Yannas, I.V., 1980. Design of an artificial skin. Part III. Control of pore structure. J. Biomed. Mater. Res. 14, 511–528. https://doi.org/10.1002/jbm.820140417

Dahlstrøm, K.K., Weis-Fogh, U.S., Medgyesi, S., Rostgaard, J., Sørensen, H., 1992. The Use of Autologous Fibrin Adhesive in Skin Transplantatio... : Plastic and Reconstructive Surgery. Plast. Reconstr. Surg. 89, 968–972.

Dai, C., Shih, S., Khachemoune, A., 2018. Skin substitutes for acute and chronic wound healing: an updated review. J. Dermatol. Treat. 1–33. https://doi.org/10.1080/09546634.2018.1530443

Dalby, M.J., Gadegaard, N., Tare, R., Andar, A., Riehle, M.O., Herzyk, P., Wilkinson, C.D.W., Oreffo, R.O.C., 2007. The control of human mesenchymal cell differentiation using nanoscale symmetry and disorder. Nat. Mater. 6, 997–1003. https://doi.org/10.1038/nmat2013

Dare, E.V., Griffith, M., Poitras, P., Kaupp, J.A., Waldman, S.D., Carlsson, D.J., Dervin, G., Mayoux, C., Hincke, M.T., 2009. Genipin Cross-Linked Fibrin Hydrogels for in vitro Human Articular Cartilage Tissue-Engineered Regeneration. Cells Tissues Organs 190, 313–325. https://doi.org/10.1159/000209230

Davies, J.T., 1957. A quantitative kinetic theory of emulsion type. I. Physical chemistry of the emulsifying agent, in: Proceedings of the 2nd International Congress Surface Activity.

de la Puente, P., Ludeña, D., 2014. Cell culture in autologous fibrin scaffolds for applications in tissue engineering. Exp. Cell Res. 322, 1–11. https://doi.org/10.1016/j.yexcr.2013.12.017

Di Stasio, E., Nagaswami, C., Weisel, J.W., Di Cera, E., 1998. Cl− Regulates the Structure of the Fibrin Clot. Biophys. J. 75, 1973–1979. https://doi.org/10.1016/S0006-3495(98)77638-6

Dikici, B.A., Sherborne, C., Reilly, G.C., Claeyssens, F., 2019. Emulsion templated scaffolds manufactured from photocurable polycaprolactone. Polymer 175, 243–254. https://doi.org/10.1016/j.polymer.2019.05.023

Dohle, D.S., Pasa, S.D., Gustmann, S., Laub, M., Wissler, J.H., Jennissen, H.P., Dünker, N., 2009. Chick ex ovo Culture and ex ovo CAM Assay: How it Really Works. J. Vis. Exp. JoVE. https://doi.org/10.3791/1620

Domingues, M.M., Macrae, F.L., Duval, C., McPherson, H.R., Bridge, K.I., Ajjan, R.A., Ridger, V.C., Connell, S.D., Philippou, H., Ariëns, R.A.S., 2016. Thrombin and fibrinogen γ′ impact clot structure by marked effects on intrafibrillar structure and protofibril packing. Blood 127, 487–495. https://doi.org/10.1182/blood-2015-06-652214

Dutta, R.C., Dey, M., Dutta, A.K., Basu, B., 2017. Competent processing techniques for scaffolds in tissue engineering. Biotechnol. Adv. 35, 240–250. https://doi.org/10.1016/j.biotechadv.2017.01.001

Ehrlichman, R.J., Seckel, B.R., Bryan, D.J., Moschella, C.J., 1991. Common Complications of Wound Healing: Prevention and Management. Surg. Clin. North Am., Complications of General Surgery 71, 1323–1351. https://doi.org/10.1016/S0039-6109(16)45593-3

Eisenbud, D., Huang, N.F., Luke, S., Silberklang, M., 2004. Skin Substitutes and Wound Healing: Current Status and Challenges. Wounds 16, 2–17.

Engler, A.J., Sen, S., Sweeney, H.L., Discher, D.E., 2006. Matrix Elasticity Directs Stem Cell Lineage Specification. Cell 126, 677–689. https://doi.org/10.1016/j.cell.2006.06.044

Eyal-Giladi, H., Kochav, S., 1976. From cleavage to primitive streak formation: A complementary normal table and a new look at the first stages of the development of the chick: I. General morphology. Dev. Biol. 49, 321–337. https://doi.org/10.1016/0012-1606(76)90178-0

Falanga, V., 2005. Wound healing and its impairment in the diabetic foot. The Lancet 366, 1736–1743. https://doi.org/10.1016/S0140-6736(05)67700-8

Falanga, V., 2004. The chronic wound: impaired healing and solutions in the context of wound bed preparation. Blood Cells. Mol. Dis., Stem Cell Plasticity 32, 88–94. https://doi.org/10.1016/j.bcmd.2003.09.020

Falanga, V., 2002. Physiology and Pathophysiology of Wound Healing, in: DSc, A.V.M., DPM, J.M.G., MD, F.W.L. (Eds.), The Diabetic Foot. Humana Press, pp. 59–73. https://doi.org/10.1007/978-1-59259-168-8_3

Falanga, Vincent., Su Wen Qian, Vincent., Danielpour, David., Katz, M.H., Roberts, A.B., Sporn, M.B., 1991. Hypoxia Upregulates the Synthesis of TGF-β1 by Human Dermal Fibroblasts. J. Invest. Dermatol. 97, 634–637. https://doi.org/10.1111/1523-1747.ep12483126

Ferry, J.D., Morrison, P.R., 1947. Preparation and Properties of Serum and Plasma Proteins. VIII. The Conversion of Human Fibrinogen to Fibrin under Various Conditions1,2. J. Am. Chem. Soc. 69, 388–400. https://doi.org/10.1021/ja01194a066

Floury, J., Desrumaux, A., Lardières, J., 2000. Effect of high-pressure homogenization on droplet size distributions and rheological properties of model oil-in-water emulsions. Innov. Food Sci. Emerg. Technol. 1, 127–134. https://doi.org/10.1016/S1466-8564(00)00012-6

Folkman, J., Hochberg, M., 1973. Self-Regulation of Growth in Three Dimensions. J. Exp. Med. 138, 745–753. https://doi.org/10.1084/jem.138.4.745

Fontenot, K., Schork, F.J., 1993. Sensitivities of droplet size and stability in monomeric emulsions. Ind. Eng. Chem. Res. 32, 373–385. https://doi.org/10.1021/ie00014a014

Franks, G.V., Moss, B., Phelan, D., 2006. Chitosan tissue scaffolds by emulsion templating. J. Biomater. Sci. Polym. Ed. 17, 1439–1450. https://doi.org/10.1163/156856206778937271

Freed, L.E., Engelmayr, G.C., Borenstein, J.T., Moutos, F.T., Guilak, F., 2009. Advanced material strategies for tissue engineering scaffolds. Adv. Mater. 21, 3410–3418. https://doi.org/10.1002/adma.200900303

Friberg, S.E., Goldsmith, L.B., Hilton, M.L., 1968. Theory of emulsions, in: Pharmaceutical Dosage Forms: Disperse Systems. Dekker, New York, pp. 49–73.

Frueh, F.S., Menger, M.D., Lindenblatt, N., Giovanoli, P., Laschke, M.W., 2017. Current and emerging vascularization strategies in skin tissue engineering. Crit. Rev. Biotechnol.

Frueh, F.S., Menger, M.D., Lindenblatt, N., Giovanoli, P., Laschke, M.W., 2016. Current and emerging vascularization strategies in skin tissue engineering. Crit. Rev. Biotechnol. 0, 1–13. https://doi.org/10.1080/07388551.2016.1209157

Fuchs, A., Lindenbaum, E.S., 1988. The two- and three-dimensional structure of the microcirculation of the chick chorioallantoic membrane. Cells Tissues Organs 131, 271–275. https://doi.org/10.1159/000146528

Gabrielli, M.G., Accili, D., 2010. The chick chorioallantoic membrane: A model of molecular, structural, and functional adaptation to transepithelial ion transport and barrier function during embryonic development. J. Biomed. Biotechnol. 2010, e940741. https://doi.org/10.1155/2010/940741

Galanakis, D.K., Lane, B.P., Simon, S.R., 1987. Albumin modulates lateral assembly of fibrin polymers: evidence of enhanced fine fibril formation and of unique synergism with fibrinogen. Biochemistry 26, 2389–2400. https://doi.org/10.1021/bi00382a046

Garcia-Gareta, E., 2019. Biomaterials for Skin Repair and Regeneration. Woodhead Publishing.

Garipcan, B., Maenz, S., Pham, T., Settmacher, U., Jandt, K.D., Zanow, J., Bossert, J., 2011. Image analysis of endothelial microstructure and endothelial cell dimensions of human arteries – A preliminary study. Adv. Eng. Mater. 13, B54–B57. https://doi.org/10.1002/adem.201080076

Geer, D.J., Swartz, D.D., Andreadis, S.T., 2002. Fibrin Promotes Migration in a Three-Dimensional in Vitro Model of Wound Regeneration. Tissue Eng. 8, 787–798. https://doi.org/10.1089/10763270260424141

Gilbert, T.W., Sellaro, T.L., Badylak, S.F., 2006. Decellularization of tissues and organs. Biomaterials 27, 3675–3683. https://doi.org/10.1016/j.biomaterials.2006.02.014

Glick, B., 1979. The avian immune system. Avian Dis. USA 23, 282–289.

Glowacki, J., Trepman, E., Folkman, J., 1983. Cell shape and phenotypic expression in chondrocytes. Proc. Soc. Exp. Biol. Med. 172, 93–98. https://doi.org/10.3181/00379727-172-41533

Goldman, R., 2004. Growth Factors and Chronic Wound Healing: Past, Present, and Future. Adv. Skin Wound Care 17, 24–35.

Goldwyn, R.M., 1969. Guillaume Dupuytren: his character and contributions. Bull. N. Y. Acad. Med. 45, 750–760.

Gorkun, O.V., Veklich, Y.I., Medved, L.V., Henschen, A.H., Weisel, J.W., 1994. Role of the alpha C domains of fibrin in clot formation. Biochemistry 33, 6986–6997.

Graham, G.P., Helmer, S.D., Haan, J.M., Khandelwal, A., 2013. The Use of Integra® Dermal Regeneration Template in the Reco... : Journal of Burn Care & Research. J. Burn Care Res. 34, 261–266.

Granville-Chapman, J., Jacobs, N., Midwinter, M.J., 2011. Pre-hospital haemostatic dressings: A systematic review. Injury 42, 447–459. https://doi.org/10.1016/j.injury.2010.09.037

Grasman, J.M., Page, R.L., Dominko, T., Pins, G.D., 2012. Crosslinking strategies facilitate tunable structural properties of fibrin microthreads. Acta Biomater. 8, 4020–4030. https://doi.org/10.1016/j.actbio.2012.07.018

Griffin, W.C., 1955. Calculation of HLB values of non-ionic surfactants. Am Perfum. Essent Oil Rev 65, 26–29.

Guest, J.F., Ayoub, N., McIlwraith, T., Uchegbu, I., Gerrish, A., Weidlich, D., Vowden, K., Vowden, P., 2015. Health economic burden that wounds impose on the National Health Service in the UK. BMJ Open 5, e009283. https://doi.org/10.1136/bmjopen-2015-009283

Guhad, F., 2005. Introduction to the 3Rs (Refinement, Reduction and Replacement). J. Am. Assoc. Lab. Anim. Sci. 44, 58–59.

Gupta, D., Venugopal, J., Prabhakaran, M.P., Dev, V.R.G., Low, S., Choon, A.T., Ramakrishna, S., 2009. Aligned and random nanofibrous substrate for the in vitro culture of Schwann cells for neural tissue engineering. Acta Biomater. 5, 2560–2569. https://doi.org/10.1016/j.actbio.2009.01.039

Gurtner, G.C., Werner, S., Barrandon, Y., Longaker, M.T., 2008. Wound repair and regeneration. Nature 453, 314–321. https://doi.org/10.1038/nature07039

Hainey, P., Huxham, I.M., Rowatt, B., Sherrington, D.C., Tetley, L., 1991. Synthesis and ultrastructural studies of styrene-divinylbenzene polyhire polymers. Macromolecules 24, 117–121.

Hamburger, V., Hamilton, H.L., 1992. A series of normal stages in the development of the chick embryo. Dev. Dyn. 195, 231–272. https://doi.org/10.1002/aja.1001950404

Hansbrough, J.F., 1990. Current status of skin replacements for coverage of extensive burn wounds. J. Trauma - Inj. Infect. Crit. Care 30, 155–159.

Hantgan, R.R., Hermans, J., 1979. Assembly of fibrin. A light scattering study. J. Biol. Chem. 254, 11272–11281.

Harding, K.G., Morris, H.L., Patel, G.K., 2002. Healing chronic wounds. Br. Med. J. 324, 160–163.

Hardy, J.J., Carrell, N.A., Mcdonagh, J., 1983. Calcium Ion Functions in Fibrinogen Conversion to Fibrin*. Ann. N. Y. Acad. Sci. 408, 279–287. https://doi.org/10.1111/j.1749-6632.1983.tb23251.x

Haw, P., 2004. The HLB System-A Time Saving Guide to Surfactant Selection.

Haynesworth, S.E., Baber, M.A., Caplan, A.I., 1996. Cytokine expression by human marrow-derived mesenchymal progenitor cells in vitro: Effects of dexamethasone and IL-1α. J. Cell. Physiol. 166, 585–592. https://doi.org/10.1002/(SICI)1097-4652(199603)166:3<585::AID-JCP13>3.0.CO;2-6

Hendrickx, B., Vranckx, J.J., Luttun, A., 2010. Cell-Based Vascularization Strategies for Skin Tissue Engineering. Tissue Eng. Part B Rev. 17, 13–24. https://doi.org/10.1089/ten.teb.2010.0315

Henschen, A., Lottspeich, F., Kehl, M., Southan, C., 1983. Covalent Structure of Fibrinogen. Ann. N. Y. Acad. Sci. 408, 28–43. https://doi.org/10.1111/j.1749-6632.1983.tb23232.x

Hentze, H.-P., Antonietti, M., 2001 Template synthesis of porous organic polymers. Curr. Opin. Solid State Mater. Sci. 5, 343–353. https://doi.org/10.1016/S1359-0286(01)00008-0

Hile, D.D., Amirpour, M.L., Akgerman, A., Pishko, M.V., 2000. Active growth factor delivery from poly(d,l-lactide-co-glycolide) foams prepared in supercritical CO2. J. Controlled Release 66, 177–185. https://doi.org/10.1016/S0168-3659(99)00268-0

Ho, H.-O., Hsiao, C.-C., Chen, C.-Y., Sokoloski, T.D., Sheu, M.-T., 1994. Fibrin-Based Drug Delivery Systems. II. The Preparation and Characterization of Microbeads. Drug Dev. Ind. Pharm. 20, 535–546. https://doi.org/10.3109/03639049409038316

Hollister, S.J., 2005. Porous scaffold design for tissue engineering. Nat. Mater. 4, 518–524. https://doi.org/10.1038/nmat1421

Hollister, S.J., Maddox, R.D., Taboas, J.M., 2002. Optimal design and fabrication of scaffolds to mimic tissue properties and satisfy biological constraints. Biomaterials 23, 4095–4103. https://doi.org/10.1016/S0142-9612(02)00148-5

Holy, C.E., Dang, S.M., Davies, J.E., Shoichet, M.S., 1999. In vitro degradation of a novel poly(lactide-co-glycolide) 75/25 foam. Biomaterials 20, 1177–1185. https://doi.org/10.1016/S0142-9612(98)00256-7

Horch, R.E., Kopp, J., Kneser, U., Beier, J., Bach, A.D., 2005. Tissue engineering of cultured skin substitutes. J. Cell. Mol. Med. 9, 592–608. https://doi.org/10.1111/j.1582-4934.2005.tb00491.x

Hrabchak, C., Flynn, L., Woodhouse, K.A., 2006. Biological skin substitutes for wound cover and closure. Expert Rev. Med. Devices 3, 373–385. https://doi.org/10.1586/17434440.3.3.373

Hutmacher, D.W., 2001. Scaffold design and fabrication technologies for engineering tissues - state of the art and future perspectives. J. Biomater. Sci. Polym. Ed. 12, 107–124. https://doi.org/10.1163/156856201744489

ICI Americas, Inc., 1984. The HLB system: a time-saving guide to emulsifier selection. ICI Americas, Inc., Wilmington.

International Organization for Standardization, 2009. ISO 13320:2009 Particle size analysis - Laser diffraction methods.

Ito, M., Liu, Y., Yang, Z., Nguyen, J., Liang, F., Morris, R.J., Cotsarelis, G., 2005. Stem cells in the hair follicle bulge contribute to wound repair but not to homeostasis of the epidermis. Nat. Med. 11, 1351–1354. https://doi.org/10.1038/nm1328

Jackson, D.MacG., 1970. In search of an acceptable burn classification. Br. J. Plast. Surg. 23, 219–226. https://doi.org/10.1016/S0007-1226(70)80045-5

Janson, I.A., Putnam, A.J., 2015. Extracellular matrix elasticity and topography: Material-based cues that affect cell function via conserved mechanisms. J. Biomed. Mater. Res. A 103, 1246–1258. https://doi.org/10.1002/jbm.a.35254

Jeon, O., Ryu, S.H., Chung, J.H., Kim, B.-S., 2005. Control of basic fibroblast growth factor release from fibrin gel with heparin and concentrations of fibrinogen and thrombin. J. Controlled Release 105, 249–259. https://doi.org/10.1016/j.jconrel.2005.03.023

Jeremias, T. da S., Machado, R.G., Visoni, S.B.C., Pereima, M.J., Leonardi, D.F., Trentin, A.G., 2014. Dermal substitutes support the growth of human skin-derived mesenchymal stromal cells: potential tool for skin regeneration. PLOS ONE 9, e89542. https://doi.org/10.1371/journal.pone.0089542

Jiang, Y., Jahagirdar, B.N., Reinhardt, R.L., Schwartz, R.E., Keene, C.D., Ortiz-Gonzalez, X.R., Reyes, M., Lenvik, T., Lund, T., Blackstad, M., Du, J., Aldrich, S., Lisberg, A., Low, W.C., Largaespada, D.A., Verfaillie, C.M., 2002. Pluripotency of mesenchymal stem cells derived from adult marrow. Nature 418, 41–49. https://doi.org/10.1038/nature00870

Jin, L., Wang, T., Zhu, M.-L., Leach, M.K., Naim, Y.I., Corey, J.M., Feng, Z.-Q., Jiang, Q., 2012. Electrospun fibers and tissue engineering. J. Biomed. Nanotechnol. 8, 1–9. https://doi.org/10.1166/jbn.2012.1360

Jockenhoevel, S., Zund, G., Hoerstrup, S.P., Chalabi, K., Sachweh, J.S., Demircan, L., Messmer, B.J., Turina, M., 2001. Fibrin gel – advantages of a new scaffold in cardiovascular tissue engineering. Eur. J. Cardiothorac. Surg. 19, 424–430. https://doi.org/10.1016/S1010-7940(01)00624-8

Jones, I., Currie, L., Martin, R., 2002. A guide to biological skin substitutes. Br. J. Plast. Surg. 55, 185–193. https://doi.org/10.1054/bjps.2002.3800

Jones, M., Gabriel, D.A., 1988. Influence of the subendothelial basement membrane components on fibrin assembly. Evidence for a fibrin binding site on type IV collagen. J. Biol. Chem. 263, 7043–7048.

Kamel, R.A., Ong, J.F., Eriksson, E., Junker, J.P.E., Caterson, E.J., 2013. Tissue Engineering of Skin. J. Am. Coll. Surg. 217, 533–555. https://doi.org/10.1016/j.jamcollsurg.2013.03.027

Kang, H.-W., Tabata, Y., Ikada, Y., 1999. Fabrication of porous gelatin scaffolds for tissue engineering. Biomaterials 20, 1339–1344. https://doi.org/10.1016/S0142-9612(99)00036-8

Kang, S.-W., Kim, Y.-B., Shin, J.-D., Kim, E.-K., 2010. Enhanced biodegradation of hydrocarbons in soil by microbial biosurfactant, Sophorolipid. Appl. Biochem. Biotechnol. 160, 780–790.

Kato, A., Fujishige, T., Matsudomi, N., Kobayashi, K., 1985. Determination of Emulsifying Properties of Some Proteins by Conductivity Measurements. J. Food Sci. 50, 56–58. https://doi.org/10.1111/j.1365-2621.1985.tb13276.x

Kaufman, T., Lusthaus, S.N., Sagher, U., Wexler, M.R., 1990. Deep partial skin thickness burns: A reproducible animal model to study burn wound healing. Burns 16, 13–16. https://doi.org/10.1016/0305-4179(90)90199-7

Kim, S.E., Park, J.H., Cho, Y.W., Chung, H., Jeong, S.Y., Lee, E.B., Kwon, I.C., 2003. Porous chitosan scaffold containing microspheres loaded with transforming growth factor-β1: Implications for cartilage tissue engineering. J. Controlled Release 91, 365–374. https://doi.org/10.1016/S0168-3659(03)00274-8

Kimmins, S.D., Cameron, N.R., 2011. Functional Porous Polymers by Emulsion Templating: Recent Advances. Adv. Funct. Mater. 21, 211–225. https://doi.org/10.1002/adfm.201001330

Kincade, P.W., Cooper, M.D., 1971. Development and distribution of immunoglobulin-containing cells in the chicken: An immunofluorescent analysis using purified antibodies to μ, γ and light chains. J. Immunol. 106, 371–382.

Klawitter, J.J., Hulbert, S.F., 1971. Application of porous ceramics for the attachment of load bearing internal orthopedic applications. J. Biomed. Mater. Res. 5, 161–229. https://doi.org/10.1002/jbm.820050613

Klin, B., Weinberg, M., Vinograd, I., Sandbank, J., Siman-Tov, Y., Astachov, L., Ayalon, O., Rochkind, S., Shahar, A., Nevo, Z., 2007. Experimental Repair of Tracheal Defects Using a New Biodegradable Membrane. J. Laparoendosc. Adv. Surg. Tech. 17, 342–349. https://doi.org/10.1089/lap.2006.0165

Klingenberg, J.M., McFarland, K.L., Friedman, A.J., Boyce, S.T., Aronow, B.J., Supp, D.M., 2010. Engineered Human Skin Substitutes Undergo Large-Scale Genomic Reprogramming and Normal Skin-Like Maturation after Transplantation to Athymic Mice. J. Invest. Dermatol. 130, 587–601. https://doi.org/10.1038/jid.2009.295

Koç, O.N., Day, J., Nieder, M., Gerson, S.L., Lazarus, H.M., Krivit, W., 2002. Allogeneic mesenchymal stem cell infusion for treatment of metachromatic leukodystrophy (MLD) and Hurler syndrome (MPS-IH). Bone Marrow Transplant. 30, 215–222.

Koç, O.N., Gerson, S.L., Cooper, B.W., Dyhouse, S.M., Haynesworth, S.E., Caplan, A.I., Lazarus, H.M., 2000. Rapid hematopoietic recovery after coinfusion of autologous-blood stem cells and culture-expanded marrow mesenchymal stem cells in advanced breast cancer patients receiving high-dose chemotherapy. J. Clin. Oncol. 18, 307–307. https://doi.org/10.1200/JCO.2000.18.2.307

Köhler, S., Schmid, F., Settanni, G., 2015. The Internal Dynamics of Fibrinogen and Its Implications for Coagulation and Adsorption. PLOS Comput. Biol. 11, e1004346. https://doi.org/10.1371/journal.pcbi.1004346

Kondo, T., Ishida, Y., 2010. Molecular pathology of wound healing. Forensic Sci. Int., Molecular Pathology in Forensic Medicine 203, 93–98. https://doi.org/10.1016/j.forsciint.2010.07.004

Kopeć, M., Latallo, Z.S., 1978. Fibrinogen and Fibrin Degradation Products, in: Markwardt, F. (Ed.), Fibrinolytics and Antifibrinolytics, Handbuch Der Experimentellen Pharmakologie / Handbook of Experimental Pharmacology. Springer, Berlin, Heidelberg, pp. 81–105. https://doi.org/10.1007/978-3-642-66863-0_3

Kourembanas, S., Hannan, R.L., Faller, D.V., 1990. Oxygen tension regulates the expression of the platelet-derived growth factor-B chain gene in human endothelial cells. J. Clin. Invest. 86, 670–674.

Kourembanas, S., Marsden, P.A., McQuillan, L.P., Faller, D.V., 1991. Hypoxia induces endothelin gene expression and secretion in cultured human endothelium. J. Clin. Invest. 88, 1054–1057.

Kravchenko, O.G., Gedler, G., Kravchenko, S.G., Feke, D.L., Manas-Zloczower, I., 2018. Modeling compressive behavior of open-cell polymerized high internal phase emulsions: effects of density and morphology. Soft Matter 14, 1637–1646. https://doi.org/10.1039/C7SM02043K

Kulkarni, M.M., Greiser, U., O'Brien, T., Pandit, A., 2011. A Temporal Gene Delivery System Based on Fibrin Microspheres. Mol. Pharm. 8, 439–446. https://doi.org/10.1021/mp100295z

Kwon Oh, J., 2011. Polylactide (PLA)-based amphiphilic block copolymers : synthesis, self-assembly , and biomedical applications. Soft Matter 7, 5096–5108. https://doi.org/10.1039/C0SM01539C

Landis, S.J., 2008. Chronic Wound Infection and Antimicrobial Use : Advances in Skin & Wound Care. Adv. Skin Wound Care 21, 531–540.

Langer, K., 1861. On the anatomy and physiology of the skin: I. The cleavability of the cutis. Br. J. Plast. Surg. 31, 3–8.

Langer, R., Vacanti, J.P., 1993. Tissue engineering. Science 260, 920–926. https://doi.org/10.1126/science.8493529

Laschke, M.W., Schank, T.E., Scheuer, C., Kleer, S., Schuler, S., Metzger, W., Eglin, D., Alini, M., Menger, M.D., 2013. Three-dimensional spheroids of adipose-derived mesenchymal stem cells are potent initiators of blood vessel formation in porous polyurethane scaffolds. Acta Biomater. 9, 6876–6884. https://doi.org/10.1016/j.actbio.2013.02.013

Leach, J.B., Schmidt, C.E., 2005. Characterization of protein release from photocrosslinkable hyaluronic acid-polyethylene glycol hydrogel tissue engineering scaffolds. Biomaterials 26, 125–135. https://doi.org/10.1016/j.biomaterials.2004.02.018

LeBaron, R.G., Athanasiou, K.A., 2000. Extracellular Matrix Cell Adhesion Peptides: Functional Applications in Orthopedic Materials. Tissue Eng. 6, 85–103. https://doi.org/10.1089/107632700320720

Lee, A.C., Yu, V.M., Lowe III, J.B., Brenner, M.J., Hunter, D.A., Mackinnon, S.E., Sakiyama-Elbert, S.E., 2003. Controlled release of nerve growth factor enhances sciatic nerve regeneration. Exp. Neurol. 184, 295–303. https://doi.org/10.1016/S0014-4886(03)00258-9

Lee, D.-H., Kim, E.-S., Chang, H.-W., 2005. Effect of Tween surfactant components for remediation of toluene-contaminated groundwater. Geosci. J. 9, 261–267.

Lee, S.B., Jeon, H.W., Lee, Y.W., Lee, Y.M., Song, K.W., Park, M.H., Nam, Y.S., Ahn, H.C., 2003. Bio-artificial skin composed of gelatin and (1→3), (1→6)-β-glucan. Biomaterials 24, 2503–2511. https://doi.org/10.1016/S0142-9612(03)00003-6

Lee, S.J., 2006. Emulsion rheology and properties of polymerized high internal phase emulsions. Korea-Aust. Rheol. J. 18, 183–189.

Leong, T.S.H., Wooster, T.J., Kentish, S.E., Ashokkumar, M., 2009. Minimising oil droplet size using ultrasonic emulsification. Ultrason. Sonochem. 16, 721–727.

Lesman, A., Koffler, J., Atlas, R., Blinder, Y.J., Kam, Z., Levenberg, S., 2011. Engineering vessel-like networks within multicellular fibrin-based constructs. Biomaterials 32, 7856–7869. https://doi.org/10.1016/j.biomaterials.2011.07.003

Levenberg, S., Lesman, A., 2014. Tissue engineering construct comprising fibrin. US20140050766 A1.

Levenson, S.M., Geever, E.F., Crowley, L.V., Oates, J.F., Berard, C.W., Rosen, H., 1965. Healing of Rat Skin Wounds. Ann. Surg. 161, 293–308.

Lewis, S.D., Janus, T.J., Lorand, L., Shafer, S., 1985. Regulation of formation of factor XIIIa by its fibrin substrates. Biochemistry 24, 6772–6777. https://doi.org/10.1021/bi00345a007

Li, H., Chang, J., 2005. pH-compensation effect of bioactive inorganic fillers on the degradation of PLGA. Compos. Sci. Technol. 65, 2226–2232.

Li, J., Chen, J., Kirsner, R., 2007. Pathophysiology of acute wound healing. Clin. Dermatol. 25, 9–18. https://doi.org/10.1016/j.clindermatol.2006.09.007

Lim, X., Potter, M., Cui, Z., Dye, J.F., 2018. Manufacture and characterisation of EmDerm—novel hierarchically structured bio-active scaffolds for tissue regeneration. J. Mater. Sci. Mater. Med. 29, 79. https://doi.org/10.1007/s10856-018-6060-6

Linnes, M.P., Ratner, B.D., Giachelli, C.M., 2007. A fibrinogen-based precision microporous scaffold for tissue engineering. Biomaterials 28, 5298–5306. https://doi.org/10.1016/j.biomaterials.2007.08.020

Liu, H., Zhang, F., Lineaweaver, W.C., 2016. A brief history of the treatment of burns. Ann. Plast. Surg.

Liu, X., Ma, P.X., 2004. Polymeric Scaffolds for Bone Tissue Engineering. Ann. Biomed. Eng. 32, 477–486. https://doi.org/10.1023/B:ABME.0000017544.36001.8e

Lobmann, R., Ambrosch, A., Schultz, G., Waldmann, K., Schiweck, S., Lehnert, H., 2002. Expression of matrix-metalloproteinases and their inhibitors in the wounds of diabetic and non-diabetic patients. Diabetologia 45, 1011–1016. https://doi.org/10.1007/s00125-002-0868-8

Loeb, L., 1909. Über Wirkungen des Fibrins. Biochem Z 16, 157. https://doi.org/10.1055/s-0029-1201395

Lovvorn, H.N., Cheung, D.T., Nimni, M.E., Perelman, N., Estes, J.M., Adzick, N.S., 1999. Relative distribution and crosslinking of collagen distinguish fetal from adult sheep wound repair. J. Pediatr. Surg., Papers Presented at the 29th Annual Meeting of the American Pediatric Surgical Association Hilton Head 34, 218–223. https://doi.org/10.1016/S0022-3468(99)90261-0

Lu, H., Oh, H.H., Kawazoe, N., Yamagishi, K., Chen, G., 2012. PLLA–collagen and PLLA–gelatin hybrid scaffolds with funnel-like porous structure for skin tissue engineering. Sci. Technol. Adv. Mater. 13, 064210. https://doi.org/10.1088/1468-6996/13/6/064210

Ma, K., Titan, A.L., Stafford, M., Zheng, C. hua, Levenston, M.E., 2012. Variations in chondrogenesis of human bone marrow-derived mesenchymal stem cells in fibrin/alginate blended hydrogels. Acta Biomater. 8, 3754–3764. https://doi.org/10.1016/j.actbio.2012.06.028

Ma, L., Gao, C., Mao, Z., Zhou, J., Shen, J., Hu, X., Han, C., 2003. Collagen/chitosan porous scaffolds with improved biostability for skin tissue engineering. Biomaterials 24, 4833–4841. https://doi.org/10.1016/S0142-9612(03)00374-0

MacNeil, S., 2007. Progress and opportunities for tissue-engineered skin. Nature 445, 874–880.

Mahjour, S.B., Fu, X., Yang, X., Fong, J., Sefat, F., Wang, H., 2015. Rapid creation of skin substitutes from human skin cells and biomimetic nanofibers for acute full-thickness wound repair. Burns 41, 1764–1774. https://doi.org/10.1016/j.burns.2015.06.011

Makogonenko, E., Tsurupa, G., Ingham, K., Medved, L., 2002. Interaction of Fibrin(ogen) with Fibronectin: Further Characterization and Localization of the Fibronectin-Binding Site. Biochemistry 41, 7907–7913. https://doi.org/10.1021/bi025770x

Mann, B.K., West, J.L., 2002. Cell adhesion peptides alter smooth muscle cell adhesion, proliferation, migration, and matrix protein synthesis on modified surfaces and in polymer scaffolds. J. Biomed. Mater. Res. 60, 86–93. https://doi.org/10.1002/jbm.10042

Marder, V.J., Aird, W.C., Bennett, J.S., Schulman, S., White III, G.C. (Eds.), 2012. Overview of basic coagulation and fibrinolysis, in: Hemostasis and Thrombosis: Basic Principles and Clinical Practice. LWW, Philadelphia, pp. 103–109.

Marshall, A.J., Barker, T., Sage, E.H., Hauch, K.D., Ratner, B.D., 2004. Pore size controls angiogenesis in subcutaneously implanted porous matrices. Presented at the Transactions - 7th World Biomaterials Congress, p. 710.

Marshall, A.J., Irvin, C.A., Barker, T., Sage, H.E., Hauch, K.D., Ratner, B.D., 2005. Biomaterials with tightly controlled pore size that promote vascular in-growth, in: Excellence in Graduate Polymer Science Research Symposium. Presented at the ACS National Meeting, Philadelphia, PA.

McClements, D.J., 2007. Critical review of techniques and methodologies for characterization of emulsion stability. Crit. Rev. Food Sci. Nutr. 47, 611–649. https://doi.org/10.1080/10408390701289292

McClements, D.J., Demetriades, K., 1998. An integrated approach to the development of reduced-fat food emulsions. Crit. Rev. Food Sci. Nutr. 38, 511–536. https://doi.org/10.1080/10408699891274291

McColl, D, MacDougall, M., Watret, L., Connolly, P., 2009. Monitoring moisture without disturbing the wound dressing. Wounds UK 5, 94–99.

McCullen, S.D., Stevens, D.R., Roberts, W.A., Clarke, L.I., Bernacki, S.H., Gorga, R.E., Loboa, E.G., 2007. Characterization of electrospun nanocomposite scaffolds and biocompatibility with adipose-derived human mesenchymal stem cells. Int. J. Nanomedicine 2, 253–263.

McGrath, J.A., Eady, R. a. J., Pope, F.M., 2004. Anatomy and organization of human skin, in: Burns, T., Breathnach, S., Cox, N., Griffiths, C. (Eds.), Rook's Textbook of Dermatology. Blackwell Publishing, Inc., Malden, Massachusetts, USA, pp. 45–128. https://doi.org/10.1002/9780470750520.ch3

McManus, M.C., Boland, E.D., Koo, H.P., Barnes, C.P., Pawlowski, K.J., Wnek, G.E., Simpson, D.G., Bowlin, G.L., 2006. Mechanical properties of electrospun fibrinogen structures. Acta Biomater. 2, 19–28. https://doi.org/10.1016/j.actbio.2005.09.008

Mengual, O., Meunier, G., Cayre, I., Puech, K., Snabre, P., 1999. Characterisation of instability of concentrated dispersions by a new optical analyser: the TURBISCAN MA 1000. Colloids Surf. Physicochem. Eng. Asp. 152, 111–123. https://doi.org/10.1016/S0927-7757(98)00680-3

Merritt, K., Shafer, J.W., Brown, S.A., 1979. Implant site infection rates with porous and dense materials. J. Biomed. Mater. Res. 13, 101–108. https://doi.org/10.1002/jbm.820130111

Mirastschijski, U., Haaksma, C.J., Tomasek, J.J., Ågren, M.S., 2004. Matrix metalloproteinase inhibitor GM 6001 attenuates keratinocyte migration, contraction and myofibroblast formation in skin wounds. Exp. Cell Res. 299, 465–475. https://doi.org/10.1016/j.yexcr.2004.06.007

Mishra, Pravin J., Mishra, Prasun J., Banerjee, D., 2016. Keratinocyte Induced Differentiation of Mesenchymal Stem Cells into Dermal Myofibroblasts: A Role in Effective Wound Healing. Int. J. Transl. Sci. 2016, 5–32. https://doi.org/10.13052/ijts2246-8765.2016.002

Mishra, Pravin J, Mishra, Prasun J, Banerjee, D., 2012. Cell-free derivatives from mesenchymal stem cells are effective in wound therapy. World J. Stem Cells 4, 35–43. https://doi.org/10.4252/wjsc.v4.i5.35

Monfort, A., Soriano-Navarro, M., García-Verdugo, J.M., Izeta, A., 2013. Production of human tissue-engineered skin trilayer on a plasma-based hypodermis. J. Tissue Eng. Regen. Med. 7, 479–490. https://doi.org/10.1002/term.548

Montagna, W., Parakkal, 2012. The Structure and Function of Skin. Elsevier.

Mooney, D.J., Cima, L., Langer, R., Johnson, L., Hansen, L.K., Ingber, D.E., Vacanti, J.P., 1991. Principles of Tissue Engineering and Reconstruction Using Polymer-Cell Constructs. MRS Online Proc. Libr. Arch. 252. https://doi.org/10.1557/PROC-252-345

Moosavi-Movahedi, A.A., 2005. Thermodynamics of protein denaturation by sodium dodecyl sulfate. J. Iran. Chem. Soc. 2, 189–196. https://doi.org/10.1007/BF03245921

Moreno-Jiménez, I., Hulsart-Billstrom, G., Lanham, S.A., Janeczek, A.A., Kontouli, N., Kanczler, J.M., Evans, N.D., Oreffo, R.O., 2016. The chorioallantoic membrane (CAM) assay for the study of human bone regeneration: a refinement animal model for tissue engineering. Sci. Rep. 6, 32168. https://doi.org/10.1038/srep32168

Mosesson, M.W., Siebenlist, K.R., Amrani, D.L., DiOrio, J.P., 1989. Identification of covalently linked trimeric and tetrameric D domains in crosslinked fibrin. Proc. Natl. Acad. Sci. 86, 1113–1117.

Mosesson, M.W., Siebenlist, K.R., Meh, D.A., 2001. The Structure and Biological Features of Fibrinogen and Fibrin. Ann. N. Y. Acad. Sci. 936, 11–30. https://doi.org/10.1111/j.1749-6632.2001.tb03491.x

Moustafa, M., Bullock, A.J., Creagh, F.M., Heller, S., Jeffcoate, W., Game, F., Amery, C., Tesfaye, S., Ince, Z., Haddow, D.B., MacNeil, S., 2007. Randomized, controlled, single-blind study on use of autologous keratinocytes on a transfer dressing to treat nonhealing diabetic ulcers. Regen. Med. 2, 887–902.

Musgrave, C.S.A., Nazarov, W., Bazin, N., 2017. The effect of para-divinyl benzene on styrenic emulsion-templated porous polymers: a chemical Trojan horse. J. Mater. Sci. 52, 3179–3187. https://doi.org/10.1007/s10853-016-0607-z

Mustoe, T., 2004. Understanding chronic wounds: a unifying hypothesis on their pathogenesis and implications for therapy. Am. J. Surg. 187, S65–S70. https://doi.org/10.1016/S0002-9610(03)00306-4

Nade, S., Armstrong, L., McCartney, E., Baggaley, B., 1983. Osteogenesis after bone and bone marrow transplantation. The ability of ceramic materials to sustain osteogenesis from transplanted bone marrow cells: preliminary studies. Clin. Orthop. 255–263.

Nair, L.S., Laurencin, C.T., 2007. Biodegradable polymers as biomaterials. Prog. Polym. Sci., Polymers in Biomedical Applications 32, 762–798. https://doi.org/10.1016/j.progpolymsci.2007.05.017

Nam, J., Huang, Y., Agarwal, S., Lannutti, J., 2007. Improved cellular infiltration in electrospun fiber via engineered porosity. Tissue Eng. 13, 2249–2257. https://doi.org/10.1089/ten.2006.0306

Nam, Y.S., Park, T.G., 1999. Biodegradable polymeric microcellular foams by modified thermally induced phase separation method. Biomaterials 20, 1783–1790. https://doi.org/10.1016/S0142-9612(99)00073-3

Nguyen, T.T., Morgan, C., Poindexter, L., Fernandez, J., 2019. Application of the Hydrophilic–Lipophilic Deviation concept to surfactant characterization and surfactant selection for enhanced oil recovery. J. Surfactants Deterg. 22, 983–999. https://doi.org/10.1002/jsde.12305

NICE, 2015. NICE Guidance NG19: Diabetic foot problems: prevention and management.

Nissen, N.N., Polverini, P.J., Koch, A.E., Volin, M.V., Gamelli, R.L., DiPietro, L.A., 1998. Vascular endothelial growth factor mediates angiogenic activity during the proliferative phase of wound healing. Am. J. Pathol. 152, 1445–1452.

Norde, W., Lyklema, J., 1991. Why proteins prefer interfaces. J. Biomater. Sci. Polym. Ed. 2, 183–202. https://doi.org/10.1080/09205063.1991.9756659

Norman, J.J., Desai, T.A., 2006. Methods for fabrication of nanoscale topography for tissue engineering scaffolds. Ann. Biomed. Eng. 34, 89–101. https://doi.org/10.1007/s10439-005-9005-4

Nowak-Sliwinska, P., Segura, T., Iruela-Arispe, M.L., 2014. The chicken chorioallantoic membrane model in biology, medicine and bioengineering. Angiogenesis 17, 779–804. https://doi.org/10.1007/s10456-014-9440-7

Okada, M., Blombäck, B., 1983. Calcium and fibrin gel structure. Thromb. Res. 29, 269–280. https://doi.org/10.1016/0049-3848(83)90039-7

Oliver, R.F., GB6, Grant, R.A., GB2, 1983. United States Patent: 4399123 - Fibrous tissue dressing or implant. 4399123.

Oltulu, P., Ince, B., Kokbudak, N., Findik, S., Kilinc, F., 2018. Measurement of epidermis, dermis, and total skin thicknesses from six different body regions with a new ethical histometric technique. Turk. J. Plast. Surg. 26, 56. https://doi.org/10.4103/tjps.TJPS_2_17

Opneja, A., Kapoor, S., Stavrou, E.X., 2019. Contribution of platelets, the coagulation and fibrinolytic systems to cutaneous wound healing. Thromb. Res. 179, 56–63. https://doi.org/10.1016/j.thromres.2019.05.001

Oreffo, R.O.C., Cooper, C., Mason, C., Clements, M., 2005. Mesenchymal stem cells: lineage, plasticity, and skeletal therapeutic potential. Stem Cell Rev. 1, 169–178. https://doi.org/10.1385/SCR:1:2:169

Otzen, D., 2011. Protein–surfactant interactions: A tale of many states. Biochim. Biophys. Acta BBA - Proteins Proteomics 1814, 562–591. https://doi.org/10.1016/j.bbapap.2011.03.003

Owen, R., Sherborne, C., Paterson, T., Green, N.H., Reilly, G.C., Claeyssens, F., 2016. Emulsion templated scaffolds with tunable mechanical properties for bone tissue engineering. J. Mech. Behav. Biomed. Mater. 54, 159–172. https://doi.org/10.1016/j.jmbbm.2015.09.019

Pal, R., 1999. Yield stress and viscoelastic properties of high internal phase ratio emulsions. Colloid Polym. Sci. 277, 583–588. https://doi.org/10.1007/s003960050429

Paljevac, M., Jeràbek, K., Krajnc, P., 2012. Crosslinked poly(2-hydroxyethyl methacrylate) by emulsion templating: influence of crosslinker on microcellular structure. J. Polym. Environ. 20, 1095–1102. https://doi.org/10.1007/s10924-012-0524-4

Pan, J.-F., Liu, N.-H., Sun, H., Xu, F., 2014. Preparation and characterization of electrospun PLCL/poloxamer nanofibers and dextran/gelatin hydrogels for skin tissue engineering. PLoS One 9, e112885.

Papini, R., 2004. Management of burn injuries of various depths. BMJ 329, 158–160. https://doi.org/10.1136/bmj.329.7458.158

Park, K., Ju, Y.M., Son, J.S., Ahn, K.-D., Han, D.K., 2007. Surface modification of biodegradable electrospun nanofiber scaffolds and their interaction with fibroblasts. J. Biomater. Sci. Polym. Ed. 18, 369–382. https://doi.org/10.1163/156856207780424997

Patel, M., Fisher, J.P., 2008. Biomaterial scaffolds in pediatric tissue engineering. Pediatr. Res. 63, 497–501. https://doi.org/10.1203/01.PDR.0b013e318165eb3e

Pays, K., Giermanska-Kahn, J., Pouligny, B., Bibette, J., Leal-Calderon, F., 2002. Double emulsions: how does release occur? J. Controlled Release 79, 193–205.

Percival, N.J., 2002. Classification of Wounds and their Management. Surg. Oxf., Basic Surgical Techniques / Wound Healing / Theatre Problems 20, 114–117. https://doi.org/10.1383/surg.20.5.114.14626

Perka, C., Arnold, U., Spitzer, R.-S., Lindenhayn, K., 2001. The Use of Fibrin Beads for Tissue Engineering and Subsequential Transplantation. Tissue Eng. 7, 359–361. https://doi.org/10.1089/10763270152044215

Perng, C.-K., Kao, C.-L., Yang, Y.-P., Lin, H.-T., Lin, W.-B., Chu, Y.-R., Wang, H.-J., Ma, H., Ku, H.-H., Chiou, S.-H., 2008. Culturing adult human bone marrow stem cells on gelatin scaffold with pNIPAAm as transplanted grafts for skin regeneration. J. Biomed. Mater. Res. A 84A, 622–630. https://doi.org/10.1002/jbm.a.31291

Pham, C., Greenwood, J., Cleland, H., Woodruff, P., Maddern, G., 2007. Bioengineered skin substitutes for the management of burns: A systematic review. Burns 33, 946–957. https://doi.org/10.1016/j.burns.2007.03.020

Pittenger, M.F., Mackay, A.M., Beck, S.C., Jaiswal, R.K., Douglas, R., Mosca, J.D., Moorman, M.A., Simonetti, D.W., Craig, S., Marshak, D.R., 1999. Multilineage Potential of Adult Human Mesenchymal Stem Cells. Science 284, 143–147. https://doi.org/10.1126/science.284.5411.143

Posnett, J., Franks, P., 2008. The burden of chronic wounds in the UK. Nurs. Times 104, 44.

Preissner, K.T., Jenne, D., 1991. Vitronectin: A new molecular connection in haemostasis. Thromb. Haemost. 66, 189–194.

Prinderre, P., Piccerelle, P., Cauture, E., Kalantzis, G., Reynier, J.P., Joachim, J., 1998. Formulation and evaluation of o/w emulsions using experimental design. Int. J. Pharm. 163, 73–79. https://doi.org/10.1016/S0378-5173(97)00368-2

Pu, J., Komvopoulos, K., 2014. Mechanical properties of electrospun bilayer fibrous membranes as potential scaffolds for tissue engineering. Acta Biomater. 10, 2718–2726. https://doi.org/10.1016/j.actbio.2013.12.060

Puisieux, F., Seillier, M., 1983. Agents de surface et émulsions, Dispersions.

Qin, Y., Guo, X.W., Li, L., Wang, H.W., Kim, W., 2013. The antioxidant property of chitosan green tea polyphenols complex induces transglutaminase activation in wound healing. J. Med. Food 16, 487–498. https://doi.org/10.1089/jmf.2012.2623

Quell, A., Sottmann, T., Stubenrauch, C., 2017. Diving into the fine structure of macroporous polymer foams synthesized via emulsion templating: A phase diagram study. Langmuir 33, 537–542. https://doi.org/10.1021/acs.langmuir.6b03762

Rajangam, T., An, S.S.A., 2013. Fibrinogen and fibrin based micro and nano scaffolds incorporated with drugs, proteins, cells and genes for therapeutic biomedical applications. Int. J. Nanomedicine 8, 3641–3662. https://doi.org/10.2147/IJN.S43945

Rapp, M., 2002. Flexible wound covering based on fibrin and process for its production. US6486377 B2.

Reed, W.L., Clark, M.E., 2011. Beyond maternal effects in birds: Responses of the embryo to the environment. Integr. Comp. Biol. 51, 73–80. https://doi.org/10.1093/icb/icr032

Regoeczi, E., Stannard, B.A., 1969. In vivo behaviour of frozen and freeze-dried fibrinogen and of that prepared from out-dated blood. Biochim. Biophys. Acta BBA - Protein Struct. 181, 287–294. https://doi.org/10.1016/0005-2795(69)90251-7

Ribatti, D., 2012. Chicken Chorioallantoic Membrane Angiogenesis Model, in: Peng, X., Antonyak, M. (Eds.), Cardiovascular Development: Methods and Protocols, Methods in Molecular Biology. Humana Press, Totowa, NJ, pp. 47–57. https://doi.org/10.1007/978-1-61779-523-7_5

Ribatti, D., 2010. The Chick Embryo Chorioallantoic Membrane in the Study of Angiogenesis and Metastasis: The CAM assay in the study of angiogenesis and metastasis. Springer Science & Business Media.

Ribatti, D., Vacca, A., Roncali, L., Dammacco, F., 2000. The chick embryo chorioallantoic membrane as a model for in vivo research on anti-angiogenesis. Curr. Pharm. Des. 1, 73–82. https://doi.org/info:doi/10.2174/1389201003379040

Riboldi, S.A., Sampaolesi, M., Neuenschwander, P., Cossu, G., Mantero, S., 2005. Electrospun degradable polyesterurethane membranes: potential scaffolds for skeletal muscle tissue engineering. Biomaterials 26, 4606–4615. https://doi.org/10.1016/j.biomaterials.2004.11.035

Riedel, T., Suttnar, J., Brynda, E., Houska, M., Medved, L., Dyr, J.E., 2011. Fibrinopeptides A and B release in the process of surface fibrin formation. Blood 117, 1700–1706. https://doi.org/10.1182/blood-2010-08-300301

Risau, W., 1997. Mechanisms of angiogenesis. Nature 386, 671–674. https://doi.org/10.1038/386671a0

Robson, M.C., 1997. WOUND INFECTION: A Failure of Wound Healing Caused by an Imbalance of Bacteria. Surg. Clin. North Am. 77, 637–650. https://doi.org/10.1016/S0039-6109(05)70572-7

Rohani, M.G., Parks, W.C., 2015. Matrix remodeling by MMPs during wound repair. Matrix Biol., Metalloproteinases in Extracellular Matrix Biology 44–46, 113–121. https://doi.org/10.1016/j.matbio.2015.03.002

Romanelli, M., Dini, V., Bertone, M., Barbanera, S., Brilli, C., 2007. OASIS® wound matrix versus Hyaloskin® in the treatment of difficult-to-heal wounds of mixed arterial/venous aetiology. Int. Wound J. 4, 3–7.

Rose, E., Dresdale, A., 1986. Fibrin adhesive prepared as a concentrate from single donor fresh frozen plasma. US4627879 A.

Sahota, P.S., Burn, J.L., Brown, N.J., MacNeil, S., 2004. Approaches to improve angiogenesis in tissue-engineered skin. Wound Repair Regen. 12, 635–642. https://doi.org/10.1111/j.1067-1927.2004.12608.x

Salager, J.L., Morgan, J.C., Schechter, R.S., Wade, W.H., Vasquez, E., 1979. Optimum formulation of surfactant/water/oil systems for minimum interfacial tension or phase behavior. Soc. Pet. Eng. J. 19, 107–115. https://doi.org/10.2118/7054-PA

Salager, J.-L., Rondón, M., Tolosa, L., Pizzino, A., Bullón, J., 2010. Emulsion formulation engineering for the practitioner, in: Encyclopedia of Surface and Colloid Science, 1. Taylor & Francis, New York, NY, USA, pp. 1–6.

Sander, E.A., Lynch, K.A., Boyce, S.T., 2014. Development of the Mechanical Properties of Engineered Skin Substitutes After Grafting to Full-Thickness Wounds. J. Biomech. Eng. 136, 051008-051008–7. https://doi.org/10.1115/1.4026290

Sasaki, M., Abe, R., Fujita, Y., Ando, S., Inokuma, D., Shimizu, H., 2008. Mesenchymal Stem Cells Are Recruited into Wounded Skin and Contribute to Wound Repair by Transdifferentiation into Multiple Skin Cell Type. J. Immunol. 180, 2581–2587. https://doi.org/10.4049/jimmunol.180.4.2581

Schagemann, J.C., Chung, H.W., Mrosek, E. h., Stone, J. j., Fitzsimmons, J. s., O'Driscoll, S.W., Reinholz, G.G., 2010. Poly-ϵ-caprolactone/gel hybrid scaffolds for cartilage tissue engineering. J. Biomed. Mater. Res. A 93A, 454–463. https://doi.org/10.1002/jbm.a.32521

Schoof, H., Apel, J., Heschel, I., Rau, G., 2001. Control of pore structure and size in freeze-dried collagen sponges. J. Biomed. Mater. Res. 58, 352–357. https://doi.org/10.1002/jbm.1028

Schulz, J.T., Tompkins, R.G., Burke, J.F., 2000. Artificial Skin. Annu. Rev. Med. 51, 231–244. https://doi.org/10.1146/annurev.med.51.1.231

Serbo, J.V., Gerecht, S., 2013. Vascular tissue engineering: biodegradable scaffold platforms to promote angiogenesis. Stem Cell Res. Ther. 4, 8. https://doi.org/10.1186/scrt156

Sergienko, A.Y., Tai, H., Narkis, M., Silverstein, M.S., 2002. Polymerized high internal-phase emulsions: Properties and interaction with water. J. Appl. Polym. Sci. 84, 2018–2027. https://doi.org/10.1002/app.10555

Shainoff, J.R., Dardik, B.N., 1983. Fibrinopeptide B in Fibrin Assembly and Metabolism: Physiologic Significance in Delayed Release of the Peptide*. Ann. N. Y. Acad. Sci. 408, 254–268. https://doi.org/10.1111/j.1749-6632.1983.tb23249.x

Shastri, V.P., Martin, I., Langer, R., 2000. Macroporous polymer foams by hydrocarbon templating. Proc. Natl. Acad. Sci. 97, 1970–1975. https://doi.org/10.1073/pnas.97.5.1970

Shea, J.D., 1975. Pressure Sores Classification and Management. Clin. Orthop. 112, 89–100.

Shea, L.D., Smiley, E., Bonadio, J., Mooney, D.J., 1999. DNA delivery from polymer matrices for tissue engineering. Nat. Biotechnol. 17, 551–554. https://doi.org/10.1038/9853

Sheikh, Z., Brooks, P.J., Barzilay, O., Fine, N., Glogauer, M., 2015. Macrophages, Foreign Body Giant Cells and Their Response to Implantable Biomaterials. Materials 8, 5671–5701. https://doi.org/10.3390/ma8095269

Shevchenko, R.V., James, S.L., James, S.E., 2009. A review of tissue-engineered skin bioconstructs available for skin reconstruction. J. R. Soc. Interface rsif20090403. https://doi.org/10.1098/rsif.2009.0403

Shikanov, A., Xu, M., Woodruff, T.K., Shea, L.D., 2009. Interpenetrating fibrin–alginate matrices for in vitro ovarian follicle development. Biomaterials 30, 5476–5485. https://doi.org/10.1016/j.biomaterials.2009.06.054

Shinoda, K., Arai, H., 1964. The correlation between phase inversion temperature in emulsion and cloud point in solution of nonionic emulsifier. J. Phys. Chem. 68, 3485–3490.

Sidawy, A.N., 2006. Diabetic Foot: Lower Extremity Arterial Disease and Limb Salvage. Lippincott Williams & Wilkins.

Sidhu, J.S., Cowan, D., Kaski, J.-C., 2003. The effects of rosiglitazone, a peroxisome proliferator-activated receptor-gamma agonist, on markers of endothelial cell activation, C-reactive protein, and fibrinogen levels in non-diabetic coronary artery disease patients. J. Am. Coll. Cardiol. 42, 1757–1763. https://doi.org/10.1016/j.jacc.2003.04.001

Siebenlist, K.R., Mosesson, M.W., Hernandez, I., Bush, L.A., Cera, E.D., Shainoff, J.R., Orio, J.P.D., Stojanovic, L., 2005. Studies on the basis for the properties of fibrin produced from fibrinogen-containing γ′ chains. Blood 106, 2730–2736. https://doi.org/10.1182/blood-2005-01-0240

Silverstein, M.S., 2014. Emulsion-templated porous polymers: A retrospective perspective. Polymer 55, 304–320. https://doi.org/10.1016/j.polymer.2013.08.068

Sneve, H., 1906. The treatment of burns and skin grafting. J. Am. Med. Assoc. XLVII, 1–8. https://doi.org/10.1001/jama.1906.25210010001001

Snyder, R.J., 2005. Treatment of nonhealing ulcers with allografts. Clin. Dermatol. 23, 388–395.

Sobisch, T., Lerche, D., 2005. Rapid emulsifier selection and evaluation of emulsion stability by analytical centrifugation, in: SCI/RSC/SCS Conference on Cosmetics and Colloids. London.

Solans, C., Izquierdo, P., Nolla, J., Azemar, N., Garcia-Celma, M.J., 2005. Nano-emulsions. Curr. Opin. Colloid Interface Sci. 10, 102–110. https://doi.org/10.1016/j.cocis.2005.06.004

Song, J.J., Ott, H.C., 2011. Organ engineering based on decellularized matrix scaffolds. Trends Mol. Med. 17, 424–432. https://doi.org/10.1016/j.molmed.2011.03.005

Šprincl, L., Kopeček, J., Lím, D., 1971. Effect of porosity of heterogeneous poly(glycol monomethacrylate) gels on the healing-in of test implants. J. Biomed. Mater. Res. 5, 447–458. https://doi.org/10.1002/jbm.820050503

Standeven, K.F., Ariëns, R.A.S., Grant, P.J., 2005. The molecular physiology and pathology of fibrin structure/function. Blood Rev. 19, 275–288. https://doi.org/10.1016/j.blre.2005.01.003

Stocker, K., Fischer, H., Meier, J., 1982. Thrombin-like snake venom proteinases. Toxicon 20, 265–273. https://doi.org/10.1016/0041-0101(82)90225-2

Sultana, N., Wang, M., 2008. Fabrication of HA/PHBV composite scaffolds through the emulsion freezing/freeze-drying process and characterisation of the scaffolds. J. Mater. Sci. Mater. Med. 19, 2555. https://doi.org/10.1007/s10856-007-3214-3

Sun, T., Norton, D., McKean, R.J., Haycock, J.W., Ryan, A.J., MacNeil, S., 2007. Development of a 3D cell culture system for investigating cell interactions with electrospun fibers. Biotechnol. Bioeng. 97, 1318–1328. https://doi.org/10.1002/bit.21309

Swartz, D.D., Russell, J.A., Andreadis, S.T., 2005. Engineering of fibrin-based functional and implantable small-diameter blood vessels. Am. J. Physiol. - Heart Circ. Physiol. 288, H1451–H1460. https://doi.org/10.1152/ajpheart.00479.2004

Swieszkowski, W., Tuan, B.H.S., Kurzydlowski, K.J., Hutmacher, D.W., 2007. Repair and regeneration of osteochondral defects in the articular joints. Biomol. Eng., Proceedings on Symposium J Surface Functionalization of BiomaterialsEMRS 2006 Fall Conference 24, 489–495. https://doi.org/10.1016/j.bioeng.2007.07.014

Szabo, G., 1967. The Regional Anatomy of the Human Integument with Special Reference to the Distribution of Hair Follicles, Sweat Glands and Melanocytes. Philos. Trans. R. Soc. B Biol. Sci. 252, 447–485. https://doi.org/10.1098/rstb.1967.0029

Szabowski, A., Maas-Szabowski, N., Andrecht, S., Kolbus, A., Schorpp-Kistner, M., Fusenig, N.E., Angel, P., 2000. c-Jun and JunB Antagonistically Control Cytokine-Regulated Mesenchymal–Epidermal Interaction in Skin. Cell 103, 745–755. https://doi.org/10.1016/S0092-8674(00)00178-1

Tadros, T.F., 2013. Emulsion Formation and Stability. John Wiley & Sons.

Tai, H., Sergienko, A., Silverstein, M.S., 2001. Organic–inorganic networks in foams from high internal phase emulsion polymerizations. Polymer 42, 4473–4482. https://doi.org/10.1016/S0032-3861(00)00820-X

Taizi, M., Deutsch, V.R., Leitner, A., Ohana, A., Goldstein, R.S., 2006. A novel and rapid in vivo system for testing therapeutics on human leukemias. Exp. Hematol. 34, 1698–1708. https://doi.org/10.1016/j.exphem.2006.07.005

Takeda, Y., 1966. Studies of the metabolism and distribution of fibrinogen in healthy men with autologous 125-I-labeled fibrinogen. J. Clin. Invest. 45, 103–111.

Tan, W.-H., Takeuchi, S., 2007. Monodisperse Alginate Hydrogel Microbeads for Cell Encapsulation. Adv. Mater. 19, 2696–2701. https://doi.org/10.1002/adma.200700433

Tarnuzzer, R.W., Schultz, G.S., 1996. Biochemical analysis of acute and chronic wound environments. Wound Repair Regen. 4, 321–325. https://doi.org/10.1046/j.1524-475X.1996.40307.x

Taylor, M.S., Daniels, A.U., Andriano, K.P., Heller, J., 1994. Six bioabsorbable polymers: in vitro acute toxicity of accumulated degradation products. J. Appl. Biomater. 5, 151–157.

Tessmar, J.K., Göpferich, A.M., 2007. Matrices and scaffolds for protein delivery in tissue engineering. Adv. Drug Deliv. Rev., Matrices and Scaffolds for Drug Delivery in Tissue Engineering 59, 274–291. https://doi.org/10.1016/j.addr.2007.03.020

Thomas, A., Goettmann, F., Antonietti, M., 2008. Hard Templates for Soft Materials: Creating Nanostructured Organic Materials. Chem. Mater. 20, 738–755. https://doi.org/10.1021/cm702126j

Thomson, R.C., Wake, M.C., Yaszemski, M.J., Mikos, A.G., 1995. Biodegradable polymer scaffolds to regenerate organs, in: Biopolymers II. Springer, Berlin, Heidelberg, pp. 245–274. https://doi.org/10.1007/3540587888_18

Tîrzui, E., Seres, M., 2010. Particularities of the Avian Immune System. Lucr. Ştiinłifice Med. Vet. 43, 269–278.

Tong, Q., Romanini, C.E., Exadaktylos, V., Bahr, C., Berckmans, D., Bergoug, H., Eterradossi, N., Roulston, N., Verhelst, R., McGonnell, I.M., Demmers, T., 2013. Embryonic development and the physiological factors that coordinate hatching in domestic chickens. Poult. Sci. 92, 620–628. https://doi.org/10.3382/ps.2012-02509

Tremblay, P.-L., Hudon, V., Berthod, F., Germain, L., Auger, F.A., 2005. Inosculation of Tissue-Engineered Capillaries with the Host's Vasculature in a Reconstructed Skin Transplanted on Mice. Am. J. Transplant. 5, 1002–1010. https://doi.org/10.1111/j.1600-6143.2005.00790.x

Trottier, V., Marceau-Fortier, G., Germain, L., Vincent, C., Fradette, J., 2008. IFATS Collection: Using Human Adipose-Derived Stem/Stromal Cells for the Production of New Skin Substitutes. STEM CELLS 26, 2713–2723. https://doi.org/10.1634/stemcells.2008-0031

Tuan, R.S., Boland, G., Tuli, R., 2002. Adult mesenchymal stem cells and cell-based tissue engineering. Arthritis Res Ther 5, 32. https://doi.org/10.1186/ar614

Tufaro, A.P., Buck, D.W., Fischer, A.C., 2007. The use of artificial dermis in the reconstruction of oncologic surgical defects. Plast. Reconstr. Surg. 120, 638–646. https://doi.org/10.1097/01.prs.0000270298.68331.8a

United States Pharmacopoeia, n.d. USP 788 Particulate Matter in Injections.

Valdes, T.I., Kreutzer, D., Moussy, F., 2002. The chick chorioallantoic membrane as a novel in vivo model for the testing of biomaterials. J. Biomed. Mater. Res. 62, 273–282. https://doi.org/10.1002/jbm.10152

Vepari, C., Kaplan, D.L., 2007. Silk as a biomaterial. Prog. Polym. Sci. 32, 991–1007.

Vidal, S.E.L., Tamamoto, K.A., Nguyen, H., Abbott, R.D., Cairns, D.M., Kaplan, D.L., 2019. 3D biomaterial matrix to support long term, full thickness, immuno-competent human skin equivalents with nervous system components. Biomaterials, Organoids and Ex Vivo Tissue On-Chip Technologies 198, 194–203. https://doi.org/10.1016/j.biomaterials.2018.04.044

Vig, K., Chaudhari, A., Tripathi, S., Dixit, S., Sahu, R., Pillai, S., Dennis, V.A., Singh, S.R., 2017. Advances in Skin Regeneration Using Tissue Engineering. Int. J. Mol. Sci. 18, 789. https://doi.org/10.3390/ijms18040789

Viswanathan, P., Chirasatitsin, S., Ngamkham, K., Engler, A.J., Battaglia, G., 2012. Cell instructive microporous scaffolds through interface engineering. J. Am. Chem. Soc. 134, 20103–20109. https://doi.org/10.1021/ja308523f

Vournakis, J.N., Demcheva, M., Whitson, A.B., Finkielsztein, S., Connolly, R.J., 2003. The rdh bandage: hemostasis and survival in a lethal aortotomy hemorrhage model. J. Surg. Res. 113, 1–5. https://doi.org/10.1016/S0022-4804(03)00161-6

Wainwright, D.J., 1995. Use of an acellular allograft dermal matrix (AlloDerm) in the management of full-thickness burns. Burns 21, 243–248. https://doi.org/10.1016/0305-4179(95)93866-I

Walters, K., Roberts, M., 2002. The Structure and Function of Skin, in: Dermatological and Transdermal Formulations. CRC Press, pp. 1–39.

Wang, B., Li, D., Wang, L.-J., Adhikari, B., Shi, J., 2010. Ability of flaxseed and soybean protein concentrates to stabilize oil-in-water emulsions. J. Food Eng. 100, 417–426. https://doi.org/10.1016/j.jfoodeng.2010.04.026

Wang, S., Zheng, Z., Weng, Y., Yu, Y., Zhang, D., Fan, W., Dai, R., Hu, Z., 2004. Angiogenesis and anti-angiogenesis activity of Chinese medicinal herbal extracts. Life Sci. 74, 2467–2478. https://doi.org/10.1016/j.lfs.2003.03.005

Wang, X., Ding, B., Li, B., 2013. Biomimetic electrospun nanofibrous structures for tissue engineering. Mater. Today 16, 229–241. https://doi.org/10.1016/j.mattod.2013.06.005

Watt, F.M., Driskell, R.R., 2010. The therapeutic potential of stem cells. Philos. Trans. R. Soc. B Biol. Sci. 365, 155–163. https://doi.org/10.1098/rstb.2009.0149

Webb, D.R., 1987. Thermal Tolerance of Avian Embryos: A Review. The Condor 89, 874–898. https://doi.org/10.2307/1368537

Weigert, R., Choughri, H., Casoli, V., 2011. Management of severe hand wounds with integra® dermal regeneration template. J. Hand Surg. Eur. Vol. 36, 185–193. https://doi.org/10.1177/1753193410387329

Weinberg, C.B., 1989. Fibrin-collagen tissue equivalents and methods for preparation thereof. US4837379 A.

Weisel, J.W., 2004. The mechanical properties of fibrin for basic scientists and clinicians. Biophys. Chem. 112, 267–276.

Weisel, J.W., 1986. Fibrin assembly. Lateral aggregation and the role of the two pairs of fibrinopeptides. Biophys. J. 50, 1079–1093. https://doi.org/10.1016/S0006-3495(86)83552-4

Weisel, J.W., Medved, L., 2001. The Structure and Function of the αC Domains of Fibrinogen. Ann. N. Y. Acad. Sci. 936, 312–327. https://doi.org/10.1111/j.1749-6632.2001.tb03517.x

Weisel, J.W., Nagaswami, C., 1992. Computer modeling of fibrin polymerization kinetics correlated with electron microscope and turbidity observations: clot structure and assembly are kinetically controlled. Biophys. J. 63, 111–128. https://doi.org/10.1016/S0006-3495(92)81594-1

West, J.L., Hubbell, J.A., 1999. Polymeric Biomaterials with Degradation Sites for Proteases Involved in Cell Migration. Macromolecules 32, 241–244. https://doi.org/10.1021/ma981296k

Whang, K., Goldstick, T.K., Healy, K.E., 2000. A biodegradable polymer scaffold for delivery of osteotropic factors. Biomaterials, Orthopaedic Polymeric Biomaterials: Applications of Biodegradables 21, 2545–2551. https://doi.org/10.1016/S0142-9612(00)00122-8

Whang, K., Thomas, C.H., Healy, K.E., Nuber, G., 1995. A novel method to fabricate bioabsorbable scaffolds. Polymer 36, 837–842. https://doi.org/10.1016/0032-3861(95)93115-3

Wieland, M., Haas, H., 2013. Stratiform perforated biomatrices. US8481802B2.

Wilcke, I., Lohmeyer, J.A., Liu, S., Condurache, A., Krüger, S., Mailänder, P., Machens, H.G., 2007. VEGF165 and bFGF protein-based therapy in a slow release system to improve angiogenesis in a bioartificial dermal substitute in vitro and in vivo. Langenbecks Arch. Surg. 392, 305–314. https://doi.org/10.1007/s00423-007-0194-1

Wilde, P., Mackie, A., Husband, F., Gunning, P., Morris, V., 2004. Proteins and emulsifiers at liquid interfaces. Adv. Colloid Interface Sci., Emulsions, From Fundamentals to Practical Applications 108–109, 63–71. https://doi.org/10.1016/j.cis.2003.10.011

Wilf, J., Gladner, J.A., Minton, A.P., 1985. Acceleration of fibrin gel formation by unrelated proteins. Thromb. Res. 37, 681–688. https://doi.org/10.1016/0049-3848(85)90197-5

Witthayapanyanon, A., Harwell, J.H., Sabatini, D.A., 2008. Hydrophilic–lipophilic deviation (HLD) method for characterizing conventional and extended surfactants. J. Colloid Interface Sci. 325, 259–266. https://doi.org/10.1016/j.jcis.2008.05.061

Wolberg, A.S., 2007. Thrombin generation and fibrin clot structure. Blood Rev. 21, 131–142. https://doi.org/10.1016/j.blre.2006.11.001

Wu, Y., Chen, L., Scott, P.G., Tredget, E.E., 2007. Mesenchymal Stem Cells Enhance Wound Healing Through Differentiation and Angiogenesis. STEM CELLS 25, 2648–2659. https://doi.org/10.1634/stemcells.2007-0226

Xiao, X., Wang, W., Liu, D., Zhang, H., Gao, P., Geng, L., Yuan, Y., Lu, J., Wang, Z., 2015. The promotion of angiogenesis induced by three-dimensional porous beta-tricalcium phosphate scaffold with different interconnection sizes via activation of PI3K/Akt pathways. Sci. Rep. 5, 9409.

Yamaguchi, R., Takami, Y., Yamaguchi, Y., Shimazaki, S., 2007. Bone marrow-derived myofibroblasts recruited to the upper dermis appear beneath regenerating epidermis after deep dermal burn injury. Wound Repair Regen. 15, 87–93. https://doi.org/10.1111/j.1524-475X.2006.00189.x

Yang, S., Leong, K.-F., Du, Z., Chua, C.-K., 2001. The Design of Scaffolds for Use in Tissue Engineering. Part I. Traditional Factors. Tissue Eng. 7, 679–689. https://doi.org/10.1089/107632701753337645

Yang, X.B., Roach, H.I., Clarke, N.M.P., Howdle, S.M., Quirk, R., Shakesheff, K.M., Oreffo, R.O.C., 2001. Human osteoprogenitor growth and differentiation on synthetic biodegradable structures after surface modification. Bone 29, 523–531. https://doi.org/10.1016/S8756-3282(01)00617-2

Yannas, I.V., Burke, J.F., 1980. Design of an artificial skin. I. Basic design principles. J. Biomed. Mater. Res. 14, 65–81.

Yannas, I.V., Burke, J.F., Stasikelis, P.J., 1985. Method for preserving porosity in porous materials. US4522753 A.

Yannas, I.V., Lee, E., Orgill, D.P., Skrabut, E.M., Murphy, G.F., 1989. Synthesis and characterization of a model extracellular matrix that induces partial regeneration of adult mammalian skin. Proc. Natl. Acad. Sci. 86, 933–937.

Yarranton, H.W., Sztukowski, D.M., Urrutia, P., 2007. Effect of interfacial rheology on model emulsion coalescence: I. Interfacial rheology. J. Colloid Interface Sci. 310, 246–252. https://doi.org/10.1016/j.jcis.2007.01.071

Yasuda, H., Kuroda, S., Shichinohe, H., Kamei, S., Kawamura, R., Iwasaki, Y., 2009. Effect of biodegradable fibrin scaffold on survival, migration, and differentiation of transplanted bone marrow stromal cells after cortical injury in rats. J. Neurosurg. 112, 336–344. https://doi.org/10.3171/2009.2.JNS08495

Yayon, A., Azachi, M., Gladnikoff, M., 2010. Freeze-dried fibrin matrices and methods for preparation thereof. US7714107 B2.

Yu, J.R., Navarro, J., Coburn, J.C., Mahadik, B., Molnar, J., Holmes, J.H., Nam, A.J., Fisher, J.P., 2019. Current and future perspectives on skin tissue engineering: Key features of biomedical research, translational assessment, and clinical application. Adv. Healthc. Mater. 8, 1801471. https://doi.org/10.1002/adhm.201801471

Zhang, H., Cooper, A.I., 2005. Synthesis and applications of emulsion-templated porous materials. Soft Matter 1, 107–113. https://doi.org/10.1039/B502551F

Zhang, H., Cooper, A.I., 2002. Synthesis of monodisperse emulsion-templated polymer beads by oil-in-water-in-oil (O/W/O) sedimentation polymerization. Chem. Mater. 14, 4017–4020. https://doi.org/10.1021/cm0206643

Zhang, Y., Chan, H.F., Leong, K.W., 2013. Advanced materials and processing for drug delivery: The past and the future. Adv. Drug Deliv. Rev., Advanced Drug Delivery: Perspectives and Prospects 65, 104–120. https://doi.org/10.1016/j.addr.2012.10.003

Zhong, S.P., Zhang, Y.Z., Lim, C.T., 2010. Tissue scaffolds for skin wound healing and dermal reconstruction. Wiley Interdiscip. Rev. Nanomed. Nanobiotechnol. 2, 510–525. https://doi.org/10.1002/wnan.100

Zhou, Q., Xie, J., Bao, M., Yuan, H., Ye, Z., Lou, X., Zhang, Y., 2015. Engineering aligned electrospun PLLA microfibers with nano-porous surface nanotopography for modulating the responses of vascular smooth muscle cells. J. Mater. Chem. B 3, 4439–4450. https://doi.org/10.1039/C5TB00051C